ASSESSMENTS OF NANOPARTICLE PROCOAGULANT PROPERTIES IN BLOOD

by

Clinton F. Jones

A dissertation submitted to the faculty of
The University of Utah
in partial fulfillment of the requirements for the degree of

Doctor of Philosophy

Department of Pharmaceutics and Pharmaceutical Chemistry

The University of Utah

May 2014

The University of Utah Graduate School

STATEMENT OF DISSERTATION APPROVAL

The dissertation of **Clinton F. Jones**

has been approved by the following supervisory committee members:

David W. Grainger	, Chair	**8/10/2012** Date Approved
Hamidreza S. Ghandehari	, Member	**8/10/2012** Date Approved
Sung Wan Kim	, Member	**8/10/2012** Date Approved
Andrew S. Weyrich	, Member	**8/10/2012** Date Approved
Michael Redd	, Member	**8/10/2012** Date Approved

and by **David W. Grainger** , Chair of

the Department of **Pharmaceutics and Pharmaceutical Chemistry**

and by David B. Kieda, Dean of The Graduate School.

ABSTRACT

The need for nanoparticle toxicity evaluations is well recognized as the number of applications for nanoparticles continues to grow. This dissertation seeks to reach beyond presently available assessments of nanoparticle-mediated toxicity and mortality to assess the consequences of intravenous nanoparticle injection upon the cellular and molecular participants in the hemostatic response. Based on published reports of severe *in vivo* coagulopathy, *in vitro* platelet aggregation and hemolysis for cationic poly(amido amine) (PAMAM) dendrimer nanoparticles, cationic generation-7 PAMAM dendrimers (G7-NH_2) were hypothesized to possess strong and specific hemostatic properties and were utilized in the adaptation and development of assays evaluating nanoparticle procoagulant properties. The latter part of this dissertation utilizes the lipopolysaccharide (LPS)-sensitive limulus amoebocyte lysate (LAL) assay a surrogate to explore the hypothesis that intrinsically heightened nanoparticle properties of surface reactivity and specific surface area may disrupt endogenous biochemical cascades.

The G7-NH_2 were found to affect all key platelet functions, evidenced by severe morphological alteration, extensive aggregation and adhesion, release of alpha granule contents, and attenuation of thrombin generation. It was further demonstrated that extensive, direct, dendrimer-mediated aggregation of fibrinogen occurs *via* a thrombin-independent, electrostatic mechanism that also included G7-NH_2 aggregation of bovine serum albumin and, by extension, the a majority of soluble plasma protein species due to their negative charge domains.

Silica nanoparticles and two types of gold nanoparticles were demonstrated to increase the LAL assay response to LPS, while carboxy latex particles attenuated the LAL assay response. This apparent increase in the rate of production for the chromogenic LAL assay product for the gold and silica nanoparticles shows the potential for nanoparticles to exacerbate endogenous inflammatory responses to toxins co-presented *in vivo*.

In summary, this dissertation demonstrates the potential for nanoparticle reactivity within or in concert with biological systems and specifically clarifies the mechanism of cationic dendrimer-induced hemostasis. Additionally, this work establishes additional models for the assessment of procoagulant properties of nanoparticles. The specific mechanistic findings presented herein represent an improvement upon the level of analysis usually performed for nanoparticles in the blood system and may guide rational design for safer nanoparticle-based, intravenous therapies.

TABLE OF CONTENTS

LIST OF FIGURES

LIST OF TABLES

ACKNOWLEDGEMENTS

I thank my dissertation advisor, Professor David W. Grainger, for his support during my graduate career. I have greatly appreciated his guidance in my research as well as his availability and careful mentorship in my professional development as a scientist. His thoughtful advice and dedication have contributed much to my problem solving methods and passion for science. Additionally, I appreciate the support and collaboration of my supervisory committee members and their respective research groups. Particularly, I wish to thank Dr. Robby Campbell for the hours in experiments and conversations that he contributed to this project. He is an excellent scientist whose assistance and expertise were indispensable in all things dealing with blood and platelets. I also wish to thank Giridhar Thiagarajan for highly useful and motivating research and conversation that helped me get this project rolling. I am also grateful to Drs. Mike Redd and Brent Bisgrove for their hours of training and advice with zebrafish embryo experiments, for always providing interesting conversation, and for their friendship and interest.

I also thank the members of the Grainger research group, past and present including Dr. Hiro Takahashi, Dr. Neil Ayres, Dr. Lisa Chamberlain, Dr. Yuwei Wang, Dr. Dolly Holt, Paul Hogrebe, Anna Astashkina, Archana Rao, Dorina Diekjurgen, Joe Aamodt, Dr. Amanda Brooks, and Dr. Ben Brooks for their technical advice and assistance, and especially for their support, encouragement and friendship,.

I owe great thanks to my family, including my parents and siblings for the support, love and individual examples of accomplishment that they provide to me. I also appreciate my parents' much needed and timely financial assistance to help us get through this experience.

Most especially, I thank my sweetheart, Camber, for her unfailing love, support, and companionship through all the ups and downs of my graduate research, having married me just before I started my graduate career. We have been blessed with two wonderful, energetic children,

Camdon and Carolina, and I thank them for loving me, praying for me, and making me a better person through their smiles, songs, and hugs every day.

Additionally, I am very thankful to the Eccles family for supporting the scholarship that funded my first year in the program, the Utah Synergy program that funded my second year, subsequent funding from a University Interdisciplinary grant, and NIH support for the all the rest.

CHAPTER 1

IN VITRO ASSESSMENTS OF NANOMATERIAL TOXICITY

Reprinted from Advanced Drug Delivery Reviews, 61(6), Clinton F. Jones, David W. Grainger, In Vitro Assessments of Nanomaterial Toxicity, pp. 438–456, with permission from Elsevier.

Advanced Drug Delivery Reviews 61 (2009) 438–456

Contents lists available at ScienceDirect

Advanced Drug Delivery Reviews

journal homepage: www.elsevier.com/locate/addr

In vitro assessments of nanomaterial toxicity☆

Clinton F. Jones, David W. Grainger *

Department of Pharmaceutics and Pharmaceutical Chemistry, University of Utah, Salt Lake City, UT 84112-5820 USA

ARTICLE INFO

Article history:
Received 5 August 2008
Accepted 30 March 2009
Available online 19 April 2009

Keywords:
Nanoscience
Nanotechnology
Nanomaterials
Nanotoxicity
In vitro
Bioassays
Toxicology
Particles

ABSTRACT

Nanotechnology has grown from a scientific interest to a major industry with both commodity and specialty nanomaterial exposure to global populations and ecosystems. Sub-micron materials are currently used in a wide variety of consumer products and in clinical trials as drug delivery carriers and imaging agents. Due to the expected growth in this field and the increasing public exposure to nanomaterials, both from intentional administration and inadvertent contact, improved characterization and reliable toxicity screening tools are required for new and existing nanomaterials. This review discusses current methodologies used to assess nanomaterial physicochemicial properties and their *in vitro* effects. Current methods lack the desired sensitivity, reliability, correlation and sophistication to provide more than limited, often equivocal, pieces of the overall nanomaterial performance parameter space, particularly in realistic physiological or environmental models containing cells, proteins and solutes. Therefore, improved physicochemical nanomaterial assays are needed to provide accurate exposure risk assessments and genuine predictions of *in vivo* behavior and therapeutic value. Simpler model nanomaterial systems in buffer do not accurately duplicate this complexity or predict *in vivo* behavior. A diverse portfolio of complementary material characterization tools and bioassays are required to validate nanomaterial properties in physiology.

Contents

☆ This review is part of the *Advanced Drug Delivery Reviews* theme issue on "Identifying and Assessing Biomaterial Nanotoxicity in Translational Research for Preclinical Drug Development".

* Corresponding author. Department of Pharmaceutics and Pharmaceutical Chemistry, College of Pharmacy, Rm 301, 30 South 2000 East, University of Utah, Salt Lake City, UT 84112-5820 USA. Fax: +1 801 581 3674.
E-mail address: david.grainger@utah.edu (D.W. Grainger).
URL: http://www.bioen.utah.edu/faculty/DWG/ (D.W. Grainger).

0169-409X/$ – see front matter © 2009 Elsevier B.V. All rights reserved.
doi:10.1016/j.addr.2009.03.005

1. Introduction

The rapid expansion of scientific, technological and commercial interests in sub-micron materials, assembly, and properties unique at this size scale has spawned the fields of nanoscience and nanotechnology. Over 500 consumer products currently on the market claim to contain elements of nanoscience and nanotechnology with new entries coming daily [1,2]. This market annually requires metric tons of raw nanomaterials, ranging from nano-sized metals and metal oxide particles to carbon nanotubes [3,4]. Such manufacturing and consumer utilization then produces multiple different sources of release of these materials into the environment, eco-system, water [5] and food supplies, and other routes of non-voluntary entry into the human body [6]. Demand for nanotechnology in medical products will grow by more than 17% annually to reach an estimated $53 billion market in 2011, with the largest share of this opportunity in pharmaceutical applications, expected to reach $18 billion in 2014 [7]. Moreover, the US National Science Foundation predicts that half of the pharmaceutical industry product line will comprise central nanotechnological design features by 2015. At least 12 nanomedicines are already approved, and progressively more are seen entering active development stages [8]. Hence, a steady succession of new nanotech-based drugs, imaging agents, and diagnostic products are anticipated to seek (and possibly gain) regulatory approvals and subsequent access to human-prescribed use. Therefore, deliberate point-sourced (i.e., drug-dosed) as well as uncontrolled, inadvertent environmental nanomaterial exposure to humans will undoubtedly increase through many different routes.

While nanomaterials are attractive for both basic science and technological reasons, increasing human exposure to nanomaterials together with the distinct properties of these materials all mandate development and validation of accurate nanodevice and materials characterization protocols and predictive toxicity and hazard capabilities. These methods must reliably predict and assess the possible spectra of effects, from benefits to possible risks, and health hazards associated with exposure to nanomaterials as they become more widespread, pervasive agents in manufacturing and medicine. The inter-agency National Toxicology Program recommends the classification of a new entity according to its plausible risks, in line with the data extant concerning the new entity. Accordingly, the entity is interrogated by a set of tests designed to characterize a given risk and characterize mechanisms for related outcomes [9]. Such an assessment regime would best consider traditional pharmacology and toxicology approaches to dose response, acute and chronic exposure, as they correlate to rigorous physicochemical characterization [10] and various levels of physiological reactivity (e.g., molecular, cellular, tissue, organ toxicity) in making risk–benefit analyses of these materials both in various manufactured forms and as incorporated within new technologies [9]. This need becomes compelling if future studies continue to bolster recent preliminary findings that claim biological responses to carbon nanotubes not unlike those observed for the well-known carcinogen/irritant, asbestos [11–13].

Importantly, new evidence showing *in vivo* immunomodulatory cell processing of intravenous nanoparticles acutely dosed for antigen presentation and vaccine induction suggests specific uptake, transport and cell processing of nanoparticles [14–17]. That such immune surveillance is also affected by non-deliberate, potentially harmful or chronic low-level nanoparticle processing remains to be shown. To this end, many materials testing methods well-established for macroscale biomaterials and for soluble pharmaceutical products are simply adapted in a variety of ways to discover correlations between nanomaterial properties and the biological responses *in vitro* to cells and *in vivo* to animal pre-clinical models. This requisite analysis precedes any human *in vivo* materials applications: such monitoring falls broadly under the scope of "biocompatibility testing" (i.e., ISO 10993), although no definitive or scientific metric exists for such assessment except the FDA-mandated safety and efficacy requirements. However, to date, two notable deficiencies in such testing exist, namely that little long-term chronic nanomaterial exposure data is available in any form, and that connections between extensive acute-exposure cell-based testing models *in vitro* with any *in vivo* response are generally lacking. Implanted biomaterials might indeed be known to do no harm to a host in various bulk forms (e.g., sheets, fabrics, milled large pieces as implants), but could be decidedly and distinctly reactive and harmful if presented to the host in a different form, e.g., as a colloid or particulate [14,16]. A particular challenge is to assert safety and efficacy for nanoscale biomedical systems, distinct from similar materials in micro- and macroscopic morphologies. Routes of biological exposure, as well as materials chemical and physical properties must be carefully considered in these nano-biocompatibility tests. Each route and each material size and form has its own pharmacological and/or toxicological properties that require unique assessment protocols and criteria for healthful versus harmful exposure outcomes. Hence, there is currently no evidence or confidence in assuming that nanoscale pieces of known biocompatibility bulk metals or metal oxides, ceramics or polymers would share accepted biocompatible properties of their bulk materials. Similar presumptions might also be made about the biocompatible relationships between micron and nanometer-sized dispersions of these materials, or various colloidal formulations of sub-micron materials (i.e. as pharmaceutical formulations for parenteral injections, inhalation, or oral administrations). Therefore, the current nanomaterials revolution in human dosing, exposure and toxicological assessments must be accompanied by an equally ambitious biomedical research effort to develop new tools, methods, pharm/tox protocols, biocompatibility and safety standards and host exposure qualifications for different nanomaterial classes.

There are indeed concerns specific to nanoscale materials in biological systems: as materials dimensions approach the nanoscale, certain properties become scale-dependent, especially in particles below 20 nm diameter. These include capillary forces, optical effects/color, melting points, conductivity, ionization potential, electron affinity, magnetism, and, significantly, surface energy and reactivity. Specific surface areas for micron-sized particles (e.g. fumed silicas and commercial carbon blacks) are typically 60–80 m^2/g, a considerable surface-to-mass ratio many times greater than their macroscopic counterparts. Commercial CB-1 carbon black and single-wall carbon nanotubes – a major current nanotechnology interest for both therapeutics and consumer products – have specific surface areas approaching 1000 m^2/g. Similar area scaling effects are seen with miniaturization of surface topology, porosity, texturing, and high-density fabrication in sub-micron features. Hence, surface structure and composition, and therefore intrinsic reactivity, are perhaps the dominant structure-determining properties in nanomaterials. Surface effects must also be considered a unique and very significant set of functional nano-properties that requires both control and careful characterization enroute to exploitation in specific nanotechnologies [18].

Such high-specific-surface-area materials have high interfacial chemical and physical reactivity that translates to biological reactivity.

Compared to bulk-phase atoms, two important, distinguishing features of surface atoms in nanosystems are (1) their lower coordination number and (2) their increased exposure to reactive species in the environment. These features translate to intrinsically higher surface atom reactivity than bulk atoms and manifestation of this reactivity in some usual ways, but also other very unique ways. As particle size decreases, the surface properties of the atoms dominate, leading to significant changes in particle reactivity. The relative fraction of surface atoms to bulk atoms in a structure, called *dispersion*, exhibits a power law scaling in the nanoscale regime. While less than 1% of a microparticle's atoms occupy surface positions, over 10% of the atoms in a 10-nm diameter metal particle reside on its surface (and 60% in a 2-nm particle!) [9,18]. This huge fractional surface presence in nanomaterials contributes to a change in surface physical and chemical properties as materials are reduced in size below 20 nm [19]. This presents unique challenges for the materials science and associated surface analytical communities to characterize and control surface properties, as well as asserts quality control specifications at the nanoscale that would help standardize different nanomaterial properties. Deploying these materials *in vivo* has even more challenges.

Significantly, the question of whether or not these nanomaterial properties, or other effects (e.g., intrinsic colloidal instability and aggregation phenomena in aqueous milieu, bio-accumulation in the environment or tissues, contaminant adsorption and transport) would permeate, become persistent in and influence biological systems remains to be determined. Currently, there is no consensus about the intrinsic risks, tolerance, hazards, toxicity or dose–response relationships for almost all classes of nanomaterials. A search of the current literature can easily provide diametrically opposed opinions on safety and tolerance of the same nanomaterial in model *in vitro* test systems (e.g., cell lines) and in small animal *in vivo* testing models. Nanotolerance and nanotoxicology are emerging fields with unique constraints placed by the size and surface properties of the materials under analysis. Few tools and methods exist that can adequately track nanomaterial properties and reactivity in biological or physiological systems. Importantly, these methods are primarily *in vitro* assays to date and, as for many biocompatibility tests conducted for related macrophase materials, could have little if any correlation or validation to *in vivo* materials tolerance [20].

This review identifies current methods commonly used to assess nanomaterial surface and bulk properties and biological reactivity in model *in vitro* systems. These assays are important to characterizing nanomaterial applications in biotechnology, ecosystems, agri- and aqua-culture, biomedical applications and toxicity screening. In large part, these methods represent direct extension of methods known for up to 4 decades for other macroscopic biomaterials compatibility or soluble drug toxicology assessments, adapted to nanoscale colloids. Few of these methods are specifically discriminatory to nanoscale properties, sizes or physical states, and many do not report sensitive information about the nanomaterial behaviors in biological systems: they simply report gross material behaviors and assay signals averaged over the system employed. Few analytical methods provide direct information on nanosystems within biological milieu (solutions of proteins, or cells, or tissues). Lacking the proper tools and sensitivity, current nanotoxicology is in many ways analogous to a blind man describing an elephant: the possible dimensionalities of what scientists seek and need to define for nanophased materials in the environment or living host are enormous. At the same time, the analytical tools available to accurately and reliably determine the pharmacological and toxicological fate of these materials are primitive enough in such complex bio-systems to provide only small, often equivocal, pieces of the resulting huge parameter space.

1.1. Pre-biological materials characterization

Before biological responses to nanomaterials may be assayed to any degree with any real scientific validity, materials properties as supplied (with probable contamination), cleaning procedures, batch-batch variability, and solution properties such as intrinsic aqueous stability, aggregation and flocculation must be thoroughly screened. This is a materials science exercise in quality control, but critically important before meaningful results may be interpreted from later *in vitro* or *in vivo* testing. Bulk materials analysis should involve purity certification, aqueous leachables, and electron microscopy of bulk nanophase morphology, polydispersity, intrinsic aggregation, solubility, and when appropriate, bulk-phase thermal analysis, conductivity or redox behavior, and spectroscopy (i.e., fluorescence, vibrational) to provide some quality control of the expected materials physical and chemical states, and stability.

1.1.1. Surface contamination

Surface contamination of biomaterials is a thermodynamically driven process of surface energy reduction through the adsorption of adventitious air- or water-borne contaminants or renovation of the biomaterial surface through chemical processes. Similarly, the surface contamination of nanomaterials may range from adventitious adsorption to surface oxidation, corrosion, charging or electron transfer reactions of the nanomaterial itself. Due to the highly reactive nature of nanophase surfaces, surface adsorption of many types of molecules in the milieu is expected to reduce surface free energy of the solid interface. Finely dispersed materials (e.g., diatomaceous earth, alumina, silica, and activated charcoals) are already used as adsorbent beds to remove dissolved species. Nanomaterials reproduce this same scenario but with substantially increased surface areas. Hence, contamination of nanomaterials in both air and in aqueous milieu is likely by spontaneous adsorption from ambient phases, and at a degree commensurate with 200–1000 m^2/g surface areas. This means that a few hundred milligrams of carbon nanotubes contaminated with a monolayer of unintentional adsorbate could introduce over a milli-mole of possible surface leachate to the solution to which they were introduced. Hence, nanomaterial surfaces could unintentionally introduce high levels of contaminants by reversible adsorption of air- or solution-borne species. That this might occur to transport high levels of unintended or toxic adsorbate species into human beings via adsorption to nanomaterials is one possibility. A second issue is alteration of nanomaterial colloidal stability by such solute or surfactant adsorption to induce aggregation and altered physical properties of the nanomaterial compared to its 'ideal' monodisperse, 'clean' state. A third concern is that assays will not distinguish toxic endogenous adsorbates from intrinsically toxic nanomaterials without careful control experiments and surface analysis. Deliberate surface modification agents used to stabilize nanomaterials (surfactants, steric and electrostatically charged stabilizers) could also slough in biological systems or partition into serum proteins or membranes (as many drugs do) to produce confounding issues with nanotoxicity or nanomaterial compatibility. Because cell-mediated particle uptake (at least at the micron-size scale) is influenced by surface properties and chemistry, surface contamination and aggregation resulting from surface contamination and/or adsorption in biological systems can affect these mechanisms of cell processing, providing a basis for skewed outcomes for impure materials used for *in vitro* and *in vivo* testing. Therefore, surface composition and its control are requisite to understanding nanomaterial interactions with living systems.

Possible sources of surface contamination of nanomaterials are diverse. The adventitious adsorption of bacteria-derived ubiquitous endotoxins – pyrogens or lipopolysaccharides (LPS) – or polyaromatic hydrocarbons (PAHs) is one concern. Surface oxidation, corrosion, charging or electron transfer reactions of the nanomaterial are also important [9,18]. Left uncharacterized, these various forms of nanomaterial surface contamination and alterations represent a substantial and confusing variable to understand the results of any experimental outcome of nanomaterials simply introduced into *in vitro* or *in vivo* pharm/tox models. In fact, it is likely that

nanomaterials will carry significant adsorbed contamination into test systems under most all conditions, with the exception rather than the rule being a clean, unreactive, or at least consistent, pure material surface chemistry [10,18]. Therefore, understanding and controlling this interface is a key challenge to understanding nanomaterial biocompatibility, risk assessment and possible toxicity mechanisms. This parallels the well-known surface analytical paradigm in macro-scale biocompatibility materials and device testing [21]. The number and varieties of different biomaterials surface characterization methods commonly implemented to assure some quality control standards to implanted materials chemistry and physical conditions is extensive [22]. This chapter lacks the breadth necessary to sufficiently describe the numerous well-known materials characterization tools used prior to any *in vitro* or *in vivo* assay. Nevertheless, such nanomaterial quality control reporting should be expected to be essential in order to understand the material characteristics prior to exposure to biological systems.

1.1.1.1. Adsorbed endotoxin contamination. One example surface contaminant is ubiquitous bacterial endotoxin, lipopolysaccharide (LPS). As a component of gram negative bacterial cell walls, LPS remains one of the most common surface-adsorbed contaminants of serious concern for all biomaterials [23]. As a ubiquitous, heavily glycosylated, phosphorylated lipid often present on skin, on all that skin has touched, in all milieu capable of supporting bacteria, and in most water sources (except expensive pyrogen-free water), LPS surface activity favors its adsorption to hydrophobic surfaces, while its phosphate groups allow it to bind to positively charged surfaces [23]. These properties allow the endotoxin to contaminate virtually any surface. Endotoxin affects biological systems strongly as a known pyrogen by raising organismal body temperature or inflammatory cellular cytokine production through its presentation to host cells of many types [23–26]. Hence, reliably discriminating its activity distinct from the nanomaterial's intrinsic inflammatory activity is important. Given the exaggerated surface-to-volume ratio for nanophase systems, the possible amounts of adsorbed endotoxin (e.g., grams adsorbed endotoxin per gram of material) are significant. Titanium dioxide (TiO_2) particles have been shown to bind LPS in such a way as to reduce *in vitro* cellular inflammatory response to LPS [27]. Other nanoparticles have been shown to bind endotoxin [28,29] and some have been evaluated for their ability to bind endotoxin from aqueous solution [30,31]. Moreover, investigations of particle–endotoxin interactions in relation to orthopedic wear particles have found that particle-adsorbed endotoxin can affect implant loosening through localized inflammation [24,32]. Therefore, endotoxin contamination is possible on a variety of nanoparticles, producing an inflammatory response that is magnified by nanomaterial presence to levels that would warrant concern over endotoxin's potent inflammatory reactivity *in vivo* and with many cell lines [23–26]. The presence of adventitious endotoxin contamination in the cell cultures or on the nanomaterials applied to cells could activate cells and generate inflammatory cytokine responses essentially indistinguishable from any response generated by the nanomaterial exposure. Additionally, such cellular activation could also alter other cell signaling pathways for cell-based assays with unintended consequences. Consequently, endotoxin contamination of nanomaterials, nanomaterial stock solutions, lab glassware, ultrafiltered lab supply water, and cell culture materials should be regularly assayed [33–35], controlled, and remediated before any cell response assay to nanomaterials is attempted [23].

The Limulus Amebocyte Lysate (LAL) assay [23] is the current standard for detecting soluble endotoxin *in vitro* because it is considered the best assay currently available and the established means for endotoxin testing in spite of its inherent inconsistencies (i.e., assay signal is relative to fixed LPS standards that may or may not reflect diverse sources or reactivity of LPS). The colorimetric variation of the LAL is widely used in biomaterials testing, particularly in pre-clinical settings, and is more accurately defined as a measure of endotoxin activity rather than endotoxin concentration. Thus, it is generally accepted that endotoxin may only be detected by these assays if it is soluble or readily displaceable (i.e., not permanently surface-bound), but some methods have been developed to correlate detectable solute endotoxin to surface-bound endotoxin for the same system [23,36,37]. For such methods to be reliable, adsorbed endotoxin concentrations would need to be shown to depend on known LPS exchange or desorption rates under the relevant *in vitro* conditions where LPS undetected by the assay in surface-bound form produced a reliable answer when surface-displaced in biological milieu. That is, irreversibly adsorbed endotoxin might be indirectly correlated by knowing its soluble, reversibly adsorbed, assayed LPS fraction in biological milieu. This rigorous analysis is simply not done on nanomaterials to date, despite the possibility of LPS being one of the most-likely, biologically reactive contaminants present at high levels from routine materials processing and manufacturing. Hence, biological of cause-and-effect tracing of adsorbed LPS and its partitioning between nanophases and biological milieu is unknown.

1.1.1.2. Other surface contaminants. Other adsorbates expected as surface-adsorbed contaminants are no less problematic. Polyaromatic hydrocarbons (PAHs) – known carcinogens [38] – commonly adsorb to surfaces exposed to ambient air, in which PAH exists ubiquitously in trace amounts. Production of carbon-based nanomaterials is now known to generate substantial toxic by-products including at least 15 PAHs [39]. Additionally, carbon nanomaterials are well-known to actively adsorb volatile PAHs co-produced as part of the carbon nanophase manufacturing process [40,41]. Other common laboratory surface-active contaminants include volatile hydrocarbons and silicones from pump exhausts and various volatile plasticizing additives (e.g., alkylated phthalates such as the ubiquitous, surface-active plasticizer, dioctylphthalate). Additionally, catalyst species or unreacted synthesis reagents residual from nano-synthesis are common contaminants in nanosystems [33] such as the Fe, Co, or Ni catalyst or amorphous carbon soot retained by carbon nanotubes following their synthesis [42]. Simple water rinsing or suspension will not remove these adsorbate layers easily or completely. Catalyst removal from carbon nanotubes is routinely performed by stirring in acid for ~2 days, while amorphous carbon is oxidized and removed by 20–70 h treatment with H_2O_2 or by thermal treatment [42,43]. Additionally, the surface-active components in biological fluids (proteins, lipids) can promote exchange and desorption of these adlayers when other cleaning methods may not have removed them. Hence, surface-adsorbed contaminants on nanomaterials may be off-competed and, replaced with biological, surface-active substances. This can produce reactions to the solubilized form of surface contaminant in the test organism. Alternatively, surface-contaminated nanomaterials may elicit substantially distinct biological responses *in vitro* and *in vivo* compared to purer or cleaner phases of the same materials. These distinctions must be carefully understood.

1.1.1.3. Detection of surface contamination. Nanoscale-specific surface analysis methods are still few in number, but surface contaminants may often be detected by one or more of many well-established surface analysis techniques including time-of-flight secondary ion mass spectrometry (ToF-SIMS), X-ray photoelectron spectroscopy (XPS) [44,45], as well as X-ray fluorescence (XRF) and related energy dispersive X-ray analysis (EDX), and surface-enhanced Raman spectroscopy (SERS)[46]. ToF-SIMS uses a beam of accelerated ions to sputter ionized atoms and molecules from the surface (<1 nm depth) of a material under ultrahigh vacuum (UHV) to produce a complex yet sensitive mass spectrum of the sample surface with a spatial resolution as fine as 40 nm [46]. XPS focuses a beam of X-rays on the sample under UHV resulting in the emission of core level

electrons whose photokinetic energy is measured. The energy of the surface-emitted electrons and relative proportions of various energized electrons yields surface chemical information concerning the origin of the electron's atomic environment and the relative proportions of those atoms in the top 9 nm of the surface, respectively. Spectral information includes atomic composition (of any elements save H and He), bonding, and oxidation state of the surface, with spatial lateral resolution as fine as 8 μm for some instruments [46]. In XRF, voltage-accelerated X-rays or gamma rays are focused into a sample where they generate secondary fluorescent X-ray photons characteristic of the atomic environment where they are produced, yielding absolute quantification of all elements (except H, He, and Li) present in the sample [47]. Energy-dispersive X-ray fluorescence scans only the top 5 μm of the sample, but provides the entire spectrum simultaneously, while wavelength-dispersive X-ray fluorescence scans up to 150 μm into the sample, providing the spectrum sequentially [47]. Though atomic absorption spectroscopy and some forms of mass spectroscopy generally have lower limits of detection, synchrotron radiation XRF is capable of elemental detection in the femtogram (10^{-15} g) range [48]. In SERS, intense (laser) light is focused upon the surface of which a small fraction loses or gains energy by inducing vibrations in the surface of the sample and then leaves the sample at a different frequency (indicative of the Raman spectral shift). This energy change reflects the chemical composition of the sample surface. When this technique is applied to a roughened metal surface, molecules on the surface enhance the Raman signal intensity more than 10^6 times leading to the distinction of 'surface enhancement' compared to traditional Raman spectroscopic methods [46].

1.1.2. Particle sizing and aggregation

By definition, nanomaterials possess at least one dimension below 100 nm. Because many unique properties of nanomaterials stem from their size, nanoparticle sizing is a critical aspect of pre-characterization. Additionally, because of intrinsic high dispersion and elevated surface energy, nanoparticle aggregation is thought to be common in complex experimental conditions such as biological media, although surprisingly few studies report much actual aggregation data. At the nanoscale, aggregation is extremely difficult to discern, especially in biological milieu (e.g., serum- containing 50–70 mg/ml of protein), but could exert a pronounced effect upon nano-specific material properties interacting with cells and tissues. Important properties affected by aggregation include colloidal stability and homogeneity, electronic and optical behavior, and cell or bacterial uptake/targeting properties, especially in the presence of proteins. Consequently, particle sizing and aggregation stability assays in various solution conditions relevant to biology are an important early-phase component of nanomaterial characterization. Commonly used methods of particle sizing currently include transmission electron microscopy (TEM), scanning electron microscopy (SEM), optical spectroscopy (UV–vis), dynamic light scattering (DLS), and fluorescence polarization. These methods are often not conclusive when applied to nanomaterials in complex systems and are therefore best utilized in pre-experimental characterization. Additionally, each method possesses its own inherent uncertainties, making corroboration of results with one or more additional methods the desirable means of sizing or aggregation determination.

1.1.2.1. Electron microscopies. TEM is a well-established technique for micro- and nano-imaging of material features: morphology, particle size distributions and aggregation. Therefore, many studies have relied upon TEM for particle shape, sizing and aggregation information [44,49–53]. Particle sizing by TEM is capable of yielding the most unequivocal sizing information available via direct electron imaging, but is generally used only for metallic samples (though the energy-filtering variation of the technique, EFTEM, may be used to image non-metallic materials [54,55]). Though TEM is a robust and widely accepted particle sizing technique, it requires ultrahigh vacuum (UHV) conditions and specialized equipment. Additionally, *ex situ* particle aggregation information observed by TEM is not necessarily representative of *in situ* aggregation states because sample preparation of a nanoparticle solution for TEM analysis most often requires careful sample dessication. During preparative sample drying, many aqueous preparations commonly produce artifacts, such as particle aggregation due to increasing ionic strength and surface tension influences. Hence, sample preparation of a nanoparticle solution for TEM analysis fails to adequately control surface tension effects of the evaporating liquid, confounding interpretation of the final particle states. Flash freezing and desiccation techniques require practice, but can eliminate some of these TEM preparation artifacts [56]. It is also quite tedious to get TEM replicates assessed for statistical significance. Therefore, TEM solution aggregation information should be corroborated by other methods (i.e., particle sizing and zeta-potential [57], spectrophotometry, and gel electrophoresis [58]). While aggregation information obtained from TEM images may be inconclusive, selected-area electron diffraction by TEM is a powerful tool to identify or confirm crystalline particulate chemistry [34] and to examine material crystal habit/aggregation [34,49,50,52] (e.g., nano-fullerene aggregate samples were distinguished from nano-fullerene crystalline samples in resin-fixed and freeze-dried cells examined by TEM micro-diffraction [59]).

SEM is a powerful surface imaging technique yielding surface features of materials in addition to material sizing and aggregation information [60,61]. Traditional SEM also requires UHV conditions and dried samples producing some experimental uncertainty on its ability to accurately represent actual *in situ* material characteristics. However, recently commercially available environmental SEM (ESEM) allows the sample to be scanned and imaged in hydrated conditions, while maintaining UHV conditions around the electron gun. Moreover, routine ESEM successfully images only the water surface and objects near the surface, but a modification (wet scanning transmission electron microscopy 'wet STEM') of standard ESEM protocols to utilize a Peltier element (for evaporation control) and the transmission mode of the instrument expands ESEM capabilities beyond the liquid surface to include the imaging of emulsions and particle suspensions [62,63].

1.1.2.2. Optical spectroscopy. Depending on metallic electronic and lattice structures, interband electron physics and excitation energies, certain metal nanoparticles and nanorods exhibit size-dependent absorption and scattering of light through excitation of the metal's plasmon band electrons by incident photons of the correct wavelength or through scattering of incident photons of the correct wavelength according to Mie theory [64,65]. Free electron physics is essential for plasmon excitation. Efficient electronic coupling of metal lattice energies and excitation interband energies are also required. These requirements are found in a few pure metals: Pb, In, Hg, Sn, Cd Ag, and Au are free electron metals that exhibit plasmon excitation bands. In most metals, the plasma frequency is in the ultraviolet, making them shiny (reflective) in the visible range. These are less interesting for nanoparticle applications for this reason. Some metals, such as copper and gold, have electronic interband transitions in the visible range, whereby specific light energies (colors) are absorbed, conveniently yielding their distinct color of interest. Other metals and metal oxides exhibit plasmons in non-visible optical energy regions, making plasmon excitation and detection of the plasmon extinction or band shifts challenging. Metal oxide formation and intrinsic surface metal lattice mis-match with excitation energies frequently distort energetic interband coupling and free electron physics, diminishing plasmon coupling effects for most metals, except those essentially oxide-free (i.e., more noble-like). Changes in surface plasmon band extinction occur in the metal by adsorbate binding, altering surface interband electronic states as manifested in altered refractive index. Surface oxide and thick adsorbed surface-stabilizing adlayers (e.g.,

organic films/coatings) can mask other adsorbate electronic influences with the metal. Surface plasmon resonance (SPR) optical effects are dependent upon shape, diameter, surface adsorbates, and distance between plasmonic particles [66]. Consequently, gold/silver nanoparticles – currently most commonly studied – are routinely sized by measuring the extinction wavelength(s) of incident light [67,68] Platinum, palladium, copper and other metals also possess plasmonic optical properties if protected from substantial contaminating oxides (i.e., copper nanoparticles within silica nanoshells) [69]. Importantly, plasmon peak absorbance progressively decreases in intensity and red shifts to higher optical wavelengths as the average particle diameter increases [69]. This yields a characteristic plasmonic optical peak absorbance for each size of metal nanoparticle defining its size [66]. Similarly, adsorption of ligands (e.g., contaminants, stabilizing layers, proteins, and DNA) onto the nanoparticle (also quantum dot) surface will also red-shift the extinction wavelength from that of the clean material by a few nanometers [58,70]. Additionally, inter-particle distances smaller than average particle diameter will result in a shift in sample absorbance [66]. Significantly, this may be used as an online indicator of particle aggregation. For instance, a gold colloidal solution color shift from red to blue indicates particle aggregation [71]. However, in biological milieu, where non-specific adsorption induces particle aggregation, effects of particle surface adsorption and resulting aggregation are difficult to distinguish.

1.1.2.3. Dynamic Light Scattering. Dynamic Light Scattering (DLS) has been widely applied for direct determinations of particle sizing in solution [57,72]. DLS of nanoparticles of similar dimensions to soluble proteins in protein milieu, or dilute serum is very complicated: few controls or calibrations are ever reported. ASTM Grade I (e.g., ultrapure) water systems use 200 nm filters to remove particulates. This means that this research-grade purified water contains endogenous populations of particles below 200 nm that confound DLS sizing of introduced nanoparticles. For example, the Millipore Simplicity® Ultrapure Water System has a final filter of 50 nm, leaving smaller particles in the water [73]. DLS is theoretically better applied in micro-scale size regimes in which particles scatter much more light than in nano-size regimes [74]. Consequently, DLS data are easily skewed by the presence of small amounts of contaminants.

Additionally, nanoparticle solutions are notoriously sensitive to changes in salt, protein, or surfactant concentration. Colloid stability decreases with increasing salt concentration as Debye length-dependent electrostatic particle–particle repulsions decrease below the order of attractive van der Waals interactions [75]. Also, charge-stabilized or charged ligand-stabilized particles will aggregate rapidly in the presence of an oppositely charged protein (such as the aggregation of lysine-capped gold nanoparticles by human serum albumin (HSA) [76]. Conversely, addition of non-polar adsorbates (polymer, surfactant, and peptide) will increase colloid stability through steric stabilization, but also change sizing and modeling fits [75]. DLS yields particle hydrodynamic size in solution, allowing measurements of particles bearing adsorbed coronas of molecules: particles adsorbed with proteins are especially relevant in this respect because of their size and abundance in physiological systems. One DLS study asserts the capability of DLS to differentiate between end-adsorbed, (111) face, and shaft-adsorbed, (110) face, bovine serum albumin (BSA) on gold nanorods [77]. However, such nano-sizing analyses by DLS require a high degree of skill to perform, careful instrument calibration, positive and negative controls, attention to reagent purities and some knowledge of optical data modeling algorithms to predict a sizing outcome consistent with many assumptions about the optical scattering physics in the solution. Many particle sizing studies, spanning metals, metal oxides and polymers, treat the technique blindly as an automated method with default scattering models and curve fitting assumptions that are neither described, justified nor validated for various sample types. In fact, the result of the above DLS study of albumin-adsorption has been contrasted by the results of a spectroscopy-based study which found no appreciable length change for gold nanorods (of similar size to those in Ref. [77]) following exposure to human serum albumin [67].

Loose adsorbates and unwanted solutes in nanoparticle systems are typically removed by dialysis [67] or centrifugation [78]. Loose particle aggregates are often broken up by bath sonication of the nanoparticle solution [44,72,78]. However, care is warranted when employing conventional sonication treatments (bath and probe) since they are difficult to standardize (density, dose, power, and local heating) [79] and sometimes have unwanted side effects, such as the addition of metal particles typically shed from the probe tip during sonication treatment, and oxidation of surface-active, stabilizing alkylthiol coatings on nanoparticle surfaces [80]. Given the foregoing, DLS sizing data, when uncontrolled and uncorroborated by other sizing techniques, are generally viewed with some skepticism since the method has great potential for skewed interpretation or ambiguity because of its dependence on user experience and model assumptions. Therefore, DLS studies of nanoparticles should be carefully designed, including sample calibration with sizing standards under conditions relevant to the experiment, and subsequent, thorough descriptions of the data analyses employed. Recently released standards now exist to aid researchers both experienced and novice to the area of particle sizing by light scattering. These aids include the ASTM Standard Guide for Measurement of Particle Size Distribution of Nanomaterials in Suspension by Photon Correlation Spectroscopy (ASTM E2490–08) and NIST gold nanoparticle standard materials (NIST RM8011, NIST RM8012 and NIST RM8013). However, complicating biological milieu (ionic strength, surfactants, and proteins) should compel researchers to seek confirmation of results using other sizing methods.

1.1.2.4. Fluorescence polarization. Currently, time-resolved fluorescence polarization anisotropy (TRFPA) is used in nanosystems for the purpose of sizing. Observed fluorescence polarization decay time is correlated to fluor or particle size (hydrodynamic radius [81]) according to the Stokes–Einstein–Debye rotational equation for particle motion. Using this method, 1–10 nm particles may be sized with 0.1 nm resolution [81]. TRFPA utilizes sub-nanosecond-resolution laser pulses and detectors to excite fluors in assay milieu, often high-throughput screening multi-well plates; these fluors could be nanoparticles. Optical excitation induces fluorescence that can be distinguished in free-floating versus receptor- or surface-bound states by emission anisotropy. Monitoring the decay of the fluorescence polarization provides information that distinguishes particle or fluor binding (i.e., to receptors, membranes, proteins) from assay components. While TRFPA is a widely used technique in drug discovery assays to monitor "hits" by drug-target binding signals, [82]. It has not yet found wide application in analogous particle or nanomaterial characterization assays. Prospectively, this technique may yet be analogously adapted to relate fluorescence anisotropy of labeled nanoparticles to nanoparticle–cell receptor interactions and elucidate pathways of toxicity through correlation with toxicity endpoints.

1.1.2.5. Other techniques. Several other techniques have been applied to nanomaterials sizing with less frequency. These include:

- large angle X-ray diffraction (XRD) used to differentiate between crystalline and amorphous samples [72];
- multi-angle laser light scattering (MALLS) is used in combination with UV–vis spectroscopy in field flow fractionation (FFF) for particle sizing and colloidal separation [83];
- small angle X-ray scattering (SAXS) and small angle neutron scattering (SANS) both of which are used to analyze both particle core and shell sizing as well as particle shape, to a spatial resolution of about 10 nm [84];

- inductively coupled plasma-mass spectroscopy (ICP-MS) used to measure trace metal impurities [72]; and
- inductively coupled plasma-atomic emission spectroscopy (ICP-AES) used to measure the concentration of gold (atoms) in cell suspensions (but notably neither size nor shape) [58].

2. *In vitro* biological testing: cell types, selection, and use

All nanomaterials exposed to *in vivo* conditions immediately and continuously encounter a broad array of biological and physiological species, including thousands of surface-active molecules, many different cell types in different tissue environments, and reactive pathological or inflammatory conditions. The interaction, influence, and possible toxicity of nanomaterials with proteins and cells are an essential focus in assessing and understanding nanomaterial compatibility versus toxicity. Cell-nanomaterial reactions of interest include cellular uptake and processing of nanomaterials in various routes, effects on cell signaling, membrane perturbations, influence on the cellular electron transfer cascades, production of cytokines, chemokines and reactive oxygen species (ROS), transcytosis and intercellular transport, gene regulation, overt toxic reactivity, no observable toxicity, and cell necrosis or apoptosis. Most often, *in vitro* culture of cell lines (commercial, typically genetically altered) or primary cells (tissue-harvested) on plastic plates, either with or without serum, with bolus dosing of nanomaterials and subsequent cell reactivity profiling is the common assessment method [85]. Wide varieties of *in vitro* assays with cells should consistently reflect the variety of possible physiologic responses to nanoparticles *in vivo* and all possible cell processing routes and natural reactions.

Typically, several major cell types are used *in vitro* for testing including phagocytic, neural, hepatic, epithelial, endothelial, and red blood cells and various cancer cell lines. In each case, the specific cell line selected for *in vitro* assay is intended to model a response or phenomenon likely observed or sensitized by particles *in vivo*. However, there are thousands of transformed cell lines to choose from, each with its own inherent shortcomings, many deposited within commercial registries (i.e., American Tissue Type Culture Collection, ATCC) each day. In all such assays, determining meaningful endpoints that reflect physiological stress, toxicity, or therapy or some other phenomenon detectable *in vivo* remains a challenge – this is a common issue involving the consistent disconnect between *in vitro* and *in vivo* results and lack of cell assay predictability of biocompatibility with biomaterials. Cell monocultures as measured by *in vitro* assays rarely react in such isolated pathways in native tissues; tissues comprise multiple, dynamically communicative cell types that produce non-linear and correlated responses to toxins and foreign materials. These effects are not often recapitulated *in vitro* in adherent cell monocultures in dilute serum media on plastic plates. A second major concern is the mounting evidence that secondary cell lines supplied by commercial vendors are either contaminated or no longer consistently or reliably represent the cell phenotype claimed. As few investigators actually validate the phenotype before assay use or against primary cell types, secondary cell lines represent an increasingly confounding, unvalidated source of information claimed to represent *in vivo* cell responses [86]. Lastly, even related cell lines can produce different results. One cell study of carbon nanotubes screened three human lung cancer cell lines, H596, H446, and Calu-1, for their response to MWCNTs, and selected H596 as the model for further study because its viability was the most sensitive to MWNT exposure and yielded the most repeatable results from the three cell lines as evaluated by the MTT viability assay [60]. Thus, specific cell lines within a given series of commonly derived cell line phenotypes may respond to a given stimulus in disparate ways and with varying intensity, making cell line selection an important aspect of experimental design. Thus, while cell lines can contribute important insights into select scientific aspects of cell-materials interactions, without consistent phenotyping and validation in culture as justification for their use, *in vitro* results may be increasingly confusing until quality control standards for cell behavior and biological relevance are implemented, compared and enforced.

There are numerous inconsistencies in secondary cell line use that are frequently ignored. Increasingly, primary cell culture use is urged, but primary phagocyte, tissue-specific and tumor cell cultures also have challenges. Isolation of the cell or progenitor of interest often requires differentiation via specialized media and inducers/growth factors [87]. Such differentiation requires cell phenotyping, making the entire isolation process expensive and tedious. Retention of cell phenotype and its accurate validation during experiments is equally onerous. Primary cultures also require much higher seeding densities *in vitro* and usually need attachment to a surface for efficient proliferation while many transformed cell lines may proliferate in suspension or without special attention to growth conditions. Immortalized cell lines often exhibit more rapid division and phagocytosis rates and capacities than their *in vivo* counterparts and sometimes a lack of reproducibility arising from passaging or sourcing. By contrast, primary cells obtained from tumor biopsy may provide a closer representation of the *in vivo* tumor cell type. However, 2-D monocultures are generally not representative of the *in vivo* case because the culture lacks the spatial interactions and phenotypic/cell-type cross-talk of the actual tumor. Therefore, co-culture and 3-D cultures are increasingly encouraged to more-closely model the complexities inherent in tumor physiology [85,88,89]. Additionally, cells normally refractory to high particle uptake in culture (i.e., primary cells of many types) might, if rapidly dividing, present internalized particles by non-specific capture during cell division. This is rarely controlled by the use of staged or non-dividing cultures with rapidly dividing cells since many assays provide better signal during proliferative phases. Additionally, primary cell culture often requires both animal resources, maintenance fees, and post-harvest animal sacrifice, raising costs, ethical controversies and significant paperwork for the investigator (ex., IACUC and IRB applications) [87]. Nevertheless, potentially misleading and costly outcomes for many poorly planned or unjustified cell culture studies should mandate careful scrutiny of secondary vs. primary cell culture designs. Clearly, all studies should be justified and validated based on careful cell phenotype selection and maintenance, and the intended outcomes for their use for nanomaterial testing. Too often, all of these components are missing from the reported experimental designs, producing serious questions about the significance of the work.

In summary, cell line-based screening for "biocompatibility", transport and processing pathways, toxicology, drug delivery, or imaging is commonly employed currently. To be useful, the major challenge remains to connect these cultured cell responses with nanomaterials *in vitro* under controlled conditions to predictions about their behaviors in more complex, relevant environmental and organismal systems. A rigorous rationale for selecting and using certain cell lines, validations of their phenotypes under specific culture conditions with further validation of *in vitro* results to *in vivo* correlations is very important.

2.1. Phagocytes

Because nanomaterial toxicity is often associated with materials uptake by cells, (see Section 3.3.2) and many early uptake responses to foreign materials introduced by multiple different exposure routes involve sentinel leukocytes and immune modulatory cells (e.g., neutrophils, macrophages, and dendritic cells), phagocytic cells (e.g., monocyte and macrophage phenotypes) have been used as experimental models for their ability to actively uptake foreign particles and respond with cytokine signaling cascades or production of ROS. Multiple cytokines are readily assayed from cell culture using commercial kits (e.g., ELISA arrays) at both message and protein

levels, and some cytokines (e.g., IL-6, TNF-alpha, and IFN-gamma) are clearly associated with cell-based *in vivo* inflammatory reactions. Characteristic ROS production upon insult by foreign materials [57,90–93] produces short-lived highly chemically reactive oxygen/nitrogen radicals of several types, often damaging the surrounding tissue [90,92,94]. While direct *in situ* ROS assay is possible, but difficult, many experimental cell models are selected on the basis of observing secondary effects of nanomaterial-cell exposure mediated by ROS injury. ROS production has also been implicated in quantum dot (QD) cytotoxicity through lipid peroxidation and resultant apoptosis through Fas receptor up-regulation [95].

Primary phagocytic cells of interest have included peripheral blood monocytes, peritoneal and lung macrophages, and bone-marrow transformed monocytes. Immortalized secondary cells representing this phenotype include RAW264.7, J774.1, IC-21, THP-1, Jurkat, Mono Mac-6, and NR8383. Table 1 shows selected examples of these types of cell uptake assays. This table surveys different particles ingested by different cells in various cultures, indicating the many chemistries and cell types that participate in particle uptake. What this table (and many of the articles referenced) cannot provide are specific mechanisms of cell uptake that might differentiate cell–particle reactivities. Unfortunately, many phagocytic cell lines are simply chosen for convenience in culture experimentation, including putative phenotype, rapid, reliable proliferation in culture, attachment dependence, and commercial availability. Additionally, increasing skepticism and criticism are cast upon the ability of immortalized secondary commercial cell lines to accurately represent their primary counterparts, or anything else *in vivo* [20,96-98]. In primary phagocytes, cell differentiation state (i.e., to terminally differentiated macrophages) significantly alters phagocytic and proliferative tendencies. The validity of macrophage differentiation and attachment dependence in culture and accuracy of cytokine profiles produced compared to *in vivo* responses remains largely unproven. Immortalized cell lines, particularly RAW cells, have at times shown a lack of repeatability stemming from simple differences in cell passage number or cell sourcing/lineage [99]. Or, as in the case of immortalized hepatic carcinoma cell lines, oncogenic cells divide more rapidly and, consequently, possess altered phagocytic behavior from their healthy counterparts [98].

Cell-based assays of nanomaterials often attempt to place the relevant particle chemistry with the cell phenotype implicated in its processing, both in a culture context. For example, pulmonary exposure to nanomaterials (e.g., by normal inhalation, passive environmental exposure, and/or deliberate use of inhaled nanomedicines) is often modeled *in vitro* by use of either immortalized secondary cell lines putatively representing a phagocyte phenotype (e.g., THP-1, RAW, J7, Mono mac 6 cells or IC-21 lines) [100–103] or primary cultures of alveolar macrophages that reside at high densities deep in the lung in the alveolar bed and scavenge inhaled foreign materials [89,104–107]. Moreover, alveolar macrophages are considered to play a key role in particle-mediated inflammation and lung disease [108]. These cells actively phagocytose in culture and are known to produce cytokines in response to materials uptake.

In terms of ROS-induced cell toxicity, Long et al. used BV2 cells (immortalized mouse microglia) to model the characteristic ROS-burst from particle insult to these macrophage-like cells in the context of the brain. As a model for brain injury occasioned by such exposure, they co-cultured these microglial cells with N27 cells (rat dopaminergic neurons) to represent brain neuronal cells most susceptible to DNA, protein, or lipid damage by ROS insult from glial cell ROS production [57]. Similarly, particle overload in the lung has been implicated in ROS production. In culture, human blood-derived monocytes release ROS, consistent with *in vivo* monocyte infiltration and subsequent inflammation in the lung as a result of particle overloading [90,104]. Furthermore, *in vitro* culture of alveolar macrophages with oil fly ash (OFA), TiO_2, and SiO_2 shows strong induction of ROS production along with high cytotoxicity, suggesting a direct correlation between ROS production and cytotoxicity [107]. Particle-mediated ROS release by polymorphonuclear leukocytes (PMNs) in culture has also been related to the content of Si, Fe, Mn, Ti, and Co as particle-associated, insoluble species introduced to cell culture [90]. Additionally, peritoneal macrophages, collected by murine abdominal lavage and used as an *in vitro* model of phagocytosis, are shown to be highly sensitive to particle coating chemistries [109,110]. *In vitro* particle uptake of polystyrene particles coated with poloxamer (surface-active FDA-approved triblock copolymer used in drug formulations) has been correlated to *in vivo* particle uptake data [109]. Hence, not only nanoparticle 'bulk' chemistry, but nanophase surface chemistry, possibly surface contamination alone, can influence phagocytosis in culture. Much work remains to fully elucidate the inter-relationships between particle exposure, particle uptake, ROS production and toxicity of cells, both those directly involved with particle uptake and those secondarily affected.

2.2. Hepatic and other hematologic cells

Nanomaterials introduced into the blood stream (e.g., via systemic injection, oral absorption, or inhalation) would immediately encounter high concentrations of platelets and red blood cells and would also have frequent contact with the blood-filtering cells of the liver and the mononuclear phagocytic system (i.e., reticuloendothelial system), including Kupffer cells and other phagocytes. *In vitro* model studies of these systems consider several cell types and phagocytes have been described in the preceding section. For circulating particles, the liver consistently plays a prominent role in normal host particle clearance, performed by liver-resident Kupffer cells and not hepatocytes [111]. Cell lines selected as models of liver toxicity include Hep2G [112], and BRL3A, an immortalized rat liver cell line chosen simply for its convenience in modeling liver cell toxicity [113]. Therefore, common cell toxicity endpoints – cellular morphology, mitochondrial function (MTT assay), membrane leakage of lactate dehydrogenase (LDH assay), reduced glutathione (GSH) levels, ROS production, and mitochondrial membrane potential (MMP) are assayed. However, in addition to showing exaggerated phagocytic behavior (as previously discussed), immortalized liver cell lines also exhibit altered ethanol toxicity and transferrin uptake (iron trafficking) behavior from normal hepatocytes [98]. This suggests phenotypic changes in these secondary transformed cell lines that might not reflect accuracy to certain traits found *in vivo*.

Other relevant cell types include endothelial cells (BAECs and HUVECs) and red blood cells (erythrocytes), platelets, and leukocytes in cultures. Platelets are not true blood cells but membrane-bound hematopoietically derived cell fragments without nuclei sourced from marrow megakaryocytes. Platelets contain over a dozen potent chemicals in granules that are excreted in response to platelet activating agents, facilitating blood coagulation. At $1–4 \times 10^9$ platelets per liter of blood, and a thousand-fold higher occurrence for red blood cells, these blood elements comprise nearly 50% of the packed cell volume and represent major interactive components with nanoparticles in blood, affecting transport, metabolism, and tissue processing. However, these anuclear elements are not typical cells, exhibiting limited metabolism and inability to culture. Primary blood harvests must be treated differently than other cell culture studies: generally only short-term particle incubation studies are possible. Importantly, calcium ion removal (EDTA addition) typically used to prevent blood coagulation in such blood collections are known to chelate other heavy metals (i.e., those introduced from nanoparticle preparations), and prevent platelet degranulation reactions important in these assays.

In terms of particle studies, red blood cells have been contrasted to a phagocytic cell line in order to model non-phagocytotic transmembrane particle movement [55,114]. Several studies determined that polystyrene particles (200 nm, 78 nm), gold nanoparticles (25 nm),

Table 1
Select cell-based *in vitro* assays to study particle internalization in cultures.

Cell line/name	Particle	Functionalization	Other details	Reference
Human umbilical vein endothelial cells	$C_{60}(OH)_{24}$ hydroxyl fullerenes		$d = 7.1 \pm 2.4$ nm	Yamawaki and Iwai [179]
Human dermal fibroblasts HDF; human liver carcinoma HepG2; neuronal human astroctytes, NHA	C_{60}	COOH, OH, Na^+	$d = 100$ nm	Sayes et al. [180]
Rat alveolar macrophage cell line NR8383; human alveolar epithelial cell line A549	SWNT (single-walled carbon nanotubes); CB14; crystalline quartz particles (DQ12)		SWNT: $d = 1$–2 nm, $l =$ up to 100 μm; CB14: size = 14 nm; DQ12: size<5 μm;	Pulskamp et al. [181]
Human 3T6; murine 3T3	SWNT (coated with FITC(fluorescein isothiocyanate))		$d = 1$ nm, $l = 300$–1000 nm	Pantarotto et al. [182]
Human lung-tumor cell lines, H596, H446, and Calu-1	MWNT; CNF; CB	MWNT: CdO, COOH, OH CNF: CdO, COOH, OH	MWNT: $d = 20$ nm, AR = 80–90; CNF: $d = 150$ nm, AR = 30–40; CB: $d =$ submicrometer, AR = 1;	Magrez et al. [60]
T lymphocytes; Jurkat T leukemia cells	MWNT; CB	MWNT: COOH, OH	MWNT: $d = 20$–40 nm, $l = 1$–5 μm	Bottini et al. [183]
RAW264.7 macrophage cells	Gold nanoparticles Au(0)	Lys, Poly-L-Lysine, FITC	$d = 3$–8 nm	Shukla et al. [184]
Vero cells	Au_3Cu_1 (gold nanoshell)	polyelectrolytes polyethylenimine (PEI), poly(acrylic acid) (PAA),	$d = 48.9 \pm 19.1$ nm, shell thickness = 5.8 ± 1.8 nm	Su et al. [185]
Hela cells	Gold nanorods	phosphatidylcholine [PC]	$w = 11 \pm 1$ nm, $l = 65 \pm 5$ nm, AR = 5.9	Takahashi et al. [186]
Rat pheochromocytoma cell line PC12M	Magnetic nanoparticles (MNPs) Fe_2O_3	DMSA	$d = 5$–12 nm	Pisanic et al. [187]
Human monocyte-macrophages (HMMs)	Fe_3O_4	Dextran	$d = 30$ nm	Muller et al. [188]
Human breast cancer cells (SK-BR-3); human dermal fibroblast cells	Fe_3O_4	PMAO-PEG	$d = 9.6$ nm	Yu et al. [189]
Primary human epidermal keratinocytes (HEKs)	QD 565; QD 655	PEG, PEG-amine, polyacrylic acid	565: $d = 4.6$ nm 655: $w = 6$ nm, $h = 12$ nm	Ryman-Rasmussen et al. [190]
Human lymphoblastoid WTK-1	CdSe QD	MUA (COOH), cysteamine (NH_2), thioglycerol (OH)	$D = 9$–48 nm	Hoshino et al. [127]
Human dermal fibroblasts and human lung epithelial cells	TiO_2 (anatase and rutile)		$d = 3$–10 nm	Sayes et al. [191]
Mouse J6456 lymphoma cells (J6456-FR), human head and neck KB cancer cells (KB-FR)	Lipodot (CdSe QD + lipid coat)	QD: 1,2 dipalmitoyl-sn-glycero-3 phosphocholine, mPEG-DSPE	QD: 2.6, 2.9 nm lipodot: 100 nm	Schroeder et al. [192]
HepG2 cell	Micellar-like core shell nanoparticles (2 types used)	Type 1: MePEG–PCL Type 2: PCL–PEG–PCL	10 to 200 nm	Hu et al. [193]
Macrophages and foam cells	dexamethasone-liposomes (in 3 sizes)		518.7 ± 49.5 nm (L500) 202.2 ± 23.1 nm (L200) 68.6 ± 6.5 nm (L70)	Chono and Morimoto [194]
Human lung fibroblasts (ATCC, MRC-9)	CeO_2 Cerium Oxide Nanoparticles		$d = 25$–50 (diffusion) up to 250–500 (sedimentation) nm	Limbach et al. [195]
Dendritic cells (DC)	Fluoresbrite™ carboxylated yellow-green microspheres; yellow-green fluorescent (505/515) carboxylate-modified FluoSpheres	FITC, (TT, PS, PA, PLL, WGA for 0.1 – 1 μm only)	Fluorebrite: 0.1, 0.5, 1.0 and 4.5 μm Fluospheres: 0.04, 10 and 15 μm	Foged et al. [196]
Hamster kidney cell line (BHK-21)	25-kDa polyethylenimine (bPEI); beta-cyclodextrin-containing polymer (βCDP)	PEG (adamantane-PEG_{5000} conjugate)	100 nm	Mishra et al. [197]
Langerhans cells (LC), DC	Human papillomavirus-like particles (HPV 6bL1 VLP)	Carboxifluorescein Diacetate (CFDA) (label)		Yan et al. [198]
Caco-2; MTX-E12 (mucus)	Polystyrene NP, chitosan NP and PLA–PEG NP; Chitosan NP	PLA–PEG and Chitosan, labeled with FITC–BSA	PS: 213 ± 8 nm Chitosan: 290 ± 7 nm PLA–PEG: 196 ± 20 nm	Behrens et al. [199]
Human alveolar epithelial cell line A549; human monocytic leukemia cell line THP-1; human monocytic leukemia cell line Mono Mac 6	Hematite ((–Fe2O3); silicasol particles (SiO2, amorphous silica) DQ-12 (reference)		Hematite: 50 ± 90 nm (mean 70 nm) silicasol S100: 80 ± 110 nm (mean 100 nm) silicasol S60: (mean 60 nm) DQ12:<5 μm	Wottrich et al. [103]
Tissues from liver, spleen, kidney, heart, lung, brain	Iron oxide MNP	Oleic acid (OA) and Pluronic	Core $d = 11 \pm 2$ nm	Jain et al. [200]
3T3 fibroblast cells	Silver nanoparticle	Phosphorylcholine (PC), phosphorylethanolamine (PE)	$D = 3.8$ nm	Chung et al. [201]
Endothelial and Kupffer cells	Liposome particle (PC, Chol, PS)		200 ± 38 nm	Rothkopf et al. [202]
Kupffer cells	PS microspheres; polystyrene–polyethylene oxide (PS-PEO) copolymer microspheres		PS: 1 μm PS-PEO: 1 μm	Harper et al. [203]
Mouse Peritoneal Macrophages (lavage)	Polystyrene nanospheres and microspheres	Poloxamer 338 and 188, Egg Lecithin, Secretory immunoglobulin A, and ^{131}I (label)	$d = 60$ nm and 5.25 μm; 160 nm (uncoated only)	Illum et al. [109]
Mouse Peritoneal Macrophages (lavage)	Fluorescent polystyrene microspheres	Various surfactants and protein isothiocyanate fluorescein (label)	$d = 0.995$ μm	Privitera et al. [110]
Rat glioma cell lines: 9L gliosarcoma (GS-9 L); RG-2; F-98; Caco-2 (control)	Doxorubicin-loaded nanoparticles (Dox-PBCA-NP); Empty NP (PBCA NP)	Poloxamine 908, polysorbate 80, poloxamer 188	Dox-PBCA-NP: 270 ± 20 nm PBCA NP: 250 ± 30 nm	De Juan et al. [204]
MG63 osteoblast-like cells; Primary human osteoblast-like cells	UHMWPE; commercially pure titanium (cpTi); Ti–6Al–4 V (Ti–A); cobalt–chrome (CoCr)		UHMWPE: $d = 1.0 \pm 0.96$ μm; cpTi: $d = 0.84 \pm 0.12$ μm; Ti–A: $d = 1.35 \pm 0.09$ μm; CoCr: $d = 1.21 \pm 0.16$ μm	Lohmann et al. [205]

and TiO_2 nanoparticle aggregates (<200 nm) were all able to enter red blood cells, independent of surface charge, but particles or particle aggregates larger than 200 nm were found adhered to the cell outer membranes and not inside the cells [114]. Untreated red blood cells and porcine lung macrophages treated with cytochalasin D (to block particle phagocytosis) both showed uptake of TiO_2 ultrafine (22 nm agglomerates of 4 nm particles) and 0.2-micron particles, but not of 1-micron particles. Because untreated macrophages did uptake 1-micron particles, active metabolic particle uptake processes were concluded to be size-dependent [55]. Red blood cells can uptake nanoparticles passively.

Platelet models of blood-related particle toxicity generally use such primary assay endpoints as platelet activation (degranulation) and aggregation. Several forms of nanomaterials were assayed in one relevant study; with the exception of carbon fullerenes, all nanomaterials produced platelet activation, including mixed carbon nanoparticles (amorphous carbon, 7% C_{60}), multi-wall nanotubes, single-wall nanotubes, and standard urban particulate matter. Moreover, introduction of these nanomaterials into a rat thrombosis model accelerated thrombosis, showing an *in vivo* correlation for the platelet model of nanoparticle toxicity [115].

2.3. Epithelial/endothelial cells

While phenotypically distinct, the epithelium and endothelium both share common cell-derived physiological barrier properties to the transport of foreign materials into the body, whether through the skin, mucosa, digestive tract or (for injectables) through the walls of the vasculature. This constitutes a very large cell surface area (i.e., intestines $\approx 200\ m^2$; lung epithelium $\approx 100–140\ m^2$) [116] exposed to nanoparticles in both environmental and therapeutic exposure. Consequently, epithelial cells employed for *in vitro* experiments are selected for their similarity to an *in vivo* epithelial phenotype including presence of mucin cell membrane coatings, microvilli, desmosomes, and lamellar bodies [61]. Cell models must distinguish between dermal, oral-gastric, colonic, pulmonary, nasal, kidney and vaginal epithelial characteristics depending upon the analogy sought through *in vitro* experiment and the desired outputs. Often cell lines selected as models of epithelial toxicity are precancerous type II pneumocytic cells [11,35] since a major result of their chronic inflammation is abnormal growth. Other common transformed epithelial lines include MDCK (kidney), HT-1080, HT29-18-C1 (colonic), and HeLa (cervical) [58]. Moreover, the paucity of culture procedures for some primary cell lines necessitates use of cancer-based transformed cell lines for cell-based assays, though some of these cancer cell lines do not contain the mutated genes common to cancers of analogous tissue. For example, RKO-transformed colon cells do not possess the mutations common to colon cancer and therefore do not reflect an *in vivo* phenotype [85].

Gastric, nasal, oral and urinary tract epithelium are all characterized *in vivo* by viscous mucin production and tissue coatings that slough and regenerate frequently, affecting particle bioadhesion, capture, uptake [117], and aggregation. Mucin thickness is thinner for nasal than for oral or intestinal epithelium, but such details are frequently ignored by cell culture studies most often using non-mucinylated epithelial cell lines, such as Caco-2, an immortalized non-mucinylated enterocytic colonic cell line used for electrophysiology and cell transport studies. Commercial Caco-2 lines can also be contaminated as supplied [86]. Hence, for most intestinal particle uptake studies, Caco-2 cells do not exhibit an appropriate phenotype, but are used regardless because of their intrinsic capacity to form tight junctions and confluent, sealed cell monolayers in culture. Alternatively, Goblet cell-like MTX-E12 cells are a mucus-secreting cell line that offers a model for mucus interactions in studies of intestinal uptake.

Mucin makes a difference to cell-particle processing. For example, direct comparison of Caco-2 cultures to MTX-E12 cultures with 200 nm polystyrene nanoparticles showed a strong particle hydrophobicity-dependent decrease in particle-cell association (consistent with *in vivo* rat studies that showed decreased polystyrene nanoparticle uptake with increasing hydrophobicity of particle surface coating); this difference effectively disappeared with the pre-treatment removal of the mucus layer from the MTX-E12 cultures. Nevertheless, most of the MTX-E12-associated particles were found to be trapped within the mucus layer that had re-formed during culture with particles. Moreover, 200–300 nm chitosan nanoparticles were found to reach a steady-state association value with MTX-E12 cells in half the time required for Caco-2 cells, due to the strong, electrostatic, chitosan–mucus interactions. Conversely, hydrophilic, 200–300 nm PLA–PEG nanoparticles showed minimal cell association for both cell types [118]. Therefore, especially in the case of hydrophobic and/or positively charged particles, mucinylated gastric epithelial cells are recommended for *in vitro* particle testing, given the high degree of uptake and aggregation state dependence for nanoparticle systems. Studies should therefore focus on ascertaining relevant characteristics of the epithelium *in vivo* relevant to the study design, and produce *in vitro* conditions to recapitulate these traits *in vitro* as accurately as possible. Cell selection and contextual justification is critical to these determinations.

Endothelial cells tightly line the various vascular conduits within the body and represent the barrier to transport of particles and other species from the blood to surrounding tissues including the blood-brain barrier which severely restricts access of foreign materials and substances to the brain [119]. Due to the varied nature of the circulatory system, endothelial cells vary widely in character from the aortic lining to the blood-brain barrier to the capillary beds of the lung [120]. Therefore, a wide variety of endothelial cells are applied to *in vitro* tests, but relatively few of these have been tested against nanoparticles. Secondary transformed endothelially derived cell lines include COS-7 (kidney) and MS-1 (pancreas). Human aortic endothelial cells (HAECs), human umbilical vascular endothelial cells (HUVECs) and human microvascular endothelial cells – all commercialized primary cell isolates – have been used as models of endothelial inflammatory response and resultant arthroscleroses inducible by circulating metal oxide particles.

Specifically in this context, alumina nanoparticles were claimed to be toxic to HUVEC cells [121], FeO_3 nanoparticles showed no toxicity to HEACs and induced no significant inflammation at even the highest levels tested while Y_2O_3 and ZnO both induced significant inflammation at the highest doses tested. Only ZnO caused any appreciable cell death, 20% and 50% cell mortality [122]. Moreover, HUVECs and porcine endothelial cells showed dose-dependent up-regulation of the inflammatory adhesion proteins, ELAM-1, ILAM-1, and VCAM-1, in response to alumina nanoparticle administration at surface area-specific doses, with increasing adhesion of activated monocytes [121]. This points to the potential of metal oxide nanoparticles to initiate/exacerbate inflammatory artherosclerotic processes in the absence of cell mortality. PLA–PGA particles also demonstrated adherence to cytokine-inflamed HUVEC as a model for inflamed endothelium *in*

Notes to Table1:
Abbreviations: AR = aspect ratio, BSA= bovine serum albumin, C+ = positive control, C− = negative control, CB = carbon black, Chol = Cholesterol, CNF = carbon nanofibers, DMSA = Dimercaptosuccinic acid, mPEG-DSPE = methoxy–polyethylene–glycol–distearoyl–phosphatidyl–ethanolamine, MePEG–PCL= di-block copolymer of methoxy poly (ethylene glycol)–polycaprolactone, MUA= 11-mercaptoundecanoic acid, PA= poly-D-L-alanine, PBCA= polybutylcyanoacrylate, PCL–PEG–PCL= polycaprolactone–poly(ethylene glycol)–polycaprolactone, PEG = poly(ethylene glycol), PLA= poly(lactic acid), PLL= poly-L-lysine, PMAO = poly(maleic anhydride-alt-1-octadecene) PS= protamine sulphate, QD = quantum dot, TT= tetanus toxoid, WGA= lectin wheat germ agglutinin.

vivo consistent with adhesive similarities between PLA–PGA particles and leukocytes (which also adhere to inflamed endothelium) [123].

By contrast, human aortic smooth muscle cells were used to assay uptake of poly (D,L-lactide-coglycolide) (PLGA) polymeric nanoparticles. Particle internalization decreased with increasing concentrations of polymer-associated polyvinyl alcohol (PVA), residual from the NP synthesis [124]. ECV304 endothelial cells (considered relevant for parenteral administration) and 3T3 fibroblasts were transfected with DNA plasmid complexes with both low- and high-molecular weight polyethylenimine (pGL3/LMW-PEI and pGL3/HMW-PEI), respectively, and tested for cytotoxicity with unconjugated HMW-PEI and LMW-PEI. HMW-PEI coated the outer membrane of the cell, inducing necrosis, while LMW-PEI did not adhere to the cell surface. Instead, small LMW-PEI aggregates were found inside ECV304 cells by TEM [125].

2.4. Tumor cell models

Aside from common precancerous cells, numerous oncogene-transformed cancerous cell lines (MSTO211H [126], HL60 [126], WTK1 [127], 1321N1 [78], and HeLa [58] are employed *in vitro* for materials testing, some for no apparent reason other than convenient culture, rapid expansion and growth, and commercial availability for experimental exploitation, others for their intrinsically high phagocytic abilities for particle uptake [126]. They are also utilized to predict pharmacologic endpoints of specific tissue-derived tumors to nano-based cancer therapies. Specifically, SH-SY5Y human neuroblastoma cells of epithelial origin, were examined for cytotoxicity from functionalized quantum dots (QDs) bearing a variety of surface chemistries. Cell-specific QD cytotoxicity (e.g., to SH-SY5Y cells) reflects both QD limitations for tissue imaging or therapy, but could also allow assessment of novel methods to simultaneously image and then treat neuroblastomas using toxic QDs [95].

Cell-based testing of many other polymer nanotherapeutics uses diverse assortments of cell lines to assay various delivery vehicles: both N-(2-hydroxypropyl)methacrylamide (HPMA) copolymer-bound doxorubicin [128] and polyamidoamine (PAMAM) G4 dendrimer-succinic acid-paclitaxel conjugates [129] have been taken up by human ovarian cancer cells (A2780); poly (D,L-lactide-coglycolide) (PLGA) polymeric nanoparticles have been assayed for uptake by human arterial smooth muscle cells (HASMC) [124]; nanoparticles of cholesteryl-3β-carboxyamidoethylene-*N*-hydroxyethylamine and Tween-80 were used to transfect human prostate tumor PC-3 cells [130]; poly(D-glucaramidoamine)-compacted DNA nanoparticles were used to transfect BHK-21 (baby hamster kidney) cells [131]; plasmid conjugates of both low- and high-molecular weight polyethylenimine (pGL3/LMW-PEI and pGL3/HMW-PEI) have been used to transfect ECV304 endothelial cells and 3T3 fibroblasts [125]; 2Mb plasmid conjugates, including NaCl-DNA, PLL-DNA, and PEI-DNA were each used to transfect HT1080 human cells [132]; plasmid-PEI-adenovirus conjugates were used to transfect immortalized (DMD) and primary human fibroblasts [133]; histidinylated polylysine–plasmid complexes were used to transfect immortalized cystic fibrosis airway surface epithelial cells (ΣCFTE29o- cells) and airway gland serous cells (CF-KM4 cells) [134]; and plasmid–polygalactosamine (pGL3/pGalN), small (15 kDa) and large (100 kDa) plasmid–chitosan complexes, and plasmid–lipofectin (pGL3/lipofectin) complexes were used to transfect human lung carcinoma A549 cells, Hela cells, and B16 melanoma cells [135].

3. Cell-based in vitro toxicity assays

Cell-based assays are currently considered central to toxicity testing [9,136], biomaterials testing [137] and environmental materials exposure testing [138]. Despite the frequent lack of consistency or predictability between *in vitro* models and *in vivo* observations, there is little rational or ethical justification to proceed directly from materials synthesis to animal models, although this appears to be increasingly done in industrial development. Cell models still seek validation as a useful screening bridge between materials quality analysis and *in vivo* deployment. The standard *in vitro* test methods are specified in ISO 10993 [139,140]. Historically, there is substantial work reported for cell-based assays on various colloids and materials particulates [104]. It follows logically that numerous cell-based assays have also been applied to characterize the response of cells to nanomaterials. Nearly all of these assays have been adapted from other applications. As a result, a degree of ambiguity or inconclusiveness is inherent in some answers from certain assays as applied to nanosystems, sometimes due to intrinsic challenges associated with the analysis of nanomaterials. For example, intrinsic photometric absorbance or fluorescence of nanosuspensions or colloids may alter colorimetric or fluorometric assay reporting. High surface energy and surface area of nanomaterials may also contribute to binding of unanticipated amounts of assay reagent or analyte. Often, ambiguity results from the spectrum of inconsistent or different cell responses observed in these assays frequently interpreted either as toxicity or adverse reactivity. Therefore, corroboration of answers from many different assays is vital to forming valid and credible conclusions about interactions of nanomaterials with cell cultures [136]. Five main assay categories, including ROS production, cell viability, cell stress, cell morphology phenotyping, and cell–particle uptake assays, are central themes in such testing. Challenges in interpreting cellular results in various 'gray scales' of toxicity or non-toxic responses include lack of consensus regarding cytokine combinations that reflect acute or chronic toxicity, assay reproducibility and reliability, assay sensitivity, and translation of results from *in vitro* to *in vivo* systems.

One particular concern is a lack of distinction currently between cell assays of nanomaterials in serum-containing media versus those in serum-free media. Serum-free media is often employed to avoid complications of protein–particle interactions in cells. Many studies acknowledge ineffective cellular delivery of nanomaterials (e.g., polymer therapeutics or gene vectors [125]) in the presence of serum proteins and, therefore, employ serum-free media. However, this introduces questions of relevance and biological equivalence since no *in vivo* exposure would occur in the absence of host proteins. This also has enormous implications for the physical presentation of nanomaterials to cells and possible effects of dispersed versus aggregated materials exposure to cell processing mechanisms and response. Serum proteins comprise several thousand different proteins identified to date amounting to 4–7 mg/ml total protein content in 10% serum media common to cell culture. Many of these are highly surface-active and rapidly promote particle aggregation and even precipitation of colloidal materials introduced into this media. Large particles (micron to sub-100 nm size) bind proteins indiscriminately and rapidly from the milieu, changing their surfaces presented to cells and causing flocculation. By contrast, sufficiently small particles (<10 nm) are actively bound to, solubilized by, and carried by serum proteins. This facilitates cellular transport mechanisms distinct from bare particles and their aggregates that require phagocytosis or pinocytosis for cell entry. Protein adsorption to particles is extremely likely and pivotal to understanding cellular processing [141,142]. However, few reliable methods outside of conventional protein radiolabeling and centrifugation and elution protocols have been reported, particularly for full serum analysis. Nonetheless, certain *in vivo* situations experience only transient exposure to plasma or serum. For examples, wound sites clotted with blood and often infiltrated with healing-associated macrophages likely are not effectively perfused with blood proteins. Hence, what cells actually experience *in vivo* in context is not consistent or necessarily modeled by either serum or serum-free culture media. Moreover, nanoparticles in serum-free media bind cytokines more

Table 2
Techniques to detect ROS and RNS *in vitro* (adapted from Ref. [34]).

Assay	ROS detected	Advantages	Disadvantages
Chemiluminescence	Oxygen radicals	Quantitative	Specificity
Salicylate	•OH and $ONOO^-$	Quantitative	Limited to •OH and $ONOO^-$ detection only
Cytochrome c	ROS and RNS	Quantitative and Simple	Only *in vitro*, no information about ROS species
DCDHF	ROS	Both intra- and extra-cellular ROS can be detected, visualized	Autocatalytic degradation, no information about ROS
Product analysis	ROS	Employs well-established analytical techniques	Does not provide unequivocal evidence
Total GSH depletion	ROS	Simple	Does not provide GSH:GSSG ratio
ESR/EPR	Free radicals	Uses both *in vitro* and *in vivo*, Quantitative, structural information	Not possible to calibrate *in vivo*
Inhibition by SOD	Superoxide	Simple, highly specific	Only applicable to superoxide
Inhibition by antioxidants	ROS	Simple	Little information about radical species

avidly because serum proteins are no longer present to compete for surface sites. This results in reduced levels of detectable cytokines in serum-free media with NP vs. serum-rich media with NP [141], requiring corroborative measurement of cytokine-specific mRNA expression. Additionally, the switch to serum-free media for cultures long-adapted to serum media often requires a specific recipe for each cell type, along with the potential for possible sub-lineage selection [87], phenotypic alteration, decreased survival [143], increased phagocytosis [144,145], increased cell stress, increased cell transport, altered cell membrane turn-over, altered transcriptional behavior and protein production, and induction of stress responses. Hence, serum-free media used without justification or testing can produce a highly artifactual cell culture condition not particularly relevant to "real world" cell-based testing. Yet, inclusion of serum complicates consistent nanomaterial presentation to the cells and complicates their bioassay [146].

3.1. ROS production assays

Cell-based ROS production was described above in Section 2.1 as a consequence of nanoparticle exposure. Since phagocytes are the predominant cell model for nanoparticle toxicity, many cell assays interrogate phagocyte ROS production [9]. (see Table 2). Care must be exercised in ROS production assays involving carbon black (CB) and TiO_2 as these have both been shown to also generate ROS in cell-free systems [147]. This behavior generally extrapolated over other chemistries that naturally produce ROS precludes accurate determination of ROS produced exclusively by cells. Nevertheless, numerous cell-particle assays have been applied to this endpoint; some seek to quantify the ROS species production by cells directly while others seek to quantify its effects on cell behavior or further production of other cell biochemical reactions.

3.1.1. ROS detection

Direct measurement of ROS in cell media has been accomplished by two similar fluorescein-compound-based tests or by Electron Paramagnetic Resonance (EPR). The reactive fluorescein probes, 2′,7′-difluorescein-diacetate (DCFH-DA) [54,72] and dichlorodihydrofluorescein diacetate (H_2 DCFDA) [113] both fluoresce when oxidized by ROS yielding an optical ROS concentration-dependent response [54,57]. EPR has the advantage of being an effective radical detection method in either the presence or absence of cells allowing for the use of a greater variety of experimental controls. For EPR detection of radicals, an adduct-forming, spin-trapping agent (5,5-dimethyl-l-pyrroline N-oxide, DMPO) for hydroxide ($OH^{\cdot -}$) or superoxide ($O_2^{\cdot -}$) radicals or a radical-consuming spin probe (4-hydroxy-2,2,6,6-tetramethylpiperidine-1-oxyl) are introduced into the culture or nanoparticle solution for a set amount of time after which the entire supernatant is collected, vortexed, and analyzed on an EPR spectrometer [34,35,51]. Additionally, though reactive nitrogen species are studied much less often in cell culture systems, $NO^{\cdot}$ is a radical commonly produced by phagocytes that may react with $O_2^{\cdot -}$ to form peroxynitrite ($ONOO^-$) [93], one of the most reactive oxidizing species. However, $ONOO^-$ readily degrades to $OH^{\cdot -}$ and may thus be detected indirectly. Nevertheless, $NO^{\cdot}$-specific detection and $ONOO^-$ may be accomplished using the EPR spin probe colloids, iron-N,N-diethyldithiocarbamate, Fe-$(DETC)_2$ and 1-hydroxy-3-carboxy-2,2,5-tetramethyl-pyrrolidine (CPH), respectively [148]. Though Fe-$(DETC)_2$ may not be used in cell solutions [148], $ONOO^-$ may also be detected in cell systems by fluorescent DCF detection (discussed earlier in this section) [149].

3.1.2. ROS effector assays

As stated above in Section 2.1, potent but short-lived reactive oxygen species (ROS) are produced by several cell types either as a natural function (e.g., inflammatory oxidative burst response) or in response to other stresses [99]. ROS is produced in response to biomaterials exposure, including particulates [57,90–92]. As ROS is indiscriminate in its biochemical oxidative reactivity, most cells have built-in defenses to neutralize ROS by using ubiquitous glutathione, an endogenous, reducing agent depleted by ROS insult. Thus, ROS encountered by a cell may be quantified by the well-known glutathione (GSH) assay [54,72,136,150]. Other assays seek to quantify ROS-effected damage to cell membranes or DNA by essentially analyzing key oxidized species. Immunocytochemistry allows for the detection of specific DNA lesions, such as the OH^- radical-specific 8-hydroxydeoxyguanosine lesion, a direct measure of ROS involvement in DNA damage [51]. Alternatively, BODIPY-C_{11} is a fluorescent dye that inserts itself into lipid bilayers allowing oxidized and unoxidized lipids to be quantified fluorimetrically and imaged by their respective green and red colors [95]. ROS-induced membrane lipid peroxidation may occur both at the cellular level and organelle level, especially in membranes of highly metabolically active mitochondria, making mitochondrial injury a common indicator of elevated intracellular ROS levels [95]. Compromised cell viability and cell death may result from this insult as well, making this a key analytical marker for ROS-induced oxidative membrane damage.

3.2. Cell viability assays

Cellular metabolism is the focus of many cell viability assays [85]. Assays of live versus dead cells in a sample provide gross estimates of the cell response to an insult and are frequently used as an overall biocompatibility assessment criterion. A number of routine, dye-based cell viability assays reviewed previously are available for this assessment [136]. Most involve differential inclusion, exclusion, or conversion of an added dye or enzymatic conversion of a dye precursor in living versus dead cells that can then be distinguished and quantified colorimetrically or fluorescently. Such dye-dependent assays include neutral red, trypan blue [51], LIVE/DEAD™, lactate dehydrogenase (LDH) [51,72,113,150], formazan-based assays (MTT [44,51,53,95,151], MTS [78], WST), Alamar blue (resazurin) [53], Coomassie blue [53], ATP-luciferin luminescence [54,57], adenylate kinase (AK) release [53], mitochondrial membrane potential (MMP) [113], and thiobarbituric (TBA) assays. These assays possess potential for side reactions and ambiguities. For instance, cysteamine-coated quantum dots have been observed to catalytically reduce MTT to formazan without cellular metabolism [127]; high-density cultures or

long incubation times have shown the potential for a secondary reduction of the Alamar blue product to a non-fluorescent, confounding species; silver nanoparticles have been shown to interfere with the LIVE/DEAD™ assay [152]; the Coomassie blue assay primarily reacts with arginine, making it composition-dependent and may be additionally confounded by small amounts of SDS in solution [153]; and many particles possess spectral properties that make them possible confounders of any spectral assay. Therefore, all such dye-based assays require careful calibration in the presence of high specific surface area particles or nanomaterials as controls to determine interference and standardization issues for reliable quantitation of cell-specific activities.

Fluorescence-activated cell sorting (FACS) is capable of categorizing and quantifying cells as healthy, dead, apoptotic, or necrotic, and can distinguish alterations in the cell-cycle dynamics of a cell population, such as an increased proportion of hypodiploid DNA cells in sub-G0/G1 phases, which is indicative of necrosis or apoptosis [61]. Additionally, FACS may be used to quantify receptor expression by cells to reveal mechanism of cell death, such as the up-regulation of the Fas receptor, an integral component in the formation of the apoptotic, death-inducing signaling complex [95]. FACS has the advantage of automation and parallel processing of multiple cell targets in single multi-color assays. However, multiple antibody-hapten non-specific cross-reactivities and specificities, and assay interference from high specific surface area nanomaterials must be determined in such assays to assert their accuracy and validity with cells.

Other cell viability assays are also pathway-sensitive indicating apoptotic DNA fragmentation and leakage from the cells. These include the enzyme-linked immunosorbent assay (ELISA) to quantify fragmented DNA [44], comet [154], Caspase Glo3/7 [57], Hoechst-DNA [57], and (TdT-mediated dUTP-biotin nick end labeling) TUNEL assays [155–157]. The comet assay measures fragmented DNA by gel electrophoresis [51,127], Caspase Glo3/7 quantifies downstream effectors of the mitochondrial apoptotic pathway, and Hoechst-DNA is a fluorescent probe that binds to adenine-thymine-rich regions on double-stranded DNA that has leaked out of the nucleus in cells under stress [57]. TUNEL measures the amount of fragmented DNA in the nucleus to quantify cell apoptosis [157]. Control assays in the presence of nanomaterials should determine assay interference in the presence of culture milieu.

Some quantitative and some more qualitative assays of cell death are accessible by microscopy. Quantitative viability results may be obtained from light microscopy by counting numbers of adherent treated cells or cell colonies relative to control cell adherence [44]. Qualitative light microscopy results range from detection of cellular debris or detached cells to identification of necrotic and apoptotic cells. Visible symptoms of apoptosis are reported to include cell detachment, rounding of cells, cytoplasm retraction, and nuclear shrinkage due to chromatin condensation [60]. This kind of qualitative visual characterization should not be used as a stand-alone viability assay, but may be used to confirm a common pathway of cell death identified in other assays for a variety of materials [60].

3.3. Cell stress assays

These assays seek to identify non-lethal injuries to cells or changes in cellular behavior resulting from environmental insult. These changes/injuries to cells are manifest in their modulation of protein or gene expression, phagocytic ability, and/or inflammation reactions that alter normal phenotype. Hence, metrics for 'normal, background' cell phenotype and its retention and stability in untreated cohorts must be convincingly and reliably determined for comparison and control.

3.3.1. Protein/gene expression

Changes in select gene/protein expression patterns may be detected by polymerase chain reaction (PCR), western blotting, and total protein assay (i.e., BCA or Bradford). Quantitative, real-time PCR (qPCR) has been applied to detect toxicity-modulated gene expression in A549 cells exposed to varying dilutions of nano-sized, propane-combustion-generated particles. Specifically, expression modulation of CDKN1A (cell-cycle arrest gene), GADD45β (DNA damage-dependent), IL-6 (inflammatory response), NFκBIA (inflammatory response), EGFP (reporter gene), and NF-κB (involved in promoter/enhancer regions of fibrotic/inflammatory growth factors, cytokines, and adhesion molecules) were assayed. GADD45β and NF-κB expression increased with time and with increasing cell mortality signaling increases in DNA damage and inflammation. Significantly, for cells treated with dilute particle solutions, wherein cell damage, but no appreciable mortality was observed, CDKN1A was up-regulated, arresting cells in G1 phase, possibly to enhance repair of DNA damage. For less dilute particle solutions that caused significant cell mortality, CDKN1A was initially up-regulated, but subsequently down-regulated, possibly indicating apoptotic activity [158]. Thus, changes in gene expression can reveal toxicity-dependent modulation of gene expression and help to elucidate possible mechanisms of toxicity.

Western blotting has been used to examine the effects of nanotubes on cell adhesion by assaying adhesion proteins: fibronectin, laminin, p-cadherin, FAK, collagen IV, β-actin, and cyclin D_3 [44]. However, cell protein production is cell-cycle dependent and altered distinctly as a function of applied insult in confluent, contact-inhibited cultures vs. non-confluent (proliferating) or non-contact inhibited cells. So, careful control measurements at similar cell densities and growth stages must be used for comparisons of relative changes. Down-regulation of protein expression from cell stress or oxidative

Table 3
Cytokines related to nanotoxicity.

Cytokine	Receptor	Source	Targets	Major function
Interleukin (IL)-1α; IL-1β	IL1RI and IL1R-AcP	Macrophages, many others	Macrophages, thymocytes, CNS, others	Inflammatory; promotes activation, costimulation, and secretion of cytokines and other acute-phase proteins; pyrogenic
IL-6	IL6Rα and gp130	Macrophages, T cells, fibroblasts, and others	Wide variety of cells: B cells, T cells, thymocytes, myeloid cells, osteoclasts	Inflammatory and costimulatory action; induces proliferation and differentiation; synergizes with TGFβ to drive Th17
IL-8	ILa and ILb	Macrophages, endothelial, keratinocyte	Leukocytes	Proinflammatory
MCP-1	CCR2, CCR12	Macrophages	Macrophages, Glial cells	Proinflammatory
MIP-2	CCR1	Macrophages	T lymphocytes, T cells	Proinflammatory, chemokine
Prostaglandin E_2	PTGER2: EP1, EP2, EP3, EP4 subtypes	Macrophages, fibroblasts	Osteoblasts, endothelial, dendritic, and carcinoma cells, various others	Inflammatory, anti-apoptotic, and neuromodulator
TNFα	Murine: TNFR,p55; TNFR,p75 Human: TNFR,p60; TNFR,p80	Macrophages, monocytes, T cells, others	Neutrophils, macrophages, monocytes, endothelial cells	Inflammatory; promotes activation and production of acute-phase proteins

Adapted from Refs. [206–209].
(to date, only inflammatory cytokines have been reported).

damage results in changes in the extracellular matrix, cytoskeleton and cell morphology as well as displacement of organelles, disturbing normal cell adhesion and spreading [44]. Total cell protein assays are routinely used in combination with protein expression assays to normalize gene/protein expression data (such as luciferin assay data) to monitor up-regulation of genome and cell transcriptional activity [157]. Changes in certain key cellular proteins involved in either toxicity pathways or inflammation (e.g., cytokines, chemokines) in cells under stress are altered compared to controls.

3.3.2. Inflammatory markers

The characteristic *in vivo* response of macrophages to insult includes some form of oxidative (ROS) burst (see Section 2.1) and chemical recruitment of additional macrophages and auxiliary cells using cytokine and chemokine chemotactic pathways to the site of disturbance. The primary ROS-independent means of assessing cellular inflammation is through qualitative observation of inflammatory protein expression by immuno-fluorescence [121] or quantification of relevant protein signaling molecules (cytokines) at the protein level (e.g., via ELISA or Western blotting) and up-regulation of the mRNA that codes for their synthesis (using PCR variant assays) [121].

Direct cytokine protein detection has traditionally focused on surface capture immuno-mediated sandwich assays in various permutations, including enzyme-linked immunosorbent assay (ELISA) [34,35,53,54,150,152]; or innovations upon the ELISA design that allow for the simultaneous detection of 8 (LINCOplex) [159] or hundreds of cytokines in multiplexed assay formats. Recent permutations of cytokine detection assays are reported. These include multiplexed cytometric bead assays, namely CBA – a distinct application of flow cytometry equipment employed for fluorescence-activated cell sorting, FACS, discussed above), but exploiting libraries of various fluorescent bead-linked antibodies for the simultaneous detection of 30 or more cytokines [160]. Also, microarray -printed immuno-capture multiplex assays such as Quansys Q-Plex™, based on 96-well plates wherein up to 25 different capture antibodies have been printed on each well surface, allow for simultaneous quantification of up to 25 unique analytes from single 5 to 30 μl samples [161]. Hundreds of unique cytokines have been discovered to-date and classified variously into several families by structure, function or targeted receptor. Cytokines are produced severally by the majority of cell types throughout the body and customarily act in concert, with some cytokines potentiating numerous others [162,163]. However, very few cytokines have been assayed and identified in nanomaterial-exposed cell cultures, with relevant publications focusing cytokine analysis on only a small list of cytokines (<10) which comprises only inflammatory cytokines (see Table 3). Thus, this present, small beginning of cytokine analysis in cell-based nanomaterial testing is set to expand tremendously as understanding continues to develop toward *in vitro* cellular responses to nanomaterials.

Cytokine detection assays, like many other bioassays, are notoriously fraught with user- and milieu-dependent variation requiring meticulous attention to multiple-step preparations and good standard curves *performed in the specific media being assayed*. Assay answers are often qualitative in nature or only indirectly and relatively quantitative compared to a standard curve that, cannot reflect accurate answers unless run under identical media conditions (i.e., spiked standards). Moreover, serum-modulated cytokine adsorption to nanoparticles has been demonstrated, particularly for the case of carbonaceous nanomaterials, such as road tunnel, wood smoke, and diesel exhaust particulate samples, as well as ultrafine carbon black. All were shown to bind cytokines in solution and modify cytokine concentrations to varying degrees. Conversely, quartz mineral particles did not alter detectable cytokine concentrations for the specific cytokines tested, including human variants of TNF-α, IL-1β, IL-6 and IL-8 [141]. Because transient nucleic acid messaging in cells during gene up-regulation and as quantified by the various PCR techniques does not necessarily get expressed as protein or correlate with the amount of its protein product, protein assays (e.g., ELISAs, and Western blots) are often encouraged to ensure such correlations. Therefore, quantification of soluble cytokines should be corroborated by concomitant quantitation of cytokine-specific mRNA message expression obtained by reverse transcriptase polymerase chain reaction (RT-PCR) of the lysates of treated cells [34,35,150] or analysis of up/down regulation of inflammation-related genes by a microarray gene expression technique such as the Affymetrix mouse genome gene chip oligonucleotide array or other appropriate gene chip modality [57].

3.3.3. Cell visualization – phagocytic activity, internalization, and organelle interaction

Cellular uptake of colloidal materials, particles, and nanomaterials is typically divided among four common routes of cell internalization, including phagocytosis, clathrin-mediated endocytosis, macropinocytosis, and non-clathrin-mediated endocytosis, though these four categories may fit under the two original internalization pathways defined by the work of Silverstein and Steinman [164,165]. Phagocytosis (typically from macrophages, monocytes and neutrophils) is the uptake of particles larger than 500 nm, often triggered by particle opsonization (i.e., protein–particle adsorption) and subsequent receptor-mediated activation of F-actin-driven pseudopods that engulf the particle in a cytoplasmic phagosome. Alternately, phagocytosis may be blocked by application of cytochalasin D [55], which blocks the polymerization of actin [166], inhibiting pseudopodial action. While macrophages, monocytes, and neutrophils are normally termed "professional phagocytes", epithelial cells, fibroblasts, and other cells also can uptake particles [166], likely by pinocytosis – a process common to nearly all cells [167]. Pinocytosis usually occurs at the sites of clathrin-coated pits (present in most animal cells) and involves the passage of particles smaller than 200 nm in an inadvertent sort of particle uptake along with cell-surrounding fluid in cell drinking. Macropinocytosis (a type of fluid-phase endocytosis) is the formation of vacuoles up to 1–5 μm by considerable ruffling of the cell membrane that may be seen frequently in certain cell types (i.e., macrophages, dendritic cells, and fibroblasts) and has also been suggested as the uptake mechanism responsible for the concentration of polymers and macromolecules seen in tumor cells manifesting enhanced permeability and retention (EPR) [168]. Caveolae-mediated uptake, or potocytosis, also occurs in most cells and is best detected after deactivation of the clathrin-dependent internalization pathways. Rather than mediating material sequestration in lysosomes or endosomes, caveolae are thought to mediate transport of material across endothelial cells (transcytosis) [167].

Cell-particle internalization may be monitored directly in culture to reflect relative cellular uptake activity, phenotype and health [55,114]. Phagocytic ability, measured by cellular uptake of colloidal 2-micron diameter gold latex beads or other fluorescent tracking particles, has been assayed as an indicator of nanomaterial toxicity in alveolar macrophage cultures. Following a 6-hour incubation with a sample array of test materials (one low and one high sample concentration for each material), cells are transferred to gold latex bead-containing media and phagocytic ability is assessed as the relative (compared to untreated controls) proportion of cells capable of ingesting 2-micron diameter gold latex beads during a 16-hour bead-in-media incubation [151]. However, uptake of a reference bead may vary significantly from the uptake experimental particles, particularly in the case of disparate sizes or surface chemistries. In some macrophages, cellular activation is prerequisite to phagocytic activity, as shown in glial cells [57] and THP1 human macrophages [169]. Hence non-activated, non-phagocytosing healthy cells must be distinguished from injured/dying cells whose phagocytic ability has been retarded by toxic insult. Particle dose-cell uptake response

relationships should be first controlled to ascertain whether the colorimetric reference particle might by itself exert an influence on the overall cell response alone, and whether there is a reliable correlate in its uptake with nanomaterial exposure (e.g., dose response or saturable response changes in phagocytic activity. Variations of this experiment using naive phagocytes exposed to conditioned media only (centrifuged away from cells and nanoparticles in pre-exposed cultures) or as transwell-insert co-cultures in various configurations exposed to nanomaterials in different ways also offer new possibilities to assay cell response to these materials in the presence of other cells, reporters or media influences.

Receptor-mediated internalization pathways are thought to be temperature dependent and are thus assayed by examining the variation of analyte uptake with temperature, with decreased or discontinued analyte uptake at lower temperatures (4 °C) being indicative of receptor-mediated uptake [164]. Clathrin-mediated pathways may be inhibited by application of chlorpromazine or by over-expression of Eps15 and thus identified. Macropinocytosis-dependent internalization may be inhibited and identified by application of 5-(*N*,*N*-diethyl)amyloidal hydrochloride, a macropinocytosis inhibitor [164]. Presence/absence of caveolae-mediated internalization pathways for a given particle may be demonstrated by BODIPY-labeled LacCer, a sphingolipid that is caveolae uptake dependent, applied in combination with filipin or genestein, inhibitors of caveolae-mediated uptake, to demonstrate caveolae dependence [164]. Cellular uptake of optically active particles may also be assessed and quantified by flow cytometry or by various microscopies. Significantly, flow cytometry is capable of sorting free particles, particle aggregates, cell-associated particles, and particle-free cells, allowing for the assessment of fractions of cells that associate with particles if the particles are intrinsically fluorescent or can be tagged post-facto with fluorescence [164,170].

Aside from cell-particle uptake assays, microscopy provides the added advantage of revealing particle localization and trafficking within the cell. High-resolution inspection of chemically fixed and carefully desiccated cell samples by TEM – its high-resolution (HR-TEM) and energy-filtering (EFTEM) embodiments – can reveal organelle–nanomaterial interactions that may help to elucidate nanomaterial-specific mechanisms of cellular toxicity [34,53–55,57,58]. Cell-nanomaterial interactions observed by TEM include differentiation of lysosomal aggregates from membrane-bound aggregates [59], nucleus migration toward membrane-bound clusters of single-walled nanotubes [44], and disordering of the cytoskeletal actin networks [44], all of which are indications of nanomaterial-modulated cell activity. Additionally, Electron Energy Loss Spectroscopy (EELS) [54] and confocal Laser Scanning Microscopy (LSM) fluorescence microscopy have also been used to image particle uptake and internalization within cell organelles (e.g., endosomes, lysosomes) or nuclear penetration [170]. Moreover, LSM offers accessibility of pseudo-3D images through image reconstruction algorithms combining several axial and lateral images [54,55].

The complexity of extra- and intracellular environments presents a variety of obstacles and interactions to particles that require elucidation in order to fully understand cellular reactions and processing. Multiple particle tracking (MPT) assays offer a method to observe and understand particle interactions with various cell components in real-time using video-interfaced phase microscopy to track particle movement through the various environments encountered in cellular trafficking. Tracking of individual particles can reveal information on pore sizes, particle adhesion, intracellular particle transport mechanism, and barriers to particle transport by observation of particle movement characteristics or immobilization behavior and localization [171]. Additionally, two-point micro-rheology, a variation of MPT, utilizes automated computer-based analysis of thousands of micrographs, including particle sizes and motions over time, to observe particle Brownian motion yielding information concerning viscosity and shear moduli in various parts of the cell [172]. MPT allows for the interrogation of cell-particle interactions not accessible by any other means. That this method is readily extended to nanoparticles in cellular systems remains to be reported.

As an alternative to determining cell reactivity to particles using mammalian cell-based assays, phenotypic behavior of other cell cultures to nanophase materials can also be used to provide cell toxicity information. For example, the single-celled ciliated protozoa, *Tetrahymena thermophila,* (grown in the absence of mammalian cells in supplemented or unsupplemented salt solutions, protease peptone yeast extract (PPYE) and Osterhout's solution, respectively) have also been used as a model of cellular stress in the presence of test materials. Intrinsic protozoan bacterivory activity (ingestion of green fluorescent protein labeled-*E. coli* bacteria) is monitored by video-enabled, phase-contrast microscopy over a period of 1–2 h in real-time cultures. Correlative symptoms of cell aggregation, matrix accumulation, diminished mobility, and death in the presence of culture stresses (chemicals, pollutants) are used to corroborate the bacterivory result. These protozoa have relevance to aquatic toxicity and specific relevance to wastewater treatment [173]. Analogous methods might also be adapted and employed to assay toxicity to nanomaterials for prokaryotes and other non-mammalian cells.

3.4. High-throughput screening methods

Recent advances in cell-based assays allow for toxicity and/or efficacy screening of multiple nanomaterials at multiple concentrations with multiple cell lines, simultaneously. This expansion of experimental design is practically enabled through the miniaturization and multiplexing of the experimental apparatus and method by utilization of either ultra-small 384-well cell culture plates or nanodrop sample chambers on a chip. The nanodrop assay setup allows for different assays with suitable detection features (e.g., fluorescence, and luminescence) to be performed in a fraction of the volume without the cell-activation or photometric effects of the culture plate since the cell culture is performed in a self-contained drop [112]. However, since cells are typically microns in size, nanodrops do not necessarily capture cells themselves, only fluidic cellular exudate for assay and analysis. By assaying numerous material types/functionalizations and material concentrations on numerous cell types, all in parallel, complex interactions between materials and cells may be ascertained through complex data analysis that correlates phenotypes with multi-well plates, cell culture, detection schemes, and recognition schemes [174].

4. Conclusions

The multi-disciplinary nature of the nanotechnology field that brings it strength in innovation also presents significant challenges in the interpretation, validation and correlation of cell and tissue toxicity data collected for nanomaterials. As others have indicated, needed advances in nanotoxicology will come from developing a valid set of reliable toxicity tests [175-177] and nanomaterial characterization protocols for application to the overwhelming variety of nanomaterials that have been produced and the even greater variety that is yet to come. Standardization against materials reference standards [178] and validation by corroboration and comparison will eventually produce some trends and increased confidence in newly developed methods that do not currently exist. The community is searching now for such reliable methods, reference materials, standard protocols and validations. Without these, the efforts have little scientific credibility and the community must be very careful about conclusions drawn from assays *in vitro*, particularly in their relevance to *in vivo* systems and organismal toxicology. The unique challenges in nanotoxicity assessments lie in addressing the current lack of appropriate tools to directly observe and interrogate nanomaterials in complex biological systems

[33]. Specifically, materials aggregation, physical, and chemical reactivity are nearly impossible to understand currently. Their individual and collective effects on dynamic living systems are even more difficult to accurately assess, predict and model. Significantly, pharmacological dose–response relationships are complicated by time- and condition-dependent nanomaterial chemical and physical states. Acute versus chronic nanomaterial exposure effects and hazards are therefore difficult to monitor.

Hence, multiple different measurement techniques must be adapted, carefully assessed for validity, and applied to complex nanomaterial systems. Similar to the blind man describing the elephant, decades of surface analytical chemistry of biomaterials has shown that one can assert most any conclusion from a single analytical measurement. No single analysis can provide sufficient information on the biomaterials surface to correlate biological response. Truths (or approaches to truths) pertaining to complex nanosystems necessitate 1) compilation of multiple experiments focused on common aspects of the same system, 2) corroboration of these results, 3) synthesis of supportive trends in the data, 4) careful exclusion of artifacts and 5) use of proper controls. Specifically, nanomaterial toxicities in biological systems present unique and complex problems. Investigators should be wary of forming conclusions based on single biological assays, isolated cell lines, or protein-free media, and strengthen observations by correlating measurements from multiple different assays.

Acknowledgments

The authors gratefully acknowledge technical discussions with J. Veranth and A. Ostafin (Utah), manuscript preparation assistance by C. Li and support of the Synergy grant program, University of Utah. This work was partially supported by NIH grant R01 EB00894.

References

[1] The Nanotech Industry Is Moving From Research to Production With Over 500 Consumer Nano Products. Business Wire [online news article] 2008 [cited July 4, 2008]; Available from: http://www.allbusiness.com/science-technology/materials-science/6786843-1.html.
[2] Nanotechnology White Paper. [External Review Draft] 2005 December 2, 2005 [cited July 4, 2008]; Available from: http://www.epa.gov/OSA/pdfs/EPA_nanotechnology_white_paper_external_review_draft_12-02-2005.pdf.
[3] A.M. Thayer, Carbon Nanotubes by the Metric Ton, in Chemical & Engineering News, 2007, pp. 29–35.
[4] B. Park, Current and Future Applications of Nanotechnology, in Nanotechnology: Consequences for Human Health and the Environment, R.M. Harrison, R.E. Hester (Eds.), The Royal Society of Chemistry, 2007.
[5] P.E. Barker, et al., Nanotechnology Briefing Paper: Clean Water Act, in Section of Environment, Energy, and Resources, American Bar Association, Chicago, IL, 2006, p. 13.
[6] R.G.K. Louis Theodore, Nanotechnology/Environmental Overview, in Nanotechnology: Environmental Implications and Solutions, 2005, pp. 1–60.
[7] US demand for nanotechnology medical products to approach $53 billion in 2011 – Report. nanotechwire.com [online News Release] 2007 March 16, 2007 [cited July 3, 2008]; Available from: http://nanotechwire.com/news.asp?nid=4446.
[8] Industry Statistics. PharmaMedDevice Bulletin [online] 2008 [cited July 4, 2008]; Available from: http://www.pharmameddevice.com/App/homepage.cfm?appname=100485&moduleID=3162&LinkID=23294.
[9] A. Nel, et al., Toxic potential of materials at the nanolevel, Science 311 (5761) (2006) 622–627.
[10] D.B. Warheit, How meaningful are the results of nanotoxicity studies in the absence of adequate material characterization? Toxicol. Sci. 101 (2) (2008) 183–185.
[11] A. Takagi, et al., Induction of mesothelioma in p53+/− mouse by intraperitoneal application of multi-wall carbon nanotube, J. Toxicol. Sci. 33 (1) (2008) 105–116.
[12] C.A. Poland, et al., Carbon nanotubes introduced into the abdominal cavity of mice show asbestos-like pathogenicity in a pilot study, Nat. Nano. 3 (7) (2008) 423–428.
[13] K. Kostarelos, A. Bianco, M. Prato, Hype around nanotubes creates unrealistic hopes, Nature 453 (7193) (2008) 280.
[14] Environmental, Health, and Safety Research Needs for Engineered Nanoscale Materials. [online] 2006 [cited July 4, 2008]; Available from: www.nano.gov/NNI_EHS_research_needs.pdf.
[15] S.C. Eisenbarth et al., Crucial role for the Nalp3 inflammasome in the immunostimulatory properties of aluminium adjuvants. Nature, 453(7198) (2008) 1122–1126.
[16] G.J. Nohynek, E.K. Dufour, M.S. Roberts, Nanotechnology, cosmetics and the skin: is there a health risk? Skin Pharmacol. Physiol. 21 (2008) 136–149.
[17] H. Vallhov et al., The Importance of an Endotoxin-Free Environment during the Production of Nanoparticles Used in Medical Applications. Nano Letters 6(8) (2006) 1682-1686.
[18] D.W. Grainger, D.G. Castner, Nanobiomaterials and nanoanalysis: opportunities for improving the science to benefit biomedical technologies, Adv. Mater. 20 (5) (2008) 867–877.
[19] C.T. Campbell, S.C. Parker, and D.E. Starr, The Effect of Size-Dependent Nanoparticle Energetics on Catalyst Sintering. Science, 298 (5594) (2002) 811-814.
[20] L.M. Chamberlain, et al., Phenotypic non-equivalence of murine (monocyte-) macrophage cells in biomaterial and inflammatory models. J. Biomed. Mater. Res. A, 2008.
[21] D.G. Castner, B.D. Ratner, Biomedical surface science: Foundations to frontiers. Surf Sci 500 (2002) 28-60.
[22] A.V. Recum, J.E. Jacobi, Surface Characterization, in Handbook of Biomaterials Evaluation: Scientific, Technical, and Clinical Testing of Implant Materials, M. LaBerge, Editor. 1998, CRC Press: New York, NY. p. 893.
[23] M.B. Gorbet, M.V. Sefton, Endotoxin: the uninvited guest, Biomaterials 26 (34) (2005) 6811–6817.
[24] D.R. Cho, et al., The role of adsorbed endotoxin in particle-induced stimulation of cytokine release, J. Orthop. Res. 20 (4) (2002) 704–713.
[25] E.M. Greenfield, et al., Does endotoxin contribute to aseptic loosening of orthopedic implants? J. Biomed. Mater. Res. A 72B (1) (2005) 179–185.
[26] K. Huttunen, et al., Comparison of mycobacteria-induced cytotoxicity and inflammatory responses in human and mouse cell lines, Inhal. Toxicol. 13 (11) (2001) 977–991.
[27] L.P. Schwab, et al., Titanium particles and surface-bound LPS activate different pathways in IC-21 macrophages. Journal of Biomedical Materials Research Part B: Applied Biomaterials, 79B (1) (2006) 66–73.
[28] C. Gretzer, M. Werthén, P. Thomsen, Apoptosis and cytokine release in human monocytes cultured on polystyrene and fibrinogen-coated polystyrene surfaces. Biomaterials, 23(7) (2002) 1639–1648.
[29] J.M. Peula-García, et al., Interaction of Bacterial Endotoxine (Lipopolysaccharide) with Latex Particles: Application to Latex Agglutination Immunoassays, J. Colloid Interface Sci. 245 (2) (2002) 230–236.
[30] R. Darkow, et al., Functionalized nanoparticles for endotoxin binding in aqueous solutions. Biomaterials, 20(14) (1999) 1277–1283.
[31] D.W. Karl, et al., Preliminary assessment of removal of pyrogenic lipopolysaccharides with colloidal zirconia adsorbents, Enzyme Microb. Technol. 13 (9) (1991) 708–715.
[32] E.M. Greenfield, J. Bechtold, What other biologic and mechanical factors might contribute to osteolysis? J. Am. Acad. Orthop. Surg. 16 (suppl_1) (2008) S56–62.
[33] M.A. Dobrovolskaia, S.E. McNeil, Immunological properties of engineered nanomaterials. Nat Nano, 2(8) (2007) 469–478.
[34] S. Singh, Toxicological Effects of Nanoparticles: *In Vitro* studies with Titanium Dioxide, in Environmental Health Research Institute, University Duesseldorf, Duesseldorf, 2007, p. 118.
[35] S. Singh, et al., Endocytosis, oxidative stress and IL-8 expression in human lung epithelial cells upon treatment with fine and ultrafine TiO2: role of the specific surface area and of surface methylation of the particles, Toxicol. Appl. Pharmacol. 222 (2) (2007) 141–151.
[36] M.B. Gorbet, M.V. Sefton, Leukocyte activation and leukocyte procoagulant activities after blood contact with polystyrene and polyethylene glycol-immobilized polystyrene beads. J. Lab. Clin. Med. 137(5) (2001) 345–355.
[37] A.A. Ragab, et al., Measurement and removal of adherent endotoxin from titanium particles and implant surfaces, J. Orthop. Res. 17 (6) (1999) 803–809.
[38] Vakharia, D.D., R., et al., Polycyclic aromatic hydrocarbon/metal mixtures: effect on PAH induction of CYP1A1 in Human HepG2 Cells. Drug Metab. Dispos. 29(7) (2001) 999–1006.
[39] Toxic Byproducts of Carbon Nanotube Manufacturing: Are There Green Alternatives? Science News [online research news] August 24, 2007 [cited November 2007]; Available from: http://www.sciencedaily.com/releases/2007/08/070821081446.htm.
[40] K. Yang, B. Xing, Desorption of polycyclic aromatic hydrocarbons from carbon nanomaterials in water. Environ. Pollut. 145 (2007) 529–537.
[41] R.J. Chen, et al., Noncovalent Sidewall Functionalization of Single-Walled Carbon Nanotubes for Protein Immobilization, J. Am. Chem. Soc. 123 (16) (2001) 3838–3839.
[42] C.P. Deck, G.S.B. McKee, K.S. Vecchio, Synthesis optimization and characterization of multiwalled carbon nanotubes J. Electron. Mater., 35(2) (2006) 211-222.
[43] B. Bendjemil, et al., Elimination of metal catalyst and carbon-like impurities from single-wall carbon nanotube raw material. Appl. Phys. A, 78 (2004) 311-314.
[44] Tian, et al., Cytotoxicity of single-wall carbon nanotubes on human fibroblasts. Toxicol *In Vitro*. 20(7) (2006) 1202–1212.
[45] M.S. Wagner, et al., Limits of detection for time of flight secondary ion mass spectrometry (ToF-SIMS) and X-ray photoelectron spectroscopy (XPS): detection of low amounts of adsorbed protein, J. Biomater. Sci. Polym. Ed. 13 (4) (2002) 407–428.
[46] B.D. Ratner, Biomaterials Science, 2nd ed., Elsevier Academic Press, London, UK, 2004, pp. 42–57.
[47] R. Grieken, A. Markowicz, in: R. Grieken, A. Markowicz (Eds.), Handbook of X-ray Spectrometry, 2nd ed., CRC Press, New York, 2001, p. 983.
[48] P. Wobrauschek, Total reflection X-ray fluorescence analysis – a review, X-Ray Spectrom. 36 (5) (2007) 289–300.
[49] K. Soto, K.M. Garza, L.E. Murr, Cytotoxic effects of aggregated nanomaterials, Acta Biomater. 3 (3) (2007) 351–358.

[50] K.F. Soto, et al., Comparative *in vitro* cytotoxicity assessment of some manufactured nanoparticulate materials characterized by transmission electron microscopy, J. Nanoparticle Res. 7 (2) (2005) 145–169.
[51] R.P. Schins, et al., Surface modification of quartz inhibits toxicity, particle uptake, and oxidative DNA damage in human lung epithelial cells, Chem. Res. Toxicol. 15 (9) (2002) 1166–1173.
[52] K.F. Soto, et al., Biological effects of nanoparticulate materials, Mater. Sci. Eng. C 26 (8) (2006) 1421–1427.
[53] M. Davoren, et al., *In vitro* toxicity evaluation of single walled carbon nanotubes on human A549 lung cells, Toxicol. In Vitro 21 (3) (2007) 438–448.
[54] M.R. Wilson, et al., Interactions between ultrafine particles and transition metals *in vivo* and *in vitro*, Toxicol. Appl. Pharmacol. 184 (3) (2002) 172–179.
[55] M. Geiser, et al., Ultrafine particles cross cellular membranes by nonphagocytic mechanisms in lungs and in cultured cells, Environ. Health Perspect. 113 (11) (2005) 1555–1560.
[56] M. Goldraich, Y. Talmon, Direct-imaging cryo-transmission electron microscopy in the study of colloids and polymer solutions, Amphiphilic Block Copolym. (2000) 253–280.
[57] T.C. Long, et al., Nanosize titanium dioxide stimulates reactive oxygen species in brain microglia and damages neurons *in vitro*, Environ. Health Perspect. 115 (11) (2007) 1631–1637.
[58] B.D. Chithrani, A.A. Ghazani, W.C.W. Chan, Determining the size and shape dependence of gold nanoparticle uptake into mammalian cells, Nano. Lett. 6 (4) (2006) 662–668.
[59] A.E. Porter, et al., Uptake of C60 by human monocyte macrophages, its localization and implications for toxicity: studied by high resolution electron microscopy and electron tomography, Acta Biomater. 2 (4) (2006) 409–419.
[60] A. Magrez, et al., Cellular toxicity of carbon-based nanomaterials, Nano Lett. 6 (6) (2006) 1121–1125.
[61] C. Albrecht, et al., *In vitro* and *in vivo* activation of extracellular signal-regulated kinases by coal dusts and quartz silica, Toxicol. Appl. Pharmacol. 184 (1) (2002) 37–45.
[62] A. Bogner, et al., Wet STEM: a new development in environmental SEM for imaging nano-objects included in a liquid phase, Ultramicroscopy 104 (3–4) (2005) 290–301.
[63] A. Bogner, et al., A history of scanning electron microscopy developments: towards "wet-STEM" imaging, Micron 38 (4) (2007) 390–401.
[64] C. Burda, et al., Chemistry and properties of nanocrystals of different shapes, Chem. Rev. 105 (4) (2005) 1025–1102.
[65] P. Jain, et al., Review of some interesting surface plasmon resonance-enhanced properties of noble metal nanoparticles and their applications to biosystems, Plasmonics 2 (3) (2007) 107–118.
[66] P. Englebienne, Use of colloidal gold surface plasmon resonance peak shift to infer affinity constants from the interactions between protein antigens and antibodies specific for single or multiple epitopes, Analyst 123 (7) (1998) 1599–1603.
[67] G. Doyle, et al., Mie scattering and surface plasmon based spectroscopy for the detection of nanoparticle protein interactions, Appl. Phys. A 89 (2007) 351–355.
[68] C.L. Haynes, et al., Nanoparticle optics: the importance of radiative dipole coupling in two-dimensional nanoparticle arrays, J. Phys. Chem. B 107 (30) (2003) 7337–7342.
[69] M.K. Patel, et al., Controlled synthesis of Cu nanoparticles in fused silica and BK7 glasses using ion beam induced defects, Surf. Coat. Technol. 196 (1–3) (2005) 96–99.
[70] M.A. El-Sayed, Small is different: shape-, size-, and composition-dependent properties of some colloidal semiconductor nanocrystals, Acc. Chem. Res. 37 (5) (2004) 326–333.
[71] N.L. Rosi, C.A. Mirkin, Nanostructures in biodiagnostics, Chem. Rev. 105 (4) (2005) 1547–1562.
[72] W. Lin, et al., *In vitro* toxicity of silica nanoparticles in human lung cancer cells, Toxicol. Appl. Pharmacol. 217 (3) (2006) 252–259.
[73] Simplicity® Ultrapure Water Systems. [online catalog] 2008 [cited July 16, 2008]; Available from: http://www.millipore.com/catalogue/module/C9210.
[74] Malvern Instruments Ltd. Zetasizer Nano Series User Manual 0317, Chapter 13: Size theory. [Instrument User Manual] Feb 2008 [cited; Available from: www.indiana.edu/~physbio/images/Zetasizer%20Nano%20user%20manual%20—%20Man0317-1.1.pdf.
[75] P.C. Hiemenz, R. Rajagopalan, Principles of Colloid and Surface Science, 3rd ed., CRC Press, New York, 1997, p. 650.
[76] N.C. Nayak, K. Shin, Human serum albumin mediated self-assembly of gold nanoparticles into hollow spheres, Nanotechnol. 19 (26) (2008) 265603.
[77] B. Pan, et al., Study on interaction between gold nanorod and bovine serum albumin. Colloids Surf. A 295 (1–3) (2007) 217–222.
[78] L. Dong, et al., Cytotoxicity of single-walled carbon nanotubes suspended in various surfactants, Nanotechnol. 19 (25) (2008) 255702.
[79] W.G. Pitt, G.A. Husseini, Ultrasound in drug and gene delivery, Adv. Drug Deliv. Rev. 60 (10) (2008) 1095–1096.
[80] D.G. Castner, Surface functionalization and characterization of nanoparticles for biomedical applications, National ESCA & Surface Analysis Center for Biomedical Problems, Departments of Bioengineering and Chemical Engineering, University of Washington, 2008.
[81] A. Bruno, et al., Characterization of nanometric carbon materials by time-resolved fluorescence polarization anisotropy, Opt. Lasers Eng. 44 (7) (2006) 732–746.
[82] T.J. Burke, et al., Development and application of fluorescence polarization assays in drug discovery. Comb chem high throughput screening, 6(3) (2003) 183–194.
[83] S. Dubascoux, et al., Optimisation of asymmetrical flow field flow fractionation for environmental nanoparticles separation. J. Chromatogr. A, 1206(2) (2008) 160–165.
[84] P.S. Goyal, V.K. Aswal, Use of SANS and SAXS in Study of Nanoparticles. Int. J. Nanosci. 4 (5/6) (2005) 987-994.
[85] J.M. Veranth, In Vitro Models for Nanoparticle Toxicology, in Nanoscience and Nanotechnology, V.H. Grassian, Editor. 2008, John Wiley & Sons, Inc.
[86] P. Hughes, et al., The costs of using unauthenticated, over-passaged cell lines: how much more data do we need? BioTechniques 43 (5) (2007) 575, 577–8, 581-2 passim.
[87] R.I. Freshney, Culture of Animal Cells. 4th ed. 2000, New York: John Wiley and Sons, Inc. p. 110-111.
[88] C.M. Sayes, K.L. Reed, D.B. Warheit, Assessing toxicity of fine and nanoparticles: comparing in vitro measurements to in vivo pulmonary toxicity profiles. Toxicol. Sci. 97 (1) (2007) 163–180.
[89] F. Tao, L. Kobzik, Lung macrophage-epithelial cell interactions amplify particle-mediated cytokine release, Am. J. Respir. Cell Mol. Biol. 26 (4) (2002) 499–505.
[90] A.K. Prahalad, et al., Ambient air particles: effects on cellular oxidant radical generation in relation to particulate elemental chemistry, Toxicol. Appl. Pharmacol. 158 (2) (1999) 81–91.
[91] J.M. Veranth, et al., Inflammatory cytokines and cell death in BEAS-2B lung cells treated with soil dust, lipopolysaccharide, and surface-modified particles, Toxicol. Sci. 82 (1) (2004) 88–96.
[92] M. Baggiolini, M.P. Wymann, Turning on the respiratory burst, Trends in Biochem. Sci. 15 (2) (1990) 69–72.
[93] B. Fubini, A. Hubbard, Reactive oxygen species (ROS) and reactive nitrogen species (RNS) generation by silica in inflammation and fibrosis, Free Radical Biol. Med. 34 (12) (2003) 1507–1516.
[94] V.L. Colvin, The potential environmental impact of engineered nanomaterials. Nat Biotechnol, 21(10) (2003) 1166–1170.
[95] A.O. Choi, et al., Quantum dot-induced cell death involves Fas upregulation and lipid peroxidation in human neuroblastoma cells, J. Nanobiotechnol. 5 (2007) 1.
[96] M.L. Godek et al., Rho GTPase protein expression and activation in murine monocytes/macrophages is not modulated by model biomaterial surfaces in serum-containing in vitro cultures. J. Biomater. Sci. Polym. Ed. 17(10) (2006) 1141–1158.
[97] M.W. Sinz, S. Kim, Stem cells, immortalized cells and primary cells in ADMET assays. Drug Discovery Today: Technologies, 3(1) (2006) 79-85.
[98] S.R. Popielarski, et al., A nanoparticle-based model delivery system to guide the rational design of gene delivery to the liver. 2. *In vitro* and *in vivo* uptake results, Bioconjugate Chem. 16 (5) (2005) 1071–1080.
[99] A.M. Palazzolo-Ballance, C. Suquet, J.K. Hurst, Pathways for intracellular generation of oxidants and tyrosine nitration by a macrophage cell line, Biochemistry 46 (25) (2007) 7536–7548.
[100] S.J. Charlebois, A.U. Daniels, R.A. Smith, Metabolic heat production as a measure of macrophage response to particles from orthopedic implant materials, J. Biomed. Mater. Res. A 59 (1) (2002) 166–175.
[101] J.E. Grabowski, et al., Acidification Enhances Peritoneal Macrophage Phagocytic Activity. J. Surg. Res. 147 (2) (2008) 206-211.
[102] Y. Zhang, N. Kohler, M. Zhang, Surface modification of superparamagnetic magnetite nanoparticles and their intracellular uptake, Biomaterials 23 (7) (2002) 1553–1561.
[103] R. Wottrich, S. Diabaté, H.F. Krug, Biological effects of ultrafine model particles in human macrophages and epithelial cells in mono- and co-culture, Int. J. Hyg. Env. Health 207 (4) (2004) 353–361.
[104] G. Oberdorster, Toxicokinetics and effect of fibrous and nonfibrous particles, Inhal. Toxicol. 14 (1) (2002) 29–56.
[105] J.A. Champion, S. Mitragotri, Role of target geometry in phagocytosis, Proc. Natl. Acad. Sci. U.S.A. 103 (13) (2006) 4930–4934.
[106] S. Becker, J.M. Soukup, J.E. Gallagher, Differential particulate air pollution induced oxidant stress in human granulocytes, monocytes and alveolar macrophages, Toxicol. in Vitro 16 (3) (2002) 209–218.
[107] S. Becker, et al., Stimulation of Human and Rat Alveolar Macrophages by Urban Air Particulates: Effects on Oxidant Radical Generation and Cytokine Production, Toxicol. Appl. Pharmacol. 141 (2) (1996) 637–648.
[108] D.M. Brown, et al., Calcium and ROS-mediated activation of transcription factors and TNF-alpha cytokine gene expression in macrophages exposed to ultrafine particles, Am. J. Physiol. Lung. Cell. Mol. Physiol. 286 (2) (2004) 344–353.
[109] L. Ilium, I.M. Hunneyball, S.S. Davis, The effect of hydrophilic coatings on the uptake of colloidal particles by the liver and by peritoneal macrophages, Int. J. Pharm. 29 (1) (1986) 53–65.
[110] N. Privitera, et al., Phagocytic uptake by mouse peritoneal macrophages of microspheres coated with phosphocholine or polyethylene glycol phosphate-derived perfluoroalkylated surfactants, Int. J. Pharm. 120 (1) (1995) 73–82.
[111] S.M. Moghimi, H.M. Patel, Serum-mediated recognition of liposomes by phagocytic cells of the reticuloendothelial system - The concept of tissue specificity. Adv. Drug Deliv. Rev., 32(1–2) (1998) 45–60.
[112] F. Lemaire, et al., Toxicity assays in nanodrops combining bioassay and morphometric endpoints, PLoS ONE 2 (1) (2007) e163.
[113] S.M. Hussain, et al., *In vitro* toxicity of nanoparticles in BRL 3A rat liver cells, Toxicol. In Vitro 19 (7) (2005) 975–983.
[114] B.M. Rothen-Rutishauser, et al., Interaction of fine particles and nanoparticles with red blood cells visualized with advanced microscopic techniques. Environ. Sci. Technol. 40(14) (2006) 4353–4359.
[115] A. Radomski, et al., Nanoparticle-induced platelet aggregation and vascular thrombosis. Br. J. Pharmacol. 2005. 146(6): p. 882–893.
[116] C.-M. Lehr, Cell culture models of biological barriers, in: C.-M. Lehr (Ed.), In-vitro Test Systems for Drug Absorption and Delivery, CRC Press, 2002.
[117] S.K. Lai, et al., Rapid transport of large polymeric nanoparticles in fresh undiluted human mucus, Proc. Natl. Acad. Sci. U.S.A. 104 (5) (2007) 1482–1487.
[118] I. Behrens, et al., Comparative uptake studies of bioadhesive and non-bioadhesive nanoparticles in human intestinal cell lines and rats: the effect of mucus on particle adsorption and transport, Pharm. Res. 19 (8) (2002) 1185–1193.

[119] N.J. Abbott, L. Ronnback, E. Hansson, Astrocyte-endothelial interactions at the blood-brain barrier. Nat. Rev. Neurosci. 7(1) (2006) 41–53.
[120] S.J. McPhee, V.R. Lingappa, and W.F. Ganong, Cardiovascular Disorders: Vascular Disease, in Pathophysiology of disease: an introduction to clinical medicine. 2005, McGraw-Hill Professional: New York. p. 761.
[121] E. Oesterling, et al., Alumina nanoparticles induce expression of endothelial cell adhesion molecules, Toxicol. Lett. 178 (3) (2008) 160–166.
[122] A. Gojova, et al., Induction of Inflammation in Vascular Endothelial Cells by Metal Oxide Nanoparticles: Effect of Particle Composition. Environ. Health Perspect, 115(3) (2007) 403–409.
[123] H. Sakhalkar, et al., Leukocyte-inspired biodegradable particles that selectively and avidly adhere to inflamed endothelium *in vitro* and *in vivo*. Proc. Natl. Acad. Sci. USA 100(26) (2003) 15895–15900.
[124] S.K. Sahoo, et al., Residual polyvinyl alcohol associated with poly (,-lactide-co-glycolide) nanoparticles affects their physical properties and cellular uptake, J. Contr. Rel. 82 (1) (2002) 105–114.
[125] D. Fischer, et al., A novel non-viral vector for DNA delivery based on low molecular weight, branched polyethylenimine: effect of molecular weight on transfection efficiency and cytotoxicity, Pharm. Res. 16 (8) (1999) 1273–1279.
[126] T. Takeuchi, M. Nakajima, K. Morimoto, A human cell system for detecting asbestos cytogenotoxicity *in vitro*, Mutat. Res. 438 (1) (1999) 63–70.
[127] A. Hoshino, et al., Physicochemical properties and cellular toxicity of nanocrystal quantum dots depend on their surface modification, Nano. Lett. 4 (11) (2004) 2163–2169.
[128] A. Malugin, P. Kopeckova, J. Kopecek, HPMA copolymer-bound doxorubicin induces apoptosis in ovarian carcinoma cells by the disruption of mitochondrial function, Mol. Pharm. 3 (3) (2006) 351–361.
[129] J.J. Khandare, et al., Dendrimer versus linear conjugate: influence of polymeric architecture on the delivery and anticancer effect of paclitaxel, Bioconjugate Chem. 17 (6) (2006) 1464–1472.
[130] Y. Hattori, W.-X. Ding, Y. Maitani, Highly efficient cationic hydroxyethylated cholesterol-based nanoparticle-mediated gene transfer *in vivo* and *in vitro* in prostate carcinoma PC-3 cells, J. Contr. Rel. 120 (1–2) (2007) 122–130.
[131] Y. Liu, et al., New poly(d-glucaramidoamine)s induce DNA nanoparticle formation and efficient gene delivery into mammalian cells, J. Am. Chem. Soc. 126 (24) (2004) 7422–7423.
[132] P. Marschall, N. Malik, Z. Larin, Transfer of YACs up to 2.3 Mb intact into human cells with polyethylenimine, Gene Ther. 6 (9) (1999) 1634–1637.
[133] P. Campeau, et al., Transfection of large plasmids in primary human myoblasts, Gene Ther. 8 (18) (2001) 1387–1394.
[134] I. Fajac, et al., Histidylated polylysine as a synthetic vector for gene transfer into immortalized cystic fibrosis airway surface and airway gland serous cells, J. Gene. Med. 2 (5) (2000) 368–378.
[135] T. Sato, T. Ishii, Y. Okahata, *In vitro* gene delivery mediated by chitosan. Effect of pH, serum, and molecular mass of chitosan on the transfection efficiency, Biomaterials 22 (15) (2001) 2075–2080.
[136] N. Lewinski, V. Colvin, R. Drezek, Cytotoxicity of nanoparticles, Small 4 (1) (2008) 26–49.
[137] A.L. Lewis, M. Driver, Blending in with the body, J. Chem. Educ. 79 (3) (2002) 321–326.
[138] S.T. Stern, S.E. McNeil, Nanotechnology safety concerns revisited, Toxicol. Sci. 101 (1) (2008) 4–21.
[139] "Biological Evaluation of Medical Devices," ISO 10993, parts 1–12. (Geneva: International Organization for Standardization, various dates).
[140] "Use of International Standard ISO 10993, Biological evaluation of medical devices—Part 1: Evaluation and Testing" G95-1 (Rockville, MD: Department of Health and Human Services, FDA, 1995).
[141] A. Kocbach, et al., Differential binding of cytokines to environmentally relevant particles: A possible source for misinterpretation of *in vitro* results, Toxicol. Lett. 176 (2) (2008) 131–137.
[142] J. Salaklang, et al., Superparamagnetic Nanoparticles as a Powerful Systems Biology Characterization Tool in the Physiological Context. Angewandte Chemie International Edition, 47 (41) (2008) 7857–7860.
[143] Invitrogen. Adaptation culture of cell cultures to a serum-free medium. [online information sheet] [cited. July 15, 2008]; Available from: http://tools.invitrogen.com/content/sfs/appendix/Cell_Culture/Adaptation%20Of%20Cells%20For%20Serum-Free%20Medium.pdf.
[144] R.J. Parod, J.D. Brain, Immune opsonin-independent phagocytosis by pulmonary macrophages, J. Immunol. 136 (6) (1986) 2041–2047.
[145] L. Walker, et al., Activation of mouse peritoneal macrophages by maintenance in serum-free medium, Immunology 73 (1) (1991) 109–113.
[146] C. Schulze, et al., Not ready to use – overcoming pitfalls when dispersing nanoparticles in physiological media, Nanotoxicology 2 (2) (2008) 51–61.
[147] R. Duffin, N.L. Mills, K. Donaldson, Nanoparticles – a thoracic toxicology perspective, Yonsei Med. J. 48 (4) (2007) 561–572.
[148] N. Kuzkaya, et al., Interactions of peroxynitrite, tetrahydrobiopterin, ascorbic acid, and thiols: implications for uncoupling endothelial nitric-oxide synthase, J. Biol. Chem. 278 (25) (2003) 22546–22554.
[149] C.A. Cohn, S.R. Simon, M.A. Schoonen, Comparison of fluorescence-based techniques for the quantification of particle-induced hydroxyl radicals, Part Fibre Toxicol. 5 (2008) 2.
[150] C. Monteiller, et al., The pro-inflammatory effects of low-toxicity low-solubility particles, nanoparticles and fine particles, on epithelial cells *in vitro*: the role of surface area, Occup. Environ. Med. 64 (9) (2007) 609–615.
[151] G. Jia, et al., Cytotoxicity of carbon nanomaterials: single-wall nanotube, multi-wall nanotube, and fullerene. Environ. Sci. Technol. 39 (5) (2005) 1378–1383.
[152] C. Santoro, N. Duchsherer, D. Grainger, Minimal *in vitro* antimicrobial efficacy and ocular cell toxicity from silver nanoparticles, NanoBioTechnology 3 (2) (2007) 55–65.
[153] S.J. Compton, C.G. Jones, Mechanism of dye response and interference in the Bradford protein assay, Anal. Biochem. 151 (2) (1985) 369–374.
[154] R.R. Tice, et al., Single cell gel/comet assay: guidelines for *in vitro* and *in vivo* genetic toxicology testing, Environ. Mol. Mutagen. 35 (3) (2000) 206–221.
[155] W. Wang, et al., Secretion of TNF-alpha by monocyte thp-1 stimulated by wear particles and apoptosis of osteoblasts induced by TNF-alpha, Wujing Yixueyuan Xuebao 15 (5) (2006) 423–426 C4.
[156] S.Y. Yang, et al., Diverse cellular and apoptotic responses to variant shapes of UHMWPE particles in a murine model of inflammation, Biomaterials 23 (17) (2002) 3535–3543.
[157] D.P. Pioletti, et al., Gene expression analysis of osteoblastic cells contacted by orthopedic implant particles, J. Biomed. Mater. Res. A 61 (3) (2002) 408–420.
[158] A. Arenz, et al., Gene expression modulation in A549 human lung cells in response to combustion-generated nano-sized particles, Ann. N. Y. Acad. Sci. 1091 (2006) 170–183.
[159] D.H. Kim, et al., Response of monocytes exposed to phagocytosable particles and discs of comparable surface roughness, Biomaterials 28 (29) (2007) 4231–4239.
[160] The most flexible way to multiplex with beads. BD™ Cytometric Bead Array System [online brochure] 2007 [cited July 11, 2008]; Available from: http://www.softflow.hu/Kereskedelem/XEUR1178-02%20-%20CBA%20brochure.pdf.
[161] What are multiplexed ELISAs? Multiplexed ELISA [online product information page] [cited July 16, 2008]; Available from: http://www.quansysbio.com/ELISA/whatAre.html.
[162] SITE VISIT: sorting out cytokines, Science 288 (5469) (2000) 1131b.
[163] H. Ibelgaufts, COPE: Horst Ibelgaufts' Cytokines & Cells Online Pathfinder Encyclopaedia. [cited January 23, 2009]; Available from: www.copewithcytokines.org.
[164] J. Rejman, et al., Size-dependent internalization of particles via the pathways of clathrin- and caveolae-mediated endocytosis, Biochem. J. 377 (Pt 1) (2004) 159–169.
[165] S.C. Silverstien, R.M. Steinman, Z.A. Cohn, Endocytosis, Annu. Rev. Biochem. 46 (1997) 669–722.
[166] R. Bronson, Is the oocyte a non-professional phagocyte? Hum. Reprod. Updat. 1998 4(6): p. 763-75
[167] I. Mellman, Endocytosis and molecular sorting. Annu. Rev. Cell Dev. Biol. Environ. 12 (1996): p. 575-625.
[168] K. Greish, Enhanced permeability and retention of macromolecular drugs in solid tumors: a royal gate for targeted anticancer nanomedicines, J. Drug Target. 15 (7-8) (2007) 457–464.
[169] Y. Geng, et al., Shape effects of filaments versus spherical particles in flow and drug delivery, Nat. Nano. 2 (4) (2007) 249–255.
[170] M.R. Lorenz, et al., Uptake of functionalized, fluorescent-labeled polymeric particles in different cell lines and stem cells, Biomaterials 27 (14) (2006) 2820–2828.
[171] J. Suh, M. Dawson, J. Hanes, Real-time multiple-particle tracking: applications to drug and gene delivery, Adv. Drug Deliv. Rev. 57 (1) (2005) 63–78.
[172] J.C. Crocker, B.D. Hoffman, E.D. YuLi Wang, Dennis, Multiple-particle Tracking and Two-point Microrheology in Cells, in Methods in Cell Biology, Academic Press, 2007, pp. 141–178.
[173] P. Ghafari, et al., Impact of carbon nanotubes on the ingestion and digestion of bacteria by ciliated protozoa, Nat. Nano 3 (6) (2008) 347–351.
[174] E. Jan, et al., High-content Screening as a Universal Tool for Fingerprinting of Cytotoxicity of Nanoparticles. ACS Nano, 2008.
[175] D.B. Warheit, et al., Development of a base set of toxicity tests using ultrafine TiO2 particles as a component of nanoparticle risk management, Toxicol. Lett. 171 (3) (2007) 99–110.
[176] G. Oberdorster, et al., Principles for characterizing the potential human health effects from exposure to nanomaterials: elements of a screening strategy, Part Fibre Toxicol. 2 (2005) 8.
[177] J.G. Teeguarden, et al., Particokinetics *in vitro*: dosimetry considerations for *in vitro* nanoparticle toxicity assessments, Toxicol. Sci. 95 (2) (2007) 300–312.
[178] NIST reference materials are 'gold standard' for bio-nanotech research. Nanotechnology Today [online news article] 2008 January 20, 2008 [cited July 5, 2008]; Available from: http://nanotechnologytoday.blogspot.com/2008/01/nist-reference-materials-are-gold.html.
[179] H. Yamawaki, N. Iwai, Cytotoxicity of water-soluble fullerene in vascular endothelial cells, Am. J. Physiol. Cell Physiol. 290 (6) (2006) C1495–C1502.
[180] C.M. Sayes, et al., Nano-C60 cytotoxicity is due to lipid peroxidation, Biomaterials 26 (36) (2005) 7587–7595.
[181] K. Pulskamp, S. Diabat, H.F. Krug, Carbon nanotubes show no sign of acute toxicity but induce intracellular reactive oxygen species in dependence on contaminants, Toxicol. Lett. 168 (1) (2007) 58–74.
[182] D. Pantarotto, et al., Translocation of bioactive peptides across cell membranes by carbon nanotubes, Chem. Commun. (Camb.) (1) (2004) 16–17.
[183] M. Bottini, et al., Multi-walled carbon nanotubes induce T lymphocyte apoptosis, Toxicol. Lett. 160 (2) (2006) 121–126.
[184] R. Shukla, et al., Biocompatibility of gold nanoparticles and their endocytotic fate inside the cellular compartment: a microscopic overview, Langmuir 21 (23) (2005) 10644–10654.
[185] C.H. Su, et al., Nanoshell magnetic resonance imaging contrast agents, J. Am. Chem. Soc. 129 (7) (2007) 2139–2146.
[186] H. Takahashi, et al., Modification of gold nanorods using phosphatidylcholine to reduce cytotoxicity, Langmuir 22 (1) (2006) 2–5.
[187] T.R. Pisanic II, et al., Nanotoxicity of iron oxide nanoparticle internalization in growing neurons, Biomaterials 28 (16) (2007) 2572–2581.

[188] K. Muller, et al., Effect of ultrasmall superparamagnetic iron oxide nanoparticles (Ferumoxtran-10) on human monocyte-macrophages *in vitro*, Biomaterials 28 (9) (2007) 1629–1642.
[189] W.W. Yu, et al., Aqueous dispersion of monodisperse magnetic iron oxide nanocrystals through phase transfer, Nanotechnology 17 (17) (2006) 4483–4487.
[190] J.P. Ryman-Rasmussen, J.E. Riviere, N.A. Monteiro-Riviere, Surface coatings determine cytotoxicity and irritation potential of quantum dot nanoparticles in epidermal keratinocytes, J. Invest. Dermatol. 127 (1) (2007) 143–153.
[191] C.M. Sayes, et al., Correlating nanoscale titania structure with toxicity: a cytotoxicity and inflammatory response study with human dermal fibroblasts and human lung epithelial cells, Toxicol. Sci. 92 (1) (2006) 174–185.
[192] J.E. Schroeder, et al., Folate-mediated tumor cell uptake of quantum dots entrapped in lipid nanoparticles, J. Contr. Rel. 124 (1–2) (2007) 28–34.
[193] Y. Hu, et al., Effect of PEG conformation and particle size on the cellular uptake efficiency of nanoparticles with the HepG2 cells, J. Controlled Release 118 (1) (2007) 7–17.
[194] S. Chono, K. Morimoto, Uptake of dexamethasone incorporated into liposomes by macrophages and foam cells and its inhibitory effect on cellular cholesterol ester accumulation, J. Pharm. Pharmacol. 58 (9) (2006) 1219–1225.
[195] L.K. Limbach, et al., Oxide nanoparticle uptake in human lung fibroblasts: effects of particle size, agglomeration, and diffusion at low concentrations, Environ. Sci. Technol. 39 (23) (2005) 9370–9376.
[196] C. Foged, et al., Particle size and surface charge affect particle uptake by human dendritic cells in an *in vitro* model, Int. J. Pharm. 298 (2) (2005) 315–322.
[197] S. Mishra, P. Webster, M.E. Davis, PEGylation significantly affects cellular uptake and intracellular trafficking of non-viral gene delivery particles, Eur. J. Cell Biol. 83 (2004) 97–111.
[198] M. Yan, et al., Despite differences between dendritic cells and Langerhans cells in the mechanism of papillomavirus-like particle antigen uptake, both cells cross-prime T cells, Virology 324 (2) (2004) 297–310.
[199] I. Behrens, et al., Comparative uptake studies of bioadhesive and non-bioadhesive nanoparticles in human intestinal cell lines and rats: the effect of mucus on particle adsorption and transport, Pharm. Res. 19 (8) (2002) 1185–1193.
[200] T.K. Jain, et al., Biodistribution, clearance, and biocompatibility of iron oxide magnetic nanoparticles in rats, Mol. Pharm. 5 (2) (2008) 316–327.
[201] Y.-C. Chung, I.H. Chen, C.-J. Chen, The surface modification of silver nanoparticles by phosphoryl disulfides for improved biocompatibility and intracellular uptake, Biomaterials 29 (12) (2008) 1807–1816.
[202] C. Rothkopf, et al., Uptake of phosphatidylserine-containing liposomes by liver sinusoidal endothelial cells in the serum-free perfused rat liver, Biochimica et Biophysica Acta (BBA) – Biomembranes 1668 (1) (2005) 10–16.
[203] G.R. Harper, et al., Steric stabilization of microspheres with grafted polyethylene oxide reduces phagocytosis by rat Kupffer cells *in vitro*, Biomaterials 12 (7) (1991) 695–700.
[204] B.S. De Juan, et al., Cytotoxicity of doxorubicin bound to poly(butyl cyanoacrylate) nanoparticles in rat glioma cell lines using different assays, J. Drug Target 14 (9) (2006) 614–622.
[205] C.H. Lohmann, et al., Phagocytosis of wear debris by osteoblasts affects differentiation and local factor production in a manner dependent on particle composition, Biomaterials 21 (6) (2000) 551–561.
[206] C.M. Tato, D.J. Cua, SnapShot: cytokines I, Cell 132 (2) (2008) 324.e1–324.e2.
[207] C.M. Tato, D.J. Cua, SnapShot: cytokines II, Cell 132 (3) (2008) 500.
[208] C.M. Tato, D.J. Cua, SnapShot: cytokines III, Cell 132 (5) (2008) 900.e1–900.e2.
[209] C.M. Tato, D.J. Cua, SnapShot: cytokines IV, Cell 132 (6) (2008) 1062.e1–1062.e2.

1.7 Statement of objectives

The purpose of the preceding Introduction was to orient the reader to the state of toxicity assessment in the field of nanotechnology with examples of the challenges and adaptations that are common to nanoanalyses and nanosystems. Because of the unique reactivities and size constraints characteristic to many nanomaterials, few (if any) ideal assays exist for the assessment of nanoparticle toxicity. The growing utilization of nanomaterials in consumer products and medical applications directly increases the potential for human exposure and demands the characterization of nanotechnology impacts upon biological systems. Thus, it is needful both to increase understanding toward existing assay applicability and to develop new methods for nanotoxicity assessment.

The long-term objectives of this project are 1) to build understanding toward the unintended consequences of nanoparticles on living systems and 2) to develop a toolkit for the assessment of currently underappreciated mechanisms of nanoparticle toxicity in blood. The work described herein seeks to advance nanoparticle toxicity assessment with expanded assessment and characterization of nanoparticle-mediated coagulopathy and platelet activation. The present characterization of nanoparticle-mediated coagulopathy begins with the application of common platelet function and activation assays to assess the toxicity mechanisms of severely activating, generation-7 cationic dendrimers upon platelet functions (Chapter 2). This is next complimented by a set of studies elucidating the basis for coagulopathic responses previously observed in G7-NH2-injected rodents by probing nanoparticle interactions with the molecular elements of coagulation (Chapter 3). Finally, the immunologic effects of nanoparticle surface adsorbates are reviewed (Chapter 4) as a segue to the assessment of nanoparticle-adsorbed lipopolysaccharide (LPS) toxin by the Limulus Amoebocyte Lysate (LAL) assay as a surrogate for coagulogenic reactions observable *in vivo* following injection of LPS-contaminated nanoparticles (Chapter 5).

The content and results of Chapters 1, 2, and 3 have been published in peer-reviewed journals, Chapter 4 has been published as part of the *Handbook of Immunological Properties of Nanomaterials*, and Chapter 5 has been submitted for publication in the Journal of the American Chemistry Society.

CHAPTER 2

CATIONIC PAMAM DENDRIMERS DISRUPT KEY PLATELET FUNCTIONS

molecular pharmaceutics

Article

pubs.acs.org/molecularpharmaceutics

Cationic PAMAM Dendrimers Disrupt Key Platelet Functions

Clinton F. Jones,[†] Robert A. Campbell,[‡] Zechariah Franks,[‡] Christopher C. Gibson,[‡,∥] Giridhar Thiagarajan,[§,∥] Adriana Vieira-de-Abreu,[‡,⊥] Sivaprasad Sukavaneshvar,[#] S. Fazal Mohammad,[#,▽,○] Dean Y. Li,[‡,◆,¶] Hamidreza Ghandehari,[†,§,∥] Andrew S. Weyrich,[‡,△] Benjamin D. Brooks,[†] and David W. Grainger*[,†,§,∥]

[†]Department of Pharmaceutics and Pharmaceutical Chemistry, Health Sciences, University of Utah, Salt Lake City, Utah 84112, United States

[‡]Program in Molecular Medicine, University of Utah School of Medicine, Salt Lake City, Utah 84132, United States

[§]Utah Center for Nanomedicine, Nano Institute of Utah, University of Utah, Salt Lake City, Utah 84108, United States

[∥]Department of Bioengineering, University of Utah, Salt Lake City, Utah 84112, United States

[⊥]Laboratório de Imunofarmacologia, Instituto Oswaldo Cruz, Fiocruz, Rio de Janeiro, Brazil

[#]Thrombodyne, Inc., Salt Lake City, Utah 84103, United States

[▽]Department of Pathology, University of Utah, Salt Lake City, Utah 84132, United States

[○]Utah Artificial Heart Institute, University of Utah, Salt Lake City, Utah 84112, United States

[◆]Division of Cardiology, Department of Internal Medicine, University of Utah, Salt Lake City, Utah 84132, United States

[¶]Department of Oncological Sciences, University of Utah, Salt Lake City, Utah 84132, United States

[△]Divisions of Pulmonary and Critical Care Medicine, Department of Internal Medicine, University of Utah, Salt Lake City, Utah 84132, United States

Supporting Information

ABSTRACT: Poly(amidoamine) (PAMAM) dendrimers have been proposed for a variety of biomedical applications and are increasingly studied as model nanomaterials for such use. The dendritic structure features both modular synthetic control of molecular size and shape and presentation of multiple equivalent terminal groups. These properties make PAMAM dendrimers highly functionalizable, versatile single-molecule nanoparticles with a high degree of consistency and low polydispersity. Recent nanotoxicological studies showed that intravenous administration of amine-terminated PAMAM dendrimers to mice was lethal, causing a disseminated intravascular coagulation-like condition. To elucidate the mechanisms underlying this coagulopathy, *in vitro* assessments of platelet functions in contact with PAMAM dendrimers were undertaken. This study demonstrates that cationic G7 PAMAM dendrimers activate platelets and dramatically alter their morphology. These changes to platelet morphology and activation state substantially altered platelet function, including increased aggregation and adherence to surfaces. Surprisingly, dendrimer exposure also attenuated platelet-dependent thrombin generation, indicating that not all platelet functions remained intact. These findings provide additional insight into PAMAM dendrimer effects on blood components and underscore the necessity for further research on the effects and mechanisms of PAMAM-specific and general nanoparticle toxicity in blood.

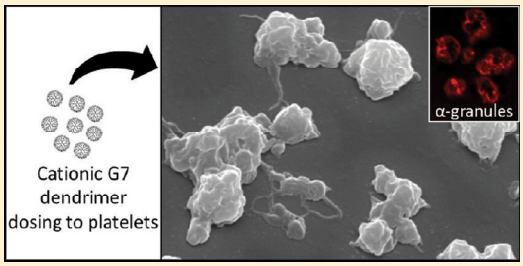

KEYWORDS: *nanotoxicity, PAMAM dendrimers, platelet activation, biocompatibility, thrombin generation*

INTRODUCTION

Dendrimers are a specialized subclass of hyperbranched polymers, produced from stepwise synthetic strategies that yield well-defined, monodisperse molecular structures. Their unique molecular structure features characteristic repeated chemical units, each with multiple equivalent terminal groups, that, through repeated end group protection and condensation chemistries, yield multifunctional, single-molecule nanoparticles with a high degree of structural and chemical consistency, defined surface chemistry, and low polydispersity.[1] Different generations of dendrimers produce different sizes and densities

Received: November 27, 2011
Revised: March 31, 2012
Accepted: April 12, 2012
Published: April 12, 2012

dx.doi.org/10.1021/mp2006054 | *Mol. Pharmaceutics* 2012, 9, 1599−1611

of terminal functional groups, each with distinct properties. With diverse technological potential, some dendrimer chemistries are proposed for a variety of pharmaceutical applications, including cell transfection,[2,3] bioimaging,[4] and drug delivery.[5−10] In particular, dendrimers receive increasing attention for drug delivery in two distinct approaches: (1) as a platform for conjugated drug molecules, especially in cancer therapeutics,[6,11−15] and (2) as an encapsulating mechanism to improve drug solubility.[16,17]

Presently, the most direct route for drug administration is via the circulatory system (i.e., intravenous) because blood-borne active compounds reach tissue targets and less-accessible sites in short times via vascular transport. However, a major problem with this strategy is that blood proteins (∼70 mg/mL in plasma) and cells (40−45% packed cell volume in blood) interact, bind, and complex with polymers and nanoparticles, often interfering with drug transport, targeting, clearance, and bioavailability.[18] Dendrimers are no exception; the ubiquitous binding of dendrimers and dendritically captured drugs to blood cells, platelets, plasma proteins, and the vascular endothelium will certainly affect drug efficacy.[19] Significantly, undesired or uncontrolled dendrimer interactions with blood components and host tissues can readily produce serious toxicity.[20−23]

Cationic (amine-terminated) polyamidoamine (PAMAM) dendrimers have been shown *in vitro* to destabilize erythrocyte membranes,[24] potentially inducing hemolysis in a manner that is both dose- and generation-dependent.[17,25] Other studies have also shown that high-generation PAMAM dendrimers induce membrane composition-specific alterations in anionic lipid vesicle morphology.[19,26] However, of greatest concern are murine experiments involving injections of high-generation PAMAM dendrimers (G7-NH_2) that resulted in hemolysis and catastrophic coagulopathy,[27] and also a very recent *in vitro* study showing size- and surface charge-dependence of PAMAM dendrimer-induced platelet aggregation.[28] For validating any *in vivo* application, careful assessment of dendrimer toxicities and biological interactions are essential, especially as injected, systemically bioavailable drugs and drug carriers. Currently, dendrimer toxicity remains relatively uncharacterized,[19,25,29−33] particularly in the specific and essential case of hematologic toxicity. Understanding specific relationships between dendrimer size and chemistry and their blood interactions and biodistributions would enable the required predictive models for assessing possible human toxicities[34] and, importantly, inform structure−property relationships for improving rational designs for *in vivo* use.

Platelets are anucleate, 2−3 μm diameter, cytoplasmic discs—the smallest formed membranous element in blood. They comprise a major metabolically active blood component, circulating constantly at $\sim 2.5 \times 10^8$ platelets/mL of blood, are highly responsive to diverse physical and biochemical stimuli with potent coagulation and growth factors, and are responsible primarily for hemostasis. Until recently, platelets have not received significant research attention regarding possible mechanisms of nanoparticle toxicity. However, platelet activation by injected drug delivery nanoconstructs could readily result in unintended—even fatal—consequences in host circulation. This potential was recently demonstrated for PAMAM dendrimers injected into systemic blood circulation in mice.[27,28] Additional mechanistic information on platelet activation and dendrimer−platelet interactions that produce these problems is required to both avoid undesired dendrimer toxicities in blood and guide dendrimer designs to avoid these issues.

In this study, we compare cationic, anionic, and polar uncharged (e.g., -NH_2, -COOH, and -OH terminated) high-generation dendrimer effects on *in vitro* platelet morphology, activation states, and hemostatic functions. Data shown for PAMAM dendrimer−platelet reactivity compliment recently published related data suggesting that cationic PAMAM dendrimers cause platelet activation and aggregation[28] by further elucidating mechanisms by which higher generation (G7), more densely cationic PAMAM dendrimers affect platelet morphology and functions in blood.

MATERIALS AND METHODS

Preparation and Characterization of FITC-Labeled PAMAM Dendrimers. G6.5-COOH, G7-OH, and G7-NH_2 PAMAM dendrimers with an ethylenediamine core were purchased from Sigma Aldrich (St. Louis, MO) and fractionated on a preparative size exclusion column (SEC, Sephadex Hiload 75, GE Healthcare, Piscataway, NJ) to remove low-molecular-weight oligomers. Characterization of the native dendrimers has been reported previously.[27] PAMAM dendrimers were labeled with fluorescein isothiocyanate (FITC) (for G7-NH_2 and G7-OH dendrimers) or 5-(aminomethyl)-fluorescein (for G6.5-COOH dendrimers), as reported previously.[35] Briefly, G7-OH (12.8 μM) and FITC (25.6 μM) (Sigma Aldrich, USA) were reacted in a molar ratio of 1:2 with a molar equivalent of triethylamine (Sigma-Alrich, USA) in DMSO for 72 h under a steady stream of nitrogen gas. G7-NH_2 (12.8 μM) and FITC (25.6 μM) were each dissolved in DMSO and conjugated overnight in nitrogen atmosphere at room temperature with feed molar ratios of 1:2. G6.5-COOH (13 μM) dissolved in DMSO and carboxyl groups were activated using NHS/EDC reagents (Sigma-Alrich, USA) at the molar ratio 1:4. Subsequently, 5-(aminomethyl)fluorescein (25 μM in DMSO) (Sigma-Aldrich, USA) was added to this mixture and allowed to react overnight under nitrogen at the molar ratio 1:2 (Supporting Information Scheme 1). Fluorescently labeled PAMAM dendrimers were dialyzed against deionized water using 500 Da molecular-weight-cutoff membranes (Spectrum Laboratories, Inc., Rancho Dominguez, USA) and subsequently fractionated on a preparative Sephadex Hiload 75 size exclusion column (SEC, GE Healthcare, Piscataway, NJ) to remove residual, free FITC, and other small molecular weight impurities. Fractionated PAMAM dendrimers were dialyzed again and lyophilized. Purified FITC-labeled PAMAM dendrimers were then characterized at unbuffered, neutral pH as previously described for the unlabeled dendrimers.[27] Zeta potential was measured using a Malvern Zetasizer NanoZS (Malvern, U.K.), particle size was verified against unlabeled dendrimer size by SEC on an analytical Superose 6 10/300 GL column (GE Healthcare, Piscataway, USA) with an elution buffer of PBS/acetonitrile (80:20) with 0.1% sodium azide, and dye labeling densities were determined at neutral pH by optical absorbance (495 nm) compared to free FITC standards and background-subtracted unlabeled dendrimer absorbance on a Cary 400 Bio UV−vis spectrophotometer (Varian, Palo Alto, CA) at ambient temperature (Supporting Information Figure 1).

Whole Blood Collection and Plasma Preparation. The University of Utah Institutional Review Board approved this study, and all subjects provided informed consent. Human peripheral venous blood (25−50 mL) from healthy, medi-

cation-free adult subjects was drawn into acid-citrate-dextrose (1.4 mL of ACD/8.6 mL of blood) through a standard venipuncture technique and used immediately upon collection. Plasma was harvested by centrifuging whole blood at 500*g* for 20 min and then once more at 13,000*g* for 2 min to remove any remaining cell contaminants.

Platelet Isolation. Human platelets were isolated from whole blood and suspended in M199 medium (Lonza, Walkersville, USA) (1×10^8 platelets/mL, final) as previously described.[36−38] Previous work has demonstrated that leukocyte contamination is minimal in platelet isolates obtained by this protocol.[38,39]

Thrombin Generation Assays. Whole blood was treated with saline controls or dendrimers for either 30 min or 4 h at 37 °C. Platelet-rich plasma (PRP) was isolated by centrifuging whole blood for 20 min at 150*g*. In some experiments, PRP was isolated before addition of agonist and treated for 30 min or 4 h. Additional $CaCl_2$ was added to the substrate reagent to reach a final concentration of 15 mM $CaCl_2$. Reagents were combined with sample plasma in duplicate according to manufacturer's instructions in a 96-well plate and read every minute for 90 min. Thrombin generation was measured with a Synergy HT multi Detection Microplate Reader (Bio-Tek Instruments, Winooski, USA) at an excitation/emission wavelength of 360 nm/460 nm. Thrombin calibration curves were performed and analyzed according to manufacturer's instructions. Falcon PRO-BIND 96-well flat bottom plates (Becton Dickinson, Franklin Lakes, USA) were used to perform the fluorogenic reactions. Fluorogenic substrate (Z-Gly-Gly-Arg-AMC; 0.5 mM, final), and RC high reagent (7.16 pM TF and 0.32 μM phospholipid micelles, final) were purchased from Technoclone (Vienna, Austria).

Immunoassays and Flow Cytometry. Platelets resuspended in M199 were treated with dendrimer or thrombin at indicated concentrations and for indicated times and centrifuged at 13000*g* for 2 min to harvest cell-free supernatants. Regulated on Activation Normal T-Expressed and Secreted (RANTES) and Platelet Factor 4 (PF4) were measured using ELISA (R&D Systems, Minneapolis, MN).[40,41] In separate experiments, platelets treated with FITC-labeled dendrimers for indicated times were stained with antihuman P-selectin (CD62) phycoerythrin (PE) (BD Biosciences, San Jose, CA). Platelets were analyzed by flow cytometry using a FACScalibur (BD Biosciences, USA). Experiments were conducted and analyzed in biological triplicate.

Confocal Microscopy. Freshly isolated platelets were fixed either immediately to assess baseline morphology or after 30-min treatment with human thrombin (0.1 U/mL, final) (Sigma-Aldrich) or FITC-labeled dendrimers (100 μg/mL final). At the end of each experimental period, buffered paraformaldehyde (2% final) was added directly to the washed platelets as previously described to maintain the native cell morphology. Fixed platelets (10,000 total for each sample) were subsequently layered onto Vectabond-coated coverslips (Vector Laboratories, USA) using a cytospin centrifuge (Shandon Cytospin; Thermo Fisher Scientific, USA). Wheat germ agglutinin (WGA, Alexa 555-labeled, Invitrogen, Carlsbad, USA) was used as a counterstain to stain granules and membranes of platelets.[42] Fluorescence microscopy and high-resolution confocal reflection microscopy was performed using an Olympus Fluoview FV1000 confocal-scanning microscope equipped with a 60×/1.42 NA oil objective for viewing platelets. An Olympus FVS-PSU/IX2-UCB camera and scanning unit and Olympus Fluoview and FV1000 image acquisition software (version 5.0) were used for recording.

Platelet Aggregometry. Dendrimers were added to citrated human whole blood or PRP to a final concentration of 100 μg/mL, and aggregation in whole blood was then measured by impedance in a whole blood aggregometer (model 592, Chronolog, Havertown, PA) or by turbidity in a light transmission aggregometer (model 560CA, Chronolog, Havertown, USA) immediately after addition of dendrimer or agonist. ADP (10 μM final, Sigma Aldrich, St. Louis, MO) was used as a positive control.

Scanning Electron Microscopy (SEM). PRP was treated with dendrimers (100 μg/mL, final) or thrombin (0.1 U/mL, final) for 45 min at room temperature. The PRP was then diluted 1:20 with Karnovsky's fixative. A small aliquot of each platelet treatment was pipetted onto glass coverslips, and the platelets were allowed to settle to the glass surface for 30 min before dehydration proceeded on the coverslip by graded ethanol solutions. Coverslips were mounted on SEM stubs, sputtered with gold for 5 min, and imaged using a JEOL CarryScope (JCM-5700). Images were taken at 2500× with a 34−55 mm working distance and a 20 kV accelerating voltage.

Platelet Shear-flow Adhesion Assay. Platelet interaction with adsorbed fibrinogen was assayed under controlled shear conditions using a parallel plate flow chamber (Ibidi 0.4 VI μ-plates, Ibidi GmbH, Germany) with six independent wells on a standard microscope slide-sized plate. Each well was coated with 0.5 mg/mL human fibrinogen at 37 °C for at least 30 min for monolayer adsorption. Platelets were fluorescently prelabeled by incubating with 1 μM CellTracker Orange CMRA (Invitrogen) for 1 h followed by a wash step. In some experiments, platelets were also treated with abciximab (0.136 μM final, University of Utah Pharmacy) for 30 min before treatment with the designated agonist. Immediately prior to platelet perfusion, the chamber was rinsed three times with PBS and mounted in a 37 °C humidified chamber (Okolab Via Campana, Italy) on an Olympus IX-81 epifluorescent microscope. Isolated platelets were treated with saline, thrombin (0.5 U/mL, final), or dendrimers (100 μg/mL, final). Thrombin-treated platelets were incubated for 5 min before perfusion, and saline- or G7-NH_2-treated platelets were immediately perfused through the flow chamber at a wall shear rate of 200 s^{-1} (1.14 mL/min flow rate) using a Harvard Apparatus syringe pump (Holliston, USA). Real-time platelet adhesion to the bottom chamber surface was viewed with a 10× objective with mercury lamp illumination (100 W, 589/15 nm excitation, 640−675 emission), and images were captured at 1-s intervals for 360 s using an ORCA-ER monochrome CCD camera (Hamamatsu). The camera and shutters were controlled by Metamorph imaging software (version 7, Meta Imaging). All image processing and analysis were performed on image stacks in ImageJ software (National Institutes of Health, USA). Two subtraction methods were employed during image processing to remove unbound bulk platelet fluorescence and intrinsic camera field noise: fluorescence from unbound platelets was eliminated by its isolation (by sequence subtraction of an identical stack offset by one image, ImageJ image calculator function) and direct subtraction of the resulting isolated unbound platelet fluorescence image sequence (ImageJ image calculator function) from the original stack. Subsequently, image stacks were background-subtracted (50-pixel sliding parabaloid options) and thresholded (dark background option).

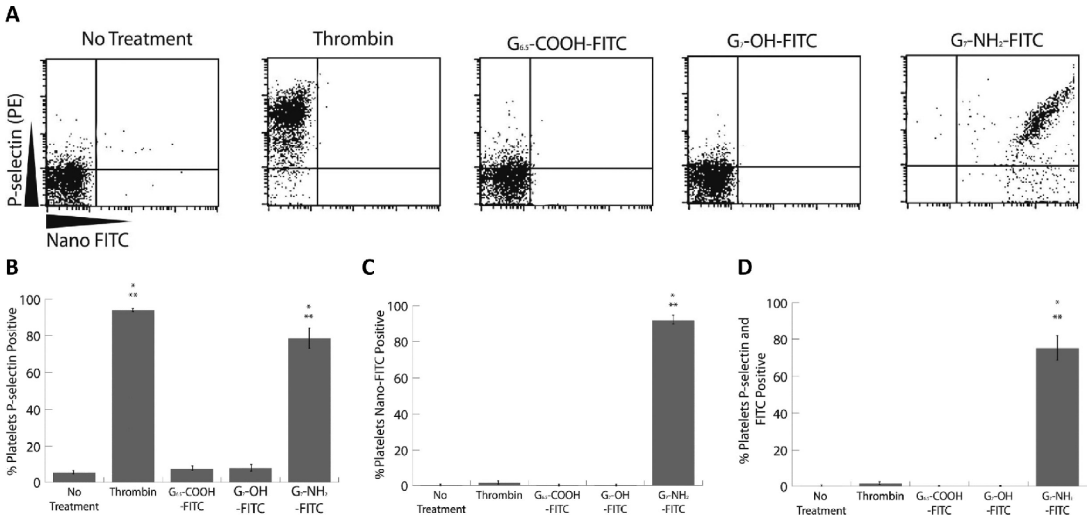

Figure 1. G7-NH_2-FITC dendrimers induce P-selectin expression on platelets (A–D). Platelets were treated with saline, thrombin, or 100 μg/mL of different functionalized dendrimers for 30 min. Thrombin induces P-selectin expression while the G6.5-COOH-FITC and G7-OH-FITC dendrimer-treated platelets express significantly less P-selectin and negatively stain for FITC, indicating no dendrimer binding. In contrast, G7-NH_2-FITC treated platelets express P-selectin and stain positively for FITC, suggesting dendrimer binding. The * indicates significantly different than no treatment ($p < 0.05$). The ** indicates significantly different than G6.5-COOH-FITC and G7-OH-FITC dendrimer ($p < 0.05$). Flow diagrams are from a single experiment and are representative of three independent experiments (A). The data represent the mean ± SEM of at least three independent experiments.

Individual platelet/aggregate size and adherent platelet coverage area were quantified by image analysis (ImageJ analyze particles function with the following criteria: dark background; particle size, 20-inf; particle circularity, 0.1–1.0), and results were exported to Excel (Microsoft) for statistical analysis. Data was grouped by treatment, and parameters analyzed included mean adhered platelet/aggregate size and average initial platelet binding rate (average of slopes for area covered by platelets vs time for first 90 s).

Statistical Analysis. Continuous variables were expressed as mean ± standard error of the mean. Pairwise comparisons were performed using a Student's *t* test. For multiple comparisons, a one-way analysis of variance (ANOVA) with a Tukey's posthoc test was used to control for error of multiple testing. Analysis for censored data was performed for lag time and time to peak. For platelet microfluidics assay, statistical analyses were performed for a given parameter and treatment by *t* tests (unpaired, two-tailed, unequal variance) on averages/slopes obtained (one per donor/treatment/parameter). A value of $p < 0.05$ was considered significant unless otherwise indicated.

RESULTS

Characterization of native dendrimers used in this study has been recently reported.[27] The impact of FITC conjugation on dendrimer properties was minimal, as indicated by comparing native dendrimer and FITC-conjugated dendrimer characterization data for each dendrimer type. Briefly, dendrimer size does not change appreciably with FITC conjugation, as evidenced by very similar SEC elution times for both labeled and unlabeled dendrimers (Supporting Information Figure 1). Moreover, as expected, FITC-dendrimer zeta potentials shifted slightly toward neutrality when compared to those of their unconjugated counterparts. These shifts in zeta potential agree with the FITC label-dendrimer ratio measured for each dendrimer type (Supporting Information Table 1 and previously published data[27]), indicating an expected slight consumption of surface functional groups and replacement with dye chemistry.

To investigate how different dendrimer functionalizations affect human platelets, G6.5-COOH-FITC, G7-OH-FITC, and G7-NH_2-FITC PAMAM dendrimers (100 μg/mL, final) were added to purified platelets for 30 min and P-selectin (a marker of platelet activation) was measured using flow cytometry. Figure 1A and B shows that platelets treated with no agonist exhibited very little P-selectin expression after a 30-min incubation, while platelets treated with thrombin (0.5 U/mL, final), a protease activator receptor-1 agonist known to induce P-selectin expression, elicited significantly ($p < 0.05$) higher levels of P-selectin expression (4.9 ± 1.6% vs 94.0 ± 1.4%, respectively). Platelet P-selectin surface expression after 30 min was significantly ($p < 0.05$) increased following G7-NH_2-FITC dendrimer treatment (78.4 ± 11.3%), but not for either G6.5-COOH-FITC (7.6 ± 3.3%) or G7-OH-FITC (8.0 ± 4.4%) dendrimers (Figure 1A and B). To assess whether dendrimers were capable of direct platelet binding, the levels of FITC staining were concurrently examined using flow cytometry. G6.5-COOH-FITC or G7-OH-FITC dendrimer-treated platelets did not stain for FITC, indicating these dendrimers did not adhere to the platelet surface or were not internalized by the platelets. Interestingly, after a 30-min incubation, G7-NH_2-FITC-treated platelets were predominantly FITC-stained (92.0 ± 4.9% FITC positive), which was significantly different from the cases of no treatment and G6.5-COOH-FITC or G7-OH-FITC stimulated platelets ($p < 0.05$). This suggests that amine-terminated dendrimers are readily capable of platelet

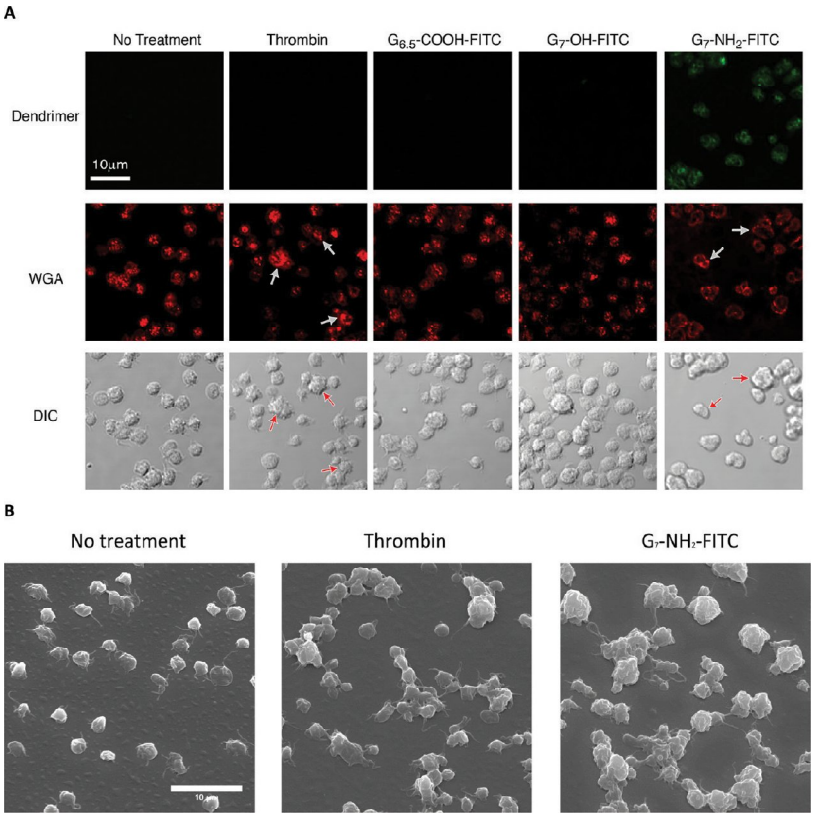

Figure 2. G7-NH_2-FITC dendrimers bind to and alter the morphology of platelets. Platelets were incubated with saline, thrombin (0.1 U/mL, final), or G6.5-COOH, G7-OH, or G7-NH_2-FITC dendrimer (100 μg/mL, final) for 45 min. Baseline platelets have few pseudopodia and intact granules compared to thrombin-activated platelets (A, second panel, see arrows). G6.5-COOH-FITC and G7-OH-FITC dendrimer-treated platelets have no apparent alterations in morphology, while G7-NH_2-FITC dendrimer treated platelets have a ruffled exterior and loss of granule morphology (see arrows) and appear green, indicating G7-NH_2-FITC binding to the platelet (A, right panels). Platelets were treated with saline, thrombin (0.1 U/mL, final), or G7-NH_2-FITC dendrimer (100 μg/mL, final) and imaged using a JEOL CarryScope SEM (B). Images were taken at 2500×, with a 20 mm working distance and a 20 kV accelerating voltage. Notice the increased number and size of platelet aggregates as well as the ruffled membrane morphology of the G7-NH_2 dendrimer treated platelets (B, right panel).

association (see Figure 1A and C). Next, populations of platelets staining positively for both G7-NH_2-FITC dendrimers and P-selectin were examined. It was determined that 92.0 ± 4.9% of platelets stained positively for dendrimer while 75.0 ± 13.1% of platelets stained positively for both dendrimer and P-selectin (shown in parts D and C, respectively, of Figure 1).

Since G7-NH_2 dendrimers were capable of both binding platelets and inducing platelet P-selectin expression, platelets were examined for morphological alterations produced by dendrimer treatment. Purified platelets were treated with no agonist or thrombin for 30 min, stained with WGA to observe the α-granule morphology, and examined using confocal microscopy. Thrombin-treated platelets exhibited increased pseudopodia formation, more platelet aggregates (Figure 2A, see red arrows in the DIC row), and centralization of granules (Figure 2A, see white arrows in fluorescence row) compared to untreated platelets. G6.5-COOH-FITC- or G7-OH-FITC-treated platelets had few pseudopodia or aggregates and distinct, individual granules similar to no treatment groups (Figure 2A). In contrast with and distinct from other dendrimer-treated platelet morphologies, G7-NH_2-FITC-treated platelets appeared to possess ruffled exterior membranes and were found in large aggregates. Interestingly, platelets stimulated with G7-NH_2-FITC dendrimer had no visible pseudopodia. Furthermore, granule staining revealed general disorder along with some apparent membrane association, contrary to the granule centralization observed in thrombin-stimulated platelets. Platelet morphology was further examined by SEM, showing that, compared to no treatment and thrombin only treated platelets, G7-NH_2-FITC dendrimer-treated platelets were much larger in size due to aggregation. In addition, SEM imaging revealed extensive membrane ruffling of G7-NH_2-FITC dendrimer-treated platelets with formation of only short pseudopodia (Figure 2B). Taken together, the confocal and SEM data demonstrate that G7-NH_2-FITC dendrimer treatment induced dramatic alterations in platelet membrane morphology and granule structure.

dx.doi.org/10.1021/mp2006054 | *Mol. Pharmaceutics* 2012, 9, 1599–1611

Given the strong surface expression of α-granule protein, P-selectin, on the platelet surface and the significant alterations in platelet structure and α-granule morphology following G7-NH_2-FITC dendrimer treatment, additional experiments were undertaken to quantify platelet α-granule protein release following dendrimer treatment. Specifically, RANTES and PF4—two α-granule proteins released upon platelet activation—were assessed in dendrimer-treated whole blood. Protein release was measured at 30 min and 4 h in whole blood treated with no agonist (control) or thrombin (0.1 U/mL, final). At both time points measured, RANTES and PF4 release were significantly ($p < 0.05$) greater in thrombin-stimulated blood compared to the case of untreated platelets (Figure 3A and B). Both G6.5-COOH-FITC- and G7-OH-FITC-treated (100 μg/mL, final) platelets released RANTES and PF4 in comparable amounts to those observed for nontreated platelets. Interestingly, G7-NH_2-FITC dendrimer platelet treatment resulted in a significant ($p < 0.05$), time-dependent release of RANTES and PF4 compared to the cases of the other two dendrimers and untreated platelet conditions (Figure 3A and B). To ensure that this granule release was dependent on a specific dendrimer-platelet interaction, a more extensive time-dependent and dose-dependent assay was undertaken on purified platelets. Thrombin treatment of purified platelets resulted in a time-dependent release of RANTES (Figure 3C) and PF4 (data not shown), whereas untreated platelets in suspension for up to four hours released only a small amount of protein. Both G6.5-COOH-FITC- and G7-OH-FITC-treatment of platelets (100 μg/mL, final) resulted in only small amounts of RANTES and PF4 release over a 4-h period that were not significantly different from the case of nontreated platelets (Figure 3C and data not shown). However, G7-NH_2-FITC-treated platelet release of RANTES and PF4 occurred after only 30 min of treatment and plateaued by 1 h (Figure 3C and data not shown).

The concentration dependence of this effect was also examined. Neither G6.5-COOH-FITC nor G7-OH-FITC treatments ranging up to 500 μg/mL exerted any observable effects on RANTES or PF4 release (Figure 3D and data not shown). However, RANTES and PF4 release from G7-NH_2-FITC-treated platelets was significantly greater than that of G6.5-COOH-FITC and G7-OH-FITC treatments at and above 1 μg/mL, with a threshold dose of 500 ng/mL (Figure 3D and data not shown).

To assess whether dendrimer treatment altered platelet-specific functions, platelet aggregation was assessed in the presence of each dendrimer type. On the basis of impedance measurements in whole blood, stimulation with adenosine disphosphate (ADP) induced significant platelet aggregation ($p < 0.05$) compared to the case of no treatment (10 ± 3 vs 0 ± 0 Ohms, respectively) (Figure 4A). Neither G6.5-COOH-FITC nor G7-OH-FITC induced a significant increase in platelet aggregation compared to the cases of no-treatment controls. However, G7-NH_2-FITC dendrimer treatment significantly increased platelet aggregation ($p < 0.05$), suggesting that platelets maintained their functional aggregation capability in response to dendrimer treatment, independent of a traditional platelet agonist (Figure 4A). Similar to aggregation trends observed in whole blood, both ADP and G7-NH_2-FITC dendrimer significantly ($p < 0.05$) increased the amplitude and the initial rate of platelet aggregation in PRP compared to the case of no treatment (Figure 4B and C).

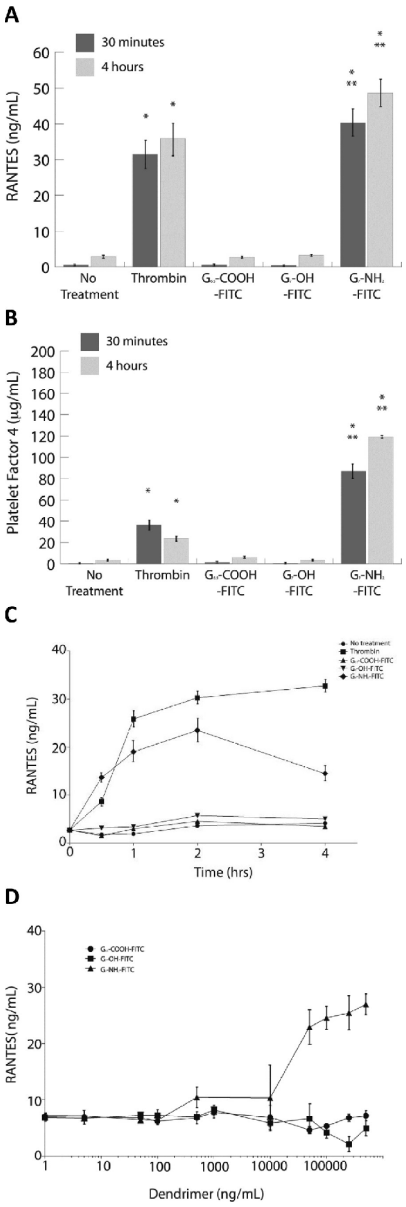

Figure 3. Human platelets release α granules contents in response to G7-NH_2-FITC dendrimers. Whole blood treated with G7-NH_2-FITC dendrimers results in significant activation of platelets based on RANTES and PF4 release after 30 min and 4 h (A and B). Purified platelets release RANTES in a dose- and time-dependent manner after treatment with G7-NH_2-FITC, but not G6.5-COOH-FITC or G7-OH_2-FITC (C and D). The * indicates a significant difference compared to the case of no treatment ($p < 0.05$). The ** indicates a significant difference compared to the cases of G6.5-COOH-FITC and G7-OH-FITC dendrimer ($p < 0.05$). The data represent the mean $\pm$ SEM of at least three independent experiments.

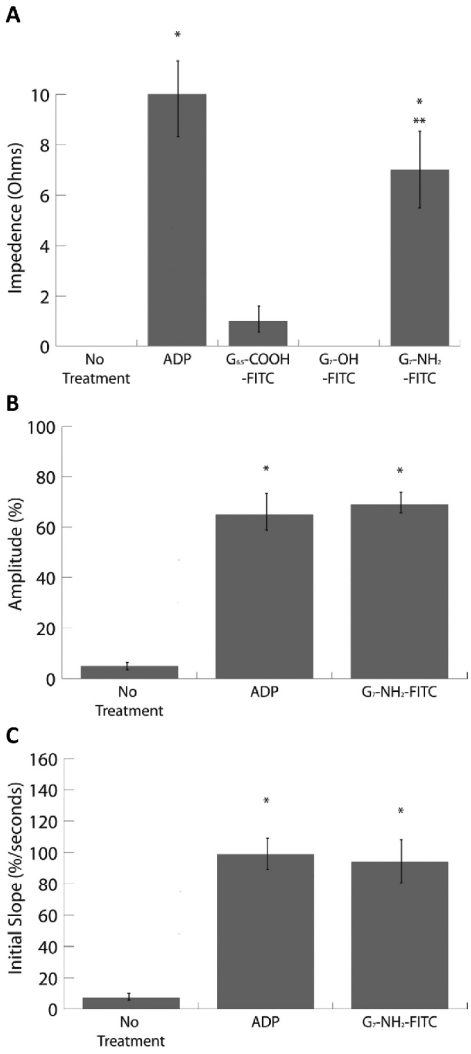

Figure 4. G7-NH_2-FITC dendrimers induce platelet aggregation. Human whole blood (A) and PRP (B and C) were treated with G6.5-COOH-FITC, G7-OH-FITC, or G7-NH_2-FITC (100 μg/mL, final), saline, or ADP (5 μM, final). G7-NH_2-FITC dendrimer treatment alone significantly increased platelet aggregation compared to no treatment (*, $p < 0.05$) and G6.5-COOH-FITC and G7-OH-FITC (**, $p < 0.05$) in whole blood. G7-NH_2-FITC treatment significantly increases platelet aggregation in PRP (*, $p < 0.05$) compared to the case of no treatment, as indicated by the increase in amplitude (B) and slope (C). The bars in panels A–C represent the mean ± SEM of three independent experiments.

Aside from aggregation and α-granule secretion, another important platelet hemostatic function is to provide a specific surface to support the formation of Factor Va/Factor Xa prothrombinase complexes for the cleavage of prothrombin to active thrombin. In turn, this thrombin activates more platelets and cleaves fibrinogen to fibrin to form a fibrin clot. The combination of fibrin and activated platelets results in the formation of a stable clot to prevent bleeding. Therefore, the critical platelet function of thrombin generation was assessed for whole blood exposed to each dendrimer type. Following treatment of whole blood, thrombin generation was assessed in isolated PRP via a thrombin-specific fluorogenic substrate. Analogous G6.5-COOH-FITC- and G7-OH-FITC-treatment of whole blood had little effect on thrombin generation parameters compared to the cases of no-treatment controls (see Figure 5A and Table 1). Additionally, no dendrimer treatments elicited any observable effect on cleavage of the thrombin-specific substrate or on the fluorimetric analysis (data not shown). Surprisingly, thrombin generation in whole blood was significantly reduced uniquely for G7-NH_2-FITC treatment as

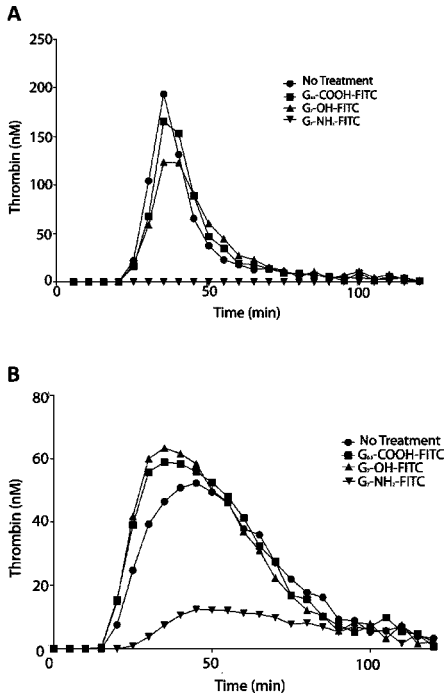

Figure 5. G7-NH_2-FITC dendrimers inhibit platelet-dependent thrombin generation in whole blood and PRP. Whole blood was treated with saline or dendrimer (100 μg/mL) for 30 min at 37 °C. After 30 min, the whole blood was centrifuged at 150*g* for 20 min and the PRP was transferred to another tube. Thrombin generation was then measured using the PRP after addition of tissue factor, $CaCl_2$, and a fluorogenic substrate. Thrombin generation was monitored with a fluorimeter for 120 min (A). G7-NH_2-FITC dendrimers inhibited thrombin generation in whole blood, while the G6.5-COOH-FITC and G7-OH -FITC dendrimers had little effect. Dendrimer alone had no effect on the rate of thrombin cleavage of the fluorogenic substrate or on the measurement of fluorescence (data not shown). Whole blood was centrifuged for 150*g* for 20 min, and PRP was transferred to another tube. PRP was treated with saline or dendrimer (100 μg/mL) for 30 min before thrombin generation was measured as described above. Similar to the case for whole blood, G7-NH_2-FITC dendrimers blunted thrombin generation in dendrimer treated PRP while G6.5-COOH-FITC and G7-OH -FITC dendrimers had no effect (B). Thrombin generation plots (A and B) depict one experiment and are representative of three independent experiments.

dx.doi.org/10.1021/mp2006054 | *Mol. Pharmaceutics* 2012, 9, 1599–1611

Table 1. Dendrimer-Treated Whole Blood Thrombin Generation[a]

treatment condition	lag time (min)	peak height (nM)	time to peak (min)	rate (nM/min)	area under the curve (nM·min)
no treatment	27.2 ± 4.2	112.4 ± 43.6	46.0 ± 8.7	8.3 ± 4.9	2449.6 ± 470.3
G6.5-COOH-FITC	27.0 ± 5.0	76.7 ± 34.0	43.8 ± 7.6	4.4 ± 2.4	2098.3 ± 595.6
G7-OH-FITC	25.3 ± 2.7	111.1 ± 40.1	46.0 ± 8.3	7.8 ± 3.8	2577.1 ± 465.0
G7-NH_2-FITC	N.D.[b]	N.D.	N.D.[b]	N.D.	N.D.[b]

[a]N.D. = nondetectable. [b]$p < 0.05$ compared to G6.5-COOH-FITC and G7-OH-FITC.

Table 2. Dendrimer-Treated Platelet-Rich Plasma Thrombin Generation

treatment condition	lag time (min)	peak height (nM)	time to peak (min)	rate (nM/min)	area under the curve (nM·min)
no treatment	20.0 ± 3.0	70.2 ± 26.4	41.7 ± 10.3	5.5 ± 3.7	2749.4 ± 347.4
G6.5-COOH-FITC	19.0 ± 2.1	65.4 ± 11.4	36.3 ± 3.1	4.1 ± 1.0	2924.1 ± 173.6
G7-OH-FITC	20.3 ± 2.5	62.3 ± 11.0	41.5 ± 9.5	4.1 ± 1.5	2787 ± 202.8
G7-NH_2-FITC	28.7 ± 2.6	9.6 ± 2[a]	65.2 ± 12.1	0.2 ± 0.2[a]	470.7 ± 144.2[a]

[a]$p < 0.05$ compared to G6.5-COOH-FITC and G7-OH-FITC.

compared to all other treatments ($p < 0.05$) based on an area-under-the-curve assessment (i.e., total thrombin generation) for each treatment (Figure 5A and Table 1). Furthermore, the onset of thrombin generation (or lag time) and the time to peak thrombin concentration were significantly shortened vs untreated whole blood (control) ($p < 0.05$). The peak thrombin concentration and rate of thrombin generation were also substantially reduced but did not reach statistical significance (Figure 5A and Table 1). Again, to ensure that dendrimers acted directly on platelets and not through other blood cell mechanisms, PRP was directly isolated from whole blood and treated with dendrimer or left untreated (control). Similar to whole blood results, G6.5-COOH-FITC- and G7-OH-FITC-treated PRP had similar thrombin-generation parameters compared to nontreated control blood. G7-NH_2-FITC caused significant decreases in thrombin generation rate, lag time, peak height, and area under the curve compared to the cases of no treatment (control) and G6.5-COOH-FITC or G7-OH-FITC dendrimer-treated PRP ($p < 0.05$) (Figure 5B and Table 2).

In vivo, platelets rapidly adhere to injured vessels, activate, degranulate, and release potent agonists to help form a hemostatic plug to prevent loss of blood. To examine if dendrimer-treated platelets were capable of adhering to surfaces under physiologic flow, purified platelets were perfused through fibrinogen-coated microchannel chambers under physiologic shear conditions and platelet adhesion was quantified. Platelets stimulated with thrombin adhered to these surfaces in greater numbers and spread to a greater extent than nontreated platelets (Figure 6A DIC column and 250% DIC column). As depicted in Figure 6C and D (see also Supporting Information Figure 2A), thrombin-treated platelets also adhered at a significantly greater rate than nontreated platelets ($p < 0.05$). Non-FITC labeled G7-NH_2-treated platelets formed large aggregates under flow, capable of both binding to and growing from the fibrinogen-coated surface (Figure 6A and E). G7-NH_2-treated platelets were morphologically similar to those observed by confocal and SEM (compare Figure 6A with Figure 2). Non-FITC labeled G7-NH_2 dendrimer-treated platelets adhered to these surfaces at significantly faster rates and covered significantly larger areas compared to the cases of untreated platelets ($p < 0.05$) (Figure 6C and D and Supporting Information Figure 2A and Videos 1 and 2).

To examine the mechanism behind the increased rates of binding and surface coverage of cationic dendrimer-treated platelets, the role of platelet−fibrinogen binding was examined. To this end, all platelet treatment groups were pretreated with abciximab, a Fab fragment-targeting integrin $\alpha_{IIb}\beta_3$ that blocks platelet aggregation and adhesion to fibrinogen.[43] Thrombin-treated platelets pretreated with abciximab adhered at significantly lower rates and covered significantly smaller areas compared to the case of thrombin-treated platelets without abciximab treatment ($p < 0.05$) (Figure 6B−D and Supporting Information Figure 2B). Dendrimer-treated platelets pretreated with abciximab adhered to surfaces at decreased rates and covered significantly smaller areas ($p < 0.05$) compared to the case of dendrimer-stimulated platelets without abciximab pretreatment (Figure 6B−D, Supporting Information Figure 2B and Videos 3 and 4). Interestingly, cationic dendrimer treatment resulted in increased platelet aggregate size, which remained unchanged after abciximab treatment, suggesting that platelet aggregation occurs independently of $\alpha_{IIb}\beta_3$ (Figure 6E).

■ DISCUSSION

Data reported here confirm and extend very recent findings on dendrimer−platelet activation effects reported *in vitro*[28] and *in vivo*.[27] This study is consistent in showing that high-generation polar neutral (hydroxyl-terminated) and anionic (carboxy-terminated) PAMAM dendrimers do not alter platelet function or morphology, while significantly, cationic (amine-terminated) G7 PAMAM dendrimers were observed to alter platelet function in both pro- and antithrombotic manners. In addition to expanding the survey of different high-generation dendrimer terminal chemistries, these data detail additional aspects of platelet biology, including platelet morphology and adhesion, and they support procoagulant surface roles that build upon and compliment previous reports focusing on dendrimer generation (size) and surface charge effects on platelet aggregation.[28] Utilizing dendrimer−FITC conjugation, the present studies demonstrate direct cationic dendrimer−platelet association. By contrast, neutral and anionic dendrimers were unable to bind platelets, while both flow cytometry and microscopic analyses demonstrated that cationic FITC-labeled dendrimers increasingly associated with platelets over time and were visually apparent on the platelet membrane (Figures 1A, 1C, and 2A), suggesting direct cationic dendrimer binding and internalization. Moreover, such potential dendrimer internalization through the platelet open canalicular system (OCS) has

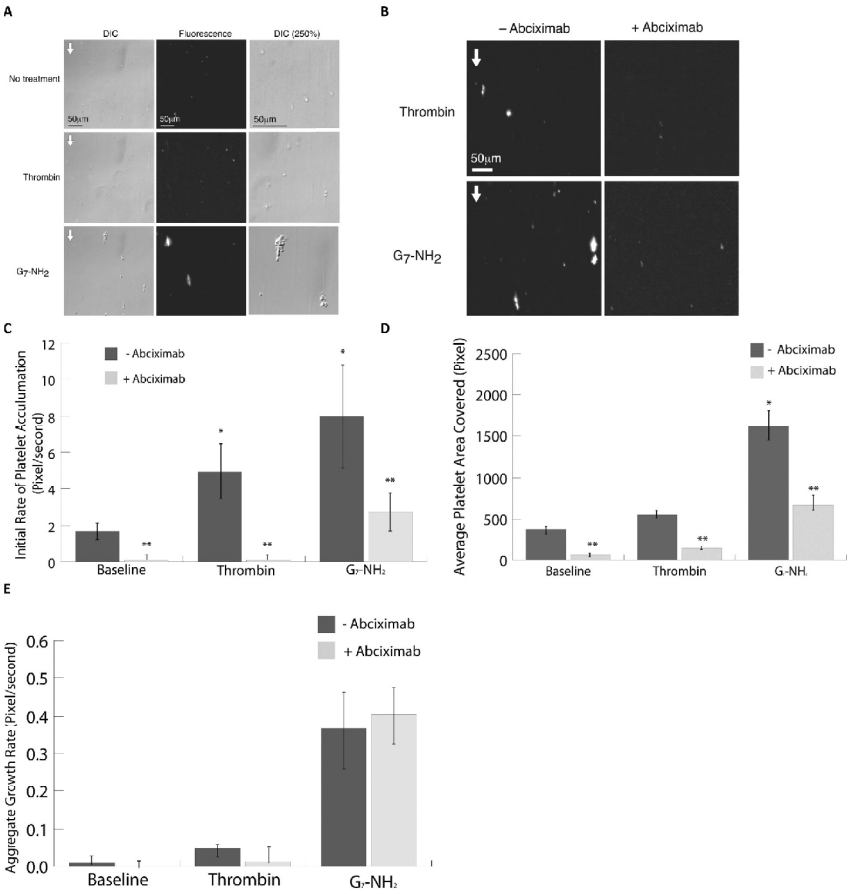

Figure 6. Platelets adhere faster and in greater numbers to fibrinogen under flow after G7-NH_2 dendrimer treatment. Platelets were left untreated or stimulated with thrombin (0.5 U/mL) or G7-NH_2 dendrimer (100 μg/mL) for 5 min and flowed at 200 s^{-1} for 6 min over Ibidi 0.4 VI plates precoated with 0.5 mg/mL fibrinogen. In some experiments, platelets were fluorescently labeled before treatment. Images were captured in real-time using an Olympus wide-field fluorescent microscope (IX-81 inverted microscope system) using an ORCA-ER monochrome CCD camera (frame rate 1 Hz). Still images from the final frame are depicted in panel A from a single experiment, representative of 12 independent experiments. Images in panel B are still images from the final frame from one experiment, representative of six independent experiments. The flow direction is indicated by the arrow in the upper left-hand corner (A and B). The DIC image has been enlarged by 250% in the right panels to show platelet morphology. The initial rate of platelet adhesion and average area covered by platelets were significantly ($p < 0.05$) increased for dendrimer-treated platelets relative to untreated controls (C and D). In some experiments, platelets were pretreated for 1 h with abciximab (0.136 μM), a Fab fragment against $\alpha_{IIb}\beta_3$, before treatment with agonist. Abciximab-treated platelets showed reduced adhesion to fibrinogen, independent of agonist treatment (B–D). However, the aggregation behavior of platelets was not significantly different for abciximab-treated platelets stimulated with cationic dendrimer (E). The bars in panels C–E represent the mean ± SEM of at least six independent experiments. The * indicates a significant ($p < 0.05$) difference compared to the case of no treatment. The ** indicates a significant ($p < 0.05$) difference compared to the case of nonabciximab-treated platelets.

additional ramifications for platelet functional perturbations that should be explored in future studies.

Similar to previous reports,[28] this study demonstrates that cationic dendrimers induced P-selectin expression on purified platelets while neutral and anionic dendrimers had no effect on P-selectin expression (Figure 1A and B). While prior hypotheses of membrane chemomechanical disruption and permeabilization explain the observed increases in P-selectin on the platelet surface in part, the present data argue further for complete release of α-granule contents from cationic G7 dendrimer-treated platelets as well: G7-NH_2-FITC dendrimer-treated platelets caused time-dependent release of α-granule proteins RANTES and PF4 (Figure 3A–C). Moreover, even as little as 500 ng/mL of the cationic G7 dendrimer elicited secretion of these α-granule proteins (Figure 3D). Upon activation by traditional platelet agonists such as thrombin or collagen followed by platelet–surface adherence, the α-granule membrane fuses with the OCS, a surface-connected membrane system, or the plasma membrane to release its contents to the extracellular milieu. This activation normally results in the flattening out of the platelet with platelet organelle and granule reorganization, causing a classic "fried egg" appearance (see Figure 6A, top two DIC 250% column panels). These changes in intracellular content are mediated through the actin

dx.doi.org/10.1021/mp2006054 | *Mol. Pharmaceutics* 2012, 9, 1599–1611

cytoskeleton that directs release of the granule contents from the platelet center. In contrast to normal platelet activation, G7-NH_2-FITC dendrimer-treated platelets exhibited ruffled exterior cellular membranes with an enlarged, spherical gross morphology. Moreover, staining of platelet granules with WGA revealed general granular disordering with some fusion to the outer plasma membrane(s) in contrast to normal granular coalescence in the center of the platelet (Figure 2A, red-fluorescent row). These unusual alterations in both gross and granular platelet morphology support widespread actin cytoskeletal disruption. Indeed, previously published reports of highly positively charged particles contacting platelets have demonstrated changes in the actin cytoskeleton ranging from attenuation of actin polymerization to degradation of the cytoskeletal structure.[44,45] This suggests that, beyond altering plasma membrane integrity to induce platelet aggregation, G7-NH_2-FITC dendrimers are capable of inducing changes in the platelet cytoskeleton, resulting in release of α-granule contents including P-selectin, RANTES, and PF4. However, this does not rule out other possibilities of direct interactions of these dendrimers with the platelet phospholipid membrane, since addition of aminated dendrimer produces visible ruffling of the platelet membrane and blunts thrombin generation that depends on phospholipid surface interactions (see below). Future studies must determine such direct interactions between dendrimer and the phospholipid membrane or the platelet cytoskeleton or both.

Aside from changes observed in platelet morphology and granule structure, G7-NH_2-FITC dendrimer-treated platelets exhibited dramatic changes in function compared to nontreated and thrombin-treated platelets. This has considerable consequences to blood coagulation when considering the array of proposed *in vivo* applications of dendrimers.[14] Similar to previous reports, amine-terminated dendrimers induced significant platelet aggregation in PRP.[28] This result was extended to whole blood for added physiological relevance, where addition of cationic G7 dendrimer was capable of inducing platelet aggregation, indicating that other blood cell and plasma protein components in blood have little effect on altering the cationic dendrimer−platelet interaction.

Interestingly, platelet-dependent thrombin generation was markedly inhibited by cationic G7 dendrimers in both whole blood and PRP systems, suggesting for the first time that cationic dendrimers also have a direct effect on procoagulant protein binding to platelets. Upon tissue injury, the central procoagulant enzyme, thrombin, is generated through the binding of coagulation proteins to phosphatidylserine (PS), a negatively charged phospholipid exposed on the platelet surface by activation.[46] Protein binding to the phospholipid surface is mediated through calcium cations associating with the γ-carboxyglutamic (GLA) protein domain, facilitating binding to the negatively charged PS lipid surface. Calcium associating with the GLA domain of Factor Xa facilitates Xa binding to the PS surface, resulting in the formation of the prothrombinase complex in combination with factor Va. Complete complex formation allows for cleavage of prothrombin and the generation of thrombin.[46] Cationic G7 dendrimer treatment prolonged the lag time (or onset) of thrombin generation and caused decreases in peak thrombin concentration, rate of thrombin generation, and total amount of thrombin produced. These data suggest direct dendrimer interference with enzyme reactions normally occurring on the activated platelet surface. An alternative platelet activation mechanism with dendrimers where PS is not actively involved is counterintuitive, but it supports the recent hypothesis of Dobrovolskaia et al.[28] that cationic dendrimers activate platelets in a nontraditional way. The present data suggest that cationic G7 dendrimers bind to platelet surfaces and alter the plasma membrane morphology to an extent that precludes procoagulant protein binding and prothrombinase complex formation, and that severely attenuates thrombin generation. A different explanation for this phenomenon is that cationic dendrimers induce the exposure of negatively charged PS through platelet activation, but immediately bind to those anionic phospholipids and block protein binding to the surface by virtue of concentration-dependent competition (i.e., 0.85 μM dendrimer vs 54 μM Factor X or 1.2 μM prothrombin potency) and also the cationic dendrimer polyvalent binding affinity exceeding that observed for procoagulant proteins on activated platelet surface sites ($K_d \approx 10^{-10}$).[46−48] With >500 formal positive charges present on an 8-nm diameter cationic G7 dendrimer surface, the surface area per amine group (70 Å^2) closely approximates the lipid headgroup density of a typical bilayer membrane, maximizing dendrimer−lipid membrane (e.g., PS) interactions, each with a contribution to the PS anionic lipid binding energy of ≈1 kcal/mol.[19] Thus, electrostatic dendrimer PS binding avidity could out-compete that of PS and Factor V with calcium. While these data suggest a direct dendrimer attenuation of platelet-mediated thrombin generation, it is also possible that amine-terminated dendrimers directly affect plasma protein procoagulant activity at platelet surfaces, altering their intrinsic ability to function as active enzymes. However, incubation of thrombin or Factor Xa (the active enzyme necessary for thrombin generation) with cationic G7 dendrimers produced no observable effect on enzyme activity (data not shown), suggesting perturbation of the plasma membrane to be a more likely explanation for the blunted thrombin response.

Of interest, Greish and co-workers[27] very recently noted a disseminated intravascular coagulation (DIC)-like condition *in vivo* resulting from intravenous cationic dendrimer injections in rodents. Superficially, this observation contradicts the present finding of decreased thrombin generation on platelet surfaces as it is thought that thrombin generation is necessary for the DIC hematologic pathology, involving extensive consumption of both platelets and coagulation proteins. However, their hypothesis that the highly positively charged dendrimer mimics the action of thrombin by independently cleaving fibrinogen to fibrin is now strengthened by the present finding of reduced thrombin generation. Therefore, a model of DIC where platelets and fibrinogen are consumed by cationic dendrimers may explain both the *in vivo* findings of Greish et al. and the present *in vitro* platelet findings.

The hypothesis of platelet consumption by high-generation cationic dendrimers is further strengthened by examining platelet adhesion under flow. Upon traditional platelet activation, the major receptor for fibrinogen, integrin $\alpha_{IIb}\beta_3$, undergoes a conformational change facilitating receptor−ligand interaction.[43] Interestingly, dendrimer-treated platelets significantly adhered to fibrinogen-coated surfaces under flow, similar to thrombin-activated platelets. However, abciximab blockage of platelet $\alpha_{IIb}\beta_3$ receptors reduced but did not eliminate some parameters of dendrimer-treated platelet adhesion, suggesting that, collectively, dendrimer-treated platelets bind to surfaces under flow by mechanisms that are potentially both fibrinogen-dependent (normal) and independent (abnormal). In these microfluidics-based experiments, abciximab at a final concen-

tration of 136 nM was preincubated with purified platelets for at least 30 min before dendrimer exposure to platelets. On the basis of reports in the literature of abciximab having a K_d in platelet-rich plasma of 6.65 ± 1.45 nM,[49] it is unlikely that the abciximab would unbind from its receptor to interact with the dendrimer.

These results may seem inconsistent with previously published reports in which the platelet $\alpha_{IIb}\beta_3$ receptor blockade by abciximab did not hinder aggregation.[28] This difference in abciximab-mediated platelet observations may be explained by distinct experimental conditions: the previous platelet aggregation studies were performed under gentle stirring conditions very different from the higher shear rates of the present microfluidics assays. Furthermore, platelet aggregation measures the ability of platelets to bind to each other whereas the microfluidics assay examines platelet binding to a more physiologic substrate, in this case adsorbed fibrinogen. Superficially, the present results suggest that dendrimer-treated platelets retain functional $\alpha_{IIb}\beta_3$ receptors with abciximab treatment. However, in the present flow-based results, only platelet adhesion to fibrinogen was reduced by abciximab treatment—the adherent platelet aggregate growth rate was unchanged by abciximab addition (Figure 6E), supporting the observation by Dobrovolskaia et al.[28] that platelet aggregation occurs independently of classic mechanisms following platelet stimulation by cationic dendrimers. Interestingly, both reports present similar data for dendrimer effects on platelet membranes, showing formation of large platelet aggregates after dendrimer treatment. Therefore, it is possible that platelet aggregation after dendrimer treatment is a function of changes in membrane properties, i.e. "stickiness" in lipid membrane, and this is independent of fibrinogen binding to $\alpha_{IIb}\beta_3$ receptors.

In conclusion, the likelihood of direct cationic dendrimer interactions with platelet membrane and internal cytoskeletal structures represents a striking new mechanism for nanocarrier toxicity in blood. At circulating concentrations of $\sim 10^8$/mL and with intrinsically rapid (millisecond) membrane response times to both chemical and mechanical stimuli, platelets could play a significant contribution in toxicity studies of nanomaterials in blood. The new data presented here, consistent with recent reports of platelet–dendrimer interactions *in vivo* and *in vitro*, support a potent activating role for increasingly amine-terminated dendrimers and, potentially, for other cationic dendrimers in high generation, densely charged forms. This seemingly precludes their direct intravenous use in this cationic form. Additionally, extracirculatory applications of cationic dendrimers should seek to prevent transport and possible host vascular access of amine-terminated dendrimer constructs. Certainly, *in vivo* toxicities reported for PAMAM dendrimers extravascularly[21−23] provide sufficient toxicity concerns for these materials as well. Applications utilizing cationic dendrimers employed either as intravenous drug carrier precursors or platforms should provide reliable characterization for conjugation or blocking of amine terminal groups prior to blood contact. Future studies should focus on dendrimer influences on plasma proteins in general and procoagulant proteins in particular as a function of dendrimer generation and chemistry (e.g., charge density, formal charge) to further identify and understand adverse effects observed for cationic dendrimers in blood *in vivo*. Specifically, particular focus on dendrimer influences on coagulation factor activation and fibrin polymerization is needed, since dendrimer toxicity may be related to direct interactions with either blood proteins or cells, or to the modulation of complex interactions between both of these blood components.

■ ASSOCIATED CONTENT

Supporting Information

Physiochemical characterization data and reaction schemes for FITC-conjugated dendrimers, additional microfluidic platelet adhesion experimental data, and microfluidic platelet adhesion videos. This material is available free of charge via the Internet at http://pubs.acs.org.

■ AUTHOR INFORMATION

Corresponding Author

*Department of Pharmaceutics and Pharmaceutical Chemistry, University of Utah, Salt Lake City, UT 84112-5820, USA. E-mail: david.grainger@utah.edu. Tel: 801-581-3715. Fax: 801-581-3674.

Author Contributions

C.F.J. and R.A.C. contributed equally to this work.

Notes

The authors declare no competing financial interest.

■ ACKNOWLEDGMENTS

The authors thank D. Lim for preparing figures. Financial support was provided by NIH Grants R01DE019050, R01EB07470, R01HL065648, R01HL066277, and R01HL091754, the American Heart Association (11POST7290019), an Interdisciplinary Seed Grant from the University of Utah, the Utah Science Technology and Research (USTAR) initiative, and a University of Utah Graduate Research Fellowship.

■ REFERENCES

(1) Tomalia, D. A.; Fréchet, J. M. J. Discovery of dendrimers and dendritic polymers: A brief historical perspective. *J. Polym. Sci., Part A: Polym. Chem.* **2002**, *40*, 2719−2728.

(2) Radu, D. R.; Lai, C.-Y.; Jeftinija, K.; Rowe, E. W.; Jeftinija, S.; Lin, V. S. Y. A Polyamidoamine Dendrimer-Capped Mesoporous Silica Nanosphere-Based Gene Transfection Reagent. *J. Am. Chem. Soc.* **2004**, *126*, 13216−13217.

(3) Bielinska, A. U.; Yen, A.; Wu, H. L.; Zahos, K. M.; Sun, R.; Weiner, N. D.; Baker, J. R., Jr.; Roessler, B. J. Application of membrane-based dendrimer/DNA complexes for solid phase transfection in vitro and in vivo. *Biomaterials* **2000**, *21*, 877−887.

(4) Svenson, S.; Tomalia, D. A. Dendrimers in biomedical applications—reflections on the field. *Adv. Drug Delivery Rev.* **2005**, *57*, 2106−29.

(5) Esfand, R.; Tomalia, D. A. Poly(amidoamine) (PAMAM) dendrimers: from biomimicry to drug delivery and biomedical applications. *Drug Discovery Today* **2001**, *6*, 427−436.

(6) Patri, A. K.; Kukowska-Latallo, J. F.; Baker, J. R., Jr. Targeted drug delivery with dendrimers: comparison of the release kinetics of covalently conjugated drug and non-covalent drug inclusion complex. *Adv. Drug Delivery Rev.* **2005**, *57*, 2203−14.

(7) Gillies, E. R.; Frechet, J. M. Dendrimers and dendritic polymers in drug delivery. *Drug Discovery Today* **2005**, *10*, 35−43.

(8) Wilbur, D. S.; Pathare, P. M.; Hamlin, D. K.; Buhler, K. R.; Vessella, R. L. Biotin Reagents for Antibody Pretargeting. 3. Synthesis, Radioiodination, and Evaluation of Biotinylated Starburst Dendrimers. *Bioconjugate Chem.* **1998**, *9*, 813−825.

(9) Cheng, Y.; Zhao, L.; Li, Y.; Xu, T. Design of biocompatible dendrimers for cancer diagnosis and therapy: current status and future perspectives. *Chem. Soc. Rev.* **2011**, *40*, 2673−2703.

(10) Sadekar, S.; Ghandehari, H. Transepithelial transport and toxicity of PAMAM dendrimers: Implications for oral drug delivery. *Adv. Drug Delivery Rev.* **2012**, *64*, 571−588.
(11) Lai, P.-S.; Lou, P.-J.; Peng, C.-L.; Pai, C.-L.; Yen, W.-N.; Huang, M.-Y.; Young, T.-H.; Shieh, M.-J. Doxorubicin delivery by polyamidoamine dendrimer conjugation and photochemical internalization for cancer therapy. *J. Controlled Release* **2007**, *122*, 39−46.
(12) Malik, N.; Evagorou, E. G.; Duncan, R. Dendrimer-platinate: a novel approach to cancer chemotherapy. *Anticancer Drugs* **1999**, *10*, 767−76.
(13) Bhadra, D.; Bhadra, S.; Jain, S.; Jain, N. K. A PEGylated dendritic nanoparticulate carrier of fluorouracil. *Int. J. Pharm.* **2003**, *257*, 111−24.
(14) Cheng, Y.; Xu, Z.; Ma, M.; Xu, T. Dendrimers as drug carriers: Applications in different routes of drug administration. *J. Pharm. Sci.* **2008**, *97*, 123−143.
(15) Thiagarajan, G.; Ray, A.; Malugin, A.; Ghandehari, H. PAMAM-camptothecin conjugate inhibits proliferation and induces nuclear fragmentation in colorectal carcinoma cells. *Pharm. Res.* **2010**, *27*, 2307−16.
(16) Shi, X.; Lee, I.; Chen, X.; Shen, M.; Xiao, S.; Zhu, M.; Baker, J. R.; Wang, S. H. Influence of dendrimer surface charge on the bioactivity of 2-methoxyestradiol complexed with dendrimers. *Soft Matter* **2010**, *6*, 2539−2545.
(17) Domanski, D. M.; Klajnert, B.; Bryszewska, M. Influence of PAMAM dendrimers on human red blood cells. *Bioelectrochemistry* **2004**, *63*, 189−191.
(18) Li, S.-D.; Huang, L. Pharmacokinetics and Biodistribution of Nanoparticles. *Mol. Pharmaceutics* **2008**, *5*, 496−504.
(19) Zhang, Z.-Y.; Smith, B. D. High-Generation Polycationic Dendrimers Are Unusually Effective at Disrupting Anionic Vesicles: Membrane Bending Model. *Bioconjugate Chem.* **2000**, *11*, 805−814.
(20) Roberts, J. C.; Bhalgat, M. K.; Zera, R. T. Preliminary biological evaluation of polyamidoamine (PAMAM) Starburst dendrimers. *J. Biomed. Mater. Res.* **1996**, *30*, 53−65.
(21) Malik, N.; Wiwattanapatapee, R.; Klopsch, R.; Lorenz, K.; Frey, H.; Weener, J. W.; Meijer, E. W.; Paulus, W.; Duncan, R. Dendrimers: Relationship between structure and biocompatibility in vitro, and preliminary studies on the biodistribution of 125I-labelled polyamidoamine dendrimers in vivo. *J. Controlled Release* **2000**, *65*, 133−148.
(22) Heiden, T. C.; Dengler, E.; Kao, W. J.; Heideman, W.; Peterson, R. E. Developmental toxicity of low generation PAMAM dendrimers in zebrafish. *Toxicol. Appl. Pharmacol.* **2007**, *225*, 70−9.
(23) Li, C.; Liu, H.; Sun, Y.; Wang, H.; Guo, F.; Rao, S.; Deng, J.; Zhang, Y.; Miao, Y.; Guo, C.; Meng, J.; Chen, X.; Li, L.; Li, D.; Xu, H.; Wang, H.; Li, B.; Jiang, C. PAMAM Nanoparticles Promote Acute Lung Injury by Inducing Autophagic Cell Death through the Akt-TSC2-mTOR Signaling Pathway. *J. Mol. Cell Biol.* **2009**, *1*, 37−45.
(24) Wang, W.; Xiong, W.; Zhu, Y.; Xu, H.; Yang, X. Protective effect of PEGylation against poly(amidoamine) dendrimer-induced hemolysis of human red blood cells. *J. Biomed. Mater. Res. B: Appl. Biomater.* **2010**, *93*, 59−64.
(25) Jain, K.; Kesharwani, P.; Gupta, U.; Jain, N. K. Dendrimer toxicity: Let's meet the challenge. *Int. J. Pharm.* **2010**, *394*, 122−142.
(26) Ottaviani, M. F.; Daddi, R.; Brustolon, M.; Turro, N. J.; Tomalia, D. A. Structural Modifications of DMPC Vesicles upon Interaction with Poly(amidoamine) Dendrimers Studied by CW-Electron Paramagnetic Resonance and Electron Spin−Echo Techniques. *Langmuir* **1999**, *15*, 1973−1980.
(27) Greish, K.; Thiagarajan, G.; Herd, H.; Price, R.; Bauer, H.; Hubbard, D.; Burckle, A.; Sadekar, S.; Yu, T.; Anwar, A.; Ray, A.; Ghandehari, H. Size and surface charge significantly influence the toxicity of silica and dendritic nanoparticles. *Nanotoxicology* **2011**, DOI: 10.3109/17435390.2011.604442.
(28) Dobrovolskaia, M. A.; Patri, A. K.; Simak, J.; Hall, J. B.; Semberova, J.; De Paoli Lacerda, S. H.; McNeil, S. E. Nanoparticle Size and Surface Charge Determine Effects of PAMAM Dendrimers on Human Platelets in Vitro. *Mol. Pharmaceutics* **2012**, *9*, 382−393.
(29) Fischer, D.; Li, Y.; Ahlemeyer, B.; Krieglstein, J.; Kissel, T. In vitro cytotoxicity testing of polycations: influence of polymer structure on cell viability and hemolysis. *Biomaterials* **2003**, *24*, 1121−31.
(30) Hong, S.; Leroueil, P. R.; Janus, E. K.; Peters, J. L.; Kober, M. M.; Islam, M. T.; Orr, B. G.; Baker, J. R., Jr.; Banaszak Holl, M. M. Interaction of polycationic polymers with supported lipid bilayers and cells: nanoscale hole formation and enhanced membrane permeability. *Bioconjugate Chem.* **2006**, *17*, 728−34.
(31) Lee, H.; Larson, R. G. Molecular dynamics simulations of PAMAM dendrimer-induced pore formation in DPPC bilayers with a coarse-grained model. *J. Phys. Chem. B* **2006**, *110*, 18204−11.
(32) Mecke, A.; Lee, I.; Baker, J. R., Jr.; Holl, M. M.; Orr, B. G. Deformability of poly(amidoamine) dendrimers. *Eur. Phys. J. E: Soft Matter Biol. Phys.* **2004**, *14*, 7−16.
(33) Hong, S.; Bielinska, A. U.; Mecke, A.; Keszler, B.; Beals, J. L.; Shi, X.; Balogh, L.; Orr, B. G.; Baker, J. R., Jr.; Banaszak Holl, M. M. Interaction of poly(amidoamine) dendrimers with supported lipid bilayers and cells: hole formation and the relation to transport. *Bioconjugate Chem.* **2004**, *15*, 774−82.
(34) Aillon, K. L.; Xie, Y.; El-Gendy, N.; Berkland, C. J.; Forrest, M. L. Effects of nanomaterial physicochemical properties on in vivo toxicity. *Adv. Drug Delivery Rev.* **2009**, *61*, 457−66.
(35) Kitchens, K. M.; Kolhatkar, R. B.; Swaan, P. W.; Eddington, N. D.; Ghandehari, H. Transport of poly(amidoamine) dendrimers across Caco-2 cell monolayers: Influence of size, charge and fluorescent labeling. *Pharm. Res.* **2006**, *23*, 2818−26.
(36) Denis, M. M.; Tolley, N. D.; Bunting, M.; Schwertz, H.; Jiang, H.; Lindemann, S.; Yost, C. C.; Rubner, F. J.; Albertine, K. H.; Swoboda, K. J.; Fratto, C. M.; Tolley, E.; Kraiss, L. W.; McIntyre, T. M.; Zimmerman, G. A.; Weyrich, A. S. Escaping the nuclear confines: signal-dependent pre-mRNA splicing in anucleate platelets. *Cell* **2005**, *122*, 379−91.
(37) Schwertz, H.; Tolley, N. D.; Foulks, J. M.; Denis, M. M.; Risenmay, B. W.; Buerke, M.; Tilley, R. E.; Rondina, M. T.; Harris, E. M.; Kraiss, L. W.; Mackman, N.; Zimmerman, G. A.; Weyrich, A. S. Signal-dependent splicing of tissue factor pre-mRNA modulates the thrombogenicity of human platelets. *J. Exp. Med.* **2006**, *203*, 2433−40.
(38) Weyrich, A. S.; Denis, M. M.; Schwertz, H.; Tolley, N. D.; Foulks, J.; Spencer, E.; Kraiss, L. W.; Albertine, K. H.; McIntyre, T. M.; Zimmerman, G. A. mTOR-dependent synthesis of Bcl-3 controls the retraction of fibrin clots by activated human platelets. *Blood* **2007**, *109*, 1975−83.
(39) Yost, C. C.; Cody, M. J.; Harris, E. S.; Thornton, N. L.; McInturff, A. M.; Martinez, M. L.; Chandler, N. B.; Rodesch, C. K.; Albertine, K. H.; Petti, C. A.; Weyrich, A. S.; Zimmerman, G. A. Impaired neutrophil extracellular trap (NET) formation: a novel innate immune deficiency of human neonates. *Blood* **2009**, *113*, 6419−27.
(40) Weyrich, A. S.; Elstad, M. R.; McEver, R. P.; McIntyre, T. M.; Moore, K. L.; Morrissey, J. H.; Prescott, S. M.; Zimmerman, G. A. Activated platelets signal chemokine synthesis by human monocytes. *J. Clin. Invest.* **1996**, *97*, 1525−34.
(41) Weyrich, A. S.; McIntyre, T. M.; McEver, R. P.; Prescott, S. M.; Zimmerman, G. A. Monocyte tethering by P-selectin regulates monocyte chemotactic protein-1 and tumor necrosis factor-alpha secretion. Signal integration and NF-kappa B translocation. *J. Clin. Invest.* **1995**, *95*, 2297−303.
(42) Schwertz, H.; Köster, S.; Kahr, W. H.; Michetti, N.; Kraemer, B. F.; Weitz, D. A.; Blaylock, R. C.; Kraiss, L. W.; Greinacher, A.; Zimmerman, G. A.; Weyrich, A. S. Anucleate platelets generate progeny. *Blood* **2010**, *115*, 3801−9.
(43) Smyth, S.; Whiteheart, S.; Italiano, J., Jr.; Coller, B. Platelet Morphology, Biochemistry, and Function. *Williams Hematol.* **2011**, *12*, 756.
(44) Ruenraroengsak, P.; Florence, A. T. Biphasic interactions between a cationic dendrimer and actin. *J. Drug Target* **2010**, *18*, 803−11.
(45) Ellis, C. E.; Naicker, D.; Basson, K. M.; Botha, C. J.; Meintjes, R. A.; Schultz, R. A. Damage to some contractile and cytoskeleton

proteins of the sarcomere in rat neonatal cardiomyocytes after exposure to pavetamine. *Toxicon* **2010**, *55*, 1071−9.
(46) Bouchard, B. A.; Butenas, S.; Mann, K. G.; Tracy, P. B. Interactions between Platelets and the Coagulation System. *Platelets* **2007**, 1343.
(47) Tracy, P.; Peterson, J.; Nesheim, M.; McDuffie, F.; Mann, K. Interaction of Coagulation Factor V and Factor Va with Platelets. *J. Biol. Chem.* **1979**, *254*, 10354−10361.
(48) Tracy, P. B.; Nesheim, M. E.; Mann, K. G. Coordinate binding of factor Va and factor Xa to the unstimulated platelet. *J. Biol. Chem.* **1981**, *256*, 743−51.
(49) Suzuki, K.-i.; Sato, K.; Kamohara, M.; Kaku, S.; Kawasaki, T.; Yano, S.; Iizumi, Y. Comparative Studies of a Humanized Anti-glycoprotein IIb/IIIa Monoclonal Antibody, YM337, and Abciximab on in Vitro Antiplatelet Effect and Binding Properties. *Biol. Pharm. Bull.* **2002**, *25*, 1006−1012.

CHAPTER 3

CATIONIC PAMAM DENDRIMERS AGGRESSIVELY INITIATE BLOOD CLOT FORMATION

Cationic PAMAM Dendrimers Aggressively Initiate Blood Clot Formation

Clinton F. Jones,[†,▽] Robert A. Campbell,[‡,▽] Amanda E. Brooks,[†] Shoeleh Assemi,[§] Soheyl Tadjiki,[⊥] Giridhar Thiagarajan,[#,△] Cheyanne Mulcock,[†] Andrew S. Weyrich,[‡,∥] Benjamin D. Brooks,[†] Hamidreza Ghandehari,[†,#,△] and David W. Grainger[†,#,△,*]

[†]Department of Pharmaceutics and Pharmaceutical Chemistry, Health Sciences, University of Utah, Salt Lake City, Utah 84112, United States, [‡]Program in Molecular Medicine, University of Utah School of Medicine, Salt Lake City, Utah 84132, United States, [§]Department of Metallurgical Engineering, University of Utah, Salt Lake City, Utah 84112, United States, [⊥]Postnova Analytics, Inc., Salt Lake City, Utah 84102, United States, [∥]Divisions of Pulmonary and Critical Care Medicine, Department of Internal Medicine, University of Utah, Salt Lake City, Utah 84132, United States, [#]Utah Center for Nanomedicine, Nano Institute of Utah, University of Utah, Salt Lake City, Utah 84112, United States, and [△]Department of Bioengineering, University of Utah, Salt Lake City, Utah 84112, United States. [▽]These authors contributed equally to this work.

ABSTRACT Poly(amidoamine) (PAMAM) dendrimers are increasingly studied as model nanoparticles for a variety of biomedical applications, notably in systemic administrations. However, with respect to blood-contacting applications, amine-terminated dendrimers have recently been shown to activate platelets and cause a fatal, disseminated intravascular coagulation (DIC)-like condition in mice and rats. We here demonstrate that, upon addition to blood, cationic G7 PAMAM dendrimers induce fibrinogen aggregation, which may contribute to the *in vivo* DIC-like phenomenon. We demonstrate that amine-terminated dendrimers act directly on fibrinogen in a thrombin-independent manner to generate dense, high-molecular-weight fibrinogen aggregates with minimal fibrin fibril formation. In addition, we hypothesize this clot-like behavior is likely mediated by electrostatic interactions between the densely charged cationic dendrimer surface and negatively charged fibrinogen domains. Interestingly, cationic dendrimers also induced aggregation of albumin, suggesting that many negatively charged blood proteins may be affected by cationic dendrimers. To investigate this further, zebrafish embryos were employed to more specifically determine the speed of this phenomenon and the pathway- and dose-dependency of the resulting vascular occlusion phenotype. These novel findings show that G7 PAMAM dendrimers significantly and adversely impact many blood components to produce rapid coagulation and strongly suggest that these effects are independent of classic coagulation mechanisms. These results also strongly suggest the need to fully characterize amine-terminated PAMAM dendrimers in regard to their adverse effects on both coagulation and platelets, which may contribute to blood toxicity.

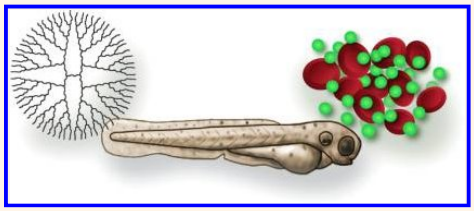

KEYWORDS: nanotoxicity · fibrinogen · protein aggregation · blood compatibility · coagulation · surface charge

Nanoparticles and other nanotechnologies promise to address a broad cross-section of biomedical needs in diverse applications such as drug delivery systems, imaging agents, and diagnostic products.[1] Medical nanotechnology markets are predicted to exceed $53 billion globally in 2012, and nanotechnology is projected to provide a component in up to half of all pharmaceutical products by 2015.[2] Dendrimers, a class of progressively hyperbranched polymers with diverse chemistries and unique properties, are proposed to be an important component in future innovations and applications of nanomaterials in medicine.[3] Their dendritic polymer structure provides highly versatile chemistry with monodisperse, multifunctional properties from geometrically and size-controlled molecules bearing high densities of terminal functional groups. Drug delivery applications for dendrimers are receiving increasing focus especially in two research areas: (1) as drug conjugates, in particular in cancer therapeutics,[4,5] and (2) as a drug solubilization technique.[6,7] Notably, both of these applications could yield new drug formulations containing dendrimers with many possible routes of *in vivo* administration, significant bioavailability, and systemic exposure in humans.

Recently, amine-terminated (PAMAM) dendrimers were shown to exhibit potent

* Address correspondence to david.grainger@utah.edu.

Received for review August 1, 2012 and accepted October 12, 2012.

Published online October 13, 2012
10.1021/nn303472r

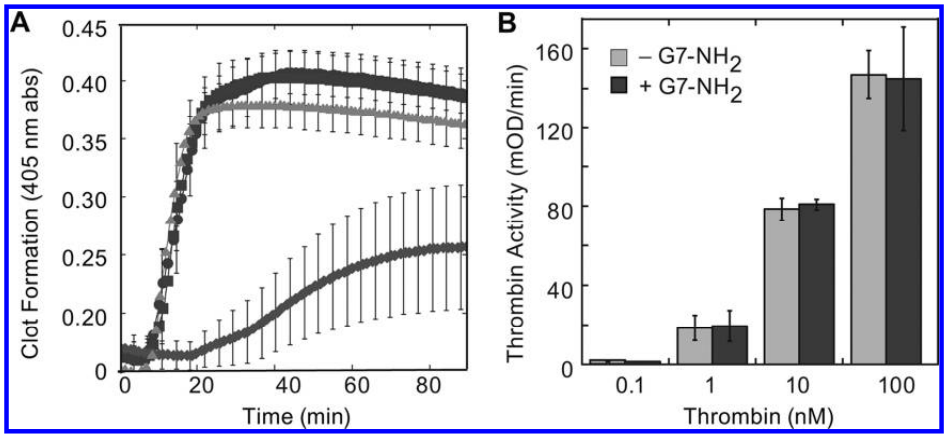

Figure 1. Cationic dendrimers blunt fibrin clot formation, but have little effect on thrombin activity. PPP was harvested as described in Methods, and clot formation induced by the addition of recombinant tissue factor (Innovin 1:10000, final) and calcium (20 mM) (triangle). In some reactions, G6.5-COOH (square), G7-OH (circle), or G7-NH_2 (diamond) (100 μg/mL, final) was added immediately before initiation of the reaction (A). To test whether cationic dendrimers directly affected the ability of thrombin to cleave fibrinogen, G7-NH_2 dendrimers were incubated with various concentrations of thrombin. The ability of thrombin to cleave a chromogenic substrate was then measured by a spectrometric plate reader at 405 nm (B).

activation reactions in whole blood, producing nanotoxicity.[8−13] Specifically, cationic dendrimers have recently been shown to extensively activate platelets, induce platelet aggregation, and comprehensively modify platelet functions both *in vitro* and *in vivo*.[8,13] Notably, some observed mechanisms of dendrimer pro-coagulant functions are unusual: cationic generation-7 PAMAM dendrimer (G7-NH_2) inhibited platelet-supported thrombin generation. Previous findings have further documented the dependence of these observed dendrimer−platelet effects on dendrimer formal surface charge and charge density that promote direct dendrimer binding to platelets and extensive platelet morphological alterations.[8,13] In rodents, intravenously injected cationic dendrimers were observed to produce a disseminated intravascular coagulation (DIC)-like condition accompanied by production of fibrinogen degradation products and rapid mortality.[14] The contrast of this fatal coagulopathy *in vivo* with observations of dendrimer inhibition of thrombin generation *in vitro* is unique and intriguing, but currently without any mechanistic understanding. This potent cationic dendrimer toxicity in blood requires further elucidation of dendrimer interactions with the coagulation cascade and its end product, the fibrin clot.

In this study, we demonstrate interactions of charge-dense, cationic (−NH_2-terminated) high-generation dendrimers with fibrinogen to generate clot-like structures. Results provide novel mechanistic data to demonstrate that cationic dendrimers induce coagulopathies through their ability to aggregate negatively charged blood proteins, including fibrinogen and albumin. Furthermore, real-time intravital observations in zebrafish embryos (ZFEs) expand previous *in vivo* observations with temporal refinement of the clot-like effect and demonstrate the significance of the formation of dendrimer-induced fibrinogen aggregation that is independent of classic coagulation pathways. Taken together, these results strongly suggest a mechanism of rapid, extensive electrostatic interaction to produce the DIC-like phenomena when densely charged cationic dendrimers contact blood.

RESULTS

Previous observations of rapid, dose-dependent *in vivo* coagulation[14] prompted by high-generation cationic dendrimer intravenous injection have no known mechanism. Attempts to better understand the interactions of these cationic dendrimers with blood components began by examining dendrimer effects on clot formation. Recombinant tissue factor and calcium chloride were added to platelet-poor plasma (PPP) in the absence or presence of G7-NH_2, G7-OH, or G6.5-COOH dendrimers. Clot formation was monitored by changes in turbidity measured at 405 nm. Figure 1A shows that cationic dendrimer-treated plasma clots formed substantially slower and to a lesser extent than both saline-treated negative controls and anionic/neutral dendrimer-treated samples. These results agree with the previous finding that cationic dendrimers inhibit thrombin generation *in vitro* in whole blood and platelet-rich plasma,[13] but seem to contradict the previous *in vivo* observations of coagulopathy.[14]

Our previous results suggested that thrombin generation was blunted in plasma in the presence of cationic dendrimer, but did not preclude the possibility for blunted thrombin activity in the presence of G7-NH_2. To determine if thrombin activity is affected, incresasing concentrations of thrombin were preincubated with a constant concentration of cationic dendrimer,

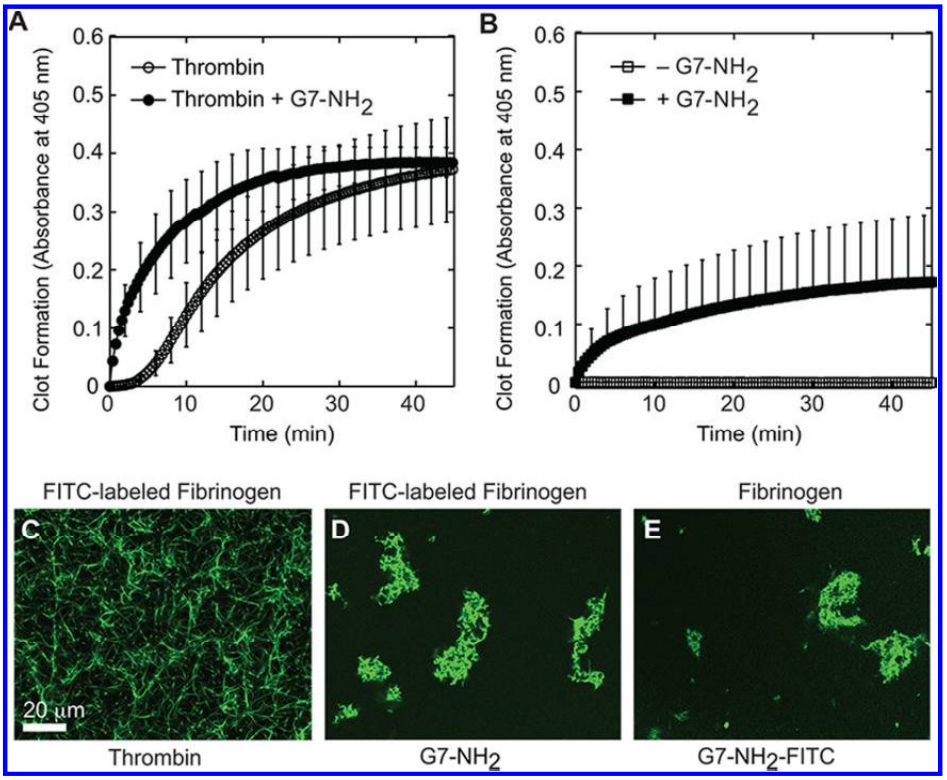

Figure 2. Cationic dendrimers induce fibrinogen aggregates. Clot formation was initiated by the addition of thrombin (2 nM, final) to fibrinogen (2 mg/mL, final) and monitored by changes in turbidity at 405 nm. In some experiments, G7-NH_2 PAMAM dendrimers (100 μg/mL, final) were added to the reaction immediately prior to thrombin addition (A). To test the effect of dendrimer directly on fibrinogen, fibrinogen with or without G7-NH_2 was monitored at 405 nm for changes in turbidity (B). Fibrin clot morphology was assessed by adding FITC-labeled fibrinogen to reactions described above. The resulting structure was then examined by laser-scanning confocal microscopy. Fibrin morphology in reactions containing FITC-labeled fibrinogen without G7-NH_2 (C), FITC-labeled fibrinogen with G7-NH_2 (D), and unlabeled fibrinogen with FITC-G7-NH_2 (E).

and thrombin's ability to cleave a chromogenic substrate was examined. As depicted in Figure 1B, cationic dendrimers do not interfere with thrombin's ability to cleave a chromogenic substrate, suggesting that thrombin's active site is unaffected by dendrimers and remains capable of cleaving fibrinogen; therefore, we decided to examine how cationic dendrimer affected fibrin formation in a purified system, where thrombin is not generated. A typical clotting response was observed for fibrinogen with the addition of thrombin, including a brief initial lag phase followed by rapid clot formation that plateaued at >45 min (Figure 2A). Upon addition of cationic dendrimer to the thrombin—fibrinogen system, the lag phase was eliminated and the rate of fibrin formation accelerated, reaching a plateau in only 30 min (Figure 2A). Notably, the presence of dendrimer did not significantly alter the peak optical absorbance attained, suggesting a similar extent of fibrin formation in the presence of dendrimer as compared to thrombin alone. Since our previous results suggested that thrombin generated was blunted in the presence of dendrimer,[13] but fibrin clot formation still occurred (Figure 1A), we examined the effect of cationic dendrimer upon fibrinogen alone, without thrombin. Cationic dendrimer addition to fibrinogen alone produced a clotting response with no lag phase and a rapid initial growth phase (Figure 2B) similar to dendrimer addition to the thrombin—fibrinogen reaction just discussed. These results demonstrate a rapid and direct (thrombin-independent) interaction between cationic dendrimer and fibrinogen. Moreover, the absence of a lag time following dendrimer addition argues for the nearly immediate formation of molecular associations between dendrimer and fibrinogen that occur in the absence of molecular cleavage. Importantly, the direct and immediate dendrimer–fibrinogen association and clot-like behavior demonstrated herein offer a compelling explanation for the immediate coagulopathy observed in all *in vivo* intravenous assessments of cationic high-generation dendrimers to date.

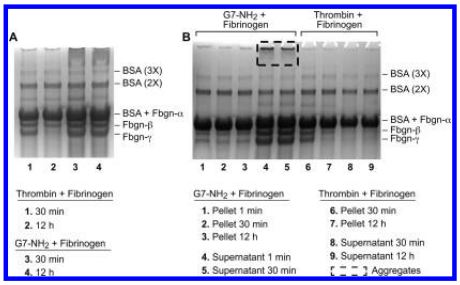

Figure 3. G7-NH_2 PAMAM dendrimers form high molecular weight aggregates with fibrinogen and albumin. Thrombin cleavage of fibrinogen results in no HMW aggregates (lanes 1 and 2), while addition of G7-NH_2 dendrimers immediately (lane 3) forms HMW aggregates, which are still visible 12 h after addition (lane 4) (A). HMW aggregates are seen only in the supernatant of fibrinogen and G7-NH_2 dendrimers (lanes 4 and 5) and are not in the pellet (lanes 1−3). HMW aggregates are not seen when thrombin and fibrinogen are incubated with each other (lanes 6−9) (B). HMW albumin aggregates are seen only in the presence of G7-NH_2 dendrimers (A, B).

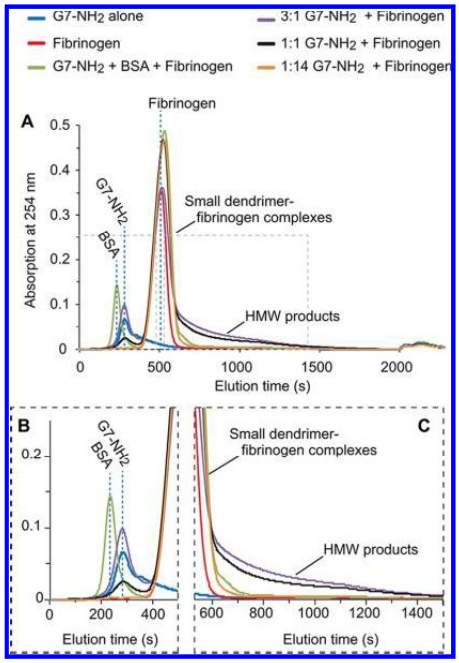

Figure 4. Cationic dendrimers induce high molecular weight fibrinogen aggregates. G7-NH_2 (blue) and fibrinogen (red) samples each provided a clean monomeric elution peak. Addition of dendrimer to fibrinogen produced a broadening of the fibrinogen peak (compare red *vs* orange) and substantial growth of the peak tail with increasing dendrimer/fibriongen molar ratio (compare orange to black to purple) (A). Insets of elution times between 0 and 500 s (B) and 600−1500 s (C) are included to better display dendrimer and product peak tails, respectively.

Microscopy of FITC-labeled fibrinogen was undertaken to characterize the product of this unusual thrombin-independent coagulation response and to visualize the dendrimer-induced perturbations on clot morphology. In the absence of cationic dendrimer, thrombin cleaves fibrinogen to form fibrin. Fibrin monomers polymerize to form protofibrils in one dimension, which then associate to produce a regular, but random, homogeneous mesh or network of fibrin (Figure 2C). In contrast, dendrimer treatment of FITC-labeled fibrinogen produced irregularly shaped, consolidated fibrinogen masses that appear to possess neither protofibrils nor defined secondary structure (Figure 2D). Additionally, separate imaging of clots with a FITC-labeled cationic dendrimer component showed dendrimer-based labeling throughout clots of unlabeled fibrinogen (Figure 2E). These results reveal pervasive dendrimer incorporation within each clot-like body and suggest the dendrimer-centric aggregation of fibrinogen, further strengthening the idea that dendrimer−fibrinogen associations underlie the DIC-like conditions observed *in vivo*. Notably, there is no evidence of fibrinogen cleavage to fibrin with dendrimer exposure (*e.g.*, fibrinopeptide cleavage), thus supporting a surrogate mechanism for this key coagulation event, independent of thrombin.

SDS-PAGE gel analysis was performed to assess the molecular products formed by dendrimer treatment of fibrinogen. Digested products of dendrimer−fibrinogen reactions were compared to thrombin-treated (positive) and untreated (negative) controls (Figure 3). Thrombin treatment of fibrinogen demonstrated a time-dependent loss of the smallest fibrinogen band, just below 50 kDa (Figure 3A, lanes 1 and 2), resulting from covalent gamma-chain cross-linking mediated by residual plasma transglutaminase (FXIIIa) in the thrombin stock, as has been shown.[15] With reaction time, these gamma-chain dimers grow to multimers that are increasingly resistant to cleavage.[15] This cleavage-mediated cross-linking was not observed following dendrimer treatment (Figure 3A, lanes 3 and 4; 3B, lanes 4 and 5). However, in addition to fibrinogen fragment bands that were similar to the untreated control, cationic dendrimer treatment of fibrinogen produced very high molecular weight (HMW) products that ran only slightly in the gel and spanned the area from the well to the faint band of residual (unreduced) fibrinogen near 340 kDa. Such HMW entities were observed in all dendrimer-treated samples, but were not observed in any other samples or controls. Moreover, PAGE banding patterns for

TABLE 1. AsFlFFF Peak Integrations (dendrimer−FBG[a] peak and tail ratios)

treatment condition	FBG peak area	FBG tail area	tail (% of total)
3:1 G7/FBG	31.69	12.63	40
1:1 G7/FBG	33.89	9.99	29
1:14 G7/FBG	26.00	2.64	10
FBG only	32.84	1.41	9

[a] Fibrinogen.

dendrimer-treated fibrinogen were similar for all time points, including 1 min, 30 min, and 12 h treatment periods (Figure 3B, lanes 1–5), demonstrating the extremely rapid formation of dendrimer–fibrinogen associations that appear to remodel very little over time. Notably, when fibrinogen was treated initially with thrombin followed by cationic dendrimer, formation of HMW products was not observed (data not shown). These results strongly suggest dendrimer-mediated aggregation of fibrinogen that is dependent upon the presence of uncleaved fibrinogen and distinct from thrombin proteolysis of fibrinogen. Interestingly, similar HMW products were observed in PAGE analysis of cationic dendrimer-treated single-protein samples of bovine serum albumin (BSA) alone (data not shown). However, unlike fibrinogen products, fractions of HMW products in BSA–dendrimer samples increased with duration of exposure to cationic dendrimer.

In sharp contrast to the foregoing PAGE results, reaction of cationic dendrimer with protamine, a small, highly cationic blood protein (5–10 kDa) composed of roughly 60% arginine, did not produce any perceptible amount of interaction product or aggregation (Supplemental Figure 1). Conversely, the reaction of anionic (generation-7 carboxylate-terminated) dendrimer with protamine (2 mg/mL) resulted in strong HMW bands that diminished with decreasing G7-COO^-/protamine molar ratios from 1:113 to 1:4760, where they vanished (data not shown). (These molar ratios were intended to bracket and include the estimated 1:340 molar ratio needed to form a complete protamine monolayer on a G7-dendrimer surface.) Together, these fibrinogen–, albumin–, and protamine–dendrimer product results demonstrate electrostatically mediated dendrimer interactions with oppositely charged proteins to produce fibrinogen/albumin HMW aggregates distinct from thrombin-mediated fibrin polymerization products.

Since cationic dendrimers alone do not electrophorese (data not shown), aggregate product sizing by electrophoresis alone was uncertain due to the potential for exposed dendrimer surface charge density in the HMW products to greatly affect product movement within the gel. Thus, to monitor the effect of dendrimer charge density and confirm and characterize the dendrimer and fibrinogen interaction products, asymmetrical flow field-flow fractionation (AsFlFFF) was employed for aggregate particle hydrodynamic size-based separation. Clean monomeric peaks were obtained for BSA (data not shown), dendrimer, and fibrinogen alone at 3.9, 4.7, and 8.5 min retention times, respectively (Figure 4A, B). With dendrimer treatment (1:14 G7-NH_2/fibrinogen ratio), the dendrimer peak vanished and the fibrinogen peak broadened, and the elution time shifted slightly from 8.2 to 8.7 min (Figure 4A, C, red *vs* orange curves). Increasing the dendrimer:fibrinogen molar ratio from 1:14 to 3:1 resulted in the appearance of a free dendrimer peak

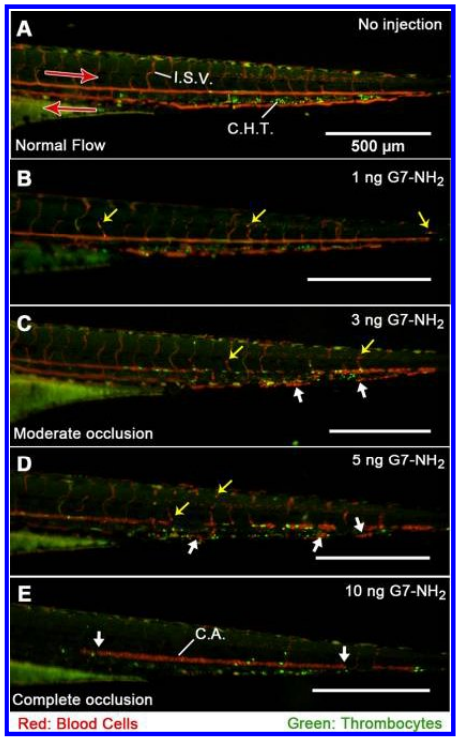

Figure 5. Dose-dependent G7-NH_2 occlusion in zebrafish embryos 1 min postinjection. ZFEs (4dpf gata-1::dsred/CD-41::EGFP) were anesthetized, mounted, injected, and imaged as described in Methods. The top panel (A) depicts unperturbed caudal blood flow as streaks of red and green light visible in the major caudal artery (CA, left to right), vein (right to left), and intersegmental vessels (ISV). Punctate green and red spots in between the major caudal artery and vein indicate the location of the caudal hematopoietic tissue (CHT). Subsequent images (proceeding downward (B–E), with increasing G7-NH_2 dose) depict increased cellular adhesion and vascular occlusion resulting from dendrimer injection, culminating in no visible blood flow following an injection of 10 ng of G7-NH_2. The yellow arrows depict individual red blood cells trapped inside the vessel, while the large white arrows show significant blood clots inside the vessels. Notice in (E) the caudal artery is completely occluded with no observable flow in the major caudal vein.

along with corresponding growth in area and length for the tail of the fibrinogen product peak (Figure 4A, C). Significantly, with dendrimer treatment, the fibrinogen peak gained a tail that increased in area from 10% to 40% of the total peak area by increasing dendrimer/fibrinogen ratios from 1:14 to 3:1 (Table 1). Moreover, this tail extended to 16 min beyond the fibrinogen peak for the 3:1 dendrimer/fibrinogen sample. Given the size-based separation inherent in the AsFlFFF technique, these results in dendrimer-treated fibrinogen samples indicate a continuum of aggregate sizes ranging from simple (possibly 1:1) dendrimer–fibrinogen associations (indicated by the large product peak with a small shift in retention time from the fibrinogen-only peak) to

progressively larger aggregates, evinced most clearly by the protracted peak tail for the 3:1 dendrimer/fibrinogen sample.

The preceding data strongly suggest rapid dendrimer-mediated aggregation of fibrinogen and provide data consistent with products of such interactions, with evidence for an electrostatic mechanism extending to many negatively charged blood components. Consequently, direct observation of *in vivo* coagulopathy was sought in the transparent zebrafish embryo model of blood coagulation to visualize the extent, character, and time dependence of the *in vivo* DIC-like condition arising from cationic dendrimer interaction in blood.[14] Hybrid CD-41::EGFP/gata-1::dsred 4dpf ZFEs, utilized for fluorescence-facilitated visualization of RBCs and thrombocytes in the circulation, were anesthetized, mounted, and injected with dendrimer preparations of various doses. Cationic dendrimer injections into ZFEs were observed to produce immediate coagulation at the injection site that rapidly resulted in caudal (tail) vessel occlusions that scaled roughly with cationic dendrimer dose (Figure 5B–E, supplemental video 1). In separate experiments, FITC-labeled cationic dendrimer injections into wild-type (AB) nonfluorescent ZFE produced fluorescently labeled clots along with diffuse staining throughout the vasculature, indicating cationic dendrimer association with the vascular endothelium (Supplemental Figure 2). This suggests that cationic dendrimers participate directly in the observed *in vivo* DIC-like events in blood and that cationic dendrimers may possess a high affinity for platelets and endothelial cells or may bind vascular endothelium, either directly or together with complexed plasma proteins. Additionally, identically administered anionic and neutral G6.5/G7 dendrimers produced no observable vascular occlusion (data not shown). This is consistent with both previous *in vivo* (rodent) observations that neutral and anionic dendrimer dosing was limited only by dendrimer solubility and not toxicity[14] and also recent *in vitro* findings demonstrating that neutral and anionic dendrimer functionalizations are minimally activating toward platelets *in vitro* (little/no platelet aggregation, morphology change, or granular release).[8,13] Functional equivalence has been previously established for zebrafish coagulation machinery in comparison to human blood.[16–18] Moreover, zebrafish blood and platelets are responsive to a variety of procoagulants and platelet agonists (*i.e.*, ristocetin, collagen, rabbit brain thromboplastin, Russell's viper venom, thrombin, adenosine diphosphate, and arachidonic acid), anticoagulants (*i.e.*, heparin, hirudin, sodium citrate, and warfarin), and antiplatelet agents (*i.e.*, acetylsalicylic acid (aspirin), abciximab, and aurin tricarboxylic acid).[19–23] Thus, a variety of anticoagulant and antiplatelet agents were applied prophylactically to ZFE to elucidate the mechanism of dendrimer-induced coagulopathy. However, none of these embryo pretreatments (administered 30 min or 2 h before dendrimer injection) prevented or noticeably diminished the occlusion resulting from a subsequent cationic dendrimer injection (3 ng, Supplemental Figure 3 and data not shown), but bleeding complications were common at the dendrimer injection site in ZFE pretreated/preinjected with warfarin, sodium citrate, lepirudin, or heparin (data not shown). Prophylactic treatments included the following agents (with maximum concentrations stated): pretreatment with warfarin (500 μM, final), sodium citrate (0.38%, final), or acetylsalicylic acid (75 μg/mL, final); preinjection (1 nL) with abciximab (42 μM), lepirudin (145 484 U/mL), or heparin sulfate (15 mg/mL) (Supplemental Figure 3). Importantly, pretreatment of ZFE by soaking in sodium citrate for 2 h (0.38%, final) was observed to block the coagulogenic action of injected human thrombin (1 nL, 3 μM), although this was only observed in roughly half of embryos tested (supplemental videos 2 and 3). The source of this inconsistency is unknown, but may be attributable to genetic variation of wild-type ZFE and nonhomology between zebrafish and human thrombin.[24]

DISCUSSION

Dose- and generation-dependent toxicity for cationic dendrimers in a variety of cell types and experimental systems has been reported (reviewed elsewhere[25]). Specifically, decreasing toxicity has been observed for decreasing dendrimer generation with higher maximum tolerated doses for lower generation dendrimers than for higher generation cationic dendrimers.[25] Previous reports of hemolysis,[14,26] platelet activation *in vitro*,[13] and fibrin degradation products in the blood of G4-NH_2 and G7-NH_2 dendrimer-injected rodents[14] consistently suggest a strong procoagulant role for cationic dendrimers in blood. Notably, these results also observed dose- and generation-dependent blood toxicity with G3 and G4 generation dendrimers.[8,13,25] Previous studies by our laboratory as well as other groups have focused on the effect of high-generation dendrimers on platelet function, but their effects on soluble coagulation proteins have been inadequately studied to date.[8,13,25] Significant platelet activation usually results in exposure of phosphatidylserine and platelet-dependent thrombin generation, but administration of cationic G7 dendrimers to plasma paradoxically inhibited thrombin generation.[13] In addition, G7-NH_2 dendrimers blunted fibrin clot formation (Figure 1A). Collectively, these findings set up an apparent *in vitro–in vivo* dichotomy of response to cationic dendrimers where the dendrimer architecture (G7) that produces the most thrombotic response has also been observed to inhibit production of the most critical coagulation enzyme, thrombin. Significantly, this dichotomy is not explainable as a simple dendrimer-mediated deactivation or binding of thrombin since thrombin retains its enzymatic activity in the presence of cationic dendrimers (Figure 1B). Thus, cationic

dendrimer attenuation of thrombin and clotting is likely to occur at the level of thrombin generation, and not thrombin activity.

Given the severe coagulopathy observed *in vivo*, the observed *in vitro* inhibition of thrombin generation (without inhibition of thrombin activity) presents an interesting potential distinction between the thrombotic actions of cationic dendrimer and thrombin resulting from competing molecular interactions with cationic dendrimer. In this respect, the simplified coagulation assay comprising only thrombin and fibrinogen demonstrated that cationic dendrimers actually accelerate clot formation and remove the lag phase observed for this simplified thrombin-clotted fibrinogen condition (Figure 2A). Further simplification of the assay demonstrated that fibrinogen clotting proceeds immediately following dendrimer addition (*i.e.*, no lag phase) (Figure 2B), producing dense, consolidated clots with pervasive dendrimer staining (Figure 2D, E) *even in the absence of thrombin*. The apparent contradiction between these accelerated clotting results and the attenuation of clotting in PPP with dendrimer exposure (Figure 1A) strongly suggests the influence of additional, competing interactions of cationic dendrimer with many of the cogulation-naïve plasma proteins present in PPP, but not present in these simplified binary or ternary coagulation assays (Figure 2).

Prior work has demonstrated interactions between cationic dendrimers and plasma proteins[27−29] to the extent that hemolysis of purified red blood cells is blunted in the presence of added human serum albumin,[30] demonstrating that both platelets and red blood cells are partially protected by the protein-rich environment of whole blood. Notably, despite previous *in vitro* analysis of dendrimer-induced platelet activation,[13] including extensive adhesion, aggregation, and proinflammatory secretions, extensive hemolysis and platelet activation have not been demonstrated *in vivo* following cationic dendrimer injection, even amidst extensive coagulopathy. Significantly, this is the first report of HMW products arising from protein−dendrimer interactions and strongly suggests that the previously reported DIC-like phenomenon may arise, in part, from dendrimer interactions with proteinaceous coagulation zymogens.

This thrombin- and (possibly) fibrin-independent interaction of cationic dendrimers with fibrinogen may simply be based on electrostatic interactions. Soluble fibrinogen (uncleaved) at physiological pH possesses a net −20 anionic charge with significant localized negative charge density on the E region (−8), which becomes positively charged (+5) upon cleavage of the fibrinopeptides to form insoluble fibrin (−7 charge overall). Thus, dendrimer−fibrinogen electrostatic interactions may be more favorable than dendrimer−fibrin interactions. This assessment is borne out in SDS-PAGE results (Figure 3) demonstrating that cationic dendrimer treatment of fibrinogen produced aggregates of otherwise unmodified fibrinogen. This was supported by the SDS-PAGE gel presence of HMW products that exceeded the size of unreduced fibrinogen (340 kDa) and, in some cases, that did not leave the loading well. These products were not present following dendrimer treatment of thrombin-activated fibrinogen (data not shown). Additionally, the similarity of dendrimer-treated fibrinogen fragment bands to the untreated fragment band patterns (*i.e.*, negative control) demonstrates an absence of the fibrinogen cleavage and cross-linking that are evident in thrombin-treated controls. Thus, dendrimer−fibrinogen molecular aggregates are proposed to form from strong electrostatic interactions between densely charged (positive) dendrimer surfaces and the oppositely charged (negative) D or E domains of uncleaved fibrinogen. Such aggregates would effectively comprise quasi dimers, trimers, and multimers of fibrinogen formed by electrostatic association between fibrinogen and cationic dendrimers. Given the numerous binding sites available on G7 dendrimers with 512 surface primary amines per molecule, such electrostatic binding of multiple fibrinogen molecules would be limited only by packing parameters and steric hindrance between adjacent fibrinogen molecules. However, since fibrinogen is roughly the size of four or five dendrimers placed end to end (9 × 45 nm long rod *vs* a 8.1 nm diameter sphere, respectively) and the negative regions of the D and E fibrinogen domains are present on opposite molecular faces, one fibrinogen molecule may interact with more than one dendrimer molecule, enhancing aggregate stabilization by charge−charge multimer cross-linking.

The AsFlFFF data demonstrate that most products formed by dendrimer−plasma protein complexes are likely simple 1:1 dendrimer−fibrinogen associations, but additionally confirm that much larger aggregates are also formed, particularly if provided dendrimer excess bias in the binary solution composition. These larger entities likely include additional dendrimers electrostatically adsorbed onto the original dendrimer−fibrinogen core, perhaps forming progressively larger multimer aggregates with alternating dendrimer−fibrinogen structure. This could occur with primary dendrimer−fibrinogen associations forming between the densely anionic E domain at fibrinogen centers and densely cationic dendrimer surfaces, and weaker, secondary associations forming between additional dendrimers and the somewhat less densely anionic D domains at the ends of the fibrinogen molecule on the opposite face from the E region charges. Further, the area relationship of the AsFlFFF product elution peak to its tail (Table 1) provides an estimated number-based proportion of small, primary aggregates relative to larger, more complex aggregate compositions. The tail's proportion to the total peak area increases with increasing dendrimer feed ratios, demonstrating the requirement for excess dendrimer for the generation of

larger FFF aggregates. The smooth decay of the product tail with increasing aggregate size demonstrates that no single binding combination is energetically most favorable beyond the major peak. Rather, the size distribution of larger aggregation products seems to be based on statistical probabilities of forming aggregates of given sizes based on alternating dendrimer−fibrinogen interactions with decreasing probability for each successive unit addition.

The most pronounced aggregate presence in gel electrophoresis results (Figure 3) was observed for dendrimer-treated samples of fibrinogen and BSA together, and the presence of BSA adds a shoulder to the dendrimer−fibrinogen product peak in the AsFlFFF results (Figure 4). BSA carries net charges of −10 and −8 on two of its three domains at neutral pH,[31] has a pH-regulating function in the blood,[32] and is highly predisposed to adsorption to foreign bodies in contact with blood.[33] At 2−3 and 40−45 mg/mL in human blood, respectively, fibrinogen and albumin together represent a substantial mass fraction of total soluble blood protein content (70 mg/mL total). They also represent two very different protein components in blood, with their drastically differing glycosylation patterns, shape (rodlike *vs* globular), structure and composition (many domains and fragments *vs* single globular strand), and function (hemostasis *vs* pH regulation and fatty acid transport). One major commonality shared by these two very disparate plasma proteins is a high negative charge density on two of their respective domains. That this property elicits electrostatically based dendrimer−fibrinogen and dendrimer−albumin interactions is seemingly confirmed by the absence of dendrimer aggregation with a densely cationic blood protein, protamine. Further, it reveals the potential for extensive "nonspecific" dendrimer-induced electrostatic protein aggregation extending well beyond a fibrinogen-only coagulation-specific response to include many blood proteins with negatively charged regions. Given up to 10 000 known proteins and 15 000 isoforms in the human plasma proteome,[34−36] most with anionic glycosylation patterns and acidic pI values,[37] there is substantial potential for cationic dendrimer−protein electrostatic interactions in whole blood. This electrostatic mechanism of aggregation is further supported by the charge-dependency demonstrated in a previous report of increased platelet aggregation observed both for increased cationic dendrimer generation and for increased intragenerational surface charge.[8] *In vivo*, such charge-based proteinaceous aggregation phenomena could rapidly produce numerous microemboli capable of adhesion to the endothelium, with subsequent consolidation into occlusions and microvasculature infarcts.

Thus, cationic G7 dendrimers are proposed to exhibit very unusual thrombogenic behaviors through strong, charge−charge interactions with a variety of many different blood components, and perhaps no one blood element preferentially. Additionally, the capacity of cationic G7 dendrimers to bind both platelets[13] and fibrinogen may also explain previous observations of platelet aggregation and adhesion to fibrinogen, each in the presence of abciximab, the platelet $\alpha_{IIb}ß_3$ (platelet fibrinogen receptor) agonist.[13] Ultimately, as an alternative to the classic enzymatic mechanism of blood coagulation, high-generation dendrimers may provide an unconventional "coagulation" mechanism consisting of complex, multicomponent interactions between platelets, dendrimers, fibrinogen, and many other anionic blood proteins. In this manner, rapid, nonspecific aggregation events could consume significant amounts of platelets and fibrinogen, as well as other negatively charged cellular and molecular elements of blood, forming aggregates and microemboli that are then consolidated by both flow and microvascular transport dynamics into massive occlusions. While the focus of the current study has been on cationic G7 dendrimers, lower generation dendrimers should also be examined carefully for similar protein aggregation properties since previous reports have demonstrated that G3 dendrimers can induce platelet activation and blood toxicity has been observed with G4 generations.[8,13,25]

These dynamics are evident in dose−response relationships observed *in vivo*. In a dendrimer-poor scenario in which DIC-like aggregation is limited by cationic G7 dendrimer concentration, dendrimer addition results in the formation of comparatively smaller aggregation products (Figure 4) and may thus result in only a minimal amount of thrombosis and vascular occlusion. This outcome was observed for the lowest doses of cationic G7 dendrimer injected into ZFE (≤1 ng) and the rodent dendrimer doses (G4- and G7-NH_2) at which some rodents survived (5−10 mg/kg).[14] Alternatively, when the dendrimer dose is comparatively and sufficiently higher, the majority of platelets and fibrinogen are consumed[13,14] by extensive aggregation that may also include significant fractions of other blood proteins (Figure 4), leading to widespread coagulopathy *in vivo*.[14] Such an extensive thrombogenic response to high-generation cationic dendrimer doses was observed *in vivo* as the total cessation of intravascular blood flow in ZFEs following the highest cationic dendrimer dose injected intravenously (10 ng, Figure 5E, supplemental video 1) and the rapid mortality of rodent subjects receiving nontolerated dendrimer intravenous doses (G4-, G7-NH_2 >10 mg/kg).[14]

Since these present *in vivo* results represent the first usage of ZFEs for assessments of procoagulant nanomaterials in blood, it is important to underscore that the components and processes of zebrafish coagulation are well-studied and have been established as functionally equivalent to their human counterparts.[16−18] Moreover, zebrafish blood and platelets are responsive to a variety of procoagulants and platelet agonists in addition to many anticoagulants and antiplatelet agents.[19−23] The

conservation of these inhibitory effects was exemplified in the prevention of human thrombin-induced clotting in some ZFEs by prophylactic treatment (see supplemental videos 2 and 3) and separate observations of increased bleeding from the dendrimer injection site in prophylactically anticoagulant/antiplatelet-treated ZFEs (data not shown), specifically those previously presoaked/preinjected with warfarin, sodium citrate, heparin, or lepirudin. In the present context, the observation that none of the inhibitors examined affected the observed dendrimer-mediated coagulopathy confirms that the dendrimers' influences on coagulation are independent of classical procoagulant mechanisms. These findings also demonstrate the utility of the ZFEs for real-time visualization and description of nanomaterial effects in blood.

CONCLUSIONS

The findings presented here describe rapid and extensive aggregation of fibrinogen and other anionic blood proteins by densely charged cationic G7 dendrimers, observed to produce HMW aggregate species by a thrombin-independent and cellular activation-free mechanism. These effects were not inhibited by any of a wide array of antithrombotic or antiplatelet agents *in vivo*. The acidic natures and high concentrations of many endogenous proteins in blood (70 mg/mL total, 2.5 mg/mL fibrinogen and 45 mg/mL albumin, respectively) predispose these blood elements to this type of rapid and extensive aggregation with G7 dendrimers having uniquely dense cationic surfaces (*i.e.*, 512 tightly packed primary amine cations per G7 dendrimer under physiological conditions). Thus, cationic G7 dendrimer architecture may provide a rare cation presentation, unshared by any linear polycations, that provides potential for more potent, stable, dendrimer-mediated electrostatic aggregation of human plasma proteins as demonstrated here for fibrinogen and BSA. This is proposed as the likely basis for adverse reactions to intravenous cationic dendrimer injection observed *in vivo* in rodents[14] and ZFEs. These findings underscore existing concerns for intravenous applications of cationic G7 dendrimers and provide a warning for their biological applications to be designed with extreme caution and careful attention to their reactivity in blood. Future studies should examine the dose-, generation-, and surface group density-dependency for these clot-like and cellular activation effects of cationic dendrimers to identify those dendrimer doses and architectures that are safe for intravenous administration.

METHODS

Materials and Reagents. G6.5-COOH and G7-NH_2 poly(amido amine) dendrimers (Sigma Aldrich, USA) were purified by preparative size-exclusion chromatography and characterized as previously described.[14] The fibrinogen clot microscopy experiments utilized fluorescein isothiocyanate-conjugated G7-NH_2 (G7-NH_2-FITC) dendrimers whose labeling, purification, and characterization was described previously.[7,13] All dendrimers were lyophilized following their purification and subsequently diluted in endotoxin-free water or phosphate-buffered saline (pH 7.4) prior to their use. Human fibronectin-free fibrinogen (Enzyme Research Lab), bovine serum albumin (fraction V, EMD Chemicals, Inc.); ethylenediaminetetraacetic acid (EDTA, 0.5 M, Gibco); human thrombin (2500 nM) and heparin (sodium salt, bovine intestinal mucosa, Sigma); sodium citrate dehydrate (Fisher Scientific); abciximab (42 μM) and lepirudin (145484 U/mL) (Hospital Pharmacy, University of Utah, Salt Lake City, USA); endotoxin-free water (Lonza); acetylsalicylic acid (gift of Dr. C. Terry, University of Utah, Salt Lake City, USA); and protamine (gift of Dr. Sivaprasad Sukavaneshvar, Thrombodyne Inc., Salt Lake City, USA) were all used as received.

Whole Blood Collection and Plasma Preparation. This study was performed as approved by the University of Utah Institutional Review Board, and all subjects provided informed consent. Human peripheral venous blood (25−50 mL) was collected into acid-citrate-dextrose (1.4 mL ACD/8.6 mL blood) from healthy, medication-free, fasting adult subjects as previously described.[13] Plasma was harvested by centrifuging whole blood at 500*g* for 20 min and then once more at 13000*g* for 2 min to remove any remaining cell contaminants to yield platelet-poor plasma.

Zebrafish Embryos. Zebrafish aquaculture has been described elsewhere.[38] Breeding colonies were maintained by the University of Utah Zebrafish Core Facility on a 14 h light/10 h dark light cycle. ZFEs were obtained from fluorescent transgenic (Tg) zebrafish, either the recombinant Tg(CD-41::EGFP) variant possessing either green fluorescent protein (EGFP)-expressing thrombocytes and thrombocyte precursors (CD-41 promoter region)[18] or hybrid Tg(CD-41::EGFP/gata-1::dsred), red fluorescent protein (dsred)-expressing red blood cells (gata-1 promoter region),[39] and EGFP-thrombocytes. For clarity, transgenic lines will hereafter be referred to without their Tg(xxxx::xxxx) nomenclature. Embryos were incubated at 28.5 °C in E3 media (aqueous 5 mM NaCl, 0.17 mM KCl, 0.4 mM $CaCl_2$, 0.16 mM $MgSO_4$) supplemented with 0.000 016% methylene blue (antifungal).

Zebrafish Embryo Injection and Imaging. All procedures were performed according to an established IACUC-approved protocol. Either CD-41::EGFP or gata-1::dsred/CD-41::EGFP ZFE, at 3-, 4-, or 6-day-postfertilization (dpf), were sorted, anesthetized topically with tricaine methanesulfonate MS222 (tricaine), and immobilized in low-melt agarose (1% in sterile water without tricaine) maintained at 42 °C, as described previously.[38] Human thrombin or PAMAM G7-NH_2 dendrimers in sterile phosphate-buffered saline (PBS) were injected (1 nL) intravenously into the venous blood flow dorsal from and immediately proximal to the heart of 3 or 6 dpf ZFEs using a YOU-1 micromanipulator (Narishige), MPPI-3 microinjector (ASI), and BP-15 backpressure unit (ASI) for injection control and a M80 Leica stereomicroscope for visualization during the injection. Injected ZFEs were quickly transferred to an upright Nikon Eclipse 600 fluorescent microscope and imaged using a CRI Nuance multispectral imaging system model N-MSI-420-FL controlled by IPL software. Alternatively, ZFEs were both injected and imaged on a Leica M165 FC microscope, and images were captured using 5.5 megapixel CCD controlled by Leica image software, LAS v4.0. For time-lapse microscopy, embryo blood flow and coagulation images were captured at a rate of 3 images per second. Single still-frame images were taken at longer shutter times (>200 ms) to offer movement-based contrast between circulating and adherent blood cells/thrombocytes. Images demonstrating FITC−dendrimer localization were obtained following injection of FITC-labeled dendrimers into wild-type ZFEs. Images of extent of vascular occlusion were obtained following injection of unlabeled dendrimers into CD-41::EGFP or gata-1::dsred/CD-41::EGFP ZFEs, respectively.

In some experiments, ZFEs were pretreated before dendrimer treatment with an anticoagulant or antiplatelet agent by direct soaking for at least 30 min and up to 12 h (before dendrimer injection) in E3 embryo media-based solutions of warfarin (500 μM, final), acetylsalicylic acid (75 μg/mL, final), or sodium citrate (0.38%, final). Such small-molecule agents have previously been demonstrated to freely diffuse into ZFEs.[20,22] In other treatments, zebrafish were pretreated with injections (1 nL) of abciximab (42 μM), lepirudin (145484 U/ml), or heparin sulfate (15 mg/mL) in sterile PBS 2 h before dendrimer injection. In other experiments, treatments occurred immediately or 30 min before dendrimer injection. Timing of drug treatments had no effect.

Thrombin Activity Assay. Thrombin activity was measured as previously described[40,41] with the notable exception that dendrimer (100 μg/mL, final) was added to the reaction. The activity of the enzyme was measured by light absorbance at 405 nm on a Spectramax VMAX plate reader (Molecular Devices).

Clotting Assays. Clot formation was initiated by addition of recombinant tissue factor (Innovin (1:10 000, final)) and $CaCl_2$ (20 mM, final) to platelet-poor plasma in the presence or absence of dendrimer (100 μg/mL, final), and clot formation was monitored by changes in light absorbance at 405 nm on a Spectramax VMAX plate reader (Molecular Devices). To examine the effect of dendrimers on only fibrinogen polymerization, thrombin (2 nM, final) and dendrimer (100 μg/mL, final) were added to purified human fibrinogen (2 mg/mL, final) in PBS (pH 7.4) supplemented with $CaCl_2$ (3 mM) and clot formation was monitored. In separate experiments, thrombin was excluded from the sample preparation to assess dendrimer-mediated clot formation in the absence of thrombin.

Clot Morphology Assessment. Clot formation and imaging were performed as described previously.[40] Briefly, clots were produced by incubating AlexaFluor-488-labeled fibrinogen (10 μg/150 μL sample, 3.2% of total fibrinogen) with $CaCl_2$ (5 mM final) and either thrombin (2 nM final) or G7-NH_2 dendrimer (100 μg/mL final) for 30 min. Confocal microscopy was accomplished using a FV300 1 $\times$ 81 microscope and FluoView software (Olympus, Center Valley, USA, Fluorescent Microscopy Core Facility, University of Utah). Both 20$\times$ and 60$\times$ objectives were used. Optical sections were collected at randomly chosen locations.

SDS-PAGE of Protein–Dendrimer Products. Purified human fibrinogen (2 mg/mL final) in 140 mM PBS supplemented with $CaCl_2$ (3 mM final) and bovine serum albumin (1 mg/mL final) was reacted with dendrimer (100 μg/mL final) or purified human thrombin (5 nM final). After reaction times of 1 min, 30 min, 2 h, 12 h, or 72 h, EDTA (20 mM, final) was added. In some experiments, clots and supernatants were separated by centrifugation (14000*g*, 4 min), and each sample fraction was digested in urea (6 M, final) and DTT (40 mM, final) with heating (60 °C, 1 h). Clot fractions did not digest completely in the case of thrombin treatment. Thus, in one experiment, centrifuged clot/pellet fractions were digested in 7.5 M urea and 40 mM DTT. Samples were mixed with loading dye, denatured, and separated on a 4–12% PAGE gel (Novex, USA) for 60–90 min. Gels were stained with Acqua Stain (Bulldog Bio, USA) for at least 20 min, and images were captured using a Molecular Imager Gel Doc XR System (Bio-Rad, USA).

Size-Based Separation of Fibrinogen–Dendrimer Reaction Products. Asymmetrical flow field-flow fractionation was employed to separate product(s) of dendrimer–fibrinogen interactions based on hydrodynamic size. G7-NH_2 dendrimer was added to fibrinogen (2 mg/mL, final) in PBS at dendrimer/fibrinogen molar ratios of 3:1, 1:1, or 1:14 and vortexed for about 5 s. In one treatment condition, dendrimer was reacted with fibrinogen (2 mg/mL, final) in PBS supplemented with $CaCl_2$ (3 mM, final) and BSA (1 mg/mL, final), as described above. Sample aliquots (20 μL) were manually injected into the FFF column (25 °C) and focused for 7 min in the mobile phase (PBS) with cross-flow (0.1 mL/min) to effect size-based particle separation. Samples were then eluted by a constant flow of 1 mL/min with a field flow of 2 mL/min for 2 min, followed by a power-decay gradient from 2 to 0.1 mL/min over 15 min, 0.1 mL/min for 10 min, and 0 mL/min for 13 min. A complete description of the instrument and relevant methodology has been reported previously.[42]

Statistical Analysis. Sample experimental replicates of at least $n = 3$ were collected from biological replicates of $n = 2$. Where applicable, pairwise comparisons were performed with a Student's t test with $p < 0.05$ considered significant.

Conflict of Interest: The authors declare no competing financial interest.

Acknowledgment. The authors gratefully acknowledge D. Lim for figure preparation. Financial support was provided by the NIH (RO1DE019050, RO1 HL066277-11, and 1U54HL112311-01), the American Heart Foundation (11POST7290019), the Utah Science Technology and Research (USTAR) initiative, a University of Utah Graduate Research Fellowship, and an Interdisciplinary Seed Grant from the University of Utah.

Supporting Information Available: Figures of SDS-PAGE analysis of protamine with cationic or anionic G7-PAMAM, vascular dendrimer distributions in ZFE following FITC-cationic dendrimer injection, and vascular occlusions in ZFE receiving warfarin or heparin prophylaxis (before dendrimer injection), videos of thrombin-induced ZFE thrombosis and its prevention by sodium citrate prophylaxis, and videos of G7-NH2 dose-dependent occlusion in zebrafish embryos. These materials are available free of charge *via* the Internet at http://pubs.acs.org.

REFERENCES AND NOTES

1. Clarke, S.; Tamang, S.; Reiss, P.; Dahan, M. A Simple and General Route for Monofunctionalization of Fluorescent and Magnetic Nanoparticles Using Peptides. *Nanotechnology* **2011**, *22*, 175103.
2. US Demand for Nanotechnology Medical Products to Approach $53 Billion in 2011, report. http://nanotechwire.com/news.asp?nid=4446 (accessed July 3, 2008).
3. Medina, S. H.; El-Sayed, M. E. Dendrimers as Carriers for Delivery of Chemotherapeutic Agents. *Chem. Rev.* **2009**, *109*, 3141–57.
4. Heath, J. R.; Davis, M. E. Nanotechnology and Cancer. *Annu. Rev. Med.* **2008**, *59*, 251–265.
5. Heath, J. R.; Davis, M. E.; Hood, L. Nanomedicine Targets Cancer. *Sci. Am.* **2009**, *300*, 44–51.
6. Frens, G. Controlled Nucleation for the Regulation of the Particle Size in Monodisperse Gold Suspensions. *Nat. Phys. Sci.* **1973**, *241*, 20–22.
7. Kitchens, K. M.; Kolhatkar, R. B.; Swaan, P. W.; Eddington, N. D.; Ghandehari, H. Transport of Poly(amidoamine) Dendrimers across Caco-2 Cell Monolayers: Influence of Size, Charge and Fluorescent Labeling. *Pharm. Res.* **2006**, *23*, 2818–2826.
8. Dobrovolskaia, M. A.; Patri, A. K.; Simak, J.; Hall, J. B.; Semberova, J.; De Paoli Lacerda, S. H.; McNeil, S. E. Nanoparticle Size and Surface Charge Determine Effects of PAMAM Dendrimers on Human Platelets *in Vitro*. *Mol. Pharm.* **2012**, *9*, 382–393.
9. Heiden, T. C.; Dengler, E.; Kao, W. J.; Heideman, W.; Peterson, R. E. Developmental Toxicity of Low Generation PAMAM Dendrimers in Zebrafish. *Toxicol. Appl. Pharmacol.* **2007**, *225*, 70–79.
10. Malik, N.; Evagorou, E. G.; Duncan, R. Dendrimer-Platinate: A Novel Approach to Cancer Chemotherapy. *Anticancer Drugs* **1999**, *10*, 67–76.
11. Malik, N.; Wiwattanapatapee, R.; Klopsch, R.; Lorenz, K.; Frey, H.; Weener, J. W.; Meijer, E. W.; Paulus, W.; Duncan, R. Dendrimers:: Relationship between Structure And Biocompatibility *In Vitro*, and Preliminary Studies on the Biodistribution of 125I-Labelled Polyamidoamine Dendrimers *in Vivo*. *J. Controlled Release* **2000**, *65*, 133–148.
12. Roberts, J. C.; Bhalgat, M. K.; Zera, R. T. Preliminary Biological Evaluation of Polyamidoamine (PAMAM) Starburst Dendrimers. *J. Biomed. Mater. Res.* **1996**, *30*, 53–65.
13. Jones, C. F.; Campbell, R. A.; Franks, Z.; Gibson, C. C.; Thiagarajan, G.; Vieira-de-Abreu, A.; Sukavaneshvar, S.; Mohammad, S. F.; Li, D. Y.; Ghandehari, H.; *et al.* Cationic PAMAM Dendrimers Disrupt Key Platelet Functions. *Mol. Pharm.* **2012**, *9*, 1599–1611.

14. Greish, K.; Thiagarajan, G.; Herd, H.; Price, R.; Bauer, H.; Hubbard, D.; Burckle, A.; Sadekar, S.; Yu, T.; Anwar, A. *et al.* Size and Surface Charge Significantly Influence the Toxicity of Silica and Dendritic Nanoparticles. *Nanotoxicology* **2012**, *6*, 713−723.
15. Siebenlist, K. R.; Mosesson, M. W. Progressive Cross-Linking of Fibrin Gamma Chains Increases Resistance to Fibrinolysis. *J. Biol. Chem.* **1994**, *269*, 28414–28419.
16. Jagadeeswaran, P. Zebrafish: A Tool to Study Hemostasis and Thrombosis. *Curr. Opin. Hematol.* **2005**, *12*, 149–152.
17. Khandekar, G.; Kim, S.; Jagadeeswaran, P. Zebrafish Thrombocytes: Functions and Origins. *Adv. Hematol.* **2012**, *2012*, 857058.
18. Lin, H. F.; Traver, D.; Zhu, H.; Dooley, K.; Paw, B. H.; Zon, L. I.; Handin, R. I. Analysis of Thrombocyte Development in CD41-GFP Transgenic Zebrafish. *Blood* **2005**, *106*, 3803–3810.
19. Hanumanthaiah, R.; Thankavel, B.; Day, K.; Gregory, M.; Jagadeeswaran, P. Developmental Expression of Vitamin K-Dependent Gamma-Carboxylase Activity in Zebrafish Embryos: Effect of Warfarin. In *Blood Cells, Mol. Dis.* **2001**, *27*, 992−999.
20. Jagadeeswaran, P.; Sheehan, J. P. Analysis of Blood Coagulation in the Zebrafish. *Blood Cells, Mol. Dis.* **1999**, *25*, 239−249.
21. Carradice, D.; Lieschke, G. J. Zebrafish in Hematology: Sushi or Science? *Blood* **2008**, *111*, 3331–3342.
22. Jagadeeswaran, P.; Sheehan, J. P.; Craig, F. E.; Troyer, D. Identification and Characterization of Zebrafish Thrombocytes. *Br. J. Hamaetol.* **1999**, *107*, 731−738.
23. Jagadeeswaran, P.; Gregory, M.; Johnson, S.; Thankavel, B. Haemostatic Screening and Identification of Zebrafish Mutants with Coagulation Pathway Defects: An Approach to Identifying Novel Haemostatic Genes in Man. *Br. J. Hamaetol.* **2000**, *110*, 946–956.
24. Jagadeeswaran, P.; Gregory, M.; Zhou, Y.; Zon, L.; Padmanabhan, K.; Hanumanthaiah, R., Characterization of Zebrafish Full-Length Prothrombin cDNA and Linkage Group Mapping. *Blood Cells, Mol. Dis.* **2000**, *26*, 479−489.
25. Sadekar, S.; Ghandehari, H. Transepithelial Transport and Toxicity of PAMAM Dendrimers: Implications for Oral Drug Delivery. *Adv. Drug Delivery Rev.* **2012**, *64*, 571–588.
26. Domanski, D. M.; Klajnert, B.; Bryszewska, M. Influence of PAMAM Dendrimers on Human Red Blood Cells. *Bioelectrochemistry* **2004**, *63*, 189–191.
27. Ottaviani, M. F.; Daddi, R.; Brustolon, M.; Turro, N. J.; Tomalia, D. A. Structural Modifications of DMPC Vesicles upon Interaction with Poly(amidoamine) Dendrimers Studied by CW-Electron Paramagnetic Resonance and Electron Spin−Echo Techniques. *Langmuir* **1999**, *15*, 1973–1980.
28. Jokiel, M.; Klajnert, B.; Bryszewska, M. Use of a Spectrofluorimetric Method to Monitor Changes of Human Serum Albumin Thermal Stability in the Presence of Polyamidoamine Dendrimers. *J. Fluoresc.* **2006**, *16*, 149–152.
29. Klajnert, B.; Cladera, J.; Bryszewska, M. Molecular Interactions of Dendrimers with Amyloid Peptides: pH Dependence. *Biomacromolecules* **2006**, *7*, 2186–2191.
30. Klajnert, B.; Pikala, S.; Bryszewska, M. Haemolytic Activity of Polyamidoamine Dendrimers and the Protective Role of Human Serum Albumin. *Proc. R. Soc. A* **2010**, *466*, 1527–1534.
31. Peters, T., Jr. Serum Albumin. *Adv. Protein Chem.* **1985**, *37*, 161–245.
32. Figge, J.; Rossing, T. H.; Fencl, V. The Role of Serum Proteins in Acid-Base Equilibria. *J. Lab. Clin. Med.* **1991**, *117*, 453–467.
33. Horbett, T. A. Chapter 13 Principles Underlying the Role of Adsorbed Plasma Proteins in Blood Interactions with Foreign Materials. *Cardiovasc. Pathol.* **1993**, *2*, 137–148.
34. Mertens, K. The Future of Plasma Derivatives. In *Transfus. Clin. Biol.* **2001**, *8*, 303−305.
35. Adkins, J. N.; Varnum, S. M.; Auberry, K. J.; Moore, R. J.; Angell, N. H.; Smith, R. D.; Springer, D. L.; Pounds, J. G. Toward a Human Blood Serum Proteome: Analysis by Multidimensional Separation Coupled with Mass Spectrometry. *Mol. Cell Proteomics* **2002**, *1*, 947–955.
36. Muthusamy, B.; Hanumanthu, G.; Suresh, S.; Rekha, B.; Srinivas, D.; Karthick, L.; Vrushabendra, B. M.; Sharma, S.; Mishra, G.; Chatterjee, P.; *et al.* Plasma Proteome Database as a Resource for Proteomics Research. *Proteomics* **2005**, *5*, 3531–3536.
37. Anderson, N. L.; Anderson, N. G.; Two-Dimensional Gel, A Database of Human Plasma Proteins. *Electrophoresis* **1991**, *12*, 883–906.
38. Wiles, T. J.; Bower, J. M.; Redd, M. J.; Mulvey, M. A. Use of Zebrafish to Probe the Divergent Virulence Potentials and Toxin Requirements of Extraintestinal Pathogenic Escherichia Coli. *PLoS Pathog.* **2009**, *5*, e1000697.
39. Traver, D.; Paw, B. H.; Poss, K. D.; Penberthy, W. T.; Lin, S.; Zon, L. I. Transplantation and *in Vivo* Imaging of Multilineage Engraftment in Zebrafish Bloodless Mutants. *Nat. Immunol.* **2003**, *4*, 1238−1246.
40. Campbell, R. A.; Overmyer, K. A.; Selzman, C. H.; Sheridan, B. C.; Wolberg, A. S. Contributions of Extravascular and Intravascular Cells to Fibrin Network Formation, Structure, and Stability. *Blood* **2009**, *114*, 4886–4896.
41. Campbell, R. A.; Overmyer, K. A.; Bagnell, C. R.; Wolberg, A. S. Cellular Procoagulant Activity Dictates Clot Structure and Stability as a Function of Distance from the Cell Surface. *Arterioscler. Thromb. Vasc. Biol.* **2008**, *28*, 2247–2254.
42. Assemi, S.; Tadjiki, S.; Donose, B. C.; Nguyen, A. V.; Miller, J. D. Aggregation of Fullerol $C_{60}(OH)_{24}$ Nanoparticles as Revealed Using Flow Field-Flow Fractionation and Atomic Force Microscopy. *Langmuir* **2010**, *26*, 16063–16070.

CHAPTER 4

SURFACE ADSORBATES ON NANOMATERIALS AND THEIR POSSIBLE ROLES IN HOST INFLAMMATORY AND TOXICOLOGICAL PROCESSING

Reprinted with permission from Frontiers in Nanobiomedical Research: Vol. 1, Handbook of Immunological Properties of Engineered Nanomaterials, Clinton F. Jones, David G. Castner, David W. Grainger, Chapter 5: Surface Adsorbates on Nanomaterials and Their Possible Roles in Host Inflammatory and Toxicological, pp. 117-149.

b1429 Handbook of Immunological Properties of Engineered Nanomaterials

Chapter 5

Surface Adsorbates on Nanomaterials and Their Possible Roles in Host Inflammatory and Toxicological Processing

Clinton F. Jones[*], *David G. Castner*[§,¶,||], *and David W. Grainger*[†,‡,**]

[*]*Center for Nanotechnology in Drug Delivery*
Division of Molecular Pharmaceutics
UNC Eshelman School of Pharmacy
University of North Carolina at Chapel Hill
Chapel Hill, NC 27599, USA
[†]*Department of Pharmaceutics and Pharmaceutical Chemistry*
and [‡]*Bioengineering, University of Utah*
Salt Lake City, UT 84112-5820, USA
[§]*National ESCA and Surface Analysis Center for Biomedical Problems*
[¶]*Departments of Bioengineering and* [||]*Chemical Engineering*
Box 351653, University of Washington
Seattle, WA 98195-1653, USA

Surface characteristics of nanomaterials are well recognized to contribute prominently to their unique properties and applications. It is less appreciated that the same surfaces have high intrinsic reactivities, typically distinct from identical bulk material chemistries. These size-dependent properties facilitate rapid, ubiquitous surface adsorption and contamination from many sources: storage containers; nanosynthesis components, by-products, and stabilizers; ubiquitous and adventitious environmental pollutants in clean room air and water; and diverse biomolecules that nanomaterials might encounter throughout their life cycle in biological, biomedical, and environmental exposures. Given their extremely large specific surface areas and high surface reactivities, nanoparticle surfaces are dynamic and rarely (if ever) the

**Corresponding author. E-mail: david.grainger@utah.edu

pure nanomaterial. Instead, such surfaces comprise complex mixtures of poorly characterized and controlled adsorbates, depending on the nanomaterial exposure history. Many adsorbates bring their own biological and toxicological activities. Significantly, surface adsorption may alter otherwise benign or innocuous adsorbates to render certain antigenic or inflammatory responses on a nanomaterial surface. To understand if such a scenario truly exists and the possible risks involved, rigorous nanomaterial surface assessments combined with careful immune system activation studies are necessary. However, the appropriate analytical tools to readily ascertain such interactions and mechanisms remain lacking.

1. Introduction

Many efforts to reduce material dimensionalities are motivated by the attractive material properties and functions unique to their nanometer regime. At the nanoscale, certain properties of matter become scale-dependent, including capillary forces, optical effects/color, melting points, conductivity, ionization potential, electron affinity, magnetism, and significantly, surface energy and surface reactivity. For example, while gold as a noble metal has a recognized low oxidation potential in bulk, properties of gold nanoclusters (e.g., Au_{55} clusters) are distinctly different, exhibiting highly oxidizable surface atoms.[1]

Optical, electronic, mass transfer, and thermal property changes that appear for materials in the nanoscale dimension are often exploited and studied. However, the impact of increasing surface areas with decreasing material dimensions must also be carefully considered as a truly impactful property. Sub-micron particles (e.g., nanoparticles with diameters of 1–300 nm) are the most popular and manipulated form in nanomaterials to date, present in increasing amounts in consumer and commercial products, and advocated for even further applications. Specific to biological exposures, nanomaterials in consumer products can enter the ecosystem in manufacturing, use, and disposal, producing some concerns over their life-cycle management, environmental tracking, and fate. Nanomaterials are also extremely popular in biomedical applications for *in vitro* immunolabeling, diagnostics, and imaging, as well as for *in vivo* diagnostics, advanced drug formulations and delivery systems, and imaging and tissue targeting functions.[2,3] In these applications, a primary feature is the direct contact of nanomaterial surfaces with metabolic cascades and literally tens of thousands of different biological components with redox properties, optical/chemical reactivity, and surfactancy. Basically, the introduction of many nanomaterials into biological milieus places two intrinsically reactive systems with dynamic properties into direct contact.

Specific surface areas for micron-sized materials (e.g., fumed silicas, commercial carbon blacks) are typically 60–80 m^2/g, a considerable surface-to-mass

ratio providing extensive utility in their applications. Further reduction of micromaterial diameter to tens of nanometers increases the specific surface area by manyfold, yielding an impressive rise in surface area per mass. Hence, commercial CB-1 carbon blacks and single-walled carbon nanotubes (CNTs) — another major material focus for nanobiotechnology — may have specific surface areas exceeding 1300 m^2/g.[4] As material size decreases, the surface properties of the atoms increasingly dominate, producing significant changes in material reactivity.[5] Relative fractions of surface atoms to bulk atoms in any structure is called "dispersion," exhibiting a power law ranging in the nanoscale regime.[5] While less than 1% of micromaterial atoms occupy surface positions, 10% of the atoms in a 10-nm diameter metal material reside on its surface (and 60% in a 2-nm material!).[6] The excess surface energy and thermodynamic instability of materials below 20 nm not only result in the appearance of surface defects and atom/lattice rearrangements that stabilize the materials, but also produce unique nanomaterial reactivities and properties.[5] Effects of size reduction on material surface topology, porosity, texturing, and high-density fabrication are observed in sub-micron scaling features, contributing to the unique performance properties of nanomaterials. Surface structure and composition, and resulting surface reactivity, dominate nanomaterial properties. Hence, surface effects are a unique and very significant functional nano-property that require both control and careful characterization for exploitation in specific nanotechnologies.[5] Direct nanomaterial interfacial contact with biological molecules and reactive metabolic pathways produces possibilities for uncontrolled or undesired effects where specific surface interactions with biology intended for nanomaterial function might be hindered, and where host responses could induce adverse reactions.[6]

Colloidal materials have a substantial history of complex physicochemical behaviors in biological milieus.[7–11] To claim that well-studied colloidal systems (e.g., lipid materials, silicas, polystyrene latexes) can be controlled predictably in physiological milieus is a gross overstatement. Classic issues with colloidal instabilities, aggregation, and flocculation dominate these behaviors due to uncontrolled adsorption and surface reactivity. Therefore, even greater difficulties in characterizing and controlling behaviors for nano-sized colloidal materials in complex biological systems are expected and in fact, routinely encountered. High specific surface area materials exhibit substantial challenges in controlling interfacial reactivity. Thus, increasing specific surface area, as is characteristic of nanomaterials, produces new issues in such control. Two important distinguishing features of surface atoms compared to bulk atoms are: 1) lower coordination numbers and 2) increased exposure to and encounter with reactive species in the environment. These distinct surface features translate to intrinsically higher surface atom reactivities than bulk

atoms, frequently manifested in certain predictable, but also other very unique, and even some exotic ways.[12]

2. Adsorption as a Natural Consequence of Surfaces

High surface energy materials of any dimension are plagued by adsorption as a spontaneous process that reduces surface free energy. This is often not a chemistry-specific phenomenon, but rather a general kinetic process involving any or all adventitious species present. Consequently, surface contamination is a thermodynamically driven process that reduces surface energy through the adsorption of adventitious air-, water-, or media-borne contaminants to yield a new adsorbate "surface" (i.e., an adlayer). Depending on the presence of other possible surface-active adsorbates, this adsorbed surface layer can be displaced, remodeled, or covered with another adsorbed layer to produce a new, even more thermodynamically stable state. Hence, the adsorption process can be dynamic and evolving, depending on the milieu, significantly changing surface composition, wettability, surface energetics and material–material two-body interactions, surface charge (ionic adsorption), and surface reactivity. Importantly, adsorption also chemically and physically alters the original material surface through adsorbate processes, including electron transfer-induced changes (redox chemistry), frequently yielding oxidized surface states in environmental systems and physical properties associated with the adsorbed layer. Few, if any, surfaces retain their original chemistry very long even under clean room conditions, and adsorption is highly ubiquitous to all surfaces even during synthesis.

Additionally, nanomaterial surface contamination may range from adventitious adsorption of adlayers to surface oxidation, corrosion, charging, or electron transfer reactions of the nanomaterial itself.[6,13] Due to dispersion, the higher intrinsic reactivity of nanophase surfaces prompts rapid and spontaneous surface adsorption of many diverse types of molecules in their milieu, reducing nanomaterial surface free energy and altering interactions with other nanomaterials (i.e., producing aggregation and flocculation) and with components in the milieu. In fact, surface adsorption is used deliberately and universally to stabilize nanomaterial solids in suspension in most commercial preparations through the intentional introduction of surface-active additives, e.g., CTAB, SDS, citrate, and charged or polar hydrophilic (co)polymers, that form stabilizing "coronas" around materials, keeping them from aggregating under shipping and storage conditions.

Due to their tremendous specific surface areas and intrinsic adsorption capacities, finely dispersed materials (e.g., diatomaceous earth, alumina, silica,

activated charcoals) are exploited commercially as adsorbent beds to remove dissolved species from solutions, even in medicine. Nanomaterials satisfy this same purpose, but with substantially increased surface areas and adsorption capacities. It follows therefore that surface contamination of nanomaterials in both air and in aqueous milieus is spontaneous and substantial, by common adsorption from any and all ambient phases, and at a level proportional to 200–1000 m^2/g nanomaterial surface areas. Hence, a few hundred milligrams of CNTs contaminated with a monolayer of unintentional adsorbates (such as Fe, Co, Ni, S, or Mn atoms from common CNT manufacturing catalysts) could introduce to their surrounding solutions nearly a millimole of these adsorbed materials as surface leachates upon introduction to solutions.[12] The take-home lesson is that adsorbate layers on nanomaterials, and not the virgin nanomaterial chemistry, are increasingly thought to be the primary surface that interacts with biological components (i.e., proteinaceous, cellular, or lipid) in complex biological environments. In fact, it is likely that nanomaterials will carry significant adsorbed contamination into other systems (i.e., environmental and physiological) under most conditions. These various adsorption/desorption pathways are schematically shown in Figure 1. Nanomaterial surface chemistry should never be presumed to be either clean or unreactive when exposed to air, water, or biological environments.[12,14]

Biological component adsorption to nanomaterials is also rapid, often irreversible and non-descript since blood, for example, contains over 70 mg/ mL of thousands of soluble proteins and enzymes, small molecule solutes, dissolved gases, oxidizing and reducing agents, hundreds of lipids, fatty acids and other surfactants, and dozens of cell types, including blood platelets at a daunting concentration of 10^8/mL, orders of magnitude higher than most nanomaterial dispersion concentrations.[15] All of these components recognize and react to nanomaterials immediately upon their introduction into the bloodstream, irreversibly influencing nanomaterial physical and chemical behaviors, aggregation, and all subsequent cellular interactions. Other physiological compartments and environments are equally complex. Cell-mediated material uptake (at least at the micron-size scale) includes a diverse array of possible cell entry mechanisms, including phagocytosis, pinocytosis, endocytosis, coated pit, and caveolae-mediated entry, and is influenced by material surface properties and chemistry, surface adsorption, contamination, and aggregation. Hence, adsorption in biological systems profoundly affects cell-material processing mechanisms, altering the behaviors of materials introduced *in vitro* and *in vivo*. Therefore, the monitoring of material surface composition and its changes in the milieus of relevance for intended applications are requisite to understanding nanomaterial interactions with living

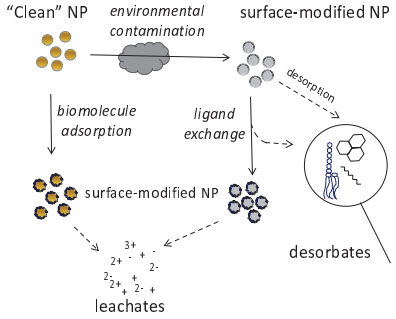

Figure 1. Environmental conditioning of nanoparticles and resulting products. Examples include contaminated nanoparticles, adsorbed stable adlayers, sloughed contaminants, and dynamically exchanging, displaced, and desorbing adlayers.

systems. Such analyses remain challenging since analytical tools to observe nanomaterial behaviors and various adsorption processes and property changes are crude and highly limited to date. Correlations to observed biological responses and behaviors in biological assays are therefore plagued by current inabilities to track nanomaterial surface and property changes within complex biological systems.[12]

Nevertheless, biological responses to nanomaterials may not be assayed with any real sense of scientific validity or confidence *before* nanomaterial properties (as supplied, with associated contamination), cleaning procedures, batch-to-batch nanomaterial variability, and solution properties (such as intrinsic aqueous stability, leachates, surfactant additives, aggregation, and flocculation) are thoroughly screened, considered, and reported. Essentially, this amounts to routine material science quality control, but remains critically important in nanomaterial research before meaningful results may be interpreted from subsequent *in vitro* or *in vivo* biological testing. Material composition must be ascertained with analytical specificity to understand its effects on the biology under assay. As one analytical routine, bulk material analysis involves material purity certification and trace contamination (e.g., soluble residual ions, leachates, organic reagents), aqueous leachables, electron microscopy of bulk nanophase morphology, polydispersity analysis (typically light scattering in aqueous dispersions of varying concentrations), intrinsic aggregation under shelf-life conditions, intrinsic nanomaterial solubility, and when appropriate, bulk-phase thermal analysis, conductivity, or redox behavior, and spectroscopy (i.e., fluorescence and vibrational) to provide some chemical quality control for physical and chemical states, and stability. This

bulk analysis provides a rational basis to then proceed with a second, critical effort in surface analysis to understand possible surface states in the nanomaterials of interest since virgin nanomaterials do not present this bulk chemistry at their surface.[6,12] Together with nanomaterial size and bulk purity, nanophase surfaces must be continuously analyzed and tightly controlled for biomedical applications where surface contamination might elicit adverse, undesired, or unexpected biological responses. Possible sources of nanomaterial-derived toxicity in physiological systems should therefore consider both the nanomaterial and, perhaps even more, the ubiquitous intrinsic nanomaterial adsorbates presented to and processed by host immune components, in both adsorbed and desorbed states in biological milieus.

Contaminants and adventitious adsorbates from diverse sources decorate nanomaterials and exert unknown consequences on biological assays. During nanomaterial synthesis, catalysts, solvents, unreacted reagents, catalysts, or synthetic by-products may be entrained into or adsorbed onto nanomaterials.[16] During and following synthesis, materials may be exposed to contaminants in their environment (e.g., in filtration and separations, in suspending water/solvents, from ambient air, and storage/processing containers and materials). Common airborne contaminants in any laboratory, even clean rooms, include plasticizers (typically surface-active phthalates) from reagent packaging and container caps and sealants, polyaromatic hydrocarbons (PAHs), volatile polydimethylsiloxanes (PDMS), hydrocarbons and fluorinated ether oligomers from pump exhausts, and ubiquitous environmental adsorbates such as airborne carbonaceous and silicate particulates and bacterial lipopolysaccharides (LPS)[6] (Figure 2).[17,18] Reagent-grade water in contact with common labware (plastic or glass) also contains substantial surface-active contamination (rarely does purified laboratory water exhibit its theoretically pure surface tension of 72.8 mN/m at 20°C for "pure" water).

Alternatively, many "pure" adsorbates are intentionally introduced to nanomaterials as suspension stabilizers. These include block copolymers, charged polymers, small molecule surfactants (SDS, CTAB, ethoxlyated alkylesters), and highly charged polyions (e.g., citrate). Many such nanomaterial-adsorbed stabilizers are known to exchange in the presence of other competitive ligand exchange reactions. Gold nanomaterials in particular are subject to ligand exchange that can alter their aggregation states.[20,21] Other common nanomaterial additives include cell uptake-modulating and protein-repelling polymers (i.e., polyethers, celluloses, polyvinyl alcohol, poloxamer, poloxamine, polyethyleneimime, and polysorbates) or biomolecules (e.g., transferrin, albumin, DNA, other proteins or synthetic peptides). While these polymers adsorb to nanomaterials and stabilize or modify nanomaterial

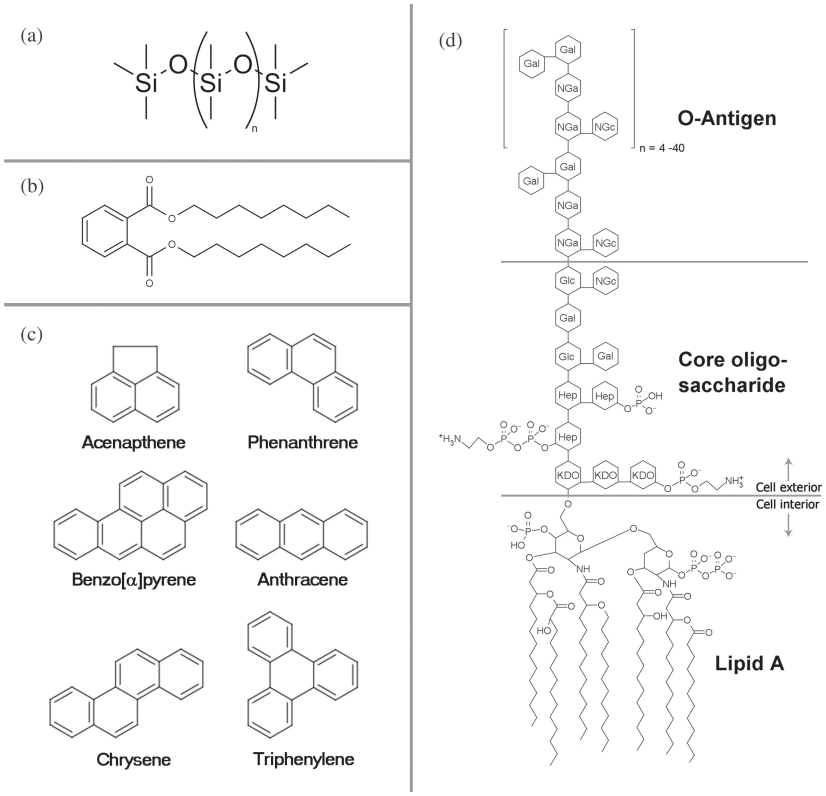

Figure 2. Selected common environmental adsorbates. Polydimethylsiloxane (PDMS) (a), dioctylpththalate (b), polyaromatic hydrocarbons (PAHs) (c), and lipopolysaccharide (d). Panels (c) and (d) were adapted with permission from Refs. 17 and 18, respectively, using ChemAxon software.

Gal: galactose; Glc: glucose; Hep: 1-glycero-d-manno-heptose; KDO: 3-Deoxy-D-manno-oct-2-ulosonic acid; NGa: N-acety1-galactosamine; NGc: N-acetyl-glucosamine.

aggregation behaviors in simple *in vitro* systems with relatively low concentrations of competitive adsorbates (i.e., low levels of plasma proteins), relatively little is known about their adsorbed stability under physiological conditions in the presence of high concentrations of proteins, lipids, and cells, alone or in any combination.

Nonetheless, understanding and controlling this nanomaterial interface in biological milieus is a key challenge to understanding nanomaterial biocompatibility, biological function and performance, risk assessment, and possible toxicity mechanisms. This rationale follows from well-known surface

analytical paradigms in conventional biomaterials and medical device biocompatibility testing.[22] Biomaterial surface characterization methods commonly used for quality control and to report on surface states of implanted material chemistry and physical conditions are diverse and extensive, with many different types and sources of information reported from each technique depending on its requirements.[23,24]

This chapter lacks the breadth necessary to sufficiently describe the numerous well-known material characterization tools appropriate for material surfaces in general, or for nanomaterial purposes in particular. Several reviews on surface issues in nanomaterial characterization have been published.[6,25,26] As with any analytical technique, one must match the measurement capabilities of a selected surface interrogation method with the information sought, and apply best practices to the characterization of nanomaterials. In any case, surface analysis should routinely accompany bulk nanomaterial analysis prior to nanomaterial introduction into any *in vitro* or *in vivo* assay. Such nanomaterial quality control reporting should be expected as essential to understand nanomaterial characteristics prior to exposure to biological systems.[12]

3. Host Processing of Nanomaterials

It is highly likely that mammalian host defenses never see a bare nanomaterial because, as mentioned above, before a nanomaterial ever sees a biological system, it is already coated with a conditioning or stabilizing layer of either an intentional or adventitious origin. Upon introduction to the body, nanomaterial adlayers are then instantly subjected to a concentrated environment of surface-active biomolecules that further overcoat both bare nanomaterial surfaces and adlayers with endogenous proteins and lipids, and can displace adlayer coatings with endogenous molecules.[27] Thus, host defenses may encounter a bare nanomaterial (rare if ever), a contaminant- or stabilizer-coated nanomaterial (possible), a protein-/biomolecule-coated nanomaterial with an underlying exogenous coating (likely), or a protein-/biomolecule-coated nanomaterial with underlying exogenous species desorbed and displaced (likely). Given the unique nanoscale size of these material–biological adsorbate entities, host recognition systems could process them in multiple ways, resulting in normal clearance or alternatively, host reactivity. Significantly, adsorbate presentation on a solid nanomaterial surface of the same approximate size as many antigenic epitopes (several nanometers) could exacerbate host responses. High intrinsic nanomaterial surface areas are capable of delivering significant amounts of surface adsorbates to immune cells via both direct nanomaterial–adsorbate presentation and adlayer desorption by biological surfactants.

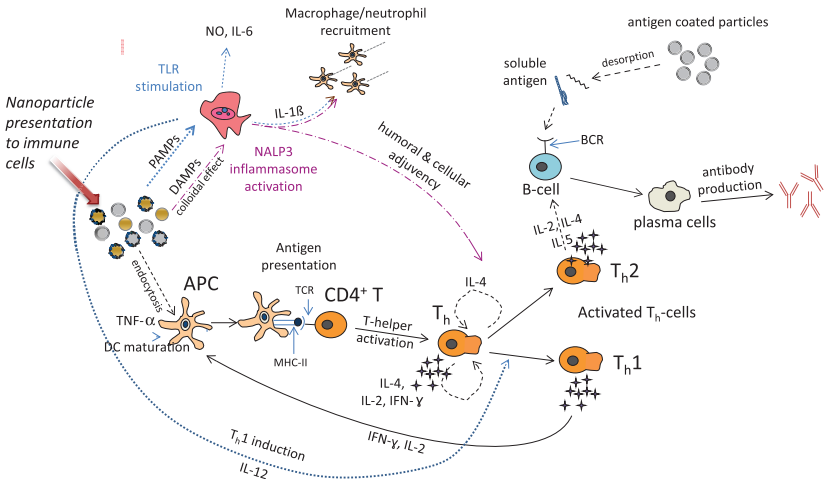

Figure 3. Possible nanoparticle processing pathways by host cellular immunological components. Nanoparticles, their desorbed adlayers, or nanoscale composites may induce a variety of immune responses. Given their size, some nanomaterials are likely to be processed as unique nanoscale composites comprising nanomaterials and adsorbed biological adlayers.

An overview of various immune processing pathways for nanomaterials and adsorbates is shown in Figure 3. In one host response scenario, the nanomaterial (coated or uncoated) may be phagocytosed by antigen-presenting cells (APCs), macrophages, dendritic cells, or neutrophils. Any peptide-based adsorbates on the material surface may be lysozomally processed and presented as digested peptide antigens by major histocompatibility complex class II (MHC-II) molecules on the APC surface. Other adlayer adsorbates carried by nanomaterials can be taken up and then desorbed within APCs and possibly presented by MHC-II molecules as antigens, although how general this processing mechanism and antigenic potential might be is very debatable. That nanomaterials can be processed intact with their adlayers as MHC-II complexes is not well described, but represents an interesting possibility. While unproven, combinations of uniquely engineered, synthetic nanomaterials with physical dimensions capable of direct immune component processing as possible antigens, high solid interfacial areas for additional adsorbate presentation and significant desorption, and unique interfacial properties and reactivities may provide unique immune stimuli, particularly when administered through previously unnatural routes (e.g., parenteral). More specifically, deliberate nanomaterial introduction into host surveillance systems by unnatural pathways in high doses (i.e., intravenous, inhaled, and subdermal) could provoke unique host immune responses.

However, this has not yet been validated. While highly variable, MHC-II antigen presentation of many molecules may activate T helper cells, leading to antibody production through the activation of B cells to plasma cells.

A second scenario involves the interaction of endogenous proteins with nanomaterials, resulting in the nucleation of protein fibrillation[28] or modification/denaturation of endogenous proteins on the nanomaterial adlayer/surface such that the protein adlayer is recognized by scavenger receptors for uptake by macrophages/endothelial cells. Moreover, protein denaturation at the particle surface could expose and present cryptic epitopes and generate haptens,[13,27,29] and the close proximity and high concentrations of proteins possible at the nanoparticle surface raise the possibility of amyloid formation that precedes disease states dependent on protein misfolding.[28]

A third scenario is the interaction of nanomaterial surface adsorbates either as presented on the nanomaterial or in their desorbed and soluble state. Adlayer molecules of pathogenic origin (pathogen-associated molecular patterns or PAMPs) may activate innate immune inflammation through the appropriate pathogen pattern recognition receptor class (TLRs, NLRs, RIG-1, MDA-5). Host cytokines released during innate inflammation may recruit phagocytes to the site of inflammation, induce cell death, generate an oxidative burst, and/or enhance an adaptive immune response. Moreover, in the case of material-presented PAMPs, the material itself acts as an adjuvant, activating the NALP-3 inflammasome to amplify the adaptive immune response to the vaccine antigen.[30] This route of action has been demonstrated for a growing list of nanomaterials that includes chitosan, poly(lactic-glycolic acid) (PLGA), polystyrene, silica, alum (aluminum oxide microparticles, the only solid-phase vaccine adjuvant approved for human use in the United States), and uric acid crystals (the only endogenous adjuvant, formed as a precipitate of accumulated uric acid released during mass necrosis).[30–32] Though the exact mechanism of NALP-3 activation and adjuvancy is not well defined, the nanomaterials themselves appear to be simply acting as an adjuvant and as such, antibodies are not likely to be generated specifically toward the nanomaterials.

Particle adjuvancy has been found to depend on antigen adsorption to particles, which is in turn affected by vaccine solution ionic strength, ionic composition (similarity to particle composition), pH, and particle and antigen isoelectric points.[33] (See Chapter 15 for more information on nanoparticle adjuvancy.) For example, adjuvant properties known for PLGA degradable polymer materials make them attractive delivery vehicles for DNA vaccines. Encapsulation, incorporation, or adsorption of antigenic DNA to PLGA–poly-L-lysine (PLL), PLGA–CTAB, or chitosan micromaterials (or some minor variation of one of these material types) have markedly improved

immunogenicity, which has been attributed to a material-based adjuvant effect comparable to that of Freund's adjuvant.[34–36] As an example, the host antibody response to the hepatitis B vaccine antigen DNA adsorbed to PLGA–CTAB nanomaterials was significantly higher (i.e., double) than that of naked antigen DNA dosed alone. This humoral response was accompanied with significant increases in interferon-gamma (IFN-γ) production (five-fold over antigen alone), cytotoxic T lymphocyte activity, extended expression by APCs, and tumor protection and animal survival following tumor cell (HBsAg-expressing CT26/S) challenge.[37] Hence, similar to known alum- and particle-based host reactivity, nanomaterial–antigen presentation synergies are implicated in adjuvant effects, likely from antigen adsorption to the material surface, enhancing host immune system recognition and processing, and perhaps exacerbating sensitivity. This scenario also introduces the possibility of activated immune system components generating auto-antibodies toward nanomaterial-adsorbed endogenous — but adulterated — proteins with exposed native or altered (and possibly) cryptic sequences.[13]

Alternatively, leached metal ion species, non-pathogenic adlayers, or desorbed molecules of environmental contaminants may elicit host responses ranging from oxidative bursts, induced by intrinsic cellular toxicity, to immunosuppression and reduction of immune cell activation or their maturation by disruption of cytokine signaling cascade components.[38,39] Thus, the vast variety of possible nanomaterial adsorbates produces a broad range of resulting endogenous responses. While not widely reported or studied, immunotoxic implications of known nanomaterial adsorbates and ostensible contaminants comprise the remainder of this chapter.

4. Polydimethylsiloxane Adsorbates

PDMS [Figure 2(a)] and their smaller oligomers represent a synthetic class of silicone-based polymers and surface-active (i.e., antifoaming) additives common to labware, vacuum pump oils, lubricants and greases, lithographic print and mold release agents, sealants and water-proofing coatings, tape adhesives, and consumer products. PDMS surface contamination of synthetic nanomaterials is extremely likely because of its many forms and pervasiveness in common synthetic chemistry and fabrication laboratory areas, and the difficulty in removing it from laboratory plasticware, glassware, and air. The intrinsic surface activity and volatility of PDMS in lower molecular weight liquids combine to make it a contaminant common in laboratories — even clean rooms — ranking it as one of the most common surface contaminants observed under high-resolution analysis.[6] PDMS transfer from slightly contaminated

synthetic glassware into many solvents and onto material surfaces is facile. Trace silicone detection with surface-sensitive X-ray photoelectron spectroscopy (XPS) is relatively straightforward except on siliceous substrates (i.e., silicate glasses, quartz, silica, or silicon wafers). Secondary ion mass spectrometry is even more sensitive than XPS for trace silicone detection, especially on siliceous substrates. Yet, the presence of PDMS on nanomaterials is rarely controlled or reported.[6]

Some level of PDMS and related siliceous surface contamination on nanomaterials is likely. Its removal is difficult without powerful oxidants and etchants (i.e., plasma gas treatment, ozonation, nitric acid, the RCA clean). As a contaminant adlayer on nanomaterials, its potential to alter nanomaterial interactions with biological systems is therefore considerable — PDMS adlayers mask intentionally adsorbed stabilizing species and also the ability to intentionally surface-modify materials with further adlayers (e.g., grafted polymer layers, functional groups, targeting ligands, or cell adhesion peptides). PDMS is known to adsorb plasma proteins readily, and alter cell and bacterial adhesion.[40] As it is hydrophobic and non-wetting, PDMS surface contamination changes droplet drying and deposition, fluidics, and wetting processes on surfaces (as in diagnostics and microfluidics devices), and adlayers can preclude ligand recognition of immobilized affinity partners at surfaces important to sandwich and affinity capture surfaces and targeting.

Silicon is the second most abundant element on earth, yet is only found in trace levels in the human body, and nearly always covalently attached to oxygen as silica or silicate networks. The silica content of human tissue varies from 10 mg to 200 mg/100 g dry weight. By contrast, silicone derivatives such as PDMS are oligomers and polymers of dimethylsiloxane (-O-Si$(CH_3)_2$-) units and related chemistries. PDMS are not found in nature or human tissues; there are no enymatic pathways known that produce or metabolize this pure chemistry. Therefore, silicones and PDMS are truly foreign materials in biological systems. This has led to the intense scrutiny of their biocompatibility and toxicology. In general, PDMS are known to have very little toxicity or biological effects, even at doses an order of magnitude above those observable in individuals with PDMS implants.[40] However, some interesting effects have been observed for specific variants. Cyclic PDMS (D_3, D_4, D_5, and D_6) are known to cause reversible liver enlargement that subsides upon the termination of exposure, but cause few additional effects other than slight dermal or ocular irritation.[40] Interestingly, decamethylcyclopentasiloxane penetrates skin slightly and octamethylcyclotetrasiloxane has demonstrated effects of reversible vaginal mucification and ovarian atrophy following inhalation exposure (12 g/m^3) or adjuvant activity (humoral only), along with transient

interferon production and a reduction in macrophage phagocytic activity following subcutaneous injection.[40] Linear decamethylsiloxane species cause more pronounced irritation with some, albeit equivocal, data for immune modulation.[40] Moreover, severe ulceration and necrosis were observed during skin exposure to PDMS precursors (non-dimethylsiloxanes), while other PDMS precursors cause minimal acute toxicity, irritation, and sensitization.[40] As is true for any non-degradable implant, PDMS implants generally trigger granulatomous reactions and fibrosis with a low incidence of solid-state sarcomas in response to PDMS gel implants.[40] Furthermore, injections of medical-grade Dow Corning 350cS PDMS fluid resulted in the observation of silicone within macrophages in regional lymph nodes and the adrenal system.[40] Thus, these compounds have the potential for bio-accumulation and immune modulation, especially at high doses. With ubiquitous environmental and industrial presence combined with high specific surface area nanomaterials, high doses are conceivable. However, more studies are needed to conclusively determine and elucidate specific effects of PDMS, either alone or with nanomaterials. Silicone and silicone gel have demonstrated adjuvant activity as an insoluble emulsifier of known antigens, but not when given separately from the antigen.[40] Silicone gel administered separately from an antigen does not exhibit adjuvant activity, but may produce a transient increase in natural killer cell activity.[40] Silicone also appears incapable of inducing classical adjuvant arthritis. Importantly, no significant links have been made between these experimental observations and any clinical immunological effect.[40]

With numerous precedents for interfacial reactivity, and also evidence for influences on biological systems, PDMS warrants careful consideration for its impact on nanomaterial properties in current biological applications. Little attention has been directed to date on significant PDMS contamination issues on material properties and behavior for high specific surface area nanomaterials.

5. Polyaromatic Hydrocarbon Adsorbates

PAHs, long known as potent carcinogens,[41] commonly adsorb to surfaces exposed to ambient air which ubiquitously contain PAHs in trace amounts, as products of combustion in transportation, manufacturing, and natural calamities. The production of carbon-based nanomaterials is now known to generate substantial toxic aromatic carbonaceous by-products including at least 15 PAHs[42,43] [Figure 2(c)]. Additionally, carbon nanomaterials are well known to actively adsorb volatile PAHs co-produced as part of the carbon nanophase manufacturing process.[44–46] Without rigorous post-synthesis

processing and cleaning steps, carbon-based engineered nanomaterials are often contaminated by PAH adsorption. Unfortunately, simple water rinsing or suspension does not remove these hydrophobic adsorbate layers easily or completely. With specific surface areas approaching 1300 m^2/g,[47] CNTs represent major transport vehicles for PAHs. Given the similar chemical nature between CNTs graphitic chemistry and PAH chemistry, the detection of PAHs as an adsorbate on carbon-based nanomaterials is difficult. As an aromatic polycyclic species, PAHs share many attributes of the underlying graphitic substrates in many carbon-based nanomaterials. Standard *in situ* surface analytical methods cannot generally distinguish PAH adlayers on CNTs by chemical fingerprinting. Only thorough material solvent extraction and mass spectrometry of the rinsed phase can determine the extent of PAH surface contamination, although this is rarely reported. Oxidizing treatments of the nanomaterials (i.e., ozonolysis, plasma treatments, nitric acid washing, and RCA-type peroxide cleaning[48,49]) can oxidize PAH species to more soluble forms, facilitating their desorption from nanomaterial substrates in a "cleaning step," but this is often performed at the risk of also modifying the material surface. Hence, PAHs represent a ubiquitous and difficult adsorbate to both distinguish and remove from graphitic nanomaterials. Without standard surface treatments to both control for and remove PAHs from carbon-based nanomaterials as contaminants, it is difficult to understand the many reports for CNT behaviors in biological and cellular milieus. Few studies provide sufficient data on the identity, purity, and chemistry of the substantial surface areas of CNTs to correlate either with observed biological responses or with each other.[6]

Surface-contaminated nanomaterials may elicit substantially different biological responses *in vitro* and *in vivo* compared to pure or cleaner phases of the same nanomaterials. As produced, unpurified CNTs are reported to induce the production of pro-inflammatory cytokines and reactive oxygen species (ROS) similar to their combustion by-product material counterparts, while cleaned CNTs (with reduced PAH and heavy metal ion content) show reduced or complete absence of these effects.[50] Moreover, diesel exhaust material inhalation has been shown to increase the incidence of pathological lung infection.[51,52] Though the mechanism is unknown, this immunosuppression has been attributed to the depression of pro-inflammatory cytokine and ROS expression and antimicrobial potential of alveolar macrophages by adsorbed organic species on a given material, rather than the material itself.[52,53] In another study, benzofuran or acrolein adsorbates impaired *ex vivo* Fc-receptor–mediated carbon black particle uptake by rat alveolar macrophages.[54] It has been hypothesized that this type of effect may result from

material overloading and lead to the co-expression of prostaglandins and corticosteroids, rather than being an adsorbate-mediated phenomenon.[55] However, several PAHs are known to be immunosuppressive (and still many others could have similar properties as most PAHs have not been extensively studied), but the mechanism of immunosuppression is not definitively demonstrated.[43] One popular hypothesis is that PAHs exert their immunesuppressive effects through cellular AhR receptor binding, but the binding strength for a given PAH is not an effective predictor of its degree of immunosuppression.[38] Moreover, AhR-deficient mice have demonstrated similar or greater immunosuppression in response to PAH exposure than AhR-competent mice.[38,56] Nonetheless, some evidence suggests that these planar, lipophilic molecules exert their immunosuppressive effects through the interruption of transmembrane/receptor signaling, disruption of interleukin signaling (IL-1, IL-2, and/or IL-3), and/or mobilization of and increases in intracellular calcium.[38] Additionally, many surface-active components present in biological fluids (proteins, lipids, fatty acids, other small molecule amphiphiles) are known to promote the exchange and desorption of these adlayers when they are not removed by other cleaning methods.[57,58] Hence, PAH contaminants on nanomaterials are likely off-competed and replaced by biological surface-active substances. This scenario produces new possible host exposures: 1) desorbed PAH reactions with cell membranes (adsorption, insertion, permeation, penetration), 2) partitioning into plasma proteins (e.g., albumins, apolipoproteins), and 3) direct biological reactions (cellular, proteinaceous) with the nanomaterial via its new, altered surface adlayer. Alas, little evidence is available to date to distinguish these phenomena *in vitro* or *in vivo*.

6. Catalyst Residues from Carbon Nanotube Synthesis

The chemical vapor deposition and ARC synthesis processes for generating CNTs utilize several catalytic reagents that include heavy metals.[59–61] As many of these become integrated into the carbon materials or tenaciously adsorbed as surface contamination, carbon-based engineered nanomaterials are often contaminated with a variety of non-carbon species, including transition metals.[62,63] In addition to the mainstay catalysts utilized in CNT synthesis (Fe, Co, Ni, Y, and Mo), neutron activation analysis and inductively coupled plasma mass spectroscopy (ICP-MS) have demonstrated an expansive list of CNT contaminants including metals/elements such as Al, As, Br, Ce, Cr, Cu, Gd, Ho, La, Mg, Na, Nd, Se, Sm, Sr, Tb, Th, Ti, V, W, Yb, Zn, and/or Zr, many of which may be employed in post-synthesis purification steps or during synthesis as catalyst dopants to favor specific CNT product attributes or improve catalyst

lifetime.[59,62] These contaminants have been observed to constitute up to 30 wt% even in commercial "purified CNTs."[62,63] Residual post-processing catalyst removal from CNTs is routinely performed by nitric acid or mixed acid reflux for approximately two days, while amorphous carbon is oxidized and removed by 20–70-h treatment with H_2O_2 or by thermal treatment.[48,49] However, metal impurities are often left entrained within the nanotube structure or ensconced in their own graphitic shell following purification, precluding complete impurity removal without concomitant destruction (or at least significant structural alteration) of the nanotubes themselves.[64] Nevertheless, in spite of graphene encapsulation, toxicologically significant quantities of metal-based catalyst impurities may be released into incubation media, particularly under mildly acidic (pH = 5, lysosomal) conditions.[63] This metal release from purified CNTs may be due to inadequate acid treatment (cleaning) time, which would kinetically limit the dissolution of catalyst metals (or their oxides) possessing slow corrosion rates such as Ni, Ti, Zn, or Mg,[62] or inadequate rinsing during purification, allowing ionic metals to adhere to CNTs, particularly at divalent cationic sites such as carboxylic groups.[62] There is some data to suggest that the avoidance of oxidizing acids during CNT purification allows for sufficient acid treatment time, while preventing the exposure of the metal that is fully encased in carbon and completely inaccessible.[62] However, an oxidizing environment or organic solvent extraction would be needed for the removal of PAH adsorbates (noted previously) and it is not known whether the *in vivo* phagocytic oxidizing environment is sufficient for the liberation of carbon-encapsulated metals. Relatively little analysis has been performed on the consequences of catalyst release from CNTs and catalyst metal release could contribute to the observed pro-inflammatory cytokine and ROS induction and/or immunosuppressive effects of CNTs as noted above in the section on PAHs. Indeed, soluble iron (Fe^{2+}) is capable of forming ROS in physiologically relevant conditions;[62,65] Cu, Co, Al, Fe, Ni, and Cr are known to be toxic by inhalation, ingestion, or dermal exposure;[65] ultrafine combustion materials, with their characteristic transition metal or sulfuric acid core with an adlayer of semivolatile organics, have been shown to induce oxidative stress;[13] and animal studies have demonstrated that Cd, V, Cr, Pb, and Ni decrease antibody formation, antigen processing, and lymphocyte processing.[66]

7. Adsorbed or Conjugated Polymer Coatings

Several polymer surface coatings are deliberately applied to nanomaterials with the intent to modify (i.e., improve) their specific interactions with host biology. Most of these polymers are hydrophilic and intended to help suspend

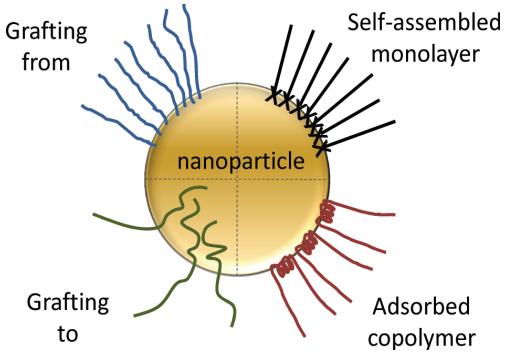

Figure 4. Common nanoparticle surface polymer functionalization schemes. These approaches include polymer growth from the surface (grafting from), polymer growth and subsequent grafting to the surface, self-assembled monolayers, and surface copolymer adsorption.

or solubilize nanomaterials in aqueous media. These polymers can be physically adsorbed to nanomaterial surfaces to form surface adlayers, or chemically conjugated to pre-existing nanomaterial surface functional groups (Figure 4). Both approaches create polymer "coronas" around the nanomaterials, dramatically altering nanomaterial surface properties, chemistry, and interactions with aqueous media. All seek to limit non-specific protein adsorption from biological milieus and improve particle suspension lifetimes in aqueous media.

Some of these polymer surface modifications aim to improve cellular uptake for imaging, drug delivery, or gene transfection. These types of particle coatings are generally simple and include polyethyleneimine, polyamines, DNA, PLL, or chitosan. Other polymer coatings on nanomaterials attempt to evade uptake and capture by the host filtration organs (i.e., the reticuloendothelial system, RES) during systemic circulation; materials such as polyethylene glycol (PEG), poloxamer block copolymers, celluloses, polyvinyl alcohol, hydrophilic polyacrylates such as polyHEMA and polyacrylic acid, and poloxamines have all been used to limit cell uptake, delay phagocytosis, and modify the host clearance of nanomaterials.[11] For more information on the specific roles of surface coatings on nanomaterial immunogenicity, please refer to Chapter 18.

PEG conjugation to nanomaterial surfaces follows countless precedents of this strategy applied to other biomaterials for the same purpose — to mask the material's surface from endogenous proteins and receptors.[11,67] However, CNTs functionalized with PEG, followed by conjugation with fluorescein

isothiocyanate as an imaging agent, produced pro-inflammatory macrophage responses, though the observed lymphocyte behavior was unchanged.[68] Anti-PEG antibodies are now recognized as well,[69–73] with evidence for complement activation (see Chapter 11 for more details) and hypersensitivity reactions,[71,73–75] particularly for hydroxy-terminated PEG,[76] indicating that PEG may have limited value *in vivo*. With the exception of PEG, PLL, polyvinyl alcohol, poloxamine and celluloses (complement activators),[71,74,76,77] and some chitosan variants (known to act as adjuvants and immunostimulants),[35,36,78–80] most of these hydrophilic designer surface coatings are used with little observable immunogenic effects. However, non-immunostimulating polymer coatings are not without their problems, especially in non-covalent, surface-adsorbed states. For example, fluorescent spectroscopy has been used to demonstrate that single-walled CNTs rapidly shed their passivating Pluronic coating in serum.[81] That this surface alteration was assessed directly is admirable, supporting no known specific binding affinity between the surface chemistries of CNT and Pluronic, and Pluronic's ready removal in serum from competing surfactancy intrinsic to many serum components. PAHs and other adsorbate contaminants common to CNT surfaces (*vida supra*) beg the question as to the true chemically bound or physically adsorbed states of other added nanomaterial and single-walled CNT polymer coatings and their stability in biological milieus. Polymer adsorbate displacement or adlayer remodeling in biological milieus may prompt other unintended property changes consequent to protein adsorption and material aggregation.[27] Poor polymer adlayer adsorption resistance to high protein surface bombardment typical of full plasma or serum (70 mg/mL protein) can bury polymer adlayers,[82] rendering any intended interaction effects of them with cells ineffective, and inducing material aggregation.

8. Biomolecule Adsorbates

Most globular proteins are highly surface-active, given their amphiphilic chemical and physical structures and abundant metastable folded states. Many proteins of diverse sizes and structures are known to adsorb rapidly to nearly all surface chemistries and known proteins are generally highly surface-active.[7,27,83] This issue remains a major unsolved challenge to the biomaterials field in general, evading solutions for over 50 years. (For more information on the impact of nanomaterial–protein adsorption/interactions on material distribution, please see Chapter 6.) Protein adsorption to nanomaterials is well documented despite various surface modifications,[29,82,84–86] occurring immediately upon or after their introduction into blood, cell culture media, food extracts, cell lysates, or other protein-containing fluids. This is expected, given that their

surface treatments are similar to those applied to conventional biomaterials for decades, and the universal failure to produce a suitable solution to this problem across all materials, regardless of size or surface. Protein adsorption is a major mechanism by which all materials are recognized and removed from circulation by filtration organs of the RES — the liver, spleen, kidney, and lung.[86,87] The process of opsonization — the non-specific adsorption of plasma proteins to circulating colloids, producing recognition by the RES tissues[75,86] — is the central mechanism of this endogenous host clearance mechanism.

With the possible exception of vitronectin and similar proteins whose adsorption may attenuate complement activation,[74] protein adsorption to materials often results in both the activation of complement with subsequent cell uptake, and activation of cell-mediated immune components.[88] For example, the intraperitoneal injection of a fullerene C_{60}–albumin conjugate into mice induced a fullerene IgG antibody response.[89] Single- and double-walled CNTs introduced into human plasma were coated primarily with fibrinogen and apolipoproteins (e.g., AI, AIV, CIII), activating the classical complement cascade though direct binding of C1q. CNTs also activated the alternative complement cascade through C3b binding.[90] Nonetheless, other studies have shown minimal roles for complement in material uptake, attributed to differing protein adsorbates and nanomaterial types. Cell uptake efficiency is optimal for CNT or polystyrene nanomaterials pre-suspended in even dilute serum or dilute albumin, respectively.[2,91] Polystyrene material data obtained from an intricate *ex vivo* spleen slice model revealed a key role for adsorbed albumin, but little uptake was observed in a purified fibronectin system and no reduction in nanomaterial cell uptake was observed for serum depleted of complement, IgG, or heparin-binding proteins.[91] This may be because albumin is the most abundant major plasma protein and is highly adsorbed to almost all materials. Nanomaterial uptake is also proposed to be mediated through macrophage scavenger receptors responding to conformational alterations in adsorbed endogenous proteins.[2,91] Moreover, the activation of scavenger receptors could attenuate innate immunity by the reduction of chemokine production or by the inhibition of inflammatory mediators.[52] Additionally, some speculate that leached ions or nanomaterial interactions with endogenous proteins could result in protein unfolding that expose normally cryptic domains or sequences, deactivate protein function, decrease bioactivity or generate new haptens, and raise allergic or autoimmune reactions.[2,13,91–93]

The inhalation route of nanomaterial exposure results in nanomaterial conditioning distinct from that of other administration/exposure routes due to the unique biomolecular environment and tissue processing present in the

lung. Material size scales inversely with the depth of material penetration into and deposition within the lung, resulting from aerodynamic effects upon inhalation. As such, larger materials are retained primarily in the upper respiratory system (throat and bronchi), where they are cleared by the mucociliatory escalator, while smaller materials penetrate deeper into the bronchiolar bed, and a small fraction of the smallest materials might reach farthest to the alveolar bed, where they become coated with lung surfactant.[94] From there, materials may interact with surfactant proteins (apolipoproteins A and D or surfactant glycoproteins A, B, or C) and enter alveolar epithelial (type I or II), abundant alveolar macrophage, or bronchiolar dendritic cells.[94] Alternatively, cellular uptake and the subsequent generation of inflammatory cytokines may result in altered material transport as inflammation increases permeability and opens up a paracellular route to the interstitium with eventual translocation to the blood circulation.[94,95]

One anecdote that possibly links nanomaterial–protein interactions to unusual host response is demonstrated through distinct host reactions to the model protein ovalbumin (OVA) in the presence and absence of CNTs. OVA and CNTs, co-administered intratracheally (in saline with Tween 80) to mice, resulted in significant increases in oxidative stress markers (e.g., heme oxygenase-1, HO-1), DNA modification (8-hydroxy-2′-deoxyguanosine, 8-OHdG), lipid peroxide products, and advanced glycation end-products [AGEs, pentosidine, and Nε-(carboxymethyl)lysine][96] commonly found in an oxidative *in vivo* environment. The binding of AGEs to corresponding receptors (RAGEs) found on many cell types contributes to chronic inflammatory diseases through pattern recognition receptor-mediated perpetuation of cellular activation.[97] Furthermore, expression levels of multiple allergy-related cytokines (IL-4, IL-5, IL-13, IL-17A, and IL-33) were elevated in the lung following OVA + CNT administration to these mice. These observed collective murine responses to OVA + CNT were significantly greater than the host response to OVA alone. While it is not known whether the adsorption of OVA to CNTs elicited the differences, or whether the observed responses resulted from a synergy of responses to the two entities together,[96] the findings suggested that the adsorptive presentation of OVA by CNTs increases the observed host response to OVA and that the adsorptive presentation of allergens or antigens by CNTs may exacerbate allergic or immunogenic responses. If consistent with host responses to other nanomaterials, biological adsorption to nanomaterials relative to activating adaptive immunity and interactions with pattern recognition receptors already implicated in nanomaterial immunotoxicity[16,98] should become a serious focus (Figure 3). As the RAGE receptor also regulates sepsis, this tentatively implicates endotoxin and

LPS processing by the host to such nanomaterial-based presentation of antigen and even LPS itself.

9. Lipopolysaccharide (Bacterial Endotoxin)

As a ubiquitous component of Gram-negative bacterial cell walls, LPS remains one of the most common surface-adsorbed contaminants of serious concern for all nanomaterials.[99] LPS is a peptidoglycan-decorated phosphorylated multi-chain lipid shed from bacterial cell walls [Figure 2(d)]. Given the considerable presence of these bacterial flora on skin, airborne of aerosols and particles, on all surfaces that comes in contact with the skin, in all milieus capable of supporting bacteria, and in most water sources (except expensive, designated "pyrogen-free" water), LPS is indeed ubiquitous. Therefore, LPS contaminates everything that most water sources and mammals have contacted, including laboratory glassware, utensils, clean rooms, and filtration equipment. Like proteins and silicones, its surface activity is particularly problematic; the LPS chemical structure and resulting surface activity favor its adsorption to hydrophobic surfaces by its multiple acyl lipid chains, while its phosphate, amine, and polar glycan chemistries facilitate binding to polar and charged surfaces.[99] These properties allow LPS to contaminate virtually any surface and remain tenaciously adsorbed. Its contamination of numerous biomaterials and medical devices is well documented.[26,100–103] Nonetheless, its detection is primarily done using assays that identify its soluble form.[12] *In situ* detection in adsorbed states is difficult and non-quantitative[6] (see Chapter 4 for more details).

Endotoxin strongly affects biological systems as a known pyrogen by raising the body temperature and inducing inflammatory cellular cytokine production through its presentation to many types of host cells.[95,102,104,105] Macrophages and other immune cells use Toll-like receptors (TLRs) to recognize and process LPS. Hence, reliably discriminating intrinsic LPS bioactivity, distinct from the nanomaterial's intrinsic inflammatory activity, is both important and technically arduous. Given the exaggerated areas and surface-to-volume ratios for nanophase systems, possible amounts of adsorbed endotoxin (e.g., micrograms of adsorbed endotoxin per gram of material) are significant. Titanium dioxide (TiO_2) materials have been shown to bind LPS in such a way that reduces *in vitro* cellular inflammatory response to LPS.[106] Other nanomaterials have also been demonstrated to bind endotoxin[14,107] and it is likely that all such materials will bind some of these contaminants. A select few biomaterials have been evaluated for their ability to bind and remove endotoxin from aqueous solution.[108,109] Moreover, investigations of

material–endotoxin interactions related to orthopedic wear debris in hip arthroplasties reported microparticle-adsorbed endotoxin effects on implant loosening through localized inflammation.[104,110] Therefore, as endotoxin contamination is nearly ubiquitous on most nanomaterials, it is capable of producing inflammatory responses magnified over those elicited from the presence of the nanomaterial alone.[12] This also provides the potential for nanomaterial–endotoxin synergy in host responses.

These effects warrant concern over the potent inflammatory reactivity of endotoxin *in vivo* and *in vitro* with many cell lines,[102,105,110,111] particularly inflammatory cell lines (e.g., macrophages lines of various lineages and maturities[12]). The presence of adventitious endotoxin contamination in cell cultures or on nanomaterials applied to cells could activate these cells and generate inflammatory cytokine responses essentially indistinguishable from any response generated by the exposure to the nanomaterial alone. Additionally, such cellular activation could also alter other crossover cell signaling pathways in cell-based assays, generating unintended consequences or confounding results. Consequently, endotoxin contamination of nanomaterials, nanomaterial stock solutions, laboratory glassware, lab-grade and even ultrafiltered water, and cell culture materials should be routinely assayed,[12,99] controlled, and remediated before any cell response assay to nanomaterials is performed.[12,99]

Unfortunately, detecting LPS on nanomaterials is currently challenging.[6] Typical endotoxin assays only respond to solution phase LPS. The Limulus Amebocyte Lysate (LAL) assay is the current standard for detecting soluble endotoxin *in vitro*, despite inherent inconsistencies (i.e., the assay signal is relative to fixed highly controlled LPS standards that may or may not reflect diverse sources, heterogeneity, purity, or reactivity of endogenous LPS). Colorimetric variation of the LAL assay in response to LPS dosing is the most widely used detection metric in biomaterial testing, particularly in preclinical settings, and is more accurately defined as a measure of relative endotoxin activity rather than absolute endotoxin concentration.[12]

Importantly, endotoxin may only be detected by these assays if it is soluble or readily displaceable (i.e., not permanently surface-bound). Nevertheless, some methods have been developed to correlate detectable solute endotoxin to surface-bound endotoxin within the same material system.[12,101–103] Furthermore, a recent murine macrophage-based commercial tool — RAW-Blue® reporter cells — facilities LPS detection or other solutes that activate the NF-κB or AP-1 transcription factor pathways. Though this reporter cell line provides LPS detection indiscernible from other possible signaling pathway activators, it yields useful information concerning the presence of soluble

agonists to the TLR family, NOD family, RIG-1 and MDA-5 receptors (RAW-Blue® cells product insert, version #11E30-MM, Invivogen, San Diego, CA).

Additional endotoxin assays are discussed in detail elsewhere[99] and in Chapter 4. However, for any of these methods to be quantitatively reliable, adsorbed endotoxin should be shown to correlate directly to known LPS exchange or desorption rates under relevant *in vitro* conditions, where LPS undetected by the assay in surface-bound form produces a reliable answer when surface-displaced in biological milieus. That is, irreversibly adsorbed endotoxin might be indirectly correlated by knowing its soluble, reversibly adsorbed LPS fraction displaced from a surface in biological milieus. This rigorous analysis is not performed on nanomaterials, despite the likelihood that LPS as a common, highly biologically reactive contaminant is present at high levels as introduced from routine material processing and manufacturing. Hence, biological tracing of adsorbed LPS and its partitioning between nanophases and biological milieus remain unknown.[12,108] Consequently, the rabbit pyrogen test has been recommended for verifying endotoxin contamination of nanomaterials to improve otherwise ambiguous results from other detection methods.[99]

10. Contaminant Detection and Assessment

Although the appreciation of the need for detailed, comprehensive surface characterization of nanomaterials exposed to environmental and biomedical applications is increasing, differences between traditional bulk material surface science and analysis of nanophases presents daunting challenges for quality control in nanomaterial applications. Surface analysis methods [e.g., XPS, low energy electron diffraction (LEED), Auger electron spectroscopy, mass spectrometries, etc.][23] have been adopted for nanomaterial use from a long history of development from surface science applied to particle-supported catalysts and microelectronics analytics for detailed characterization of nanomaterial, but typically for nanomaterials prepared and analyzed under well-defined conditions. Such analysis requires specialized instrumentation and standard, validated experimental protocols to prepare, store, and transport samples in specific, well-defined conditions (oxidized, reduced, ligand-protected, sulfided, etc.) (see Refs. 6, 111, 112 and references cited therein). Nonetheless, surface analytical tools capable of elucidating specific nanoscopic details are still limited, even under the best high vacuum analysis conditions.[114] Most of these tools do not have the spatial resolution to examine individual nanoparticles or nanomaterial features; all

results thus average area-based values from ensembles of nanomaterials and from background sources in spaces beneath and around them, and from bulk nanomaterials in multilayers.

Due to the complexity intrinsic to most biological environments, surface science methods for nanomaterials in complex milieus are lacking; the direct translation of traditional ultrahigh vacuum (UHV) surface science methods to nanomaterials placed into aqueous, proteinaceous environments provides very limited useful information. Recent studies have developed quantitative XPS methods for determining the overlayer thickness on functionalized gold particles[115] and the core-shell structures of quantum dots (QDs).[116] These studies along with others have used XPS, ToF-SIMS, and NMR methods to identify the presence of surface contaminants on gold particles and QDs.[115–119] While these and other systematic surface analysis studies[120] of functionalized nanoparticles are an important starting point for developing tools for the better characterization of nanomaterial surface chemistry, they do not address ultimate challenges of characterizing the nanomaterial surface chemistry *in situ* under biologically relevant conditions. Nonlinear optical methods offer promise to contribute information about the surface chemistry of nanomaterials in aqueous solutions. For example, sum-frequency generation in a scattering geometry has been used to characterize micro- and nanomaterials in solution.[121,122] The scattering patterns provide information about the structure of the materials (core-shell, etc.), while vibrational spectra yield information about surface species.

Current reliance of the field to date on transmission electron microscopy (TEM) to describe nanomaterial properties and behaviors is insufficient and misleading since it is performed *ex situ* after dessication, and provides little surface information. The increasingly common scenario reported in the biomedical literature involves placing a very complex, poorly defined, and highly reactive nanomaterial into an *even* more complex biological system. This routine starkly contrasts the carefully controlled ways that, for example, supported materials are studied and handled for gas-phase structure–property surface catalysis experiments (i.e., for heterogeneous catalysis). The biological results for nanomaterials are often not definitive, elucidating, mechanistic, or very good science needed to inspire approaches to improving nanotechnology, or for understanding either surface adsorbate behaviors or mechanisms of how nanomaterials interact with biological or environmental systems. The situation begs the question about how to improve (nano)science to provide accurate information on nanomaterial interactions in complex biological scenarios.[6]

11. Conclusions

Nanomaterial interactions with biological, environmental, and biomedical systems are a growing concern with increasingly diverse material sources and chemistries exposed to humans in their daily routines. A large part of this concern is focused on the surfaces of nanomaterials that comprise the majority of their interactions with human response elements. Nanomaterial surface properties and their modifications over time and in various conditions are therefore critical to elucidate in nanomaterial presentation to various immune, inflammatory, and APCs. Pathways for cellular particle, particle–adsorbate, and adsorbed antigen processing are known, but the specifics of nanomaterial involvement in such host cell-based processing are severely lacking.

Nonetheless, technical challenges for characterizing nanophase materials with significantly enhanced specific surface areas and reactivities are daunting, particularly in extending analysis beyond the UHV environment and into complex real systems. Increased analytical power is essential to produce new information capable of elucidating nanomaterial surface adsorbate chemistries, adsorption/desorption phenomena including stability, dynamics, and exchange reactions in complex media, and how these nanomaterial compositions influence host responses. Tools for such sensitive nanomaterial analyses are not yet sufficiently developed to provide the quality of information necessary to discern mechanisms and distinguish material properties in biological systems. Currently detectable cell-based toxicities and immune responses can only be correlated indirectly to nanomaterials; direct, reliable, and sensitive causal information linking observed cellular reactions to specific nanomaterials can only be inferred at best. The generation of reliable nanomaterial structure–property relationships in host immune and toxicity processing requires sensitive and versatile analytical methods to detect adsorbate classes, understand cell–material interactions, and the ways in which nanomaterials present chemistry to host inflammatory mediators. Beyond isolated, anecdotal gross histological, or morphological evidence for nanomaterial toxicity and inflammatory provocation, very little definitive information exists to demonstrate nanomaterial-induced adverse host events. Hence, the link between host cell responses and nanomaterial surface properties, conditioning, and delivery of adsorbates is poorly understood. As such, no mechanistic or structure–property relationships implicated in any possible or alleged nanomaterial toxicity risks can be rationally asserted. Improving on this scientific challenge will be essential to best understand, control, and exploit the unique features of nanoscale properties and materials in their various human and mammalian applications.[6]

Acknowledgments

The authors acknowledge support from NIH grants EB-00894 (CFJ and DWG) and EB-002027 (DGC).

References

1. Turner M, Golovko VB, Vaughan OPH, *et al.* Selective oxidation with dioxygen by gold nanoparticle catalysts derived from 55-atom clusters. *Nature* 2008;454(7207):981–983.
2. Nel AE, Mädler L, Velegol D, *et al.* Understanding biophysicochemical interactions at the nano–bio interface. *Nat Mater* 2009;8(7):543–557.
3. Petros RA, DeSimone JM. Strategies in the design of nanoparticles for therapeutic applications. *Nat Rev Drug Discovery* 2010;9(8):615–627.
4. Pumera M. Electrochemistry of graphene: New horizons for sensing and energy storage. *Chem Rec* 2009;9(4):211–223.
5. Auffan M, Rose J, Bottero JY, Lowry GV, Jolivet JP, Wiesner MR. Towards a definition of inorganic nanoparticles from an environmental, health and safety perspective. *Nat Nano* 2009;4(10):634–641.
6. Grainger DW, Castner DG. Nanobiomaterials and nanoanalysis: Opportunities for improving the science to benefit biomedical technologies. *Adv Mater* 2008;20(5):867–877.
7. Gray JJ. The interaction of proteins with solid surfaces. *Curr Opin Struct Biol* 2004;14(1):110–115.
8. Norde W, Lyklema J. Protein adsorption and bacterial adhesion to solid surfaces: A colloid-chemical approach. *Colloids Surf* 1989;38(1):1–13.
9. Jacob K. Surface interactions with adsorbed macromolecules. *J Colloid Interface Sci* 1986;111(2):305–313.
10. Andrade J, Hlady V. Protein adsorption and materials biocompatibility: A tutorial review and suggested hypotheses. *Adv Polym Sci* 1986;79(1):1–63.
11. Owens DE, Peppas NA. Opsonization, biodistribution, and pharmacokinetics of polymeric nanoparticles. *Int J Pharm* 2006;307(1):93–102.
12. Jones CF, Grainger DW. *In vitro* assessments of nanomaterial toxicity. *Adv Drug Delivery Rev* 2009;61(6):438–456.
13. Nel A, Xia T, Mädler L, Li N. Toxic potential of materials at the nanolevel. *Science* 2006;311(5761):622–627.
14. Peula-García JM, Molina-Bolivar JA, Velasco J, Rojas A, Galisteo-González F. Interaction of bacterial endotoxin (lipopolysaccharide) with latex particles: Application to latex agglutination immunoassays. *J Colloid Interface Sci* 2002;245(2):230–236.
15. Barrett KE, Barman SM, Boitano S, Brooks H. *Ganong's Review of Medical Physiology*, McGraw-Hill Medical, 2009.
16. Dobrovolskaia MA, McNeil SE. Immunological properties of engineered nanomaterials. *Nat Nano* 2007;2(8):469–478.
17. Yuan T, Marshall WD. Catalytic hydrogenation of polycyclic hydrocarbons over palladium/γ-AI203 under mild conditions. *J Hazard Mater* 2005;126(1–3):149–157.
18. Petsch D, Anspach FB. Endotoxin removal from protein solutions. *J Biotechnol* 2000;76(2–3):97–119.

19. Woehrle GH, Brown LO, Hutchison JE. Thiol-functionalized, 1.5-nm gold nanoparticles through ligand exchange reactions: Scope and mechanism of ligand exchange. *J Am Chem Soc* 2005;127(7):2172–2183.
20. Swift J, Butts CA, Cheung-Lau J, Yerubandi V, Dmochowski IJ. Efficient self-assembly of archaeoglobus fulgidus ferritin around metallic cores. *Langmuir* 2009;25(9):5219–5225.
21. Castner DG, Ratner BD. Biomedical surface science: Foundations to frontiers. *Surf Sci* 2002;500:28–60.
22. Castner DG, Grainger DW. Surface analytical methods: *In situ* and UHV techniques. In: Healy K, Ducheyne P, Grainger D, Kirkpatrick J, Hutmacher D (eds.), *Comprehensive Biomaterials — an on-line compendium*. Vol. 3(1), Elsevier, 2011, pp. 1–22.
23. Recum AV, Jacobi JE. Surface characterization. In: LaBerge M (ed.), *Handbook of Biomaterials Evaluation: Scientific, Technical, and Clinical Testing of Implant Materials*, CRC Press, 1998, pp. 893.
24. Baer DR, Gaspar DJ, Nachimuthu P, Techane SD, Castner DG. Application of surface chemical analysis tools for characterization of nanoparticles. *Anal Bioanal Chem* 2010;396(3):983–1002.
25. Richman EK, Hutchison JE. The nanomaterial characterization bottleneck. *ACS Nano* 2009;3(9):2441–2446.
26. Lynch I, Cedervall T, Lundqvist M, Cabaleiro-Lago C, Linse S, Dawson KA. The nanoparticle-protein complex as a biological entity; a complex fluids and surface science challenge for the 21st century. *Adv Colloid Interface Sci* 2007;134–135(0): 167–174.
27. Linse S, Cabaleiro-Lago C, Xue WF, *et al*. Nucleation of protein fibrillation by nanoparticles. *Proc Natl Acad Sci U S A* 2007;104(21):8691–8696.
28. Lynch I, Dawson KA, Linse S. Detecting cryptic epitopes created by nanoparticles. *Sci STKE* 2006;2006(327):pe14.
29. Sharp FA, Ruane D, Claass B, *et al*. Uptake of particulate vaccine adjuvants by dendritic cells activates the NALP3 inflammasome. *Proc Natl Acad Sci U S A* 2009;106(3):870–875.
30. Eisenbarth SC, Colegio OR, O'Connor W, Sutterwala FS, Flavell RA. Crucial role for the NALP3 inflammasome in the immunostimulatory properties of aluminium adjuvants. *Nature* 2008;453(7198):1122–1126.
31. Martinon F, Petrilli V, Mayor A, Tardivel A, Tschopp J. Gout-associated uric acid crystals activate the NALP3 inflammasome. *Nature* 2006;440(7081):237–241.
32. Gupta R, Rost B, Relyveld E, Siber G. Adjuvant properties of aluminum and calcium compounds. In: Powell M, Newman M (eds.), *Vaccine Design: The Subunit and Adjuvant Approach*, Plenum Press, 1995, pp. 229–248.
33. O'Hagan DT, Singh M, Ulmer JB. Microparticle-based technologies for vaccines. *Methods* 2006;40(1):10–19.
34. Arca HC, Günbeyaz M, Senel S. Chitosan-based systems for the delivery of vaccine antigens. *Expert Rev Vaccines* 2009;8(7):937–953.
35. Şenel S. Chitosan-based particulate systems for non-invasive vaccine delivery. In: Jayakumar R, Prabaharan M, Muzzarelli RAA (eds.), *Chitosan for Biomaterials I*. Vol. 243, Springer, 2011, pp. 111–137.
36. He X, Jiang L, Wang F, *et al*. Augmented humoral and cellular immune responses to hepatitis B DNA vaccine adsorbed onto cationic microparticles. *J Controlled Release* 2005;107(2):357–372.

37. White K, Kawabata TT, Ladics G. Mechanisms of polycyclic aromatic hydrocarbon immunotoxicity. In: Dean JH (ed.), *Immunotoxicology and Immunopharmacology*. Vol. 2, 1994, pp. 123–149.
38. Kundsin RB, Walter CW. Detection of endotoxin on sterile catheters used for cardiac catheterization. *J Clin Microbiol* 1980;11(3):209–212.
39. Bondurant S, Ernster VL, Herdman R. *Committee on the Safety of Silicone Breast Implants*. National Acadamic Press, Institute of Medicine, 2000, pp. 540.
40. Vakharia DD, Liu N, Pause R, *et al*. Polycyclic aromatic hydrocarbon/metal mixtures: Effect on PAH induction of CYP1A1 in human HepG2 cells. *Drug Metab Dispos* 2001;29(7):999–1006.
41. Plata DeL, Hart AJ, Reddy CM, Gschwend PM. Early evaluation of potential environmental impacts of carbon nanotube synthesis by chemical vapor deposition. *Environ Sci Tech* 2009;43(21):8367–8373.
42. Saboori A, Newcombe D. Environmental chemicals with immunotoxic properties. In: Newcombe DS, Rose NR, Bloom JC (ed.), *Clinical Immunotoxicology,* Raven Press, 1992, pp. 365–400.
43. Yang K, Xing B. Desorption of polycyclic aromatic hydrocarbons from carbon nanomaterials in water. *Environ Pollut* 2007;145:529–537.
44. Chen RJ, Zhang Y, Wang D, Dai H. Noncovalent sidewall functionalization of single-walled carbon nanotubes for protein immobilization. *J Am Chem Soc* 2001;123(16): 3838–3839.
45. Kah M, Zhang X, Jonker MTO, Hofmann T. Measuring and modeling adsorption of PAHs to carbon nanotubes over a six order of magnitude wide concentration range. *Environ Sci Technol* 2011;45(14):6011–6017.
46. Hiraoka T, Izadi-Najafabadi A, Yamada T, *et al*. compact and light supercapacitor electrodes from a surface-only solid by opened carbon nanotubes with 2200 m^2 g^{-1} surface area. *Adv Funct Mater* 2010;20(3):422–428.
47. Deck CP, McKee GS, Vecchio KS. Synthesis optimization and characterization of multi-walled carbon nanotubes. *J Electron Mater* 2006;35(2):211–222.
48. Bendjemil B, Borowiak-Palen E, Graff A, *et al*. Elimination of metal catalyst and carbon-like impurities from single-wall carbon nanotube raw material. *Appl Phys A* 2004; 78:311–314.
49. Pulskamp K, Diabaté S, Krug HF. Carbon nanotubes show no sign of acute toxicity but induce intracellular reactive oxygen species in dependence on contaminants. *Toxicol Lett* 2007;168(1):58–74.
50. Veranth J, Ghandehari H, Grainger DW. *Nanoparticles in the lung. Comprehensive Toxicology*. Vol. 8, Elsevier, 2010.
51. Castranova V, Ma J, Yang HM, *et al*. Effect of exposure to diesel exhaust particles on the susceptibility of the lung to infection. *Environ Health Perspect* 2001;109(Suppl 4): 609–612.
52. Yeates DB, Mauderly JL. Inhaled environmental/occupational irritants and allergens: mechanisms of cardiovascular and systemic responses. Introduction. *Environ Health Perspect* 2001;109(Suppl 4):479–481.
53. Jakab GJ, Risby TH, Sehnert SS, Hmieleski RR, Gilmour MI. Suppression of alveolar macrophage membrane-receptor-mediated phagocytosis by model particle-adsorbate complexes: Physicochemical moderators of uptake. *Environ Health Perspect* 1990;89:169–174.

54. Gilmour MI, Daniels M, McCrillis RC, Winsett D, Selgrade M. Air pollutant-enhanced respiratory disease in experimental animals. *Environ Health Perspect* 2001;109(Suppl 4): 619–622.
55. White KL. Immunosuppression by polycyclic aromatic hydrocarbons: A structure-activity relationship in B6C3F1 and DBA/2 mice. *Immunopharmacology* 1985;9(3):155–164.
56. Brewer SH, Glomm WR, Johnson MC, Knag MK, Franzen S. Probing BSA binding to citrate-coated gold nanoparticles and surfaces. *Langmuir* 2005;21(20):9303–9307.
57. Nonckreman CJ, Fleith S, Rouxhet PG, Dupont-Gillain CC. Competitive adsorption of fibrinogen and albumin and blood platelet adhesion on surfaces modified with nanoparticles and/or PEO. *Colloids Surf B Biointerfaces* 2010;77(2):139–149.
58. Öncel Ç, Yürüm Y. Carbon nanotube synthesis via the catalytic CVD method: A review on the effect of reaction parameters. *Fullerenes Nanotubes Carbon Nanostruct* 2006;14(1):17–37.
59. Jadhav N, Shah MD, Nair K, Shirote P, Bhatia NM. Methods of carbon nanotube and nanohorn synthesis: A review. *Pharm Rev*. 2007;5, from http://www.pharmainfo.net/reviews/methods-carbon-nanotube-and-nanohorn-synthesis-review.
60. Duncan R, Stolojan V, Lekakou C. Manufacture of carbon multi-walled nanotubes by the arc discharge technique. *Proc World Congr Eng* 2007;2:1391–1395.
61. Ge C, Li W, Li Y, *et al*. Significance and systematic analysis of metallic impurities of carbon nanotubes produced by different manufacturers. *J Nanosci Nanotechnol* 2011;11(3):2389–2397.
62. Liu X, Gurel V, Morris D, *et al*. Bioavailability of nickel in single-wall carbon nanotubes. *Adv Mater* 2007;19(19):2790–2796.
63. Liu X, Guo L, Morris D, Kane AB, Hurt RH. Targeted removal of bioavailable metal as a detoxification strategy for carbon nanotubes. *Carbon N Y* 2008;46(3):489–500.
64. Buzea C, Pacheco, II, Robbie K. Nanomaterials and nanoparticles: Sources and toxicity. *Biointerphases* 2007;2(4):MR17–71.
65. Kowolenko M, Mc-Cabe M, Lawrence D. Metal induced alterations of immunity. In: Newcombe D, Rose N, Bloom C (eds.), *Clinical Immunotoxicology*, Ravenial, 1992: pp. 401–419.
66. Dobrovolskaia MA, Aggarwal P, Hall JB, McNeil SE. Preclinical studies to understand nanoparticle interaction with the immune system and its potential effects on nanoparticle biodistribution. *Mol Pharm* 2008;5(4):487–495.
67. Dumortier H, Lacotte S, Pastorin G, *et al*. Functionalized carbon nanotubes are non-cytotoxic and preserve the functionality of primary immune cells. *Nano Lett* 2006;6(7):1522–1528.
68. Armstrong JK, Hempel G, Koling S, *et al*. Antibody against poly(ethylene glycol) adversely affects PEG-asparaginase therapy in acute lymphoblastic leukemia patients. *Cancer* 2007;110(1):103–111.
69. Ganson NJ, Kelly SJ, Scarlett E, Sundy JS, Hershfield MS. Control of hyperuricemia in subjects with refractory gout, and induction of antibody against poly(ethylene glycol) (PEG), in a phase I trial of subcutaneous PEGylated urate oxidase. *Arthritis Res Ther* 2006;8(1):R12–R21.
70. Knop K, Hoogenboom R, Fischer D, Schubert US. Poly(ethylene glycol) in drug delivery: Pros and cons as well as potential alternatives. *Angew Chem Int Ed Engl* 2010;49(36):6288–6308.

71. Richter AW, Akerblom E. Antibodies against polyethylene glycol produced in animals by immunization with monomethoxy polyethylene glycol modified proteins. *Int Arch Allergy Appl Immunol* 1983;70(2):124–131.
72. Sroda K, Rydlewski J, Langner M, Kozubek A, Grzybek M, Sikorski AF. Repeated injections of PEG-PE liposomes generate anti-PEG antibodies. *Cell Mol Biol Lett* 2005;10(1):37–47.
73. Moghimi SM, Andersen AJ, Hashemi SH, *et al.* Complement activation cascade triggered by PEG-PL engineered nanomedicines and carbon nanotubes: The challenges ahead. *J Controlled Release* 2010;146(2):175–181.
74. Vittaz M, Bazile D, Spenlehauer G, *et al.* Effect of PEO surface density on long-circulating PLA-PEO nanoparticles which are very low complement activators. *Biomaterials* 1996;17(16):1575–1581.
75. Arima Y, Toda M, Iwata H. Complement activation on surfaces modified with ethylene glycol units. *Biomaterials* 2008;29(5):551–560.
76. Al-Hanbali O, Rutt KJ, Sarker DK, Hunter AC, Moghimi SM. Concentration dependent structural ordering of poloxamine 908 on polystyrene nanoparticles and their modulatory role on complement consumption. *J Nanosci Nanotechnol* 2006;6(9–10):3126–3133.
77. Wen ZS, Xu YL, Zou XT, Xu ZR. Chitosan nanoparticles act as an adjuvant to promote both Th1 and Th2 immune responses induced by ovalbumin in mice. *Mar Drugs* 2011;9(6):1038–1055.
78. Ghendon Y, Markushin S, Akopova I, Koptiaeva I, Krivtsov G. Chitosan as an adjuvant for poliovaccine. *J Med Virol* 2011;83(5):847–852.
79. Vauthier C, Bertholon I, Labarre D. Integrated development of glycobiologics: From discovery to applications in the design of nanoparticular drug delivery systems. In: Gad SC (ed.), *Handbook of Pharmaceutical Biotechnology*, John Wiley and Sons, 2006, pp. 125–160.
80. Cherukuri P, Gannon CJ, Leeuw TK, *et al.* Mammalian pharmacokinetics of carbon nanotubes using intrinsic near-infrared fluorescence. *Proc Natl Acad Sci U S A* 2006;103(50):18882–18886.
81. Bertholon I, Vauthier C, Labarre D. Complement activation by core-shell poly(isobutylcyanoacrylate)–polysaccharide nanoparticles: Influences of surface morphology, length, and type of polysaccharide. *Pharm Res* 2006;23(6):1313–1323.
82. Sadana A. Protein adsorption and inactivation on surfaces. Influence of heterogeneities. *Chem Rev* 1992;92(8):1799–1818.
83. Cedervall T, Lynch I, Foy M, *et al.* Detailed identification of plasma proteins adsorbed on copolymer nanoparticles. *Angew Chem Int Ed Engl* 2007;119(30):5856–5858.
84. Lynch I, Dawson KA. Protein-nanoparticle interactions. *Nanotoday* 2008;3(1–2):40–47.
85. Moghimi SM, Hunter AC, Murray JC. Long-circulating and target-specific nanoparticles: Theory to practice. *Pharmacol Rev* 2001;53(2):283–318.
86. Li S-D, Huang L. Nanoparticles evading the reticuloendothelial system: Role of the supported bilayer. *Biochim Biophys Acta* 2009;1788(10):2259–2266.
87. Ratner BD, Hoffman AS, Schoen FJ, Lemons JE. *Biomaterials Science — An Introduction to Materials in Medicine,* Elsevier, 2004.
88. Chen BX, Wilson SR, Das M, Coughlin DJ, Erlanger BF. Antigenicity of fullerenes: Antibodies specific for fullerenes and their characteristics. *Proc Natl Acad Sci* 1998;95(18):10809–10813.

89. Salvador-Morales C, Flahaut E, Sim E, Sloan J, H. Green ML, Sim RB. Complement activation and protein adsorption by carbon nanotubes. *Mol Immunol* 2006;43(3):193–201.
90. Demoy M, Andreux JP, Weingarten C, Gouritin B, Guilloux V, Couvreur P. *In vitro* evaluation of nanoparticles spleen capture. *Life Sci* 1999;64(15):1329–1337.
91. Donaldson K, Aitken R, Tran L, *et al.* Carbon nanotubes: A review of their properties in relation to pulmonary toxicology and workplace safety. *Toxicol Sci* 2006;92(1):5–22.
92. Gatti AM, Tossini D, Gambarelli A, Montanari S, Capitani F. Investigation of the presence of inorganic micro-and nanosized contaminants in bread and biscuits by environmental scanning electron microscopy. *Crit Rev Food Sci Nutr* 2008;49(3):275–282.
93. Mühlfeld C, Rothen-Rutishauser B, Blank F, Vanhecke D, Ochs M, Gehr P. Interactions of nanoparticles with pulmonary structures and cellular responses. *Am J Physiol Lung Cell Mol Physiol* 2008;294(5):L817–L829.
94. Choi HS, Ashitate Y, Lee JH, *et al.* Rapid translocation of nanoparticles from the lung airspaces to the body. *Nat Biotech* 2010;28(12):1300–1303.
95. Inoue K, Yanagisawa R, Koike E, Nishikawa M, Takano H. Repeated pulmonary exposure to single-walled carbon nanotubes exacerbates allergic inflammation of the airway: Possible role of oxidative stress. *Free Radic Biol Med* 2010;48(7):924–934.
96. Liliensiek B, Weigand MA, Bierhaus A, *et al.* Receptor for advanced glycation end products (RAGE) regulates sepsis but not the adaptive immune response. *J Clin Invest* 2004;113(11):1641–1650.
97. Klippstein R, Fernandez-Montesinos R, Castillo PM, Zaderenko AP, Pozo D. Silver nanoparticles interactions with the immune system: Implications for health and disease. In: Perez DP (ed.), *Silver Nanoparticles*, In Tech, 2010, pp. 309–324.
98. Dobrovolskaia MA, Neun BW, Clogston JD, Ding H, Ljubimova J, McNeil SE. Ambiguities in applying traditional Limulus Amebocyte Lysate tests to quantify endotoxin in nanoparticle formulations. *Nanomedicine (Lond)* 2010;5(4):555–562.
99. Giljohann DA, Seferos DS, Daniel WL, Massich MD, Patel PC, Mirkin CA. Gold nanoparticles for biology and medicine. *Angew Chem Int Ed Engl* 2010;49(19): 3280–3294.
100. Gorbet MB, Sefton MV. Leukocyte activation and leukocyte procoagulant activities after blood contact with polystyrene and polyethylene glycol-immobilized polystyrene beads. *J Lab Clin Med* 2001;137(5):345–355.
101. Gorbet MB, Sefton MV. Endotoxin: The uninvited guest. *Biomaterials* 2005; 26(34):6811–6817.
102. Ragab AA, Van De Motter R, Lavish SA, *et al.* Measurement and removal of adherent endotoxin from titanium particles and implant surfaces. *J Orthop Res* 1999;17(6): 803–809.
103. Greenfield EM, Bechtold J. What other biologic and mechanical factors might contribute to osteolysis? *J Am Acad Orthop Surg* 2008;16(Suppl 1):S56–62.
104. Huttunen K, Jussila J, Hirvonen MR, Iivanainen E, Katila ML. Comparison of mycobacteria-induced cytotoxicity and inflammatory responses in human and mouse cell lines. *Inhal Toxicol* 2001;13(11):977–991.
105. Schwab LP, Xing Z, Hasty KA, Smith RA. Titanium particles and surface-bound LPS activate different pathways in IC-21 macrophages. *J Biomed Mater Res B Appl Biomater* 2006;79B(1):66–73.

106. Gretzer C, Werthén M, Thomsen P. Apoptosis and cytokine release in human monocytes cultured on polystyrene and fibrinogen-coated polystyrene surfaces. *Biomaterials* 2002;23(7):1639–1648.
107. Darkow R, Groth T, Albrecht W, Lützow K, Paul D. Functionalized nanoparticles for endotoxin binding in aqueous solutions. *Biomaterials* 1999;20(14):1277–1283.
108. Karl DW, Magnusson JC, Carr PW, Flickinger MC. Preliminary assessment of removal of pyrogenic lipopolysaccharides with colloidal zirconia adsorbents. *Enzyme Microb Technol* 1991;13(9):708–715.
109. Cho DR, Shanbhag AS, Hong C-Y, Baran GR, Goldring SR. The role of adsorbed endotoxin in particle-induced stimulation of cytokine release. *J Orthop Res* 2002; 20(4):704–713.
110. Greenfield EM, Bi Y, Ragab AA, Goldberg VM, Nalepka JL, Seabold JM. Does endotoxin contribute to aseptic loosening of orthopedic implants? *J Biomed Mater Res A* 2005;72B(1):179–185.
111. Castner D. Chemical modification of surfaces. In: Czanderna A, Powell C, Made T (eds.), *Specimen Handling, Beam Effects and Depth Profiling*, Plenum Press, 1998, pp. 209–238.
112. Castner DG, Watson PR, Chan IY. X-ray absorption spectroscopy, X-ray photoelectron spectroscopy, and analytical electron microscopy studies of cobalt catalysts. 2. Hydrogen reduction properties. *J Phys Chem* 1990;94(2):819–828.
113. Baer D, Engelhard M, Gaspar D, *et al*. Challenges in applying surface analysis methods to nanoparticles and nanostructured materials. *J Surf Anal* 2005;12(2):101–108.
114. Techane S, Baer DR, Castner DG. Simulation and modeling of self-assembled monolayers of carboxylic acid thiols on flat and nanoparticle gold surfaces. *Anal Chem* 2011;83(17):6704–6712.
115. Zorn G, Dave SR, Gao X, Castner DG. Method for determining the elemental composition and distribution in semiconductor core-shell quantum dots. *Anal Chem* 2011;83(3):866–873.
116. Techane SD, Gamble LJ, Castner DG. X-ray photoelectron spectroscopy characterization of gold nanoparticles functionalized with amine-terminated alkanethiols. *Biointerphases* 2011;6(3):98–104.
117. Min H, Kim Y, Yu H, *et al*. Probing the surface of organic and bioconjugated nanocrystals by using mass spectrometric imaging. *Chemistry* 2008;14(28):8461–8464.
118. Morris-Cohen A, Donakowski M, Knowles K, Weiss E. The effect of a common purification procedure on the chemical composition of the surfaces of CdSe quantum dots synthesized with trioctylphosphine oxide. *J Phys Chem C* 2010;114(2):897–906.
119. Techane SD, Gamble LJ, Castner DG. Multi-technique characterization of self-assembled carboxylic acid terminated alkanethiol monolayers on nanoparticle and flat gold surfaces. *J Phys Chem C Nanomater Interfaces* 2011;115(19):9432–9441.
120. de Beer AGF, Roke S. Nonlinear Mie theory for second-harmonic and sum-frequency scattering. *Phys Rev B* 2009;79(15):155420–155428.
121. de Beer AG, Roke S. Obtaining molecular orientation from second harmonic and sum frequency scattering experiments in water: Angular distribution and polarization dependence. *J Chem Phys* 2010;132(23):234702–234708.

CHAPTER 5

NANOPARTICLE INTERACTION WITH ENDOTOXIN CONFOUNDS *IN VITRO* ASSAY QUANTITATION

5.1 Abstract

Surface-adsorbed toxins are increasingly implicated in adverse responses to parenteral nanoparticle (NP) formulations *in vivo*. Endotoxin from gram negative bacteria (lipopolysaccharide, LPS) is a ubiquitous surface-active biomolecule that exerts significant inflammatory effects (*i.e.*, pyrogen) on mammalian systems and may induce unique reactivity in the presence of nanoparticles. Unfortunately, few methods exist to reliably detect LPS adsorbed on materials and none have been verified for high specific surface area nanomaterials, namely nanoparticles (NP). Furthermore, direct nanoparticle interference with the classical Limulus Amoebocyte Lysate (LAL) assay detection format for LPS may confound its quantification *in vitro*, though this interference has not previously been elucidated in any detail. NP-LPS interaction is demonstrated for three distinct NP materials as well as material-dependent NP interference with the kinetic chromogenic LAL (KQCL) assay format, including amplification of the biochemical LAL assay response to LPS. Notably, NP assay interference is demonstrated following NP removal from the analyte test solution, suggesting a potential for irreversible NP modification to either the assay components or to LPS bioactivity. These results demonstrate the potential for NPs to confound LPS quantitation and suggest the possibility that NPs may exacerbate biological responses to LPS. This calls for careful assessment and mitigation of LPS contamination in nanomaterials and nanoparticle formulations exposed to mammalian host responses.

5.2 Introduction

Nanomaterials are increasingly prevalent in biomedical applications such as contrast agents and targeted drug delivery carriers as well as in consumer products directly contacting human

tissue.[1-4] However, intrinsic toxicity and human risk assessments of nanoparticles generally lag behind scientific advancements in nanotechnology. Increasing numbers of studies show that some nanoparticles have associated adverse effects, including pyrogenicity (systemic inflammatory response),[5-8] immunogenicity,[9,10] coagulopathy,[11,12] and general toxicity.[13] These adverse host reactions to nanoparticles are variable, dose-dependent and often proposed to result from their size and intrinsic properties (e.g., high specific surface areas (100-400 m^2/g)[13]), but may also result from environmental contaminants and toxins adsorbed to nanoparticle surfaces.[5,6] High specific surface area increases the opportunities for surface adsorption, contamination and surface-binding of toxins compared to an analogous mass of bulk material. Since nanoparticle surfaces are in direct contact with host cells and receptors, their behavior and host reactivity *in vivo* appear to be highly dependent on material surface properties and phenomena.[7,14] However, some evaluations of nanoparticles report surface area-dependent nanomaterial toxicity[15] while others have found toxicity to be largely independent of surface area.[13] This controversy typifies a primary issue with nanoparticle use: detailed analysis of the unique surface interactions of nanomaterials is difficult if not impossible with current techniques and is not routinely performed.[14,16] As a result, little is known about nanomaterial surface-specific reactivity in biological systems and even less is actually done to assert material quality control and form comparisons to standards to understand reported variations in host responses. Recent evidence suggests substantial batch-to-batch variations in nanocarriers that confound determination of cause-and-effect relationships for interpreting *in vivo* host responses to nanomaterials.[17] Thus, the debate continues over whether observed nanomaterial *in vivo* toxicity is primarily a surface area-driven effect or something more, and what specific health risks are associated with nanomaterial surfaces.

Nanomaterial toxicity and biological assays are often complicated by interference of nanoparticles with common *in vitro* assay signal generating mechanisms.[6,18] Nevertheless, material sourcing, particle production, and subsequent laboratory handling are recognized as providing many opportunities to deliberately or inadvertently introduce a variety of adventitious and ubiquitous molecular species commonly found in lab environments as unintended adsorbates

on nanoparticles.[5,6,14] This “conditioned surface” then becomes the actual interface introduced to cells, tissues and biological pathways. Without either sufficient surface analysis or quality control, this major unknown in nanomaterial production represents a significant variable in nanomaterials toxicological assessments.

One ubiquitous nano- and biomaterial adsorbate is lipopolysaccharide (LPS), or endotoxin, a pyrogen of gram-negative bacterial origin that can elicit serious inflammatory responses *in vivo*,[8] and alter cell phenotypes in culture.[19,20] As a result, the FDA has issued guidance backing testing guidelines <85> and <161> by the United States Pharmacopeia (USP) and <ST72:2002> by the Association for the Advancement of Medical Instrumentation (AAMI) for the evaluation of bacterial endotoxin on biomaterials, implanted devices, drugs, and drug carriers using the Limulus Amebocyte Lysate assay (LAL).[7] LPS is an amphiphilic glycosylated phospholipid comprising a polar, highly diverse glycan domain conjugated to a lipid A-based highly hydrophobic acylated domain, with a high degree of both inter- and intraspecies chemical and structural heterogeneity between LPS variants across bacterial species, ranging in molecular weight from 5-80 kDa.[21] With its dual hydrophobic/polar character, LPS is soluble in aqueous environments (up to 5 mg/ml) and is also highly surface-active, able to bind both polar and non-polar surfaces. LPS forms nearly spherical, nano-scale (50-500nm) micelles and aggregates in water at critical concentrations (CMCs) between 4-38 µg/ml, with specific CMC values dependent upon polysaccharide region length.[21,22] As a product of both living and dead gram-negative bacterial commensally colonizing dermal organisms, LPS covers mammalian skin and is shed and transferred in many forms. Consequently, LPS is ubiquitous in most lab-grade water sources, even ASTM Research grade 1-filtered (e.g., “Millipore”) water, and on nearly every surface in a common laboratory (*i.e.*, glassware, water supplies, pipettes, even sterilized instruments) and is difficult both to detect and to eliminate.[23]

The most widely used and accepted assay for LPS detection is the LAL.[24] This assay is based on the coagulogenic pathogen defense mechanism utilized by the horseshoe crab, *Limulus polyphemus*, to trap invading pathogens in an LPS-induced clot in its bloodstream. This clot is the end-product of a multistep biochemical coagulation cascade, analogous to the human coagulation

cascade.[25] Relevant zymogens of the *L. polyphemus* cascade have been harvested, isolated, and harnessed for the purpose of *in vitro* LPS detection by chromogenic, turbidimetric, or gel clot assay endpoints.[25-27] However, the LAL assay is primarily limited to detecting soluble LPS that interacts with the assay zymogens.[23] Notably, the assay read-out is also prone to nanoparticle interference as reported anecdotally.[24] For example, cationic dendrimers cause the LAL assay to under-report actual LPS content, while solid nanoparticles have also been observed to interfere with readout, but may result in either over-reported or under-reported LPS concentrations, depending on the specific particle type and experimental conditions.[28]

The reliability of the LAL assay is a particular concern when assaying nanoparticle-containing samples because 1) nanoparticle interference may result in under-reporting of LPS levels and could thus yield false-negative pyrogenicity results, 2) LPS is only detected in soluble form in the LAL assay, and 3) nanomaterials, with their high specific surface areas (200-400 m^2/g) represent a substantial potential reservoir of insoluble LPS not readily detected by the LAL format. These known deficiencies in LAL assay reporting could have serious unintended consequences, particularly for contaminated parenteral nanoparticle formulations (*i.e.*, nanoparticles as drug carriers and imaging agents). Possible *in vivo* evidence for this bioanalytical shortcoming toward nanomaterials is also observed in literature reporting: combinations of LPS and nanoparticles are reported to be responsible for exacerbated systemic and local inflammatory reactions [8,29,30] and elevated fibrinogen and von Willebrand factor levels in the blood have been observed roughly 24 hours following contaminated nanoparticle exposure.[29] In related work, LPS and nanomaterials have resulted in leukocytic mediator release (cathepsin B, elastase, TNF, neopterin) and collateral prothrombin activation and coagulopathy.[31] Meanwhile, deviations from LPS content monitoring in medical devices and drugs procedurally violate FDA guidances.[7] Significantly, interactions of nanoparticles with endotoxin and host coagulogenic enzymes could imbue altered molecular activity or increased host responses to administered nanoparticles.[18] Moreover, high specific surface area nanomaterials could act as sorbents in their preparation environments, scavenging even trace amounts of LPS, later presenting or shedding substantial adsorbed LPS quantities as reactants in biological systems.

Moreover, when compared to soluble LPS in physiological milieu, such NP-adsorbed LPS could possess distinct transport and biodistribution properties, further altering the native host responses to LPS. Yet, no studies are published that investigate NP-mediated LPS effects *in vitro* or *in vivo*, or that elucidate possible NP-LPS interactions. This represents a liability in understanding the general toxicology of nanoparticles since the potential is generally high for LPS contamination of nanoparticles during preparation and handling, with consequent adverse effects that may counter and confound the intent of nanoparticle therapeutics.

This study seeks to elucidate LPS endotoxin association with model nanoparticles, demonstrate nanoparticle-endotoxin effects on the LAL assay response and document potential assay anomalies, clarifying the potential of a possible amplified immunologic response to nanoparticle-associated endotoxin *in vivo*. This study utilizes the commercialized kinetic QCL (LAL-based) assay as a detection method for these comparisons and a surrogate for a variety of biochemical processes.

5.3 Materials and methods

5.3.1 Materials and Reagents. Tetrachloroauric(III) acid ($HAuCl_4$•aq), tannic acid, and sodium citrate (Sigma, USA); sterile, 96-well, nontissue-culture-treated, polystyrene plates (Falcon, USA); Dulbecco's modified phosphate-buffered saline (DPBS, Gibco, USA); and endotoxin-free water, chromogenic LAL endpoint assay kit (QCL-1000), Kinetic QCL (KQCL) reaction kit (50-650U) and *E. coli* O55:B5 endotoxin (N185, Lonza, USA) were used as received.

5.3.2 Nanoparticle synthesis and sourcing. All dilutions and reconstitutions were performed in endotoxin-free water. All glassware and reaction-contacting equipment was depyrogenated by extended soaking (> 48 hours) in a 10% v/v HCl/ethanol bath and rinsing with endotoxin-free water. Gold nanoparticles were prepared by chloroauric acid (0.01%) reduction as described elsewhere.[32,33] Synthesized gold nanoparticles were sized by averaging the measurements of 120 particles on a TEM micrograph (University of Utah Imaging Core Facility) using ImageJ (NIH freeware, USA). Carboxylate-capped gold nanoparticles (20nm, part #11-20-100, Nanopartz, USA); carboxyl latex (polystyrene) nanoparticles (20nm, Invitrogen, USA); and silica

nanoparticles (SiNP, 50 nm, gift from Dr. H. Ghandehari, University of Utah, USA)[11,34] were used as received. See Table 5.1 for a summary of nanoparticle properties.

5.3.3 Inductively Coupled Plasma—Mass Spectrometry (ICP-MS). Gold content of sample solutions was assessed by heating sample aliquots in a small quantity of aqua regia (1:10 volume) held at boiling for at least 1 hour, and then evaporated to dryness and diluted with 5% aqua regia for analysis. Analyses were performed on an Agilent 7500ce, quadripole mass-spectrometer, using a quartz, double-pass spray chamber, PTFE nebulizer, quartz injector, and Ni cones with an Au standard solution (Inorganic Ventures) and Ir internal standard.

5.3.4 Kinetic Chromogenic Limulus Amoebocyte Lysate Assay (KQCL). All particle handling steps (dilutions, reconstitutions, and centrifugations) were performed in endotoxin-free water (Lonza) and polypropylene tubes (Eppendorf). Note: though LPS adsorbs to plastics more strongly than glass, it was necessary to use plastic for the centrifugation steps in this study, requiring all standards and samples to be handled in identical polypropylene tubes to minimize any tube-specific effect(s). Carboxylate-capped gold nanoparticles (AuNP, 20nm, Nanopartz, USA), tannic acid/citrate gold nanoparticles (5.2nm), commercial polystyrene nanoparticles (20nm), and silica nanoparticles (50nm) were centrifuged at 20.8k x g for 30 minutes, resuspended in graded concentrations (described below) of LPS (reconstituted from 1 $x10^6$ EU/ml

Table 5.1 Nanoparticle properties

NP type	Diameter (nm) †	ζ (mV)
AuNP (Nanopartz)	20 +/- 1.5 *	-30 *
AuNP (synthesized)	5.2 +/- 1.3	ND
SiNP	48.6 +/- 4.5 ‡	-61 +/- 8.6 ‡
PSNP	24 +/- 5 *	Negative ǂ

† measured by TEM
* vendor-supplied data
‡ ref [11]
ǂ vendor specifies 70 charges per particle

E. coli endotoxin (Lonza), and incubated overnight at room temperature. NP-containing samples were then serially centrifuged three times (20.8k x g or 40k x g, where specified, for 30 minutes) to remove the nanoparticles by aspirating and centrifuging just the supernatant each time, prior to LPS assay of the final supernatant by chromogenic LAL assay (KQCL). Three-step centrifugation was judged sufficient for NP removal due to the absence of any visible NP pellet at the end of the third centrifugation step. Samples (supernatants) were warmed to 37°C and the reconstituted KQCL assay reagent was added to final sample supernatants and standard aliquots in a 96-well plate. Data collection and analyses were performed according to manufacturer instructions. Briefly, addition of LAL chromogenic reagent to the plate initiated the assay and optical absorbance was read at 405nm on a microplate reader (BioTek Synergy 2) at 150-second intervals over a period of 97.5 minutes with continual incubation at 37°C. For each well, the reaction onset time (onset OD) was calculated as the time required for sample absorbance to increase 0.2 units from its baseline (t=0) value. Sample LPS content was calculated from the best data fit for the measured onset OD values of an LPS standard dilution series (log onset OD vs. log concentration) of log-order dilutions spanning 0.005-50 EU/ml). Limit-of-detection (LOD) values were calculated from endotoxin-free water blanks (n=8) as 3*SD of apparent LPS concentrations (determined from the linear correlation of onset OD vs. [LPS] data for the LPS standard series mentioned above).

In preliminary experiments, AuNPs were incubated (25°C) overnight in endotoxin-free water with a range of known, spiked LPS concentrations and analyzed by QCL-1000 endpoint and KQCL kinetic assays without nanoparticle removal prior to assay (*i.e.*, co-incubation of LAL assay reagents in the presence of the nanoparticles). Both assays were performed according to manufacturer instructions (25% v/v acetic acid (in endotoxin-free water) was utilized as the stop reagent in the QCL-1000 sample analysis).

5.3.5 Lipopolysaccharide-AuNP binding assessment by high-performance liquid chromatography. Gold nanoparticles (AuNP, 20nm, Nanopartz) were centrifuged at 20.8k x g for 30 minutes, resuspended in endotoxin-free water or LPS-containing solutions (prepared as described in KQCL method) and allowed to incubate at room temperature overnight. Solutions

were injected (10 μl) onto a Hypersil Gold C-18 column using an isocratic water: acetonitrile (95:5) mobile phase at a flow rate of 1 ml/min. Eluting peaks were detected optically at 210nm and 250 nm. Known concentrations of 1) LPS (analogous to KQCL assay standard solutions described above) without AuNPs and 2) pure AuNPs without addition of LPS were analyzed as control conditions.

5.4 Results

In preliminary experiments, AuNPs were spiked with known concentrations of LPS, incubated and assessed by both endpoint and kinetic versions of the chromogenic LAL assay, QCL-1000 and KQCL, respectively, all in the presence of AuNPs (*i.e.*, no precentrifugation to remove particles). Results of these experiments clearly demonstrated AuNP interference with assay quantification of LPS, evidenced by a consistent artifactual assay signal increase in the presence of AuNPs, but these data were highly variable, inconsistent and uninterpretable (data not shown). Specifically, these preliminary assay response data did not correlate to their corresponding known (spiked) LPS concentrations and the complexity of the optically derived signals from this mixed AuNP-LPS system precluded mechanistic interpretation or elucidation of the optical assay anomalies. Therefore, further studies were conducted to elucidate sources of observed NP assay interference.

5.4.1 Gold NPs interfere with KQCL-LAL LPS assay signal linearity. First, the well-known intrinsic AuNP plasmon optical absorption (data not shown)[35] directly interferes with the LAL assay optical read-out (assessed by 405nm optical density). Therefore, to minimize AuNP-based plasmonic spectral interference with the LAL assay, all succeeding nanoparticle-incubated samples were serially centrifuged three times to remove the NPs, and the KQCL analysis was then performed on the final centrifugal supernatant (vida infra). That is, NPs spiked with LPS were removed by centrifugation after incubation so that the KQCL LPS assay reagents and AuNPs were not present in the same assay solution simultaneously. Further, the kinetic form (KQCL) of the LAL assay was employed exclusively for this and all subsequent analyses because it utilizes an OD-based method of endotoxin quantification that excludes background sample absorbance. Thus, any plasmonic absorbance of residual AuNPs (a constant background

absorbance value) is intrinsically included in the initial assay absorbance reading and consequently subtracted out of subsequent signal-based increases in time point absorbance readings (assay signal). Importantly, no assay signal was observed for nanoparticles with chromogenic substrate alone (without any added LAL cascade factors, data not shown), excluding the possibility of signal generation by nonspecific AuNP interactions with the KQCL chromogenic substrate.

To assess nanoparticle interactions with LPS, log-order LPS concentrations (*i.e.*, assay standard concentration spikes) were quantified by KQCL assay both with and without prior incubation with AuNPs. Specifically, AuNPs were spiked and incubated with LPS concentrations ranging from 0.005-500 EU/ml, then serially centrifuged three times, with KQCL analysis performed on the final supernatant (Figure 5.1, filled circles). Assay responses to AuNP-incubated LPS solutions above 0.5 EU/ml LPS demonstrated a concentration-dependent

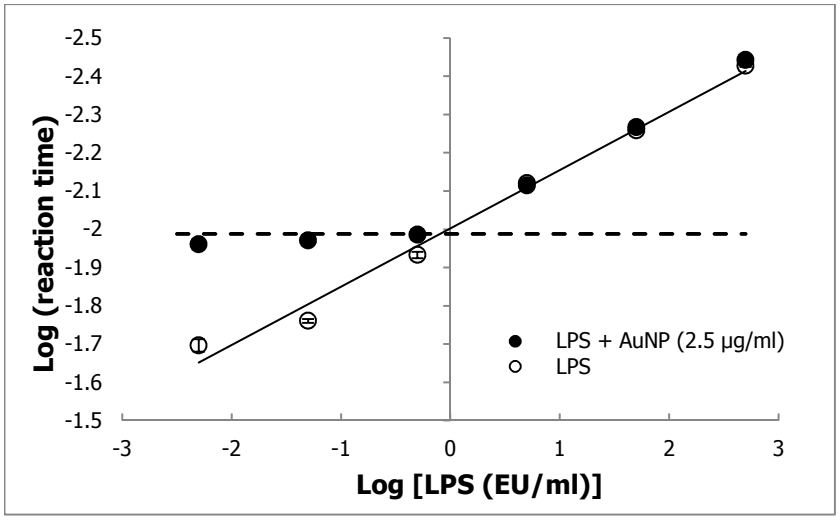

Figure 5.1 Gold nanoparticle interference of the KQCL kinetic LAL assay response to LPS spiked standards. Gold nanoparticle presence (filled circles) in LPS standards results in a loss of assay response-time fidelity at LPS concentrations below ≈1 EU/ml LPS (dotted line, log {reaction time} = -2). Nanoparticle-free samples demonstrate assay response linearity over six orders of magnitude in LPS concentration (open circles). Note: some error bars are smaller than the data point symbols, n=2 technical replicates.

response similar to that of the LPS standards at identical concentrations. However, AuNP-incubation with LPS standard solutions below ≈1 EU/ml LPS produced higher-than-expected assay responses that did not scale linearly with LPS concentration (Figure 5.1). This loss of linear KQCL response fidelity to LPS concentration (in the lower portion of the log-order concentration range) following incubation with AuNP suggests AuNP interference with the KQCL assay. The deviation is observed at lower LPS concentration as a flat response to increasing LPS presence, well above the calculated limit-of-detection of LPS under these conditions (LOD=0.001 EU/ml) (see Figure 5.1). Notably, and as expected, LPS assay standards (no NP added, open circles) exhibited a log-linear dependent assay response to LPS-spiked concentrations over 6 orders-of-magnitude (0.005-500 EU/ml, R^2=0.99), as expected for this assay.

Though AuNPs were centrifugally separated from the samples prior to assay, loss of assay linearity following AuNP incubation with LPS may be attributed to either direct AuNP interference (*i.e.*, spectral overlap with assay chromophores or adsorption of assay enzymes) or to a potential increase in LPS background introduced by contaminating LPS in the NP sample, given the ubiquitous nature of LPS contamination in laboratory environments and the lack of effective analytical surface detection and validation of depyrogenation methods. Therefore, various concentrations of AuNPs were next assayed without LPS spikes to determine the intrinsic influence of the AuNPs on the KQCL assay. These AuNP-containing samples produced KQCL assay responses increasing from 0.6 EU/ml for 2.5 μg/ml AuNP to 30.6 EU/ml for 250 μg/ml AuNP (see Figure 5.2). Superficially, these data could suggest possible background LPS contamination from added AuNPs that increases assay response directly with added AuNP mass loading, but this nonlinear, inverse relationship between AuNP concentration and mass AuNP-normalized LAL assay response shows only weak NP concentration dependence. While some minor level of background LPS contamination is probably NP-sourced, such AuNP-derived contamination alone cannot explain the observation that assayed LPS concentration does not scale directly with added AuNP concentration as it would in the event of LPS adsorbate (contaminant) shedding from nanoparticles. Rather, thes data more strongly support a hypothesis that direct physical LPS-NP interactions result in an over-reporting of actual LPS

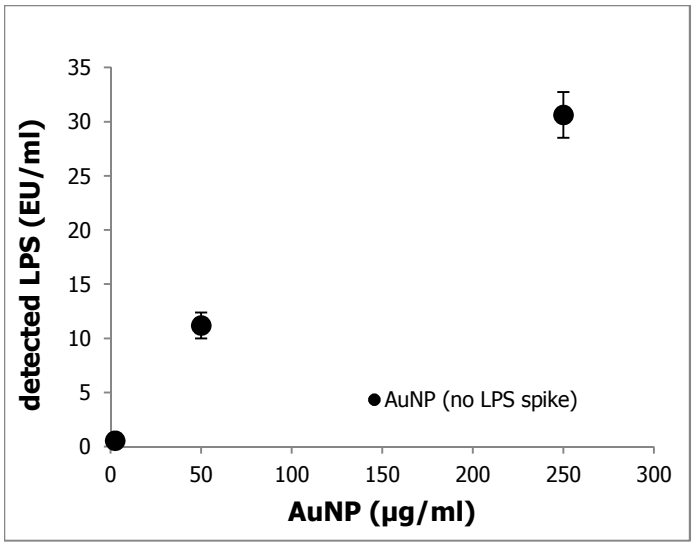

Figure 5.2 Intrinsic activity of added gold nanoparticles (NPTZ-sourced) in the KQCL assay (no LPS added). AuNP were assayed without LPS spike. A 100-fold increase in AuNP concentration resulted in a 60-fold increase in KQCL assay response (0.5-30.5 EU/ml) with no LPS present or added.

content. Further, these results were also observed to depend on the precipitation method (specific centrifugation force and/or addition of PBS) utilized for AuNP removal from these samples prior to their assay (Table 5.2). Table 5.2 shows a trend of decreasing KQCL response with increasing centrifugation, suggesting an exacerbated KQCL response with increasing residual NPs. However, though inductively coupled plasma mass spectrometry (ICP-MS) data did not show a correlation between residual gold content and assay response (data not shown), trace residual gold was detectable in all samples (not exceeding 200 ppb in any sample.

Next, a high concentration (50 EU/ml) of LPS was incubated with increasing concentrations of AuNPs to further assess the impact of AuNP-LPS interactions on KQCL assay independent of background LPS contamination introduced by the AuNPs. Thus, a 50 EU/ml LPS spike was utilized to dwarf any background contamination (e.g., 50 EU/ml LPS spike vs. ≤0.014 EU/ml LPS contamination in endotoxin-free water incubated with AuNPs, see Table 5.2 and Figure 5.2). Following incubation with 250 µg/ml AuNPs, the detected LPS (KQCL response) was three times the spiked LPS amount and double the response observed for an equivalent LPS spike incubated

Table 5.2 KQCL assay of LPS response depends on incubated AuNP (NPTZ-sourced) concentration and centrifugation conditions utilized for AuNP removal.

	Centrifugation force applied, serial supernatant spins			
AuNP amounts	20.8k x g (5, 90-min each) + PBS (no Ca^{2+}/Mg^{2+})		45k x g (3, 30-min each)	
µg/ml	EU/ml	EU/mg	EU/ml	EU/mg
2.5	0.047	0.019	0.566	0.226
50	0.445	0.009	11.189	0.224
250	0.873	0.003	30.621	0.122

with only 2.5 µg/ml AuNPs (shown in Figure 5.3). Moreover, AuNP mass-normalization of the KQCL assay responses revealed that only a small amount of AuNPs (≤ 2.5 µg/ml) were necessary to generate a KQCL response magnification, and that additional AuNP amounts yielded only marginal further increases in assay response with respect to incubated AuNP concentrations (Figure 5.3B). These results demonstrate that AuNP incubation with LPS drastically alters the KQCL response in comparison to native LPS detection and confounds the assessment of LPS content in AuNP-contacting solutions despite AuNP removal by centrifugation prior to assay. Importantly, since these samples were serially centrifuged three times before KQCL analysis of the supernatant, this result confirms the loss of KQCL assay fidelity in the presence of potentially miniscule AuNP quantities (<200 ppb).

Results in Figures 5.1-5.3 were performed using the same commercial source and type of gold nanoparticles (Nanopartz) and the data implied slight (<0.5 EU/mg) NP-sourced background LPS contamination. To minimize any possible response from background LPS contamination and also assess particle sourcing dependence on assay response, further studies were replicated using gold nanoparticles with minimal surface functionalization (*i.e.*, citrate/tannic acid-reduced gold particles, d=5.6 nm), produced using depyrogenated synthesis glassware, equipment and certified USP endotoxin-free water. These measures were taken to eliminate background LPS

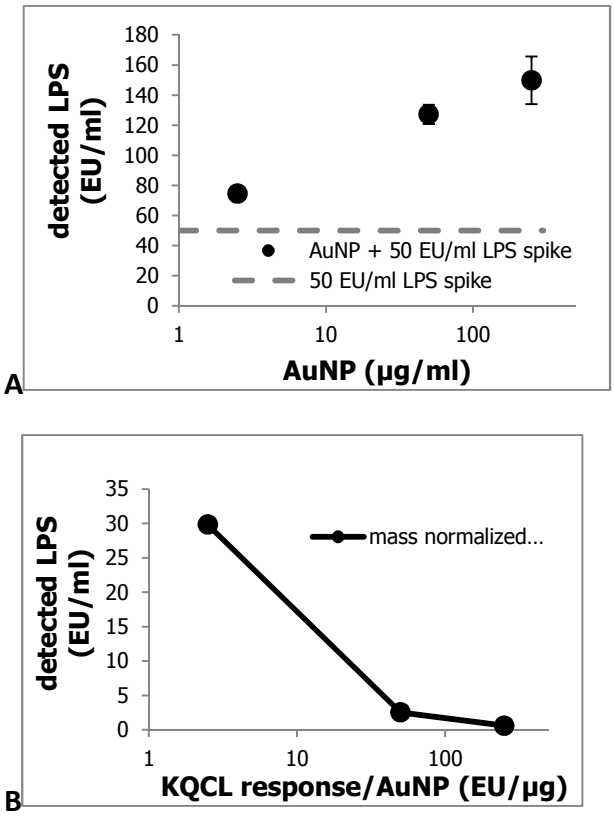

Figure 5.3 Commercial gold nanoparticles (NPTZ-sourced) magnify the LAL assay response in a high-concentration LPS solution. (A) The LAL assay response to an identical LPS spike (50 EU/ml, dotted line) doubles over three orders of magnitude of added, incubated AuNP concentrations (2.5-250 µg/ml). (B) AuNP concentration normalization of the KQCL assay data reveals that the LAL assay response magnification decreases with increasing AuNP concentration.

and any ligand effects arising from the commercial nanoparticles. In a procedure similar to that producing Figure 5.3 data, the AuNPs resulting from this reaction were incubated with a spike of 50 EU/ml LPS, then removed by serial (three times) centrifugation. Following AuNP removal, these LPS-spiked solutions produced elevated KQCL responses that were related to AuNP concentration, starting at a 390 EU/ml assay response for the lowest Au nanoparticle concentration (2.5 ug/ml) and increasing to assay responses exceeding 500 EU/ml for higher AuNP concentrations (25 and 250 µg/ml, Figure 5.4). Significantly, incubation of citrate/tannic

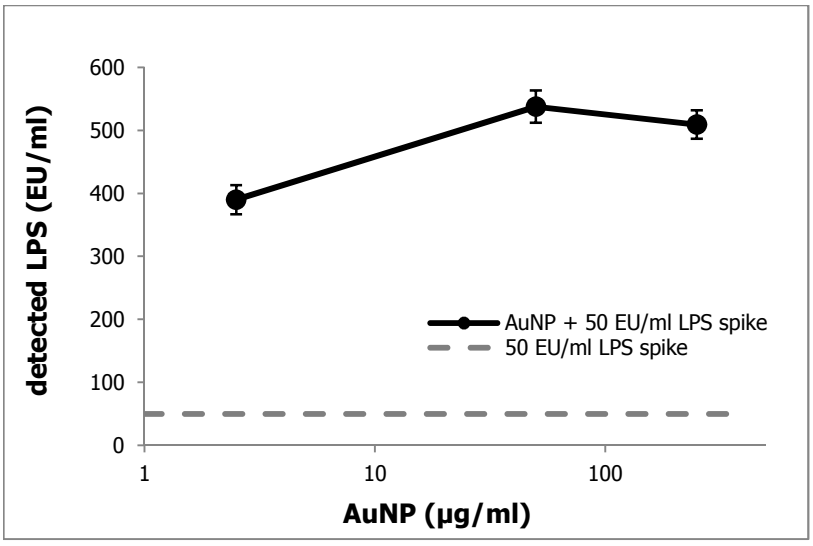

Figure 5.4 Citrate/tannic acid-reduced AuNPs amplify the KQCL LAL assay response. Incubation of citrate/tannic acid-stabilized gold nanoparticles with LPS resulted in highly amplified LAL assay responses to a constant 50 EU/ml LPS spike. These responses were observed to increase and plateau with increased incubated AuNP concentration.

acid-stabilized AuNPs with LPS before KQCL reagent addition and assessment amplified the KQCL assay response analogous to the assay results obtained following LPS incubation with the commercially sourced, AuNP (shown in Figure 5.4). Notably, for this gold nanoparticle chemistry, an unspiked (no LPS) nanoparticle-only sample control (50 µg/ml AuNP) produced a response of only 0.01 EU/mL in the KQCL assay (Table 5.3). These results demonstrate that, unlike the commercial AuNP source used in Figures 5.1-5.3, the in-house synthesized AuNPs are ostensibly "clean" and minimally interact with the assay in the absence of LPS. Between the results from these disparate AuNP types, the confirmation of trend and effect of AuNP on the KQCL assay response supports the conclusion that the AuNP themselves are responsible for the observed KQCL assay response amplification, rather than the direct effect of some sort of proprietary additive in the commercial AuNPs (e.g., exogenous steric or electrostatic colloidal stabilizer) or shedding of NP-contaminating LPS.

5.4.2 Influence of tetrachloroaurate anion on LPS assay. As gold nanoparticles are routinely produced by reduction of gold acid salt, tetrachloroauric acid ($HAuCl_4$), to zero

Table 5.3 KQCL responses to synthesized citrate/tannic acid gold, silica, and polystyrene nanoparticles resuspended in endotoxin-free water compared to $AuCl_4^{(-)}$-spiked solution.*

Particle/material type	AuNP	SiNP	PSNP	$AuCl_4^-$
Material concentration (μg/ml)	50	50	40	0.069
LPS detected (EU/ml)	0.014	0.004	0.014	0.002

*LOD = 0.001 EU/ml, lowest LPS standard = 0.005 EU/ml

valent Au metal, the potential exists for trace amounts of $HAuCl_4$ to remain in solution as AuCl4- anions following salt reduction to AuNP. Additionally, any shedding of Au^{3+} ions from AuNP surfaces into the surrounding solution would rapidly produce $AuCl_4^-$, the most stable, aqueous-soluble species of gold.[36] Thus, possible effects of residual or NP-shed $AuCl_4^-$(aq) anion interactions with the KQCL LPS assay were assessed in LPS-spiked $AuCl_4^-$ ion solutions. Added $AuCl_4^-$ concentrations were assumed as a generous upper-bound, representing a 1% portion of reactant $AuCl_4^-$ ion remaining in solution following reductive generation of AuNP. Since $AuCl_4^-$ anion is the conjugate base of the starting material used to produce these samples, pH was verified within pH=6-8 (stated KQCL assay guidelines) to avoid secondary acid-base interference. KQCL assay response to the $AuCl_4^-$ anion solution without LPS spike was below the LOD, 0.001 EU/ml, demonstrating a pyrogen-free precursor salt material without detectable colorimetric interaction with the KQCL assay (Table 5.3). Additionally, KQCL assay responses to a uniform 25 EU/ml LPS spiked concentration remained steady between 25-30 EU/ml in the presence of added $AuCl_4^-$ anion over a broad concentration range of 0.345-345 ng/ml $AuCl_4^-$ (Figure 5.5). This result sharply contrasts the KQCL assay response amplifications observed for both AuNP types reported in Figures 5.1-5.4 and demonstrates that $AuCl_4^-$ anion does not contribute significantly to KQCL assay response amplification following AuNP-LPS incubation.

5.4.3 Effect of soluble divalent cations (DPBS). Because of its amphiphilic character, LPS self-associates in aqueous solution by forming micelles and aggregates.[37,38] LPS intermolecular interactions are strengthened in the presence of divalent cations such as Ca^{2+} and Mg^{2+} that serve to bridge anionic phosphate groups on adjacent LPS molecule glycan domains.[37] To assess the effects of the AuNP-LPS interaction on LPS self-association, LPS assay standards (0.005-500 EU/ml) were assayed by KQCL in the presence of DPBS (140mM, containing 0.9/0.5

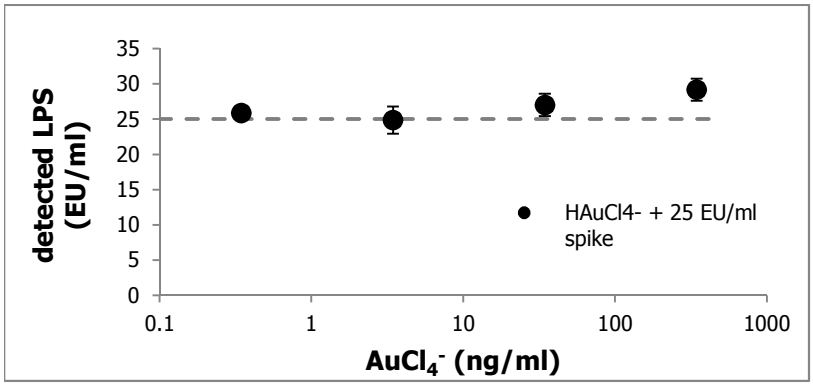

Figure 5.5 Gold anion ($AuCl_4^-$) additions and KQCL assay response. KQCL assay response to a uniform LPS spike of 25 EU/ml was not significantly altered by the presence of added $AuCl_4^-$ anion over 4 orders of magnitude in concentration.

mM Ca^{2+}/Mg^{2+}), both with and without AuNP incubations to further elucidate AuNP effect on LPS solution-phase aggregation. In the absence of AuNPs, the divalent cations of DPBS promoted intermolecular LPS interactions that blocked all KQCL assay responses to LPS concentrations ≤ 5 EU/ml as shown in Figure 5.6. Moreover, in the absence of any AuNP exposure, this divalent cation-mediated assay response inhibition in DPBS continued indefinitely and was noted as the absence of visual assay chromogenic activity (*i.e.*, yellow color) through 72 hours of assay observation (data not shown). However, incubation of 50μg/ml AuNPs (commercial, Nanopartz) in these DPBS-containing LPS concentrations restores nonzero KQCL assay responses for all LPS standards (0.005-50 EU/ml). Additionally, direct AuNP interference with KQCL was confirmed, as the actual LPS concentration fidelity of the assay was not restored by addition of AuNPs, with no substantial changes in KQCL assay response to log-order reductions in LPS concentration ≤ 5 EU/ml (Figure 5.6), similar to DPBS-free observations (Figure 5.1). This result suggests that AuNP-LPS interactions may be strong enough to disrupt self-association of solute LPS, possibly via disrupting LPS-cation (e.g., Ca^{2+}/Mg^{2+}) bridging interactions and LPS surface adsorption. Additionally, this result further confirms direct AuNP interference with the KQCL assay, resulting in loss of assay fidelity, especially for the lower LPS concentration range, ≤ 5 EU/ml.

5.4.4 Other nanoparticle chemistries influence LAL assays. Since AuNPs clearly influence the KQCL-based assay response to endotoxin, other nanoparticle types were selected based on

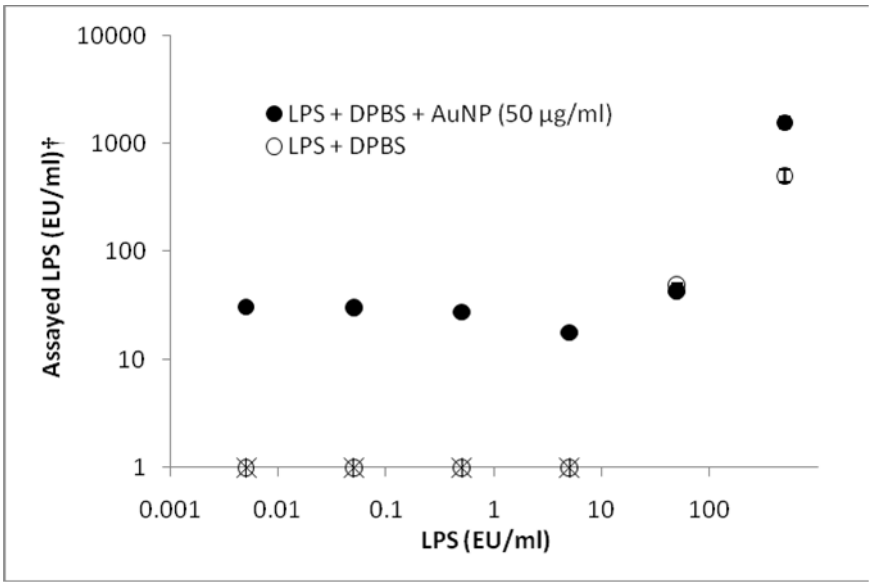

Figure 5.6 Gold nanoparticle effects on the KQCL assay of LPS in the presence of cation-containing DPBS buffer. Presence of 140mM DPBS completely inhibited the KQCL assay color generation for spiked LPS (≤ 5 EU/ml, star symbols). This inhibition was overcome by incubating with added AuNP (50 µg/ml, Nanopartz), but assay fidelity to LPS concentration was not restored. †Assayed LPS values are normalized to nonzero DPBS responses.

their lack of optical activity in the region of KQCL detection (405 nm absorbance). Specifically, silica and polystyrene nanoparticle effects were assessed using methods identical to the AuNP-based KQCL experiments already discussed. Similar to AuNP-influenced results (e.g., Figures 5.3A and 5.4), a 50 EU/ml LPS spike produced higher-than-spiked KQCL responses of 332 and 461 EU/ml following incubation with 2.5 and 250 µg/ml SiNP, respectively (Figure 5.7). Notably, the KQCL assay response to SiNP supernatant alone (50 µg/ml, no LPS spike) was below the assay LOD (0.001 EU/ml), demonstrating an ostensibly clean SiNP lot. Importantly, these results and the combined AuNP results support a synergistic effect that NPs exert only in the presence of LPS.

In contrast, analogous incubations of polystyrene nanoparticle (PSNP) in 25 EU/ml LPS produced a trend opposing that observed for both AuNP- and SiNP-based assays (shown in Figures 5.3A, 5.4 and 5.7). LPS incubation with increasing concentrations of PSNPs (1.5, 15, and 150 µg/ml) decreased assay responses (to 24.8, 9.7, and 0.6 EU/ml, respectively) all of

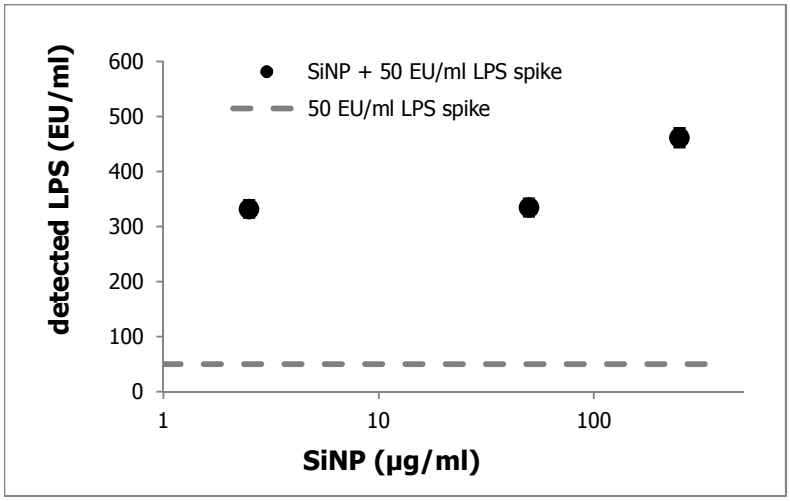

Figure 5.7 Effects of added silica nanoparticles (SiNP) on the KQCL assay response. The KQCL produced amplified assay responses to LPS (50 EU/ml spike, dotted line) following LPS incubation with SiNP.

which registered below the (constant) spiked LPS amount of 25 EU/ml (Figure 5.8). KQCL assay of unspiked PSNP was below the assay LOD (0.001 EU/ml).

The discrepancies between KQCL assay results for LPS-spiked samples of different nanoparticle types and concentrations (both with and without possible interfering intrinsic optical activity) suggest that physical NP-LPS interactions alter KQCL reporting. This is supported by the lack of baseline perturbation in KQCL assays of all assayed NPs alone without spiked LPS, and also for AuNPs incubated with the KQCL chromogenic substrate alone (peptide-nitrophenyl ester) without the required LAL zymogens present (data not shown).

Finally, LPS incubation with AuNPs or SiNPs also appears to increase the KQCL assay reaction rate, evidenced by a shift to the left (*i.e.*, shorter time) in the KQCL absorbance vs. time rate curves, corresponding to increasing amounts of added, incubated AuNPs (see Figure 5.8). Notably, the final assay absorbance values are very similar regardless of NP incubation time or NP amounts, suggesting that these NPs do not change the assay's final reaction end product chromophore concentrations, but instead change the rate of signal production. Since the KQCL assay is kinetic (rate dependent) by design,[39] this result strongly implicates a catalyst-like interference activity for AuNPs and SiNPs in the KQCL reaction cascade. However, confirming

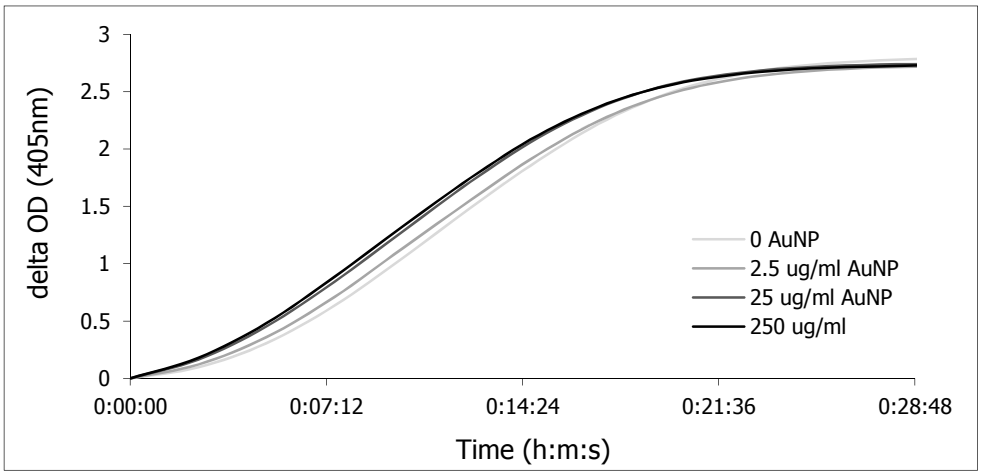

Figure 5.8 AuNPs increase the rate of KQCL chromophore generation to a 50 EU/ml LPS spike. Increasing incubated AuNP concentrations increased the rate of KQCL assay response to equivalent 50 EU/ml LPS spikes as demonstrated by a left-ward shift in the assay absorbance vs. time curves.

this particular interpretation is confounded by the procedural necessity of first removing nanoparticles from samples by serial centrifugation before addition of the chromogenic substratefor KQCL assessment of samples. Significantly, greater KQCL response amplification was observed with NPs remaining in the samples than with centrifugally separated nanoparticle samples, as noted in Figures 5.3, 5.4 and 5.7). This supports the mechanistic concept that direct NP-LPS interactions are central to assay perturbations.

5.5 Discussion

Findings described in this study demonstrate that LPS association with solid nanoparticles fundamentally alters chromogenic LPS assay results. The KQCL assay is based on the rate of end product chromaphore production (*i.e.*, enzymatic cleavage of a peptide substrate nitophenyl ester to produce the optically active *p*-nitrophenyl aniline in solution) in proportion to activation by LPS. In this assay, LPS initiates the autocatalytic activation of Factor C and with it the *L. polyphemus*-derived biochemical cascade which proceeds through Factor B and clotting enzyme to the release of *p*-nitroaniline (yellow chromaphore) from a colorless peptide substrate.[40,41] The data presented herein support two distinct KQCL assay outcomes arising from the proposed solution-phase NP-LPS interaction. The PSNP concentration-dependent decrease in KQCL

assay responses to a uniform LPS spike (Figure 5.8) appears to have a straightforward interpretation. LPS is depleted from solution by adsorption to PSNPs that are then centrifugally separated from the solution. However, analogous assays of fixed-spike LPS concentrations incubated with increasing AuNP and SiNP concentrations resulted in drastically and artificially elevated KQCL assay responses (Figures 5.3, 5.4, and 5.7) that are more difficult to interpret consistently with this explanation. Additionally, divalent cations inhibited KQCL reporting of LPS alone, but not in solution phases incubated with AuNPs (centrifugally removed before LPS assay, Figure 5.6). These results, along with HPLC partitioning retention time assays showing co-elution of LPS and LPS-exposed NPs strongly support AuNP adsorption of LPS. Nonetheless, the anomalous amplification of KQCL assay responses to LPS observed following initial nanoparticle-LPS incubation and subsequent particle removal from the solution (*i.e.*, NP removal by serial centrifugation prior to KQCL reagent addition and assay) confound a simple single mechanistic explanation. That the KQCL assay response alteration is not attributable to residual ionic and colorimetric species is evident from controls, supported both by the observed kinetic stability of the assay in the presence of $AuCl_4^-$ anion addition (Figure 5.5) and by the minimal KQCL responses to endotoxin-free water incubated with each nanoparticle type alone (Table 5.2). However, NP-LPS synergy is such that even trace amounts of residual NP in samples produce exaggerated KQCL responses to LPS, while large amounts of NP in samples produce unintelligible KQCL responses. Additionally, centrifugal NP removal from the samples before KQCL analysis minimizes direct NP interference with the assay components, *i.e.*, via competitive spectral absorption interference or assay reagent-NP adsorption.

These distinct effects of PSNP from both AuNP and SiNP on the LAL assay response are interesting, but also without mechanistic explanation. Though carboxylated to maintain some electrostatic stability in media (*i.e.*, zeta potential is ≈ -42 mV in pH=7.5, 0.15 M NaCl),[42] PSNP are the most hydrophobic of the three nanoparticles studied.[43,44] We propose that LPS adsorption to nanoparticles results in assay perturbations that distort the fidelity of the KQCL assay following NP exposure. The attenuation of KQCL response to LPS spikes in the presence of PSNP may arise from irreversible hydrophobic interactions between LPS lipid-A regions and exposed

hydrophobic surface domains on PSNP. Factor C, the LAL "biosensor" enzyme for LPS, is activated by interaction with lipid-A. Moreover, two domains of Factor C are known to interact cooperatively with LPS, [41] and LPS may concurrently engage more than one Factor C molecule.[45] Thus, lipid-A mediated adsorption of LPS to a hydrophobic surface (*i.e.*, PSNP) may inhibit cooperative binding of multiple Factor C regions or molecules to lipid A through NP association with lipid A and thus slow the kinetics of the Factor C-initiated response to LPS. In contrast, the KQCL-amplifying effects of SiNP or AuNP incubated with LPS suggest an improved presentation or stabilization of lipid A to yield more favorable interactions with Factor C and higher enzyme catalytic turnover, increasing the assay signal artifactually. However, a basis for AuNP/SiNP interactions with LPS is unknown and the mechanism of such assay over-response remains elusive.

Experiments to effectively test this hypothesis for NP-induced alteration of LPS conformation or LPS-Factor C interactions in the assay are currently stymied by a lack of specific molecular or interfacial hypothetical bases by which NP-LPS interactions alter LPS-Factor C interactions or Factor C function. Moreover, since the assay response amplification is observed for LPS incubated with NPs, even following their removal from the assay by centrifugation prior to reagent additions, may indicate that any AuNP- or SiNP- LPS associations are transient. Moreover, given the NP centrifugation step, it is also possible that some LPS is removed as NP adsorbate, meaning that the amplified KQCL responses observed are ultimately an under-representation of the actual NP interference phenomenon. This is supported by further-amplified KQCL answers to NP-incubated LPS spikes not centrifuged before LPS assay assessment (data not shown). However, experimental scenarios to adequately test these hypotheses are difficult because little is known concerning the molecular basis for hydrophobic Factor C-lipid A interactions in the presence of NPs.

5.6 Conclusions

In conclusion, this study shows a variety of nanoparticle interactions with the gram-negative endotoxin, LPS, in a variety of aqueous solutions that confound its precise detection using a common colorimetric version of the standard LAL assay for LPS. This assay interference by NPs

is of serious concern due to the known regulatory vigilance to certify and report endotoxin contents in medical devices and drugs,[7] the increasing application of nanoparticles in medicine, and the ubiquitous endotoxin contamination of laboratory reagents, glassware and synthetically prepared nanomaterials. The resulting potential adverse consequences for under-reporting LPS contamination on both commercial and investigational nanomaterials that enter biological test systems or *in vivo* applications are substantial. This problem is compounded by the lack of routine surface analysis results reported for most nanomaterials in biomedical applications, and the technical difficulty of performing adequate, sensitive, surface characterization of nanomaterials.[6,8] Of possibly greater concern is the present observation of a significant nanoparticle potential to amplify the KQCL assay response, particularly as a harbinger for enhanced immunologic and inflammatory responses *in vivo* through precisely the same biochemical, positive feedback pathways that this assay uses for its signal generation. Thus, this same adsorption phenomenon (yielding LPS-contaminated NPs) could possibly elicit host endotoxic responses *in vivo* that are distinct from those arising toward either endotoxin or nanoparticles alone.

Nanomaterial-based LPS adsorption was demonstrated for three distinct, but commonly studied NP chemistries (gold, silica, and polystyrene). However, potential alteration of biological and assay responses to LPS may extend more generally to a diverse variety of other nanoparticles. Thus, future efforts should seek to: 1. elucidate a mechanistic basis for these anomalous chromogenic assay results; 2. identify alternative methods to better quantify LPS on nanoparticle surfaces; and 3. address potentially serious biological risks of unreliable LPS assay in NP to improve both the safety and efficacy of nano-enabled biomaterials and theranostic formulations *in vivo*.

5.7 References

1. Salata O. Applications of nanoparticles in biology and medicine. *J Nanobiotechnology.* 2004;2:3.

2. Burgess R. Medical applications of nanoparticles and nanomaterials. *Studies in Health Technology and Informatics.* 2009;149:257-283.

3. Tiwari R, Takhistov P. Nanotechnology-Enabled Delivery Systems for Food Functionalization and Fortification. *Nanotechnology Research Methods for Foods and Bioproducts*: Wiley-Blackwell Pub.; 2012:55-101.

4. Bolzinger M-A, Briançon S, Chevalier Y. Nanoparticles through the skin: managing conflicting results of inorganic and organic particles in cosmetics and pharmaceutics. *Wiley Interdisciplinary Reviews: Nanomedicine and Nanobiotechnology.* 2011;3:463-478.

5. Jones CF, Castner DG, Grainger DW. Surface adsorbates on nanomaterials and their possible roles in host inflammatory and toxicological processing. In: Dobrovolskaia MA, McNeil SE, eds. *Handbook of Immunological Properties of Engineering Nanomaterials*. Singapore: World Scientific Pub Co Inc; 2013.

6. Jones CF, Grainger DW. In vitro assessments of nanomaterial toxicity. *Adv Drug Deliv Rev.* 2009;61:438-456.

7. Guidance for Industry: Pyrogen and Endotoxins Testing: Questions and Answers. In: Services USDoH, Human, eds. Rockville, MD: Food and Drug Administration; 2012.

8. Vallhov H, Qin J, Johansson SM, et al. The importance of an endotoxin-free environment during the production of nanoparticles used in medical applications. *Nano Lett.* 2006;6:1682-1686.

9. Zolnik BS, González-Fernández A, Sadrieh N, Dobrovolskaia MA. Nanoparticles and the immune system. *Endocrinology.* 2010;151:458-465.

10. Dobrovolskaia MA, McNeil SE. Immunological properties of engineered nanomaterials. *Nat Nano.* 2007;2:469-478.

11. Greish K, Thiagarajan G, Herd H, et al. Size and surface charge significantly influence the toxicity of silica and dendritic nanoparticles. *Nanotoxicology.* 2011.

12. Jones CF, Campbell RA, Franks Z, et al. Cationic PAMAM dendrimers disrupt key platelet functions. *Mol Pharm.* 2012;9:1599-1611.

13. Buzea C, Pacheco, II, Robbie K. Nanomaterials and nanoparticles: sources and toxicity. *Biointerphases.* 2007;2:MR17-71.

14. Grainger DW, Castner D. Nanobiomaterials and nanoanalysis: opportunities for improving the science to benefit biomedical technologies. *Adv Mater.* 2008;20:867-877.

15. Waters KM, Masiello LM, Zangar RC, et al. Macrophage responses to silica nanoparticles are highly conserved across particle sizes. *Toxicol Sci.* 2009;107:553-569.

16. Baer DR, Engelhard MH, Gaspar DJ, et al. Challenges in applying surface analysis methods to nanoparticles and nanostructured materials. *J. Surf. Anal.* 2005;12:101-108.

17. França R, Zhang XF, Veres T, Yahia L, Sacher E. Core-shell nanoparticles as prodrugs: possible cytotoxicological and biomedical impacts of batch-to-batch inconsistencies. *J Colloid Interface Sci.* 2013;389:292-297.

18. Kroll A, Pillukat MH, Hahn D, Schnekenburger J. Current in vitro methods in nanoparticle risk assessment: limitations and challenges. *Eur J Pharm Biopharm.* 2009;72:370-377.

19. Chamberlain LM, Godek ML, Gonzalez-Juarrero M, Grainger DW. Phenotypic non-equivalence of murine (monocyte-) macrophage cells in biomaterial and inflammatory models. *Journal of Biomedical Materials Research - Part A.* 2009;88:858-871.

20. Holt DJ, Grainger DW. Senescence and quiescence induced compromised function in cultured macrophages. *Biomaterials.* 2012;33:7497-7507.

21. Aurell CA, Wistrom AO. Critical aggregation concentrations of gram-negative bacterial lipopolysaccharides (LPS). *Biochemical and Biophysical Research Communications.* 1998;253:119-123.

22. Santos NC, Silva AC, Castanho MA, Martins-Silva J, Saldanha C. Evaluation of lipopolysaccharide aggregation by light scattering spectroscopy. *Chembiochem: A European Journal of Chemical Biology.* 2003;4:96-100.

23. Gorbet MB, Sefton MV. Endotoxin: the uninvited guest. *Biomaterials.* 2005;26:6811-6817.

24. Dobrovolskaia MA, Aggarwal P, Hall JB, McNeil SE. Preclinical studies to understand nanoparticle interaction with the immune system and its potential effects on nanoparticle biodistribution. *Mol Pharm.* 2008;5:487-495.

25. Levin J, Bang FB. The role of endotoxin in the extracellular coagulation of limulus blood. *Bulletin of the Johns Hopkins Hospital.* 1964;115:265-274.

26. Novitsky TJ, Roslansky PF. Quantification of endotoxin inhibition in serum and plasma using a turbidimetric LAL assay. *Progress in Clinical and Biological Research.* 1985;189:181-196.

27. Tsuji K, Martin PA, Bussey DM. Automation of chromogenic substrate limulus amebocyte lysate assay method for endotoxin by robotic system. *Applied and Environmental Microbiology.* 1984;48:550-555.

28. Dobrovolskaia MA, Germolec DR, Weaver JL. Evaluation of nanoparticle immunotoxicity. *Nat Nanotechnol.* 2009;4:411-414.

29. Inoue K-i, Takano H. Facilitating effects of nanoparticles/materials on sensitive immune-related lung disorders. *J. Nanomaterials.* 2011;2011:1-6.

30. Hussain S, Al-Nsour F, Rice AB, et al. Cerium dioxide nanoparticles do not modulate the lipopolysaccharide-induced inflammatory response in human monocytes. *Int J Nanomedicine.* 2012;7:1387-1397.

31. Himmelreich G, Jochum M, Bechstein WO, et al. Mediators of leukocyte activation play a role in disseminated intravascular coagulation during orthotopic liver transplantation. *Transplantation.* 1994;57:354-358.

32. Frens G. Controlled nucleation for the regulation of the particle size in monodisperse gold suspensions. *Nature Phys Sci.* 1973;241:20-22.

33. Jiang S. Recipe for Au nanoparticles. http://web.mit.edu/sjiang2/www/Resources/Gold%20nanoparticle.pdf. Accessed March 10, 2011.

34. Yu T, Malugin A, Ghandehari H. Impact of silica nanoparticle design on cellular toxicity and hemolytic activity. *ACS Nano.* 2011;5:5717-5728.

35. Eustis S, El-Sayed MA. Why gold nanoparticles are more precious than pretty gold: noble metal surface plasmon resonance and its enhancement of the radiative and nonradiative properties of nanocrystals of different shapes. *Chemical Society Reviews.* 2006;35:209-217.

36. Cotton S. Gold and Silver. *Chemistry of precious metals*. London; New York: Blackie Academic & Professional, Edition: 1st ed.; 1997:273-327.

37. Petsch D, Anspach FB. Endotoxin removal from protein solutions. *Journal of Biotechnology.* 2000;76:97-119.

38. Li Y, Pham JQ, Johnston KP, Green PF. Contact angle of water on polystyrene thin films: effects of CO2 environment and film thickness. *Langmuir.* 2007;23:9785-9793.

39. Williams KL. *Endotoxins: Pyrogens, LAL Testing and Depyrogenation.* 3 ed. New York: Informa Healthcare, Edition: 3rd ed.; 2007.

40. Gorny RL, Douwes J, Versloot P, Heederik D, Dutkiewicz J. Application of the classic Limulus test and the quantitative kinetic chromogenic LAL method for evaluation of endotoxin concentration in indoor air. *Annals of Agricultural and Environmental Medicine: AAEM.* 1999;6:45-51.

41. Tan NS, Ng ML, Yau YH, Chong PK, Ho B, Ding JL. Definition of endotoxin binding sites in horseshoe crab factor C recombinant sushi proteins and neutralization of endotoxin by sushi peptides. *FASEB J.* 2000;14:1801-1813.

42. Lundqvist M, Stigler J, Elia G, Lynch I, Cedervall T, Dawson KA. Nanoparticle size and surface properties determine the protein corona with possible implications for biological impacts. *Proc Natl Acad Sci.* 2008;105:14265-14270.

43. Vinogradova OI, Yakubov GE, Butt H-J. Forces between polystyrene surfaces in water--electrolyte solutions: long-range attraction of two types? *The Journal of Chemical Physics.* 2001;114:8124-8131.

44. Thormann E, Simonsen AC, Hansen PL, Mouritsen OG. Interactions between a polystyrene particle and hydrophilic and hydrophobic surfaces in aqueous solutions. *Langmuir.* 2008;24:7278-7284.

45. Li P, Sun M, Wohland T, Ho B, Ding JL. The molecular mechanism of interaction between sushi peptide and Pseudomonas endotoxin. *Cellular & Molecular Immunology.* 2006;3:21-28.

CHAPTER 6

CONCLUSIONS AND FUTURE WORK

6.1 Conclusions

This dissertation describes assessment of specific well-known nanoparticles for unintended effects and toxicological complications within hemostatic systems. Cationic generation-7 poly (amido amine) (PAMAM) dendrimers (G7-NH_2) were demonstrated to affect every major platelet function, including induction of procoagulant signaling, thrombin generation (inhibition), and morphological alteration for platelet aggregation and adhesion. These G7-NH_2 dendrimers were also demonstrated to alter not only platelet-supported thrombin generation, but also fibrinogen and blood protein aggregation through molecular interactions, providing a plausible basis for extensive coagulopathic outcomes observed in animal models. In the biochemical LAL assay cascade (based on the LPS-initiated, *Limulus* coagulation cascade), AuNP and SiNP were demonstrated to increase LAL assay response to LPS. Together, the studies of this dissertation specifically demonstrate the reactivity of nanoparticles in hemostatic systems and further, illustrate the potential for nanoparticles to disturb a variety of complex biological cascades and processes.

6.1.1 Amine-terminated generation-7 dendrimers are highly activating toward platelets. The increasing use of nanoparticles in intravenous drug delivery design presents a corresponding need for suitable assessment of specific nanoparticle impact on blood hemostasis and coagulation function. Amine-terminated generation-7 (G7-NH_2) PAMAM dendrimers were employed as a model nanoparticle to build an *in vitro* toolkit to assess nanoparticle coagulation-relevant properties and relate them to observed *in vivo* procoagulant functions. G7-NH_2 dendrimers were applied to platelets in concentrations corresponding to dendrimer doses observed to be hemostatic when administered intravenously to rodents.[1] Platelet assays

employed encompassed all major functions of platelets following exposure to nanoparticles (G7-NH_2) and included flow cytometry-based assessment of adhesion molecule expression, microscopy-based visualization of platelet morphology, impedance/absorbance-based measurement of aggregation, ELISA-based quantitation of platelet secretions, fluorogenic-substrate-based assessment of thrombin generation, and shear flow-based assessment of platelet adhesion. Platelets were found to be highly activated by cationic dendrimers resulting in strong expression of platelet adhesion molecule P-selectin and platelet-released inflammatory molecules RANTES and PF-4, unconventional aggregation, morphological alteration, and adhesion phenotypes, along with inhibition of thrombin generation. In light of previous reports of extensive, cationic dendrimer-induced coagulopathy, attenuation of thrombin generation was a surprising, unusual result. However, since thrombin generation depends upon platelet membrane phosphatidyl serine exposure for the assembly of the prothombinase complex, the extensive alteration of platelet membranes could also produce a loss of thrombin generation capacity. The basis of the observed morphological alterations should be further explored through examination of dendrimer interactions with the platelet cytoskeleton.

6.1.2 G7-NH_2 aggregate blood proteins. The new mechanism presented here for G7-NH_2 procoagulant activity was used to explain the apparent contradiction between the disparate G7-NH_2 effects of *in vivo* hemostasis and *in vitro* attenuation of thrombin generation. G7-NH_2 were assessed for their fundamental interactions with the key endpoints of the coagulation cascade, thrombin and fibrinogen, and further evaluated for their broader activity toward other plasma proteins. In agreement with the above findings of decreased thrombin generation, coagulation in platelet poor plasma was attenuated by G7-NH_2. Moreover, in a simplified version of coagulation containing only thrombin and fibrinogen, G7-NH_2 were shown to increase the rate of coagulation and produce morphologically dense reaction products with fibrinogen, irrespective of thrombin presence/absence in the milieu. This result is remarkable since traditional clotting requires the thrombin-mediated cleavage of fibrinogen. Further examination of the products of this fibrinogen-dendrimer interaction revealed that aggregates were rapidly being formed with G7-NH_2 and, not only with fibrinogen, but also with the most abundant plasma protein, albumin. Notably, these two

blood proteins both present densely anionic surface domains and this surface charge trend was further confirmed with the finding that G7-NH_2 did not produce aggregates with a cationic plasma protein, protamine. Thus, it was hypothesized that cationic dendrimers aggregate fibrinogen and albumin *via* cationic electrostatic interactions with the anionic protein domains, and that this mechanism may extend to include a wide range of plasma proteins possessing negative charge domains. In coagulation assays *in vitro*, a lack of fibrin generation with aggregation of plasma protein results in an apparent attenuation of clotting while these same aggregates could consolidate intravascularly (e.g., in capillary beds) to produce coagulopathy and ischemic conditions *in vivo*, with further hemostatic contributions coming from activated platelets. The question of critical charge density required to affect these coagulogenic aggregation events under physiological conditions remains central to proving this mechanism.

6.1.3 An in vitro toolkit for nanoparticle procoagulant assessment. These results demonstrate the establishment of a toolkit for the assessment of nanoparticle procoagulant effects. This includes assessments of dendrimer nanoparticle impact on the major functions of platelets in hemostasis, such as platelet morphological changes, adhesion, adhesion molecule expression, aggregation, inflammatory molecule secretion, and thrombin generation, as well as dendrimer nanoparticle-platelet binding. This toolkit also encompasses assessments of nanoparticle procoagulant effects relative to both the reactive molecules of the coagulation cascade and other circulating molecular components of blood plasma, including assays of Factor Xa and thrombin enzymatic activity, clotting in platelet poor plasma, clotting of purified thrombin and fibrinogen, visual inspection of resulting clots/products, fibrinogen fragment-based assessments, and size-based separation analysis of coagulation products (as a screen for general serum protein aggregation). Collectively, these assays probe both the mechanism and results of nanoparticle procoagulant and hemostatic properties. Further experiments will apply this toolkit to the analysis of other suspected procoagulant nanoparticles.

6.1.4 Zebrafish embryos for in vivo coagulopathic assessment. Following the preceding elucidation of G7-NH_2 hemostatic mechanisms, zebrafish embryos (ZFE) were successfully applied to elucidate whole-organism coagulogenic effects *in vivo* by real-time intravital

microscopy following intravascular microinjection of G7-NH_2. Transgenic fluorescent protein-expressing zebrafish lines were employed to facilitate fluorophore-specific microscopic observation of red blood cells and platelet-analogue thrombocytes. G7-NH_2 injections into ZFE were observed to produce immediate coagulation and vascular occlusion responses that scaled in magnitude with G7-NH_2 dosing. Though qualitative, this optically based method of nanoparticle coagulogenic effect provided clear insights into the extent and temporal progression of coagulopathy *in vivo* that were previously unavailable using existing (rodent) models. The specific challenges of the ZFE method for blood contacting assessments reside in the difficulty of dose administration, the scarcity of blood/tissue availability for *ex situ* assessments, and restriction of endpoint assessment to image-based quantitation. The strength of this ZFE-based coagulation assessment method lies in its speed, low cost and ease/clarity of assessment. Moreover, it was demonstrated cross-species efficacy of many well-known clinical anticoagulants and antiplatelet agents allows for mechanistic elucidation of nanoparticle-mediated blood activation. The ZFE model also is genetically tractable and offers relative ease of mutant generation and the existence of several convenient transgenic, morpholino-knockdown, or mutant variants with specific relevance to mechanistic or genetic screens of coagulation. Thus, the ZFE model seems well-suited to initial, gross, temporal and mechanistic assessments of nanoparticle procoagulant properties *in vivo* to identify specific areas for further study in appropriate blood-, platelet-, and small animal-based models.

6.1.5 Nanoparticles confound accurate quantitation of lipopolysaccharide in the KQCL assay. In addition to G7-NH_2 disruption of the human clotting cascade, nanoparticles were also shown to potentially alter the function of another biochemical cascade, the KQCL assay cascade which is derived from the Limulus Polyphemus coagulation system. Silica nanoparticles (SiNP) and two types of gold nanoparticles (AuNP) were observed to exaggerate the assayed lipopolysaccharide (LPS) concentration in samples containing as little as ppb quantities of AuNP or SiNP, independent of background LPS contamination or residual $HAuCl_4$ synthesis reagent. Moreover, the kinetic traces of assay product formation indicated a direct relationship between incubated AuNP/SiNP concentration and rate of product formation. While this suggests potential catalytic

NP behavior for these particle types in the KQCL assay, this phenomenon could alternately stem from proprietary stabilizers or other components of the Lonza KQCL assay reagents or lipopolysaccharide. Notably, polystyrene nanoparticles (PNP) exerted an opposite effect upon KQCL assay response, decreasing product formation in direct relation to incubated PNP concentration, strongly suggesting quantitative PNP adsorption and removal of LPS during centrifugative sample preparation. Future studies should evaluate additional nanoparticle types, sources of LPS, and forms of the LAL assay to determine the generality of the results reported herein.

6.2 Future work

The overall objective of this dissertation is to improve and expand the tools and techniques available for the assessment of nanoparticle toxicity, with a specific emphasis on pharmaceutically relevant nanoparticles that could have extensive systemic bioavailability. The immediate objective was to build a toolkit for nanoparticle coagulogenic assessment and to establish a positive control nanomaterial for the assessments comprising the toolkit. Having identified a robust and highly activating dendrimer nanoparticle and a variety of effective assessment methods for demonstrating its impacts upon the components of hemostasis, the task remains to broaden the toolkit with additional coagulation-relevant assessments, as needed. Specifically, interesting questions remain unexplored in relation to the procoagulant properties of G7-NH_2 that will require additional assays to elucidate.

The assay toolkit presented herein should be applied to a representative assortment of nanoparticles, encompassing the wide array of materials with potential for blood contact. Subsequently, with that established matrix of nanoparticle evaluations, this toolkit may be used to assess procoagulant properties for virtually any given nanoparticle.

6.2.1 Additional assessments of G7-NH_2 platelet activation. Following exposure to G7-NH_2, platelets undergo substantial morphological changes, extensive aggregation, and decreased thrombin generation capacity,[2] demonstrating strong G7-NH_2 interactions. These observed abnormalities in activated platelet morphology, when considered with confocal imaging that is suggestive of dendrimer interaction with alpha granules[2] and unpublished data demonstrating

platelet actin cytoskeleton abnormalities, suggest that G7-NH_2 may be penetrating into the platelet. The demonstration of such G7-NH_2 penetration into platelets could enable the loading of autologous platelets with a dendrimer-conjugated thrombolytic agent, by virtue of the 512 surface amine groups present on G7-NH_2. Conjugate size could present an obstacle to the G7-NH_2-mediated loading of the platelets, but the abundance of surface amines on G7-NH_2 could allow for the attachment of a carefully tuned, but substantial, amount of thrombolytic agent to the dendrimer surface simultaneous with the preservation of some positive charge density threshold necessary for platelet penetration. Alternatively, a mixture consisting of both native G7-NH_2 and drug-conjugated G7-NH_2 may produce the appropriate balance of platelet activation/membrane perturbation for dendrimer-drug loading. Since G7-NH_2 treatment imbues an activated and "sticky" phenotype to platelets,[2,3] drug loaded platelets may thus be ideally primed for targeted adhesion to the site of activation and infarction once injected back into the patient for the treatment of acute ischemic events.

6.2.2 Fibrinopeptide quantitation as a measure of fibrin production by G7-NH_2 exposure. Results in this dissertation strongly suggest the dendrimer-induced aggregation of plasma proteins. However, in order to conclusively demonstrate a (non)fibrinolytic mechanism for dendrimer procoagulant activity, fibrinogen cleavage products (fibrinopeptides A and B, FpA and FpB) should be demonstrably absent in G7-NH_2 fibrinogen sample supernatants. Fibrinopeptide quantification has been performed previously utilizing reverse-phase HPLC for thrombin-cleaved fibrinogen,[4] but HPLC sample analysis of fibrinopeptide generation was unsuccessful in these studies. However, HPLC analysis may be successful in this study through the dedication of a method-appropriate, previously unused column to the study. Alternatively, dendrimer- and thrombin-treated fibrinogen samples could be produced in scaled-up reaction volumes of reported methods[5] to allow for sample supernatant concentration of fibrinopeptides and subsequent quantitation by Asymmetric Flow Field Flow Fractionation (AsFlFFF). However, such a size-based separation method would be insensitive to the subtle size differences between FpA and FpB and would yield only quantification of the collective fibrinopeptide content of the sample. Yet another experimental alternative lies in a reported competitive enzyme-linked immunoassay (CELIA)- or

enzyme-linked immunosorbent assay (ELISA)-based detection of FpA and FpB with detection limits in the low picomolar range,[6] to allow for fibrinopeptide detection in unconcentrated samples. A variety of available FpA- and FpB-specific monoclonal antibodies and ELISA kits (e.g., MyBioSource, cat# MBS311826 and MBS726379; Abcam, cat#ab14790, ab48256, and ab86455) may be applied to this analysis.

6.2.3 Initial set of representative nanoparticles for procoagulant assessment. The results contained in this dissertation establish G7-NH_2 as a strong positive nanoparticle control for many known aspects of blood and platelet activation. However, G7-NH_2 represents only one of many nanoparticle classes and may not provide a suitable positive control for many classical activation pathways, given its unusual procoagulant mechanisms. Future efforts should extend the present set of assessments with dendrimers to include all of the major classes of nanoparticles (i.e., metallic nanoparticles, oxide nanoparticles, carbon nanomaterials, quantum dots, and polymeric nanoparticles). It would be best to begin such a matrix-based expansion with particles already known or suspected to have adverse coagulogenic effects such as iron oxide particles, polymeric poly(ethyleneimine) (PEI) particles, RGD-conjugated particles, silica particles, silver particles, and diesel exhaust particles. Comprehensive assessment of these representative nanoparticles would further demonstrate and expand the applicability of this toolkit for procoagulant assessment and may also yield classically activating nanoparticle controls for specific mechanisms of coagulation and platelet activation applicable for use in future nanoparticle assessments.

6.2.4 Utilizing zebrafish to elucidate cellular trafficking, fate, and consequences of particle uptake. Particle fate is of concern for any formulation utilizing nondegradable nanoparticles and understanding is still lacking relative to the transport of phagosome-sequestered particles and their secondary effects within the host. The transparent character of ZFEs allows for the facile visualization of cellular compartments filled with phagocytosed fluorescent nanoparticles and unpublished observations revealed the potential to visualize the *in vivo* cellular trafficking of injected fluorescent nanoparticles in real time. This unique ZFE model should be leveraged to help answer these basic questions of particle trafficking and ultimate fate. A variety of nanoparticle administration routes could be examined by utilizing injection to various

compartments of the body, solution-based diffusive dosing (topical), or oral administration. Assessment would first yield a rough evaluation of initial particle distribution, with uptake being assessed as the appearance of visible particle concentrations within host phagocytes. Subsequent particle trafficking would then be observed as the movement of cells containing high particle burdens continues throughout the animal. Such observations, distributed over a sufficient period of embryo development may yield insights into the interactions of phagocytes with particle elimination mechanisms within the animal or may suggest permanent particle sequestration within phagocytes. Such particle sequestration could result in senescence or compromised immune cell function as has been observed with the foreign body response to biomaterial implants and accompanying increased risk for infection[7] and could be assessed as outlined in the following section.

6.2.5 Assessing consequences of intracellular particle loading on immune function. As a companion to the above study of particle transport and fate in ZFE, the impairment of wound healing and antipathogen responses should be assessed for phagocytes possessing high particle burdens. This would begin with the administration and phagocytosis of fluorescently labeled nanoparticles. Subsequently, well-characterized infection and wound resolution responses would be observed and contrasted for normal and nanoparticle-dosed ZFE. Such assessments would examine the dependency of nanoparticle loading in observed modulations of cellular chemotaxis and activity in a fin-wounding assay,[8,9] cellular capacity for pathogenic phagocytosis,[10] cellular response to both local and systemic infections,[10] and persistence of pathogen loads within the host.[10] Moreover, time-lapse imagery could provide valuable insights into the specific functionality of particle-loaded cells with transgenic ZFE fluorescent neutrophil[11] Tg(MPO::EGFP) or fluorescent macrophage[9] Tg(mpeg1:Gal4-VP16/UAS:Kaede) counter labeling to injected nanoparticle fluorescence. Thus, image based-analysis could be applied to contrast localization and motility for particle-loaded cells relative to unloaded cells in the same animal. Such data would offer valuable insight into the impacts of nanoparticle phagocytosis on the subsequent cellular and systemic immune capacity for response to injury or pathogenic challenge.

This dissertation and future work outlined here offer improved assessment and better

understanding of the adverse effects consequent to systemic nanoparticle administration. The focus on the procoagulant effects of therapeutically applied nanoparticles helps to fill a deficiency in current nanoparticle assessment. The current and future application of basic cellular, molecular, and ZFE-based assessments to determine fundamental nanoparticle procoagulant properties provides a useful toolkit for the characterization of blood contacting nanoparticles. Ultimately, such comprehensive response-based characterization will aid in the design of safer nanoparticle-enabled formulations for a variety of injectable therapeutics.

6.3 References

1. Greish K, Thiagarajan G, Herd H, et al. Size and surface charge significantly influence the toxicity of silica and dendritic nanoparticles. *Nanotoxicology.* 2012;6(7):713-723.

2. Jones CF, Campbell RA, Franks Z, et al. Cationic PAMAM dendrimers disrupt key platelet functions. *Mol Pharm.* 2012;9(6):1599-1611.

3. Dobrovolskaia MA, Patri AK, Simak J, et al. Nanoparticle size and surface charge determine effects of PAMAM dendrimers on human platelets in vitro. *Mol Pharm.* 2012;9(3):382–393.

4. Cooper AV, Standeven KF, Ariens RA. Fibrinogen gamma-chain splice variant gamma' alters fibrin formation and structure. *Blood.* 2003;102(2):535-540.

5. Ng AS, Lewis SD, Shafer JA. Quantifying thrombin-catalyzed release of fibrinopeptides from fibrinogen using high-performance liquid chromatography. *Methods Enzymol.* 1993;222:341-358.

6. Soria J, Soria C, Ryckewaert JJ. A solid phase immuno enzymological assay for the measurement of human fibrinopeptide A. *Thromb Res.*1980;20(4):425-435.

7. Holt DJ, Grainger DW. Senescence and quiescence induced compromised function in cultured macrophages. *Biomaterials.* 2012;33:7497-7507.

8. Redd MJ, Kelly G, Dunn G, Way M, Martin P. Imaging macrophage chemotaxis in vivo: studies of microtubule function in zebrafish wound inflammation. *Cell Motil Cytoskeleton.* 2006;63(7):415-422.

9. Ellett F, Pase L, Hayman JW, Andrianopoulos A, Lieschke GJ. mpeg1 promoter transgenes direct macrophage-lineage expression in zebrafish. *Blood.* 2011:117(4):e49-56.

10. Wiles TJ, Bower JM, Redd MJ, Mulvey MA. Use of zebrafish to probe the divergent virulence potentials and toxin requirements of extraintestinal pathogenic Escherichia coli. *PLoS Pathog.* 2009;5(12):e1000697.

11. Renshaw SA, Loynes CA, Trushell DM, Elworthy S, Ingham PW, Whyte MK. A transgenic zebrafish model of neutrophilic inflammation. *Blood.* 2006;108(13):3976-3978.